THE SYNTHESIS AND CHARACTERIZATION OF MOLECULARLY IMPRINTED MATERIALS

Thesis by

Alexander Katz

In Partial Fulfillment of the Requirements

for the Degree of

Doctor of Philosophy

California Institute of Technology

Pasadena, California

1999

(Submitted August 10, 1998)

to my parents

Marat G. Katz and Sophia E. Katz

Acknowledgment

assistance with X-ray crystallography and Dana L. Roth for many useful literature searches.

I would also like to thank two teachers from the past, Professor Michael D. Ward at the University of Minnesota, Twin Cities and my first science teacher, Mr. James T. Threinen, from the Technology Learning Campus in Robbinsdale, Minnesota for their many words of wisdom about education and life in general during my graduate career.

I am indebted to many of my peers and to my family. First and foremost in this category, I would like to thank my parents, Marat G. Katz and Sophia E. Katz, for their constant encouragement and support. I would also like to thank my sister, Julia K. Mirman, for all of her life-experience-based advice. Finally, I would like to acknowledge some of my best friends here at Caltech who made my graduate school tenure stimulating and fun: Paul A. Wagner, Hector Gonzalez, Wayez R. Ahmad, Shervin Khodabandeh, and Larry and Dara Beck. Whether it was a strenuous hike in the Angeles National Forest or a relaxing get-together at one of our many favorite places in the vicinity of Los Angeles, these outings with friends over the past several years provide memories that I will cherish for a long time to come.

Abstract

Current advances in chemical protection strategies, analytical methods such as solid-state NMR and EPR spectroscopies and biological catalysis make it an ideal time to reinvestigate molecular imprinting as a viable method for the synthesis of catalysts for small molecule transformations. In the past, imprinting has been pursued mainly as a method for creating separation media for dealing with issues of adsorption/separation of small molecules. In a few instances, these materials have also been investigated as catalysts. Most imprinted systems to-date have employed non-covalent interactions to achieve functional group positioning, and this type of an approach can lead to other undesired effects such as binding site heterogeneity (as shown in this thesis for one particular system that employs self-assembly to achieve imprinting). Site heterogeneities can be extremely detrimental for selective catalysis. The objective of this work is to determine the origins of site heterogeneity and attempt to overcome these issues in order to synthesize new catalysts via molecular imprinting.

To gain further insight into the causes responsible for site heterogeneity in imprinted materials, the nature of molecular recognition in an imprinted polymer that is known to exhibit strong binding site heterogeneity is investigated. The system is formed by the self-assembly of a binding monomer and an imprint through non-covalent interactions. Based on observations of bulk phase separation in the system investigated, an

alternative mechanism for molecular recognition in the imprinted polymer is proposed. This mechanism involves remaining, occluded imprint molecules that provide for binding via imprint-imprint intermolecular interactions. Support for this mechanism is provided from polymers prepared using a combination of imprint and mimic, which remains covalently bound in the polymer and is shown to increase the rebinding of imprint while not significantly affecting the binding of the opposite enantiomer of the imprint. Elucidation of this mechanism provides insight into the nature of site heterogeneity in imprinted polymer systems.

Based on the findings from the self-assembly system, a new molecular imprinting approach is developed that utilizes the controlled distance method. In this approach, silica is used for the inert crosslinking framework instead of an organic polymer due to its significantly greater mechanical rigidity (300 times more rigid and not susceptible to swelling in organic media). Instead of non-covalent interactions as the driving force for functional group positioning, covalent interactions are used. The method positions several amine functionalities (up to three demonstrated), within the three-dimensional porous structure of silica. This imprinting process is characterized by FTIR and solid state NMR spectroscopies. The imprinted silicas show microporosity specifically resulting from the imprinting process, with the amount of microporosity added consistent with the extent of imprint removal. The imprinted amines which reside in the microporous void space

are able to bind molecules such as benzoic acid and acetylacetone and also perform shape-selective catalysis. To ascertain the degree of control over functional group positioning with this imprinting approach, fluorescence measurements with a pyrenebutyric acid probe molecule were performed on the imprinted silicas. The results demonstrate that the imprinting process employed gives local functional group ordering for the case of three amines per site and gives well-isolated functional groups for the case of one amine per site. The imprinted silicas thus provide a foundation from which further investigations towards elucidating quantitative distance information between imprinted functionalities in these materials can be developed.

Table of Contents

Chapter One   *Introduction and Objectives*

Chapter Two   *Rational Catalyst Design via Imprinted Nanostructured Materials*

Chapter Three   *Investigations into the Mechanisms of Molecular Recognition with Imprinted Polymers*

Chapter Four   *A New Method for the Molecular Imprinting of Silica with Amine Functionality*

List of Schemes

List of Tables

Chapter 4

List of Figures

Chapter 1

Chapter 2

Chapter 4

Figure 4.4.15.   Monofunctional product solution concentration versus time for the Knoevenagel condensation of isophthalaldehyde and malononitrile. Filled triangles represent aminopropyl, surface functionalized silica, filled circles represent the one-point imprinted silica, and filled squares represent the two-point imprinted silica.

Figure 4.4.16.   Bifunctional product solution concentration versus time for the Knoevenagel condensation of isophthalaldehyde and malononitrile. Filled triangles represent aminopropyl, surface functionalized silica, filled circles represent the one-point imprinted silica, and filled squares represent the two-point imprinted silica.

Figure 4.4.17.   Conversion of isophthalaldehyde versus time for the Knoevenagel condensation of isophthalaldehyde and malononitrile. Filled circles represent aminopropyl, surface functionalized silica, filled diamonds represent the one-point imprinted silica, and filled squares represent the two-point imprinted silica. The rates given in the right-hand-corner of the graph represent initial rates in turnovers per amine site per hour.

CHAPTER ONE

INTRODUCTION AND OBJECTIVES

1.1   Introduction

The goal of molecular imprinting is to precisely position chemical functionalities within a void space of controlled dimensions in a solid material.[1] A schematic representation of a molecularly imprinted material is shown in Figure 1.1.1.

Imprinted Material

Target Molecule Adsorption

Bound Imprinted Site
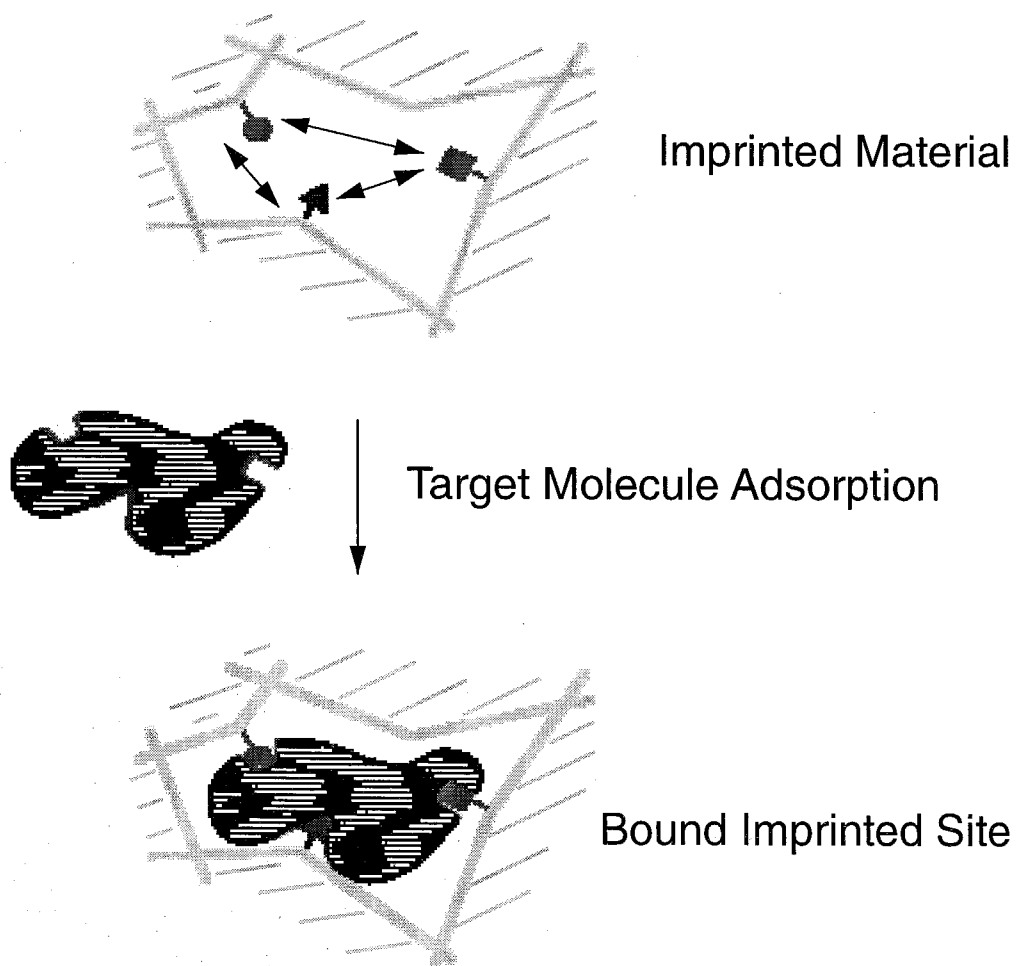
Figure   1.1.1.   Conceptual illustration of an imprinted material and its use as an adsorbent (see text for further descriptions).

The periphery of the binding site is comprised of the bulk material (usually amorphous) that serves as the scaffold for mechanically supporting the functional group organization created by the imprinting process. The filled shapes in Figure 1.1.1 represent different functional groups positioned in three-dimensions relative to one another, with the double-sided arrows in the schematic representing both well-defined distances, typically over the length scale of several Ångstroms, and angles. Such a configuration of functional groups can be used to bind a molecule that is chemically complementary to the binding site as shown in Figure 1.1.1. This principle forms the basis for the use of imprinted materials as specific adsorbents.[2] For the case in which the imprinted binding site is complementary to a transition-state analogue for a particular chemical transformation, the site may be able to provide interactions to a transition-state in order to lower the energy for the transformation and thereby catalyze the transformation in a manner consistent with the lock-and-key principle of Emil Fischer.[3] This last aspect of imprinted materials is discussed in detail in Chapter 2, which gives a general review of catalysis in nanostructured media.

From the context of catalysis, the local organization created within a material by molecular imprinting can be used for synthesizing a catalyst with both high activity and high selectivity. Nowhere is this concept more elegantly illustrated than in nature with protein-based catalysts, where the

correct functional group placement can afford rate accelerations that can approach greater than 10^{17} over thermal background, with retention of stereoselectivity (versus thermal background).[4] Figure 1.1.2 shows examples of an enzyme and antibody active site for a representative transformation involving (-)-chorismate to prephenate. The key point is that although the enzyme is not created via an imprinting-like process, the catalytic antibody was, with the use of reactive immunization which elicits an antibody against a hapten that serves as a transition-state analogue.[5] Thus catalytic antibodies demonstrate the viability of an imprinting approach to the synthesis of novel catalysts. Figure 1.1.2 shows the transition-state analogue-bound active site structure of the enzyme and antibody for the transformation of (-)-chorismate to prephenate, as determined by X-ray crystallography.[6] The enzyme active site in this case has a higher density of functional groups positioned for interaction with the substrate relative to the antibody. The increased complexity of the enzyme manifests itself in a *ca* 1000 time catalytic rate enhancement of the enzyme catalyst over the antibody for this case.

With the use of biology and its impressive capability to synthesize catalytic environments that possess precisely positioned functional groups,[7] one can ponder the question of whether non-biologically based materials with multi-functional group positioning are necessary and can have engineering applications.
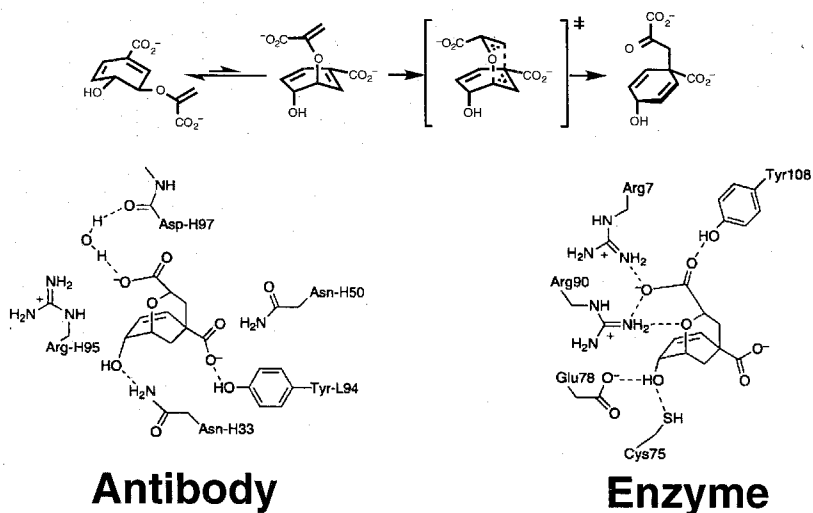
Antibody   **Enzyme**

Rate (Enzyme) > $10^{2\text{-}4}$ Rate (Antibody) > 10^6 Rate (Uncatalyzed)

Figure 1.1.2.   Antibody and enzyme active sites compared for the transformation of (-)-chorismate to prephenate.

Biologically-based catalysts, however, despite their intricate complexities and remarkable rate enhancements and specificities, have several drawbacks that limit their utility as industrially viable catalytic materials. Enzymes and antibodies have limited temperature stability, and severe problems are encountered when using these catalysts in organic solvent environments. Of most importance, however, is the issue of space-time-yield (turnover per unit reactor volume). Weisz has established a rule-of-thumb that an industrial catalytic reactor should operate at a space-time-yield (STY) that is approximately 10^{-6} mol/(cm^3·s).[8] Higher values of the STY give mass and heat transfer limitations on the rate while lower values yield reactor sizes of excessive dimensions. Despite enzymes' and antibodies' high

turnover rate, their low active site density in a reactor makes the value of the space-time-yield significantly lower than the optimum. Direct consequences of this are observed in the large operating costs associated with water removal to recover end-products and large reactor sizes that are necessary to give reasonable turnover rates, which render protein-based catalysts economically unfavorable for many applications. To deal with these shortcomings of biological systems, investigators have devised several approaches that represent a marriage between ideas borrowed from nature's catalysts and those from man-made systems. These have ranged from immobilizing protein catalysts on heterogeneous supports[9] to creating "artificial" enzymes by positioning functional groups in a convergent manner[10] around molecular scaffolds such as cyclodextrins[11] and fused aromatic systems.[12] As an extension of the latter concept to amorphous materials, molecular imprinting offers a strategy for synthesizing convergently positioned chemical functionalities in precise geometries. Thus, if molecular imprinting can be accomplished, it makes feasible the design of a solid-phase catalyst for operation at an industrially optimal space-time yield.

A significant problem to-date in the synthesis of molecularly imprinted materials has been a large binding site heterogeneity in the sites created by the imprinting method.[13] That is to say, a fraction of the sites may be as designed in the imprinted material (as illustrated in Figure 1.1.1); there are

other sites that may only contain one or two of the three imprinted functional groups or those that contain all three, but the functional groups are not positioned in the correct geometry. From the perspective of batch separations, having a heterogeneous binding site population is a problem if the selective sites become saturated due to their smaller number density. The degree of separation achieved is then governed by the less-selective heterogeneous sites, which may give poor selectivity as in the case of chiral separations of amino acid derivatives, where a sharp drop in enantioselectivity is observed upon increasing the sample loading on the imprinted material.[14] For continuous, column-based separations, the degree of separation achieved can be dominated by the selective sites and non-selective sites just act to dilute the concentration of binding sites inside the column. From the perspective of catalytic applications, however, it is crucial to have a homogeneous population of catalytic sites, as even a small fraction of less selective sites can ruin the observed selectivity, due to their amplification by the turnover frequency. Imprinted site heterogeneity happens to be particularly problematic when using the method of molecular imprinting by non-covalent self-assembly, which until recently has been the main approach investigators have used to synthesize imprinted materials. Possible mechanistic sources of this heterogeneity will be described in the investigation of an organic polymer imprinted by non-covalent self-assembly in Chapter 3.

The method of molecular imprinting by non-covalent self-assembly is illustrated in Scheme 1.1.1. Conceptually it involves the ability of an imprint species to self-assemble with a binding monomer in the presence of an inert crosslinking monomer. Polymerization of the monomers typically results in a macroporous support with the binding monomer fragments supposedly positioned for optimal interaction with the imprint. Extraction of the imprint is proposed to create molecular cavities that contain the binding monomer fragments strategically positioned to readsorb the imprint. A variety of applications such as enantioselective separations,[15] heterogeneous catalysis[16] and antibody mimicry[17] have been reported using non-covalent molecular imprinting by self-assembly. However, despite a history of using this approach to create imprinted sites since the days of Dickey at Caltech nearly five decades ago,[18] a material bearing a homogeneous distribution of imprinted binding sites has not been reported to-date with this approach.

The first report of a molecularly imprinted material that may provide a homogeneous distribution of non-covalent binding sites was made by Whitcombe et al. in 1995.[19] They prepared a molecularly imprinted polymer selective towards cholesterol that exhibits a Langmuirian binding isotherm (linear Scatchard plot) upon rebinding cholesterol from hexane solutions. Their general approach is represented in Scheme 1.1.2.
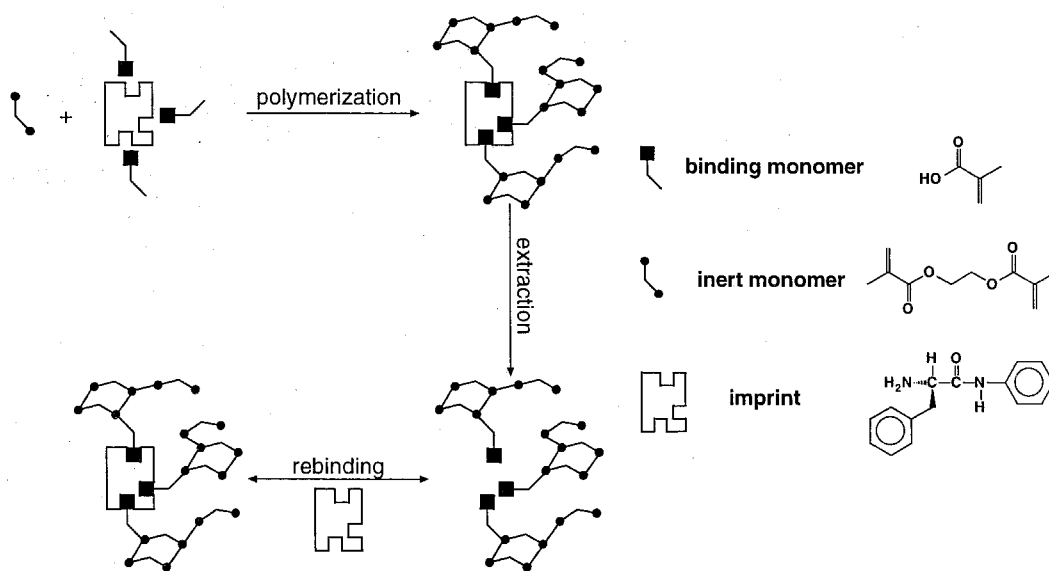
Scheme 1.1.1. Diagram illustrating the various steps involved in creating a molecularly imprinted material by non-covalent self-assembly. On the right-hand-side of the scheme are examples of typical monomers and imprints used and include methacrylic acid as binding monomer, ethylene dimethacrylate as inert crosslinking monomer, and L-phenylalanine anilide as imprint.
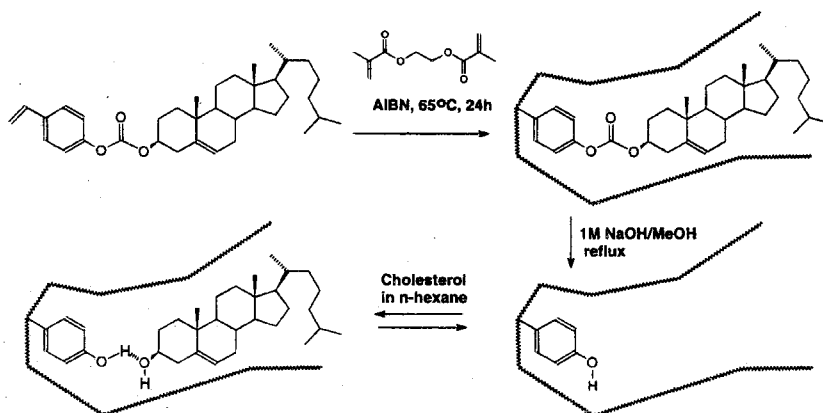
Scheme 1.1.2. Schematic of controlled distance imprinting method developed by Whitcombe et al. (Ref. 19) to create a homogeneous distribution of binding sites for the imprint cholesterol, based on the shape-selectivity of the cavity and the single-point interaction between the hydroxyl of the binding monomer fragment and cholesterol.

Whitcombe et al. used chemical synthesis to covalently fix the distance between the binding monomer fragment and the molecular porogen, which carries shape-selective information in the composite molecule that serves as the imprint, by synthesizing the 4-vinylphenyl carbonate ester of cholesterol as the imprint. In this approach, the imprint is copolymerized via free-radical initiation with the inert cross-linking monomer. This generates a crosslinked amorphous network possessing a fragment of the imprint dispersed therein. The carbonate of the imprint fragment is deprotected via base-catalyzed hydrolysis to yield an imprinted binding site that has the shape of cholesterol and a hydroxyl group strategically positioned for binding cholesterol via a single point OH···OH hydrogen bond. The important difference between the procedure developed by Whitcombe et al. and the non-covalent imprinting approach is that in the former, the binding monomer is positioned with covalent interactions, i.e., typically involving bond energies of upwards of 80 kcal/mol, while in the latter the binding monomer is positioned with non-covalent interactions, i.e., typically involving bond energies significantly smaller than 10 kcal/mol.

The significantly weaker enthalpic driving force for creating order in the non-covalent imprinting scenario is the intrinsic cause for its limited success as manifested in the binding site heterogeneity typically observed with this approach, as I will show in Chapter 3.

1.2 Objectives

The objective of my research is to attempt to prepare imprinted solid materials with homogeneous active sites for application as catalysts. As mentioned previously, homogeneity is of major importance for catalytic use. Initially, I performed a critical evaluation of the literature on nanostructured materials prepared by imprinting (Chapter 2). Based on this overview, it was clear that all imprinted materials used for catalysis (other than enzymes and antibodies) reveal site heterogeneity. In order to better understand the reasons for the observed site heterogeneity, I investigated one of the more well-studied systems, namely one that uses ethylene glycol dimethacrylate, methacrylic acid and L-phenylalanine anilide as the crosslinking monomer, binding monomer and imprint, respectively, to assemble the imprinted polymer. In Chapter 3, I present my findings on the origin of site heterogeneity when using the self-assembly method of imprinting. Because of these findings, it is clear that this synthetic methodology is not likely to yield a solid material with a homogeneous active site population. In light of these conclusions, I concentrated on developing a controlled distance imprinting procedure to allow for multiple-point interactions using silica as the inert scaffold, and my results are given in Chapter 4. Silica has several distinct advantages over organic polymers as an inert crosslinking scaffold due to its greater crosslinking density and mechanical rigidity (greater than

300 times the Young's modulus of crosslinked ethylene glycol dimethacrylate)[20] and its proven ability to withstand high temperature and organic solvent without swelling. In the past, investigators have imprinted the interior surface of silica particles by reacting suitable monomers with the hydroxyls of the particle surface to create binding sites with covalent anchors.[21] However, to-date, the cocondensation of an organosilane with a silane to create a non-covalent, imprinted binding site in three-dimensions has not been accomplished. Note that in this case molecular imprinting by non-covalent self-assembly cannot be used as a method due to the Brönsted acids and bases that are present as catalysts for sol-gel hydrolysis and condensation (interference with the architecture of the non-covalent binding monomer and imprint self-assembly will result). I developed a new method of imprinting that allows the positioning of amine moieties in silica. It relies on a controlled distance approach that is represented in Scheme 1.2.1. Here, symmetric benzene carbamates are used as templates to direct the precise positioning of up to three propylamine residues. Three molecularly imprinted silicas and one control silica were synthesized with this new approach containing: 1) no imprint (0-point control); 2) isolated propylamine residues (1-point); 3) propylamine pairs comprising a separation distance of approximately 10 Å within a pair (2-point) and 4) propylamine triads comprising a separation distance of approximately 6 Å

within a triad (3-point). The synthesis and characterization of these imprinted silicas is discussed in Chapter 4.

composite molecule synthesis

+

polymerization

bond cleavage

rebinding

binding monomer
CH_3CH_2O—Si—$(CH_2)_3$—NH_2 (with OCH_2CH_3 groups)

inert monomer
CH_3CH_2O—Si—OCH_2CH_3 (with OCH_2CH_3 groups)

molecular porogen
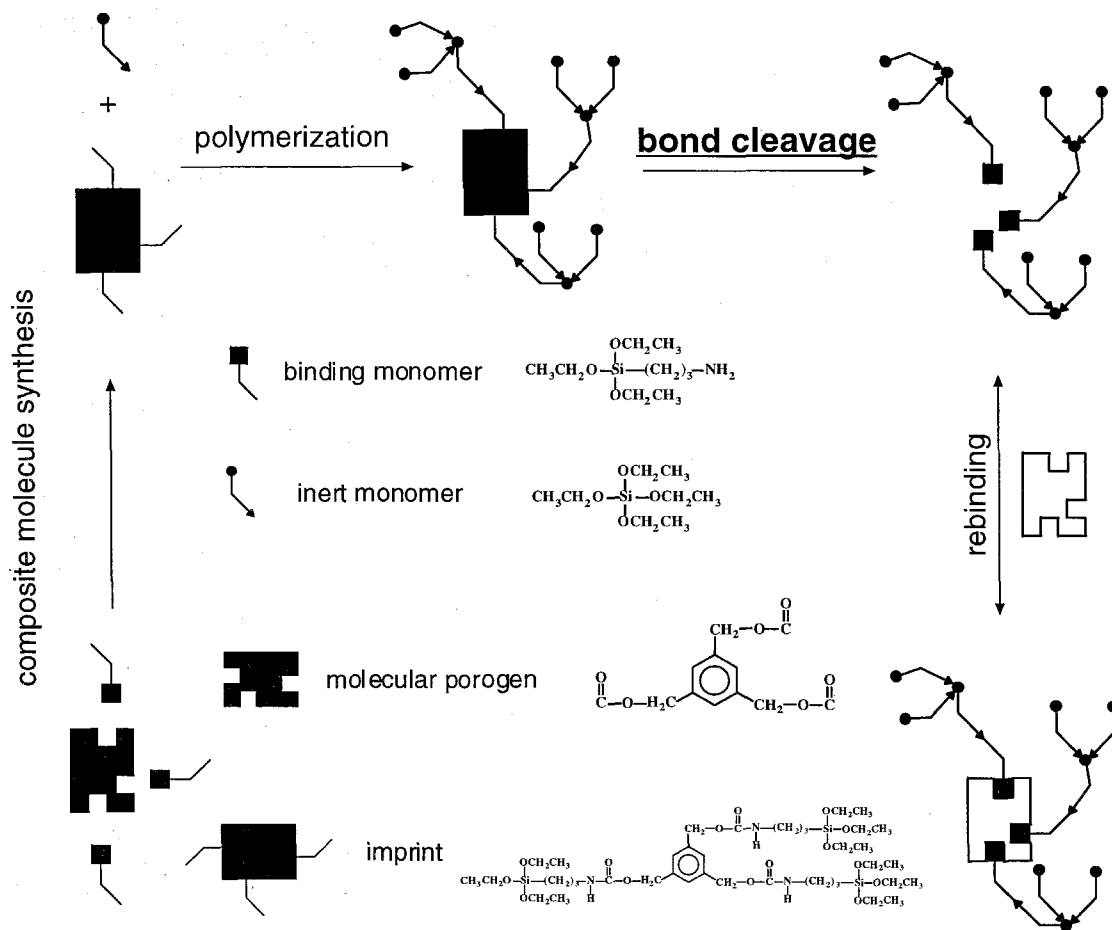
imprint

Scheme 1.2.1. Diagram illustrating the various steps involved in creating a molecularly imprinted silica by the controlled distance approach. In the center of the scheme are examples of typical monomers and imprints used and include 3-aminopropyltriethoxysilane as binding monomer, tetraethylorthosilicate as inert crosslinking monomer, and [3-(triethoxysilyl)propyl]-1,3,5-benzenetriyltris(methylene)carbamate as imprint. Imprint is cleaved to remove the molecular porogen via deprotection represented as bond cleavage (analogous to the extraction procedure in the non-covalent self-assembly imprinting method).

1.3 References

[1]   Wulff, G. In *Polymeric Reagents and Catalysts*; Ford, W. T., Ed.; ACS Symposium Series 308; American Chemical Society: Washington, DC, 1986.

[2]   Snyder, L. R. *Principles of Adsorption Chromatography*; Marcel Dekker: New York, New York 1968.

[3]   Fischer, E. *Ber. Dtsch. Chem. Ges.* **1890**, *23*, 2611.

[4]   Radzicka, A. and Wolfenden, R. *Science* **1995**, *267*, 90.

[5]   (a) Tramontano, A.; Janda, K. O.; Lerner, R. A. *Science* **1986**, *234*, 1566. (b) Pollack, S. J.; Jacobs, J. W.; Schultz, P. G. *Science* **1986**, *234*, 1570.

[6]   Haynes, M. R.; Stura, E. A.; Hilvert, D.; Wilson, I. A. *Science* **1994**, *263*, 646.

[7]   (a) DelaFuente, G.; Lagunas, R.; Sols, A. *Eur. J. Biochem.* **1970**, *16*, 226. (b) Morton, A. and Mathews, B. W. *Biochem.* **1995**, 34, 8576.

[8]   Weisz, P. B. Chemtech **1982**, *12*, 424.

[9]   Petro, M.; Svec, F.; Fréchet, J. M. J. *Biotech. Bio.* **1996**, *49*, 355.

[10]   (a) Rebek, Jr., J. *J. Heterocycl. Chem.* **1990**, *27*, 111. (b) Wolfe, J.; Muehldorf, A.; Rebek, Jr., J. *J. Am. Chem. Soc.* **1991**, *113*, 1454.

[11]   Breslow, R. *Acc. Chem. Res.* **1995**, *28*, 146.

[12]   Rojas, C. M. and Rebek, Jr., J. *Bioorg. Med. Chem. Lett.* **1996**, *6*, 3013.

[13]   (a) Matsui, J.; Miyoshi, Y.; Doblhoff-Dier, O.; Takeuchi, T. *Anal. Chem.* **1995**, *67*, 4404. (b) Matsui, J.; Kaneko, A.; Miyoshi, Y.; Yokoyama, K.; Tamiya, E.; Takeuchi, T. *Anal. Lett.* **1996**, *29*, 2071. (c) Tomioka, Y.; Kudo, Y.; Hayashi, T.; Nakamura, N.; Niizeki, M.; Hishinuma, T.; Mizugaki, M. *Biol. Pharm. Bull.* **1997**, *20*, 397.   (d) Sellergren, B.; Shea, K. J. *J. Chromatogr.* **1995**, *690*, 29.

[14]   (a) Sellergren, B. *Chirality* **1989**, *1*, 63. (b) Sellergren, B. *Makromol. Chem.* **1989**, *190*, 2703.   (c)   Sellergren, B.; Shea, K. J. *J. Chromatogr.* **1993**, *635*, 31.

[15]   (a) Kempe, M.; Mosbach, K. *J. Chromatogr.* **1995**, *694*, 3.   (b) O'Shannessy, D. J.; Ekberg, B.; Andersson, L. I.; Mosbach, K. *J. Chromatogr.* **1989**, *470*, 391. (c) Andersson, L. I.; Mosbach, K. *J. Chromatogr.* **1990**, *322*, 313. (d) Kempe, M.; Mosbach, K. *Int. J. Peptide Protein Res.* **1994**, *44*, 603. (e) Kempe, M.; Mosbach, K. *Anal. Lett.* **1991**, *24*, 1137. (f) Andersson, L. I.; Miyabayashi, A.; O'Shannessy, D.; Mosbach, K. *J. Chromatogr.* **1990**, *516*, 323.

[16]   Davis, M. E.; Katz, A.; Ahmad, W. R. *Chem. Mater.* **1996**, *8*, 1820.

[17]   (a) Andersson, L. I.; Nicholls, I. A.; Mosbach, K. In *Immunoanalysis of Agrichemicals*, Nelson, J. O.; Karu, A. E.; Wong, R. B., Eds.; ACS Symposium Series 586; American Chemical Society: Washington,

DC, 1995. (b) Ramström, O.; Ye, L.; Mosbach, K. *Chem. Biol.* **1996**, *3*, 471. (c) Burow, M. and Minoura, N; *Biochem. Biophys. Res. Commun.* **1996**, *227*, 419. (d) Mosbach, K. and Ramström, O.; *Bio/Technology* **1996**, *14*, 163. (e) Kempe, M. *Anal. Chem.* **1996**, *68*, 1948. (f) Vlatakis, G.; Andersson, L. I.; Müller, R.; Mosbach, K. *Nature* **1993**, *361*, 645. (g) Nilsson, K.; Lindell, J.; Norrlöw, O.; Sellergren, B. *J. Chromatogr.* **1994**, *680*, 57. (h) Andersson, L. I.; Müller, R.; Vlatakis, G.; Mosbach, K. *Proc. Natl. Acad. Sci. USA* **1995**, *92*, 4788.

[18]   (a) Dickey, F. H. *Proc. Natl. Acad. Sci. USA* **1949**, *35*, 227. (b) Dickey, F. H. *J. Phys. Chem.* **1955**, *59*, 695.

[19]   Whitcombe, M. J.; Rodriguez, M. E.; Villar, P.; Vulfson, E. *J. Am. Chem. Soc.* **1995**, *117*, 7105.

[20]   Lungu, A. and Neckers, D. C. *J. Polym. Sci. Part A Polym. Chem.* **1996**, *34*, 3355.

[21]   (a) Wulff, G.; Heide, B.; Helfmeier, G. *J. Am. Chem. Soc.* **1986**, *108*, 1089. (b) Wulff, G.; Heide, B.; Helfmeier, G. *React. Polym.* **1987**, *6*, 299. (c) Glad, M.; Norrlöw, O.; Sellergren, B.; Siegbahn, N.; Mosbach, K. *J. Chromatogr.* **1985**, *347*, 11. (d) Tao, Y.; Ho, Y. *J. Chem. Soc., Chem. Commun.* **1988**, *6*, 417. (e) Hwang, K.; Yakura, Y.; Ohuchi, F. S.; Sasaki, T. *Mater. Sci. Eng. C* **1995**, *3*, 137. (f) Tahmassebi, D. C. and Sasaki, T. *J. Org. Chem.* **1994**, *59*, 679.

CHAPTER TWO

RATIONAL CATALYST DESIGN VIA IMPRINTED NANOSTRUCTURED MATERIALS

Reprinted with permission from the article

[M. E. Davis, A. Katz and W. R. Ahmad, *Chem. Mater.* **1996**, *8*, 1820]

RATIONAL CATALYST DESIGN VIA IMPRINTED NANOSTRUCTURED MATERIALS

Mark E. Davis*, Alexander Katz and Wayez R. Ahmad

Chemical Engineering
California Institute of Technology,
Pasadena, California 91125
Phone: (818) 395-4251
Fax: (818) 568-8743

ABSTRACT

Progress on the use of imprinting (templating) for the synthesis of nanostructured catalysts is reviewed. In the context of providing a foundation for synthetic mimics, the basic principles of enzyme catalysis are enumerated. With these paradigms in mind, catalytic antibodies, imprinted polymers, imprinted amorphous metal oxides and zeolites are discussed with respect to their preparation procedures and catalytic properties. These synthetic catalysts are contrasted to one another in order to highlight the advantages and disadvantages of each system. Suggestions for future work on preparing enzyme-mimicking materials by imprinting are provided.

*To whom correspondence should be addressed.

2.1 Introduction

Nanostructured solids encompass a broad spectrum of material types whose applications are quite diverse. Areas of science and technology that have significantly benefited from advances in the physicochemical properties of nanostructured materials are mainly those that involve molecular recognition, such as separations, medical diagnostics, drug delivery, sensors and catalysis. Although molecules and/or materials derived from natural systems, *e.g.*, enzymes for catalysis, antibodies for immunoassays, cyclodextrins for chiral separations, can be utilized for many of the aforementioned functions, there are situations where these entities are unsuitable for application, *e.g.*, harsh environments, regeneration from fouling, etc. Thus, the desire for materials that contain synthetic receptors is high and continues to increase. In this paper, we concentrate on advances in the preparation and physicochemical properties of nanostructured materials for catalysis by design. Several reviews concerning primarily polymeric materials with imprinted receptor sites for use as separation and drug assay media can be found elsewhere.[1-5]

The lofty goal of catalysis by design has been the dream of many who have worked on abiological as well as biological catalysts. A particularly powerful conceptual approach to abiological catalysis by design has been and continues to be the attempt to translate the principles of enzyme catalysis to non-biologically derived catalytic materials. It is this line of thought that we illustrate in this review by showing the current progress in fabricating nanostructured materials that attempt to mimic biological, macromolecular catalysts.

Approximately 50 years ago Linus Pauling and colleagues prepared the first nanostructured solids for molecular recognition by molecularly imprinting (or templating) silica gels.[6] Pauling speculated that biological machinery in living systems constructed antibodies by using molecules as imprints or templates.[7] Although this idea is now known to be incorrect, the concept of imprinting to create nanostructured, abiological materials was quickly exploited.[8] Dickey prepared nanostructured silica gels by imprinting the formation of the silica with homologs of methyl orange. Subsequent removal of the imprint molecules yielded gels capable of specific adsorption (see Table 2.1.1). Thus, nanostructured solids with specific molecular recognition sites have been reported nearly a half a century ago. It is not obvious to us why these initial encouraging results did not stimulate further work until the 1970's. Although it is clear that these silicas possessed very limited stability,[9,10] the adsorption results are comparable with most of the best data obtained from present day materials. Additionally, there was even an early claim of extending this technique to produce silica gels capable of chiral separations.[11] However, it was not until the 1970's that nanostructured materials for molecular recognition surfaced again in the work of Wulff and colleagues who imprinted cross-linked polymers.[1,12] Since the 1970's, and particularly in the 1990's, work on imprinted, nanostructured materials for molecular recognition has burgeoned significantly, particularly in the area of imprinting via non-covalent interactions, to a large extent due to the work of Mosbach and colleagues.[3,4]

Here we provide an overview of imprinted (templated), nanostructured materials for catalytic applications. Enzyme catalysis is briefly introduced to

set the stage for all the other synthetic mimics. Next, catalytic antibodies are discussed since these macromolecules are catalysts that involve preparation by design and set the benchmarks from which all abiological materials will be compared. Finally, imprinted polymers, amorphous metal oxides and crystalline metal oxides (molecular sieves, zeolites) will be reviewed and their advantages and disadvantages as designed nanostructured materials for catalysis enumerated.

2.2   Enzyme Catalysis: A Model

The elegance of enzyme reactivity is unparalleled in synthetic catalytic materials. Beginning from the time when Emil Fischer proposed his classic lock-and-key theory for enzyme specificity[13] to the now generally accepted induced fit theory of Koshland,[14,15] enzyme catalysis sets the standard to which all other catalytic transformations are compared. In order to introduce a concept as complex as enzyme catalysis, a brief overview of some of the accepted principles is provided below. A more comprehensive presentation of enzyme structure and function can be found elsewhere.[16]

A limiting-case enzyme model that addresses several important issues related to enzyme catalysis is the induced fit theory of Koshland that is schematically represented in Figure 2.2.1. The critical components of this theory are: (*i*) that there is a precise three-dimensional configuration of the amino acid functional groups that must interact with an appropriate reactant (substrate) in order for catalysis to occur, (*ii*) that the binding (chemisorption) of the reactant produces an appreciable change in the three-dimensional conformation of the amino acids at the active site and (*iii*) that the changes in

the protein structure produced by substrate binding bring about the proper alignment between protein function groups and the substrate to allow catalytic reactions to occur. A non-substrate may still be able to bind but not react due to misalignment of the appropriate interactions. Thus, as Koshland states, the process is not like a "lock-and-key" fit but rather a "hand-in-glove" fit allowing for flexibility.[15] Virtually all enzymes have been shown to have conformational changes upon binding. Gerstein *et al.* have reviewed the types of movements observed in proteins.[17] They report that nearly all large proteins are built from domains, *e.g.*, β-sheets, α-helices, etc. Gerstein *et al.* suggest that when a substrate binds to a particular domain, thermal fluctuations can bring a second domain into contact with the bound substrate and the newly formed interactions stabilize the "closed" or "bound" conformation.[17] The protein-substrate interactions can be numerous and consist of combinations of interlocking salt bridges, hydrogen bonds and van der Waals interactions that account for the stability and specificity of this state. These domain closures often exclude water from the active site giving rise to a plausible argument for why numerous enzymatic reactions can take place in aqueous media without utilizing water as a nucleophile.[15] In addition to excluding water and providing the proper positioning of catalytic groups, the "closed" state confines substrates and prevents the escape of reaction intermediates. Gerstein *et al.* conclude that domain closure must be fast, that the energy barrier between the "open" and "closed" states must not be large, that these states are only slightly different in energy and that they are in dynamic equilibrium.[17] An important feature of this concept is that the alignment of the catalytic and binding groups are

optimized for the transition-state and that the attainment of this state is energetically unfavorable unless it is supplied with the energy of substrate binding. Figure 2.2.2 is a schematic illustration of the energy diagram for a single substrate, enzyme mediated reaction (enzyme assumed saturated with substrate). Proper substrate binding allows for the bound (closed) state (ES) to be in dynamic equilibrium with free substrate. Upon domain closure, catalytic reaction can occur to transform the bound state (ES) to an energetically less stable state than the open state of the protein by altering the interactions between the protein and the bound molecule.[17] Note that the upper limit on the rate of catalytic reaction should therefore be fixed by the rate of domain movements. Correlations between the time scales of enzyme movements and catalytic activities have been discussed for enzyme catalysis in low-water environments and show that decreased conformational flexibility yields lower activity.[18] Since the open state is more energetically favored, the product will desorb to return the enzyme to the open state.

As was advanced by Pauling,[19] enzymes accelerate reactions by lowering the activation barrier to the transition-state (see Figure 2.2.2). How this is accomplished involves a complex sequence of events as illustrated above. Upon initial reflection, it might be expected that evolution has selected to optimize enzymes for their bound (closed) state. However, the induced fit model leads to the conclusion that evolution has selected the protein that optimized both the open and closed states.[15]

Although the aforementioned description of enzymes is simplified for illustrative purposes, some of the essential ideas pertaining to catalysis have

been discussed. Thus, it is clear that an extremely complex set of events occur to allow enzyme catalysts to have high activity and selectivity. The question now arises as to how many of the basic principles of enzyme catalysis must be captured in the preparation of synthetic catalysts in order to achieve some form of enzymatic mimicking. Enzymes have been shown to accelerate rates to greater than 10^{17} over background.[20] Weisz has stated that for industrial practice, turnover frequencies of around 1 s^{-1} are sufficient.[21] In numerous cases, enzymatic turnover frequencies are many orders of magnitude higher than the Weisz criterion, *e.g.*, enzymatic turnover frequencies have an upper limit of ~10^7 s^{-1}. Thus, enzyme mimics may not have to reveal enzymatic rate accelerations in order to be practical catalysts. We believe that the critical feature of enzymatic catalysis that must be preserved is the selectivity at rates around the 1 s^{-1} limit. Additionally, synthetic catalysts must show high product yields and robustness (two features not common in most enzymes) for practical application. This is because it is expected that the cost of a "designed" enzyme mimicking catalyst would be high and its lifetime productivity must therefore justify its use. With these thoughts in mind, below are illustrated general classes of synthetic catalysts that attempt to mimic features of enzyme catalysis.

2.3   Catalytic Antibodies

Pauling first proposed about a half a century ago that a difference between enzymes and antibodies is that enzymes selectively bind transition-states of reactions while antibodies bind molecules in their ground state.[22] This paradigm led to the successful construction of catalytic antibodies.

Lerner and coworkers[23] and Schultz and colleagues[24] independently demonstrated that antibodies raised (templated) to stable transition-state analogues (TSA) have catalytic activity (see Figure 2.3.1). This enormous breakthrough in the rational design of catalytic materials relies on biological machinery for the production of the catalytic antibody. Reviews on the types of reactions catalyzed by catalytic antibodies are available.[25-29] Although catalytic antibodies show higher binding affinities for their transition-state analogues than reaction substrates (implying that they function by stabilizing the reaction transition-state), the differences in magnitude in the binding affinities are not sufficient to completely account for the observed rate accelerations.[27] Thus, the question arises of whether the catalytic antibody can in fact catalyze the reaction in a pathway similar to the uncatalyzed or enzyme catalyzed reactions. Hilvert and co-workers have addressed this issue.[30]

Catalytic antibodies that are capable of the unimolecular conversion of (-)-chorismate into prephenate with rate accelerations in the range of $10^2 - 10^4$ over uncatalyzed have been prepared using template **1**.[31-33]
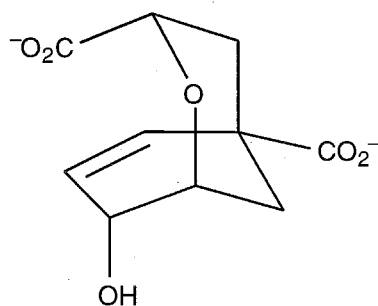
1

This reaction is also catalyzed by the enzyme chorismate mutase with an acceleration of greater than 2×10^6 over the uncatalyzed reaction. Thus, the designed (**1** is prepared to approximate the transition-state of the reaction as shown in Figure 2.3.2) catalytic antibody is about two to four orders of magnitude less active than the enzyme.[30] Haynes *et al.* solved the structure of a catalytic antibody with chorismate mutase activity when it was bound with **1**[30] and compared the structure to that of chorismate mutase bound **1**.[34] Schematic representations of the two bound complexes are shown in Figure 2.3.3.[30] The structural data reveal that both the enzyme and antibody provide environments complementary to a conformationally restricted transition-state analogue and strongly suggest (by inference) that they both catalyze the isomerization of chorismate by stabilizing the same transition-state that occurs in the uncatalyzed reaction.[30] Close inspection of the binding environments reveals combinations of hydrophobic, coulombic and hydrogen bonding interactions, *i.e.*, numerous non-covalent interactions are working in concert. There are 37 van der Waals contacts and three hydrogen bonds between **1** and the antibody[30] while the enzyme provides a greater number of hydrogen bonding interactions.[34] Haynes *et al.* speculate that these differences in specific interactions are likely to account for the lower activity of the antibody compared to the enzyme.[30] Thus, this work provides direct evidence that antibody catalysis can be reflected in the design of the transition-state analogue and that it can incorporate some features of enzyme catalysis. As has been cautioned above, there are clear examples where the rate accelerations of catalytic antibodies cannot be

completely attributable to templating alone. For example, Thorn *et al.* catalyzed the base-promoted reaction:
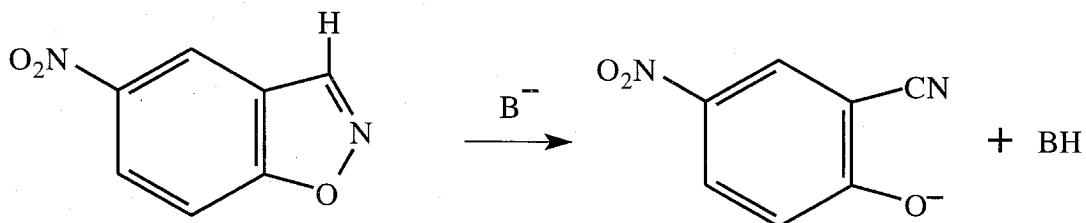
using a catalytic antibody that revealed a rate acceleration of greater than 10^8 over an acetate-promoted reaction rate.[35] However, rate acceleration of this order of magnitude can be achieved by conducting the acetate-promoted reaction in dry acetonitrile rather than water.[36] Thus, Thorn *et al.* were not able to separate the effects of individual factors such as the apolar nature of the antibody active site region (partitioning of substrate from aqueous media to "dry" active site; solvation of carboxylate active site more like dry acetonitrile than water) and the proper alignment of active site base (templating).[35]

The work of Hilvert and colleagues clearly demonstrates that the concepts currently employed in the preparation of catalytic antibodies can be successful in allowing the rational design of catalytic materials that do not appear to function too differently than enzymes. However, Stewart and Benkovic have recently placed limits on the expected behavior of catalytic antibodies.[37] First, Stewart and Benkovic state that the affinity of enzymes can reach values of 10^{-24} M while the best antibodies give 10^{-9} M. This difference in binding suggests that significant progress in the design of

catalytic antibodies needs to be made for their rate accelerations to match those of enzymes. However, as previously mentioned, this may not be necessary for the practical application of catalytic antibodies. Second, antibodies are elicited to a single specific structure while enzymes have evolved to bind a series of structures along the reaction pathway[37] (see previous discussion on open and closed states of enzymes and their evolution). Therefore, the structural dynamics of antibodies are not optimized for catalysis as are those of enzymes. These conclusions are intuitively obvious by considering biological applications of antibodies and enzymes.

The ultimate goal of the rational design of catalytic materials involves two principles: (*i*) that the atomic structure-reaction property relationships are known, and (*ii*) that synthetic methodologies to create defined atomic arrangements are available. For catalytic antibodies, point (*ii*) is possible via the use of biological machinery. For point (*i*), the structure-property relationships are not known but induced by the use of a transition-state analogue (TSA) as imprint. The degree to which the TSA actually approximates the true transition-state can have a large effect on the magnitude of the rate acceleration.[16] Also, dissimilarity of the TSA to the product is useful in minimizing product inhibition,[35] which may be particularly important for reactions that are not strongly exothermic, as discussed in the next section. In our opinion, catalytic antibodies are good demonstrations of the rational design of catalysts. Catalytic antibodies can be prepared to catalyze disfavored reactions[29] (see Fig. 3) and reactions that cannot be accomplished by enzymes (over 60 different reactions have been

catalyzed by antibodies including chiral conversions: see ref. 37 and references therein).

There is little doubt that catalytic antibodies will find applications in niche areas of fine chemicals synthesis and medical diagnoses. Several factors currently limit their use in other sectors of catalytic technology. For example, and as with enzymes, catalytic antibodies are not able to function in harsh physical, *e.g.*, high temperature, or chemical, *e.g.*, high or low pH environments. Also, to our knowledge, no report on the long-term stability of catalytic antibodies has appeared. Other issues such as the lifetime productivity (non-millimolar product concentrations; gram scale preparations of single enantiomers have now been reported[38]), the cost, and the sophistication and scale of antibody synthesis all currently limit their applicability for use in large-scale chemical synthesis. Despite these shortcomings, the invention of catalytic antibodies is a revolution in rational catalyst design. We note that from a practical standpoint, rational catalyst design must compete with combinatorial synthesis/selection methods for application. (The preparation of catalytic antibodies employs a rational design of the TSA and a selection method for obtaining the antibody.) For biologically-based synthetic methods/catalysts, it appears that combinatorial technologies show many advantages over pure, rational catalyst design in ultimately achieving the objective of preparing a catalyst for a particular reaction. However, for abiologically-based preparations/catalysts, combinatorial methods have thus far not revealed the same types of successes as shown in biological systems. Therefore, the question of post-synthetic selection (combinatorial methods) versus pre-synthetic

selection (design) is a question that will continually be asked and whose answer will continually change. Next, we discuss nanostructured abiological materials whose preparations have in many respects borrowed concepts from the field of catalytic antibodies in order to attempt to achieve the rational design of catalytic materials that overcome the aforementioned disadvantages of catalytic antibodies.

2.4 Imprinted Polymers

The imprinting of organic polymers represents a general strategy to endow randomly oriented, carbonaceous materials with a "memory" for a particular molecule. This "memory" is created by positioning functional groups of the polymer into a specific geometric arrangement that affords bonding interactions between the polymer and the imprint. This procedure is similar in principle to the early work of Dickey on imprinting silicas.[8,9] However, the advantage of polymer systems is that functional groups other than hydroxyl groups (the only functional group in silica) are available to provide interactions with the imprint. When imprinting polymers, several synthetic methods have been developed,[1,4,39] and new ones are continually being reported,[40] to design the positioning of the polymer functional groups for optimum imprinting efficiency. Early work in this area employed covalent re-binding interactions between the polymer framework and the adsorbing molecule.[1] That is to say, a side chain on the imprint was prepared such that it could be incorporated into the polymer backbone. More recently, non-covalent interactions, which are the method of choice in natural systems such as antibodies and enzymes, have generally gained preference for the

synthesis of imprinted solids because of the relative ease of preparation.[4,41] It is noteworthy that hydrogen bonding interactions have become particularly important in non-covalent polymer imprinting due to the specific geometric directionality associated with such bonds.[42] Because the molecular recognition characteristics of imprinted polymers are a direct consequence of their rigidly cross-linked surface structure,[1] applications of the imprinting method rely on the "lock-and-key" principle.[13] These applications include catalysis, which is accomplished by imprinting the polymer with a TSA in a fashion similar to that described for antibody catalysis. The critical component in optimizing imprinted polymers for a particular application is the design of the binding interactions between the imprint molecule and the polymer functional groups.

Imprinted polymers are typically copolymers prepared from two or more monomers. One of the monomers is used to create the inert "scaffolding" that provides mechanical support for the imprinted, nanoporous structure. The selection of these monomers is based on the ability to achieve high cross-link densities. An example of such a monomer is ethylene glycol dimethacrylate 2.
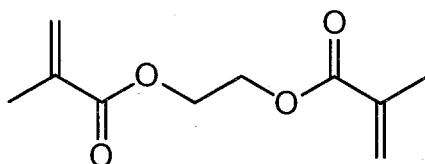
2

A second monomer is used in an imprinted polymer as the binding monomer and is selected based on its ability to form favorable binding interactions to the imprint molecule. Examples of binding monomers include methacrylic acid **3** for base-containing imprints and 4-vinylpyridine **4** for acid-containing imprints.
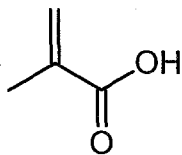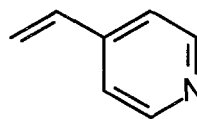
3   **4**

The binding monomer forms the interface between the bulk inert monomer and the imprint molecule as illustrated in Figure 2.4.1. A compilation of the different monomers that have been used in imprinted polymer synthesis can be found elsewhere.[4]

Two general methods of regulating the molecular-level positioning of the binding monomer have been reported for imprinted polymers utilizing non-covalent re-binding interactions: the controlled distance method and the self assembly method. The controlled distance method places the binding monomer in a predetermined geometric position relative to the imprint molecule and usually involves the synthesis of a molecule that is a composite of the imprint molecule and the binding monomer linked by covalent bonds.[40,44-46] Removal of the imprint by chemical reaction from the imprinted polymer leaves the residuals of the binding monomers in positions determined by the imprint molecule. The resulting nanopore has binding

monomers situated in predetermined conformations and distances from one another. An example of this type of preparation is illustrated in Figure 2.4.2. An advantage of this method includes limited binding to the imprint molecule by the solvent (and other non-specific binding molecules) in the monomer solution prior to polymerization. This advantage is manifested in the fact that imprinted polymers synthesized by the controlled distance method show only a very weak selectivity dependence on the solvent that is used in the polymerization.[1] This is in contrast to polymers synthesized by the self-assembly method (*vide infra*). However, considering the extremely sharp distance dependence of hydrogen bonding and van der Waals interactions,[47] it is not at all obvious that the controlled distance method affords any practical advantages in bringing about optimum binding configurations for maximum interaction between the binding monomer and the imprint over the self assembly method.

The self assembly method of imprinted polymer formation is schematically represented in Figure 2.4.3.[4,41] With this method, the binding monomer and imprint molecule are allowed to self assemble in the pre-polymerization mixture in a way that maximizes the binding interactions between the two species. After polymerization, the imprint is extracted from the polymerized material, leaving a nanopore that is supposedly selective to the binding of the imprint molecule (due to the complementary positioning of the binding monomers). The self assembly method suffers from a severe dependence on the specifics of the polymerization conditions such as the particular solvent and temperature.[43,48,49] Since no systematic comparisons of the controlled distance and self assembly methods for non-covalent polymer

imprinting have been reported to date, it is unclear at this time whether one method is really superior to the other.

The potential advantages of imprinted polymers over catalytic antibodies for practical applications are straightforward to envision. Imprinted polymers are relatively simple to prepare and can be formed rapidly (2-3 days) in large scale. They also show good mechanical, chemical, and thermal stability, due to their highly cross-linked nature. Additionally, imprinted polymers can be re-used over one-hundred times and stored in the dry state at ambient temperatures for several years without loss of recognition capabilities.[41] In addition, the potential to reuse the polymers time and time again without loss of molecular recognition capability may be of value.[41]

Despite the apparent advantages of imprinted polymers over biologically produced materials, significant work remains before imprinted polymers approach the selectivity and catalytic efficiency of their antibody counterparts. This is illustrated below. Imprinted polymers have been prepared for use as chiral separation media and this area has been reviewed elsewhere.[4] Most enantiomeric separations have selectivities less than 10 with imprinted polymers. This represents an approximate binding energy difference of 1.4 kcal/mol at room temperature, which is significantly less than the average energy of a single hydrogen bond.[42] This apparent paradox can be explained by the fact that imprinted polymers are comprised of a few selective sites (that can sometimes rival the molecular recognition capabilities of antibodies[50]), and a vast majority of relatively non-selective sites. The site heterogeneity present in an imprinted polymer has been investigated by FTIR and ^{13}C CP/MAS NMR experiments.[51] Dynamic

binding experiments were performed on a two-site imprinted polymer that covalently bound a diketone molecule to the polymer with the release of up to two water molecules (shown in Figure 2.4.4). Results from this investigation suggest that nanopores in the imprinted polymer consist of a combination of one point and two point binding sites. Upon rebinding the diketone to the polymer with initially vacant nanopores (shown in Figure 2.4.4b), the percentage of overall binding sites occupied that were two point binding sites continuously decreased with binding time, exemplifying the heterogeneous nature of the imprinted polymer surface. Note that some of the nanopores that comprised one point binding sites could be converted to two point binding sites by performing a Soxhlet extraction of water immediately following rebinding.[51] This result suggests that the water molecule released during the binding of the first ketone group of the imprint molecule may non-covalently bind to the second ketone group of the imprint molecule and thereby impede the covalent binding of the second ketone group to the polymer framework in the same nanopore. It is apparent, however, that factors other than water contamination may be responsible for the existence of the one point binding sites observed in this particular system, since the imprinted polymer still possessed both one and two point binding sites even after the water extraction procedure. A further manifestation of the existence of heterogeneous binding sites can be found in the work of Sellergren and colleagues on non-covalently imprinted polymers.[43,48,49,52] This group investigated polymers that were imprinted with amino acid amide derivatives using both equilibrium batch and kinetic chromatographic binding experiments. These two methods consistently

gave the same picture of the imprinted polymer surface as one that contains very few selective sites and a vast majority of non-selective sites. Typical values for the percentage of sites that were found to be non-selective are on the order of 99.8% of the total number of possible binding sites based on the amount of imprint originally extracted from the polymer.[48] The heterogeneous nature of the binding sites in imprinted polymers highlights the cause of the main limitation of imprinted polymers for molecular recognition: few selective sites are available for binding and catalysis with the majority of the binding sites offering relatively poor selectivity. The existence of non-selective sites is a fundamental difference between imprinted polymers and enzymes and antibodies.[53]

Comparisons of the binding specificity found in antibodies and imprinted polymers have been reviewed elsewhere.[54] Vlatakis *et al.* investigated the binding of the drugs theophylline and diazepam on imprinted polymers synthesized by the self assembly method.[55] Both the theophylline and diazepam imprinted polymers performed favorably in their selective rebinding of the imprint drug over various other compounds and in some cases revealed higher selectivities than natural antibodies. However, the inherent heterogeneous nature of the imprinted polymer surface was apparent in this study by the fact that a three-site binding model was necessary to numerically fit the experimentally-measured adsorption isotherm for the case of diazepam (a two-site binding model was necessary for theophylline). Furthermore, the most selective sites on the diazepam imprinted polymer, which had binding constants in the nanomolar regime, comprised only 0.45% of the total binding sites, while the remaining sites

had binding constants in the micromolar regime. These results are graphically summarized in Figure 2.4.5 for the diazepam and theophylline imprinted polymers. Other investigations comparing imprinted polymer performance to antibodies have been completed with similar results concerning the heterogeneous population of sites in the polymer.[50] The main limitation of the imprinted polymers in these investigations is that the sites have varying degrees of affinity for the imprint molecule. We note that no known studies have yet been performed that compare the relative magnitude of the binding constant of an antibody to that obtained with an imprinted polymer for the same compound and under the same conditions.

Imprinted polymers have been used to catalyze various organic chemical reactions. The strategy used with imprinted polymer catalysts is to stabilize the transition-state for a particular reaction, thus lowering the activation energy barrier for reaching the transition-state and thereby increasing the rate of reaction.[56,57] Therefore, the use of a TSA imprint is employed in analogy to catalytic antibodies. Of importance to understanding the reactivity is the fact that the TSA molecules are rigidly held in a particular conformation in the polymer and that the lack of conformational flexibility of the polymer does not allow for an "induced fit" as with enzyme catalysis. Thus, product inhibition can be a significant problem in the catalytic applications of imprinted polymers (and imprinted amorphous metal oxides, which are discussed in the next section). If the product is structurally too similar to the transition-state that is being stabilized by the imprinted material, it will be difficult to desorb it from the polymer framework once turnover has been achieved. It would be useful to be able to predict *a priori*

the reactions that are most likely to proceed on an imprinted polymer catalyst. We believe that the Hammond postulate most likely can provide some useful information in this regard. This postulate states that for an exothermic reaction, the transition-state resembles the reactants, and for an endothermic process, it resembles the the products.[58] It is therefore conceivable that exothermic reactions will avoid product inhibition to a greater degree than endothermic ones for a rigid catalyst, with the degree of exothermicity representing the degree to which product inhibition is avoided as schematically represented in Figure 2.4.6. It is anticipated that this will be true of catalytic antibody systems[35] and especially true of rigid catalytic systems such as imprinted polymers and silicas, which are highly cross-linked. Reactions performed with imprinted polymer catalysts are given in Tables 2.4.1 and 2.4.2, and in Table 2.4.2 our calculated standard enthalpies of reaction for selected reactions conducted on imprinted solids and antibodies using *ab initio* methods[59] are presented. Most of the reactions performed on imprinted polymers, antibodies, and imprinted silicas that are listed in Table 2.4.2 are indeed exothermic, including those that are difficult to accomplish by alternative techniques.[60,61]

A general history of catalysis with imprinted polymers can be found elsewhere.[1,2,39] Here, we discuss a few specific examples to illustrate points of concern when using imprinted polymer catalysts. The esterolysis of *p*-nitrophenyl acetate (Reaction **F** in Table 2.4.2 and below) by imprinted polymer catalysts has been investigated by several research groups.[62-65]

5
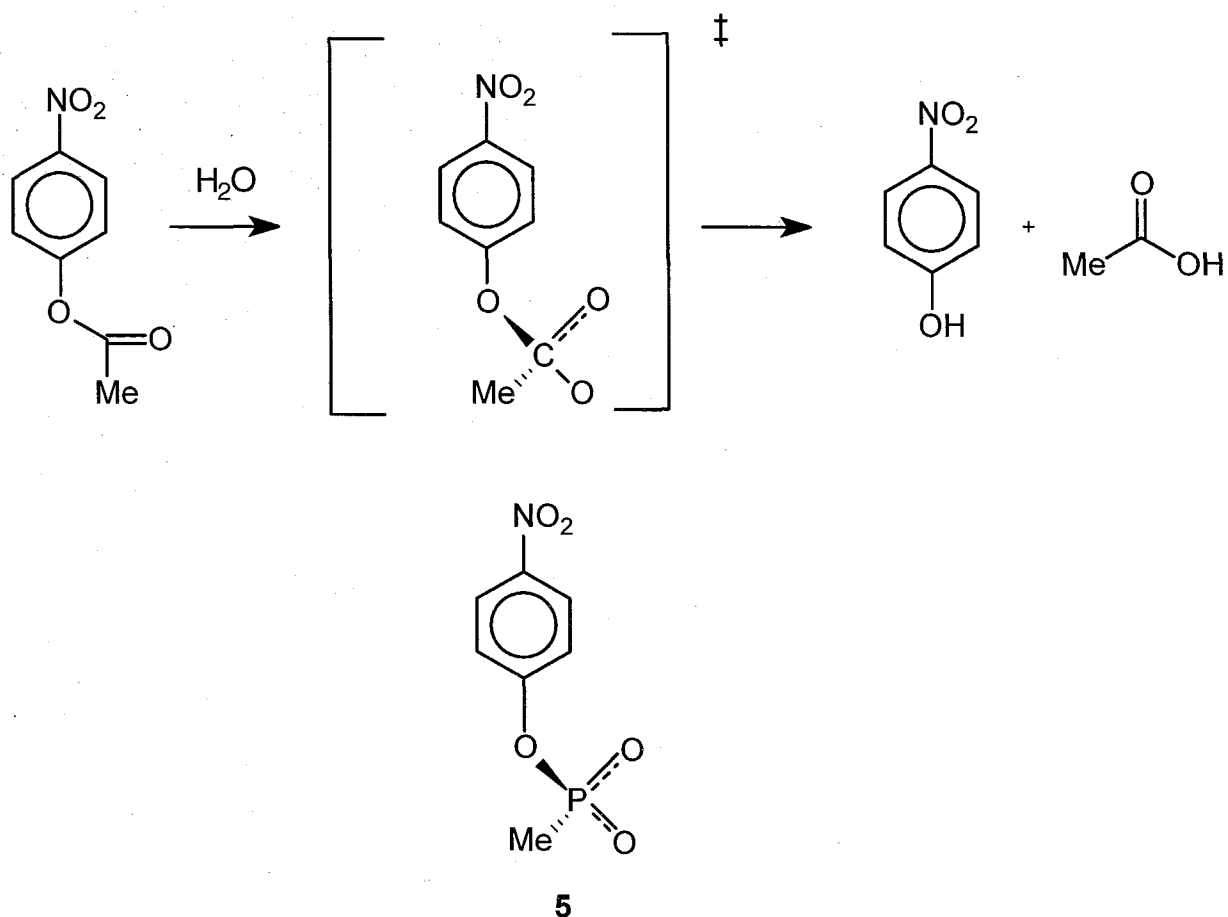
Robinson and Mosbach used an organophosphorous TSA **5** to imprint the polymer.[63] This imprint is used to mimic the transition-state geometry of the reactant carbonyl carbon by providing a tetrahedral arrangement within the TSA by the use of phosphorus. The catalytic results from this imprinted polymer show only a mild rate enhancement that is approximately a factor of 1.6 larger than a non-imprinted reference polymer for 10% methanol in water (pH 8.0).[63] Ohkubo *et al.* used *ab initio* methods to verify the correspondence in bond lengths and angles between the organophosphorous TSA **6** and the transition-state for the same reaction.[64]
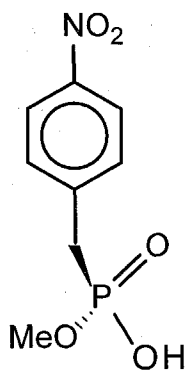
6

On imprinting TSA **6** with a polymeric system that was similar to the one used by Robinson and Mosbach, Ohkubo *et al.* reported a rate acceleration of up to 6.7 times greater than that for the uncatalyzed reaction for 10% methylsulfoxide in water (pH 7.0). For comparison, a homogeneous catalyst comprised of an imidazole-bisresorcinol derivative was reported to increase the relative rate of *p*-nitrophenyl acetate esterolysis by a factor of approximately 16 over the uncatalyzed reaction for 10% acetonitrile in water (pH 8.2).[67] Ohkubo *et al.* also calculated the activation enthalpy, entropy and free energy for the imprinted polymer-catalyzed reaction and the uncatalyzed reaction. However, it is not clear to us what method was used to calculate these thermodynamic state functions. The calculations show that the imprinted polymer stabilized the free energy of the reaction transition-state by only 0.3 kcal/mol over that of the uncatalyzed reaction.[64] This corresponds to a relative rate increase of about 1.6 over the uncatalyzed reaction,[56,57] which is significantly less than the experimentally measured value of 6.7 discussed above. We note that calculations of the activation free energy in a separate system also lead to similar

inconsistencies.[68] (Also refer to Reaction **G** in Table 2.4.2). We note that similar mild rate enhancements have been observed in other imprinted polymer-catalyzed reactions, and this trait that appears to be common amongst imprinted polymer catalysts reported to-date.[66,68]

The dehydrofluorination of 4-fluoro-4-(*p*-nitrophenyl)butan-2-one (Reaction **D** in Table 2.4.2 and below) has been conducted with both imprinted polymers and antibody catalysts.[69-71]

7
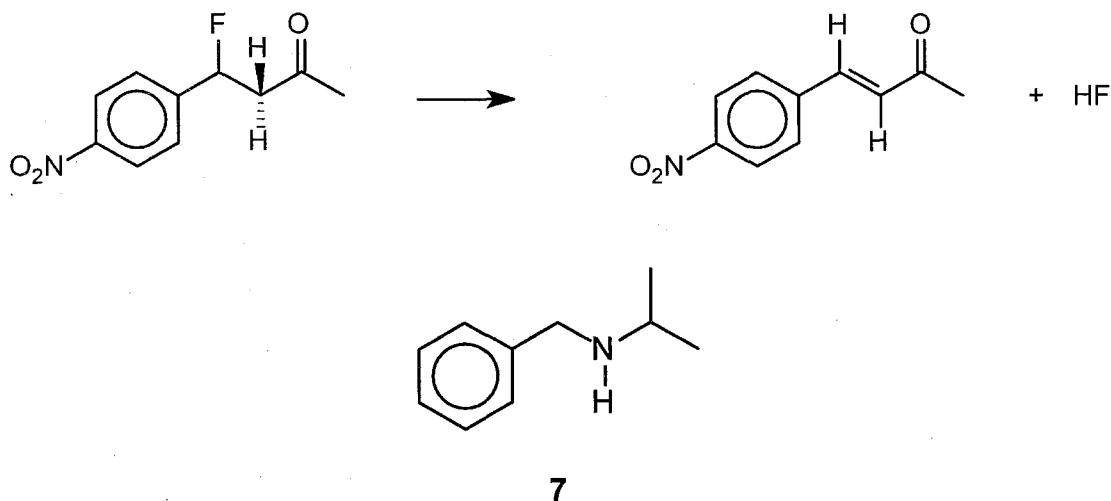
Müller *et al.* prepared an imprinted polymer in acetonitrile with N-benzylisopropylamine **7** as the transition-state analogue.[69] These workers used the TSA **7** to prepare the catalyst as schematically illustrated in Figure 2.4.7. The secondary amine of the TSA probably interacts via a single point binding with the carboxylic acid group of the binding monomer. This procedure supposedly creates a nanopore with a strategically placed carboxylic acid group that is capable of acid catalyzing the elimination reaction. Despite the apparent simplicity of this one-point binding approach,

a factor of 2.4 in the relative rate constant (imprinted polymer rate constant divided by non-imprinted polymer rate constant) was reported between the imprinted and non-imprinted polymers when conducting the elimination reaction in acetonitrile solvent. However, even though the reaction is exothermic (see Table 2.4.2), Müller *et al.* report that product inhibition appears to be a significant problem when conducting the reaction in an aqueous environment, supposedly since both reactant and product adsorbed strongly in a non-specific manner to the hydrophobic polymer surface. The lack of common solvent between the Müller *et al.* system and the catalytic antibody system[71] which was conducted in an aqueous solvent environment, prohibits a direct comparison of the two cases (it is not possible to separate the independent effects of different catalytic approaches and different solvent environments).

A more sophisticated approach to imprinting a polymer catalyst for the elimination reaction involved a two-point binding site.[70] Benzylmalonic acid **8** was used as the TSA to supposedly position amine functionalities of two binding monomers in each nanopore as schematically illustrated in Figure 2.4.8.
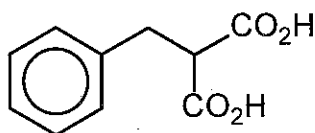
8

The concept is that one of the two binding monomers is used to anchor the reactant into the nanopore via the carboxylic oxygen, and the other to bring

about the base catalyzed elimination reaction by providing a basic environment near the α-hydrogen. Note that this approach of providing two binding sites per nanopore increased the relative rate constant by a factor of 1.46 over the Müller *et al.* one-point binding site approach. Product inhibition similar to that observed by Müller *et al.* may also have been present in the two-point binding site, since the effect of the imprinted catalysis declined for polar solvents, as shown by the data provided in Table 2.4.3. Comparison of the Beach and Shea results with those from a catalytic antibody on the same reaction demonstrate that the rate constant observed in the case of imprinted polymers is significantly lower than that reported for the antibodies.[71] The results of this comparison are summarized in Table 2.4.4, where it is shown that the catalytic antibody reveals a Michaelis-Menten binding constant of at least 148 times less and a relative rate constant (see Table 2.4.4 for definition) of 198 times larger than the Beach and Shea imprinted polymer.

As with the Müller *et al.* system, we note that a direct comparison of the antibody and imprinted polymer systems is not warranted in this case, since the imprinted polymer catalysis was conducted in benzene. It is expected, however, that the catalytic antibody binding (and corresponding transition-state stabilization) was significantly more specific than for the imprinted polymer, since the antibody did not show product inhibition of the reaction in an aqueous environment as did both imprinted polymer systems. Additionally, the antibody reactivity was completely inhibited by the addition of free hapten, which suggests that the antibody rate accelerations were indeed due to the specific binding afforded by the antibody.[71] Similar types

of inhibition experiments with the Beach and Shea imprinted polymer were less conclusive about the role of the imprinted nanopores in the observed catalysis. Upon contacting the imprinted polymer with a five-fold excess of diethyl benzylmalonate **9**, the rate of dehydrofluorination dropped only 16%.[70]

$$C_2H_5\text{---}O \overset{O}{\underset{\underset{C_6H_5}{\overset{H}{\underset{|}{H\text{---}C\text{---}H}}}}{\|}} \overset{H}{\underset{}{C}} \overset{O}{\|} O\text{---}C_2H_5$$
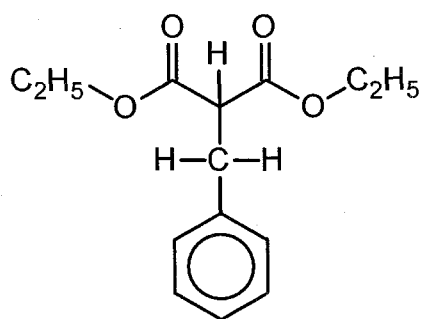
9

This small decrease in reaction rate on binding site inhibition raises serious questions as to the nature of the catalytically active sites in the Beach and Shea imprinted polymer. Binding inhibition of the catalytically active sites is not in general a problem with imprinted polymer catalysts, as inhibition experiments on other imprinted polymer systems have shown to fully suppress catalytic turnover.[62,65]

There have also been attempts to impart reaction stereoselectivity with imprinted polymer catalysis. Early studies by Damen and Neckers showed that it is possible to affect the stereochemical direction of the photochemical dimerization of *trans*-cinnamate esters using polymers imprinted with α-truxillic, β-truxinic and δ-truxinic acids (see Figure 2.4.9).[72] A sample of

the catalytic results of Damen and Neckers is shown in Table 2.4.5. Note that dimerization of *trans*-cinnamate esters bound to a non-imprinted polymer exclusively formed α-truxillic acid.[72] It does appear that some stereoselectivity is obtained with β and δ truxinic acid-imprinted polymer catalysts. More recently, Wulff and Vietmeier obtained a 36% enantiomeric excess for a threonine and allothreonine producing reaction.[73] One of the most impressive examples of imprinted polymer catalysis to date is the selective reduction of steroid 3- and 17- (Reaction **H** in Table 2.4.2) ketones with LiAlH$_4$ by Byström *et al*.[74] In this example, polymer imprinting was used to selectively place a reactive LiAlH$_4$ group into a nanopore that had the shape of the steroid ketone reactant molecule. The regio- and stereo-selectivity of the resulting reduced products could then be controlled to a remarkably high degree, in some cases showing a complete preference for the reduction along the imprinted pathway. Most recently, Sellergren and Shea produced imprinted polymers that were capable of enantioselective ester hydrolysis (Reaction **I** in Table 2.4.2).[75] The relative rates of enantiomer production differed by up to a factor of 1.85, thus giving an enantiomeric excess of almost 30%. Note that an antibody catalyst has been reported to conduct a similar amide hydrolysis reaction enantiospecifically.[76]

As described above, there has been a considerable amount of work that attempts to endow imprinted polymers with the binding selectivity of antibodies. In certain cases, the binding selectivity of the imprinted polymer sites approaches that of the antibody. However, for most cases, these selective sites are few and accompanied by a large excess of poorly

selective sites. We believe that the fundamental problem in imprinted polymer catalysis is the control of the binding site heterogeneity and this remains as the significant challenge of the future. Several questions that need to be addressed in this regard include what is the driving force for heterogeneous surface formation in these materials, and how can this driving force be controlled to give the desired binding site selectivity for a given application? Secondary issues also arise from the existence of site heterogeneity on imprinted polymers. For example, it is not at all clear what the rigorous interpretation of a Lineweaver-Burk plot is for such a truly heterogeneous system. Perhaps calculated values for the kinetic and binding parameters represent average values; correct implementation of the Michaelis-Menten analysis should be limited to a homogeneous surface such as provided by monoclonal antibodies or enzymes.[16]

Next, we discuss another class of amorphous materials for which imprinting has been employed to create catalytic materials, *i.e.*, amorphous silica-based catalysts. The imprinting methods are similar to those described above for polymers and the issues raised previously concerning the polymer-based catalysts must also be addressed with amorphous silica-based catalysts.

2.5 Imprinted Amorphous Metal Oxides

Since the pioneering work of Dickey,[8,9] different oxides, such as silicas and mixed metal oxides have been imprinted in attempts to prepare adsorbents, separation media and catalysts. To date, amorphous metal oxides have not revealed the same level of success as imprinted polymers

for separation and catalytic applications. However, there are difficulties associated with using polymers as discussed above. In addition, the thermal stability of polymeric systems limits the method of imprint removal to liquid-liquid extraction, which inevitably leaves a small amount of residual imprint in the polymer matrix.[43] The remaining imprint creates uncertainty regarding the mechanism of molecular recognition in the resulting imprinted material. For example, it has been argued that a recrystallization mechanism may be partially responsible for the observed imprinting effect in binding experiments.[9,79,80] On the other hand, with metal oxides, the imprint can be removed virtually completely by harsher techniques such as combustion with dioxygen. Finally, polymers are unsuitable for use in severe industrial environments such as high temperatures and pressures and reactive organic solvents. The use of metal oxides such as silica can overcome these difficulties while expanding the range of materials available for imprinted molecular recognition sites and ultimately selective catalysis.

Wulff and coworkers investigated the binding capabilities of imprinted silicas by using the controlled distance method that was described in the previous section.[45,46] Aryl bridged cyano compounds **10** and **11** were used to produce positioned amine binding sites by first attaching these species with dimethylmethoxysilane moieties to a silica surface. The bridging groups were subsequently cleaved leaving behind silica bound amino groups at well-defined positions and distances from each other (see Figure 2.5.1). The surface was then treated with hexamethyldisilazane to minimize non-selective interactions. The binding affinities of the corresponding dialdehydes **12** and **13** were measured.

10

11

12

13
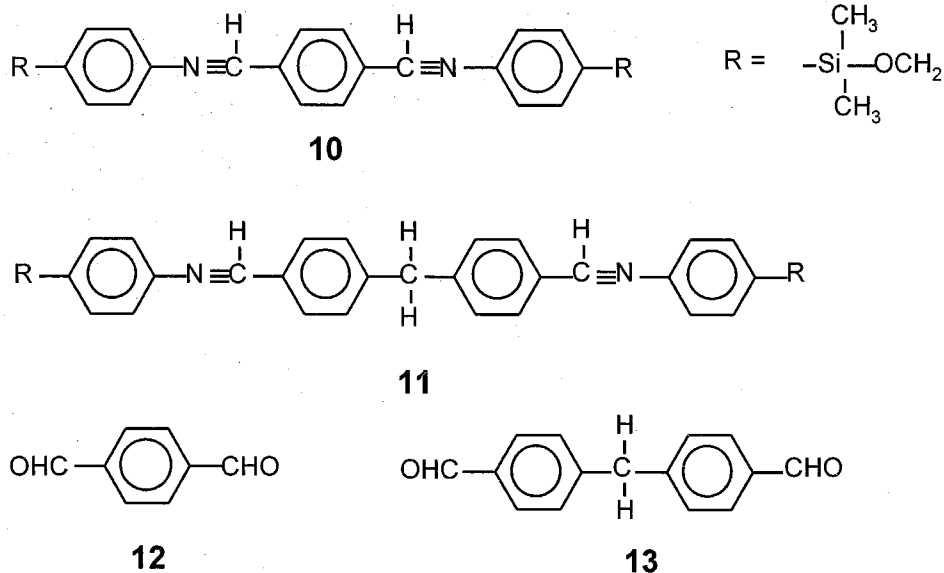
The binding selectivities shown in Table 2.5.1 suggest that a slightly preferential binding is possible from the imprinted silica surface. Although the effects are not large, this investigation is the first report of controlled distance binding of an imprint to a silica substrate. Like all previous work on imprinted metal oxides, these studies were limited to investigations involving adsorption alone.

The first example of an imprinted silica used to catalyze a reaction was reported by Morihara and coworkers.[81] Modification of silica by isomorphic substitution of Al^{3+} ions into the silicate matrix was used to generate Lewis acid sites. Morihara and coworkers imprinted an aluminated silica with a TSA for the butanolysis of benzoic anhydride that contained a Lewis base to preferentially bind to the Al^{3+} active sites. After aging the gel, the imprint was removed by Soxhlet extraction to supposedly leave behind cavities that are able to catalyze the butanolysis of benzoic anhydride (Reaction **J** in Table 2.4.2). This work was aptly termed "footprint catalysis." Morihara's group

has since published a series of papers on the subject covering several different reactions. In addition to basic kinetic studies, investigations into competitive inhibition and limited analysis of the active site affinities have also been reported.[81-86]

An illustrative example of a "footprint" catalyzed reaction is the 2,4 dinitrophenolysis of benzoic anhydride (Reaction **K** in Table 2.4.2 and below). The reaction was accomplished using catalysts that were imprinted with the TSAs **13**,[83] **14** and **15**.[85] A selection of reactivity results are shown in Table 2.5.2. With imprints **13** and **14**, the relative Michaelis-Menten constant, K_m, decreases over the control material (indicating improved binding) as does the reaction rate constant k_{cat}. A different trend is observed with TSA **15** that contains a tetrahedral phosphorous group. For **15**, the relative binding affinity increases by an order of magnitude and the reaction rate constant increases as well.
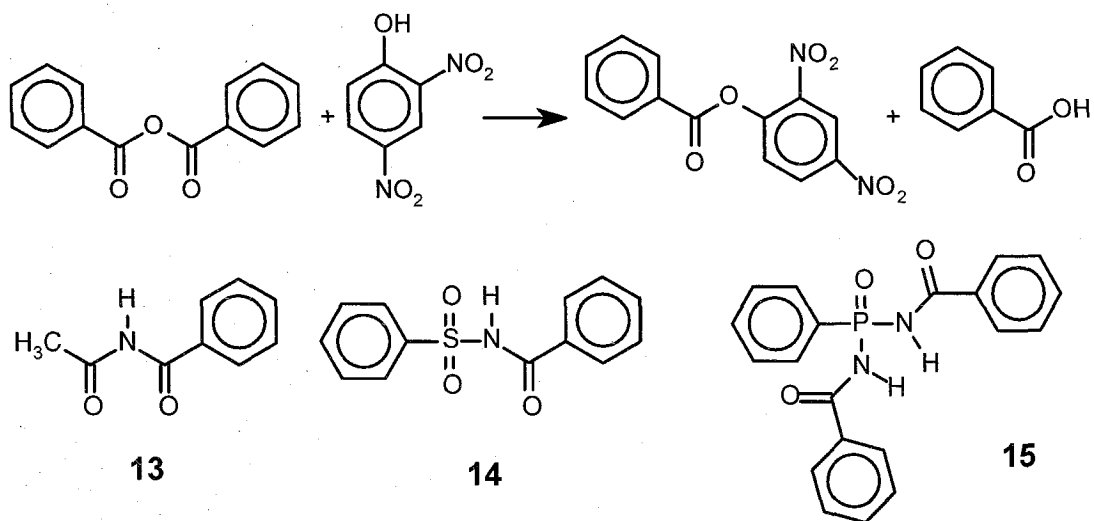
This suggests that the design of the TSA requires more than just a simple gross structural match between the transition-state and its analogue, since all of the imprints are structurally similar. We investigated these results further by assessing the Lewis basicity of the imprints using molecular mechanics calculations.[59] (Recall that the footprints are formed by preferential binding of a Lewis base to the Al^{3+} sites during the imprinting process.) The results of this molecular mechanics calculation, which are shown in the last column of Table 2.5.2, demonstrate that TSA **15** contains the strongest Lewis base and hence is more likely to produce a stronger interaction, *i.e.*, an imprint site, than TSAs **13** and **14**. This observation may explain the enhanced substrate specificity observed with this compound. Morihara and coworkers also report inhibition of the reaction on addition of the corresponding TSAs; however, turnover is never suppressed completely in these inhibition studies so only a limited conclusion about the activity of the imprinted sites can be drawn.

In a demonstration of chiral recognition, Morihara and coworkers imprinted, N-benzoyl-(N^a-benzyloxycarbonyl)-L-alaninamide **16** onto an Al^{3+} doped silica gel[87] (see Figure 2.5.2). This imprinted catalyst was used to catalyze the reaction involving the enantioselective 2,4-dinitrophenolysis of N-benzyloxycarbonyl-L-alanine anhydride **17** (Reaction **L** in Table 2.4.2 and below).
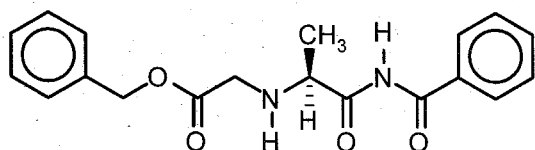
16
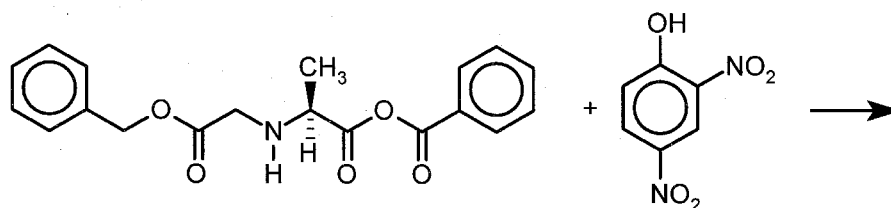
17
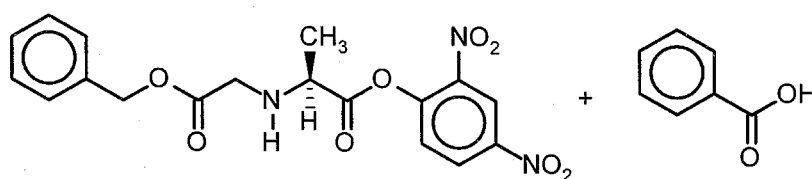
Kinetic resolution was reported. The enantioselectivity was explained by a productive and non-productive binding mechanism as illustrated in Figure 2.5.2.[88,89] Chiral imprint **16** produces 3 subsites in the aluminated silica substrate corresponding to residues of the alanine substructure. Productive binding is speculated to occur only with the L-enantiomer that places **17** in a favorable conformation on the acid site of the silica for nucleophilic attack by the dinitrophenoxide. The D-enantiomer cannot undergo the same reaction since it is sterically hindered by the methyl group.

Although Morihara and his group have achieved some success in imprinting amorphous oxides for catalysis, several significant limitations remain that need to be overcome in order to achieve the efficacy of catalytic

antibodies. The most significant problems that need to be addressed are the low enhancements of catalytic activity, poor selectivity and long term stability. This could be largely due to the heterogeneity of the catalytic sites. Moreover, the aluminum dopant used is itself a catalytically active site for these reactions. Thus, it is unclear as to what fraction of the catalysis is indeed attributable to the imprinted sites in the silica. Further characterization of the active sites is therefore necessary to address this issue. It should also be pointed out that many of the "footprint" catalyzed reactions release organic acids, and these may provide for autocatalysis. This underscores the need for additional control experiments. In view of the Hammond postulate discussed in the previous section, we believe that the low reported activities may be largely attributable to product inhibition due to the endothermicity of Reactions **K** and **L** (listed in Table 2.4.2).

Using a different approach, Heilmann and Maier recently reported a selective silica catalyst for the transesterification of ethyl phenylacetate to hexyl phenylacetate[90] (Reaction **M** in Table 2.4.2). This reaction normally occurs only with measurable rates in the presence of acid or base catalysts. A possible transition-state for the acid catalyzed reaction **18** was used in designing **19** as a TSA. The copolymerizable triethoxysiloxy moiety on **1 9** was employed to chemically bind the TSA into the silica gel during an acid catalyzed sol-gel process with a 100-fold molar excess of the monomer $Si(OEt)_4$ (similar to the self assembly method described previously for imprinted polymer synthesis). Heilmann and Maier remove the TSA by combustion in air to supposedly leave behind a silica based solid with well-defined three-dimensional cavities (supposedly, phosphorous remains on

the silica and is the active site for the catalysis). They claim that since the TSA is covalently attached to the silica prior to calcination, this imprinting procedure is more robust than the approach of Morihara et al.[81-87] Heilmann and Maier observed that the transesterification reaction was catalyzed by the imprinted solid and as a test for the selectivity of the imprinted site, the rates of transesterification of ethyl napthylacetate vs. ethyl phenylacetate were investigated. No reaction was reported when using the napthyl compound. They also reported that the catalyst was able to discriminate between hexyl and phenyl alcohols for the transesterification reaction. The success of their catalyst was attributed to three-dimensional imprinted cavities containing acid sites.[90]

18

19
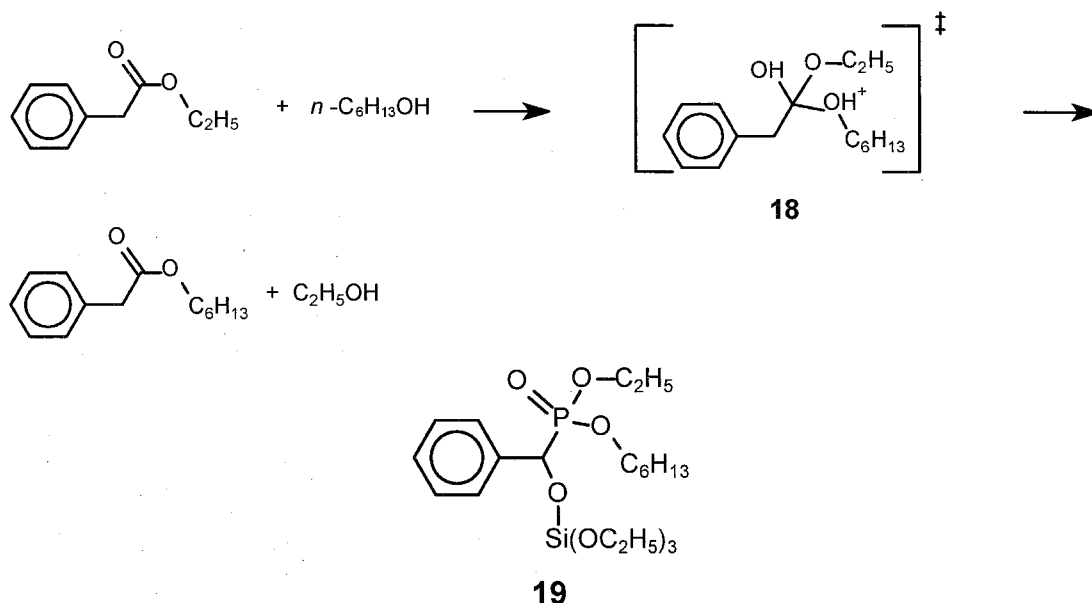
The promising results of Heilmann and Maier motivated us to further investigate this system.[91] We observed comparable rate enhancements for both the napthyl and phenyl esters and no inhibition of the reaction using the

selective inhibitor **20**. In our investigation, we were unable to find evidence for molecular recognition and catalysis from an imprinted site.
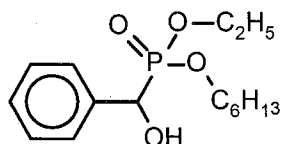
20

In a report of an antibody-catalyzed unimolecular reaction, Benkovic and coworkers elicited a monoclonal antibody against the stable TSA **21** (*cf.* **22a**) of an intramolecular six-membered ring cyclization reaction that was capable of stereospecific catalysis.[92] A single enantiomer of d-lactone **23a** from a racemic mixture of d-hydroxyester **24a** was formed with an 167-fold rate acceleration to give an enantiomeric excess of 94% (analogous to Reaction **E** in Table 2.4.2). Inhibition of the catalyzed reaction was observed to occur linearly with addition of the **21**. Motivated by these significant results, Heilmann and Maier followed an analogous procedure to that described above for the transesterification reaction to prepare an imprinted silica catalyst for the achiral intramolecular lactonization reaction of **24b** to **23b**. Heilmann and Maier used the TSA **25** to imprint the silica[93] (*cf.* **22b** and Reaction **E** in Table 2.4.2). The catalyst reportedly accelerated the intramolecular lactonization; however, control experiments revealed that the enhancement in activity was not attributable to the imprinted cavity.

24 (a) R=Z or (b) R=H

22 (a) R=Z or (b) R=H

23 (a) R=Z or (b) R=H

where Z =

21

25
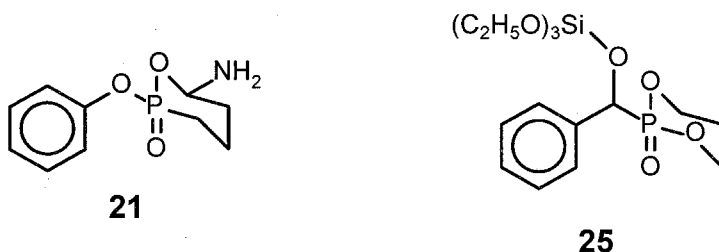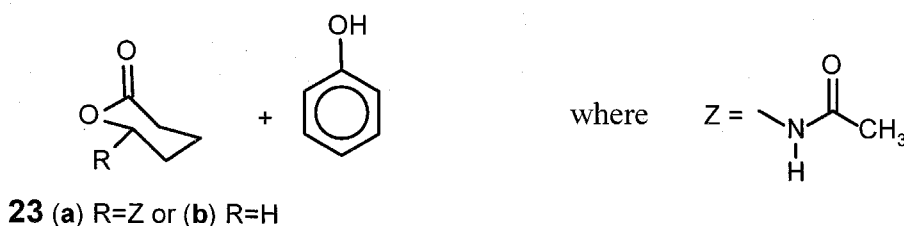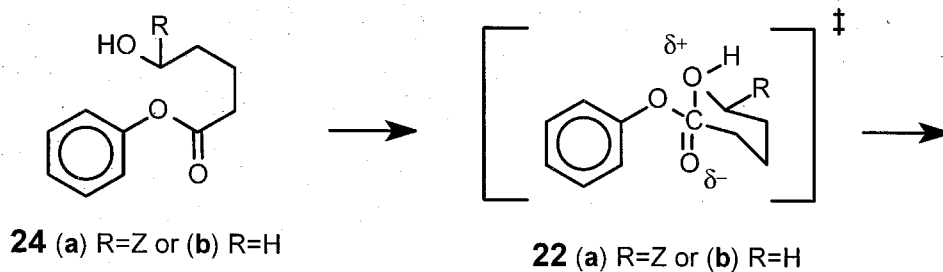
Like the imprinted polymers, imprinted amorphous metal oxides have shown some indication of catalysis that can be attributed to the imprinting process. However, it appears that site heterogeneities are prevalent and limit reaction selectivities. Next, we discuss crystalline metal oxides that have significantly less site heterogeneity than either polymers or amorphous metal oxides.

2.6 Zeolites

Zeolites are *crystalline* aluminosilicates that have pore sizes in the range of 2-10Å. Because these metal oxide materials are not amorphous, they can have very uniform pore size distributions that are fixed by the atomic

arrangements of their unit cells (repeat unit of the crystal). The existence of non-varying pore diameters that are in the size range of small molecules endows zeolites with extraordinary molecular discrimination abilities. For example, zeolite A can adsorb linear paraffins while rejecting branched hydrocarbons, e.g., n-butane vs. isobutane. The difference in kinetic diameter between the two butane isomers is 0.3 Å. Thus, zeolites have been called molecular sieves for obvious reasons. A brief review of zeolites can be found elsewhere.[94]

There is a close connection between the nanometer scale structure and the macroscopic properties of zeolite catalysts. Venuto has recently provided an exhaustive review (579 references) on the catalysis of organic molecules over zeolite catalysts.[95] Thus, it is obvious that we cannot provide an overview of all catalysis over zeolites because the field is so large; here we will limit our discussions to those issues relevant to the theme of this review. In general, the continuing commercial successes of zeolite catalysts are largely due to the constant discovery of new materials that enables process improvements and the development of new technologies. The ability to control the zeolite properties through synthetic efforts is and will continue to be of great importance. At present, the control of zeolite properties mainly involves molecular level manipulations of structural features, e.g., pore size and location of active sites.[96] That is to say, the chemical and/or electronic nature of the catalytically active site is not

normally controlled. Rather, the three-dimensional structure surrounding the active site is fabricated.[97] In the 1970's and 1980's, "catalyst design" with solid materials normally implied the manipulation of the porous solid material to affect the mass and energy transport properties of the catalyst (length scales of 10^{-2}-10^{-8} m). Today, with zeolite catalysts, "design" implies manipulation at the nm to Å length scale and involves the complementarity between the active site and reactant/product geometries.[97]

Zeolite catalysis has centered around shape-selective, acid-mediated reactions. Zeolites are anionic oxide structures that require cations for maintaining electrical neutrality (the amount of the anionic sites are on the order of meq./g zeolite). If the balancing cation is proton, then the zeolite can function as a solid acid catalyst. Since these sites are contained within the pore space of the zeolite crystal, access to these catalytic sites is through the sub-nanometer sized pores. This is why zeolites can perform shape-selective catalysis. The primary forms of shape-selective catalysis are illustrated in Figure 2.6.1 and are reactant, product and transition-state selectivity.[98] For a short review on primary and secondary shape-selective catalysis with zeolites see ref. 102. Here, it is sufficient to illustrate only primary shape-selective catalysis. Reactant and product shape-selectivity involve molecular discrimination between reactant and product molecules, respectively. There are numerous examples of reactant shape-selectivity and this type of catalysis is easy to recognize and test for, *i.e.*, by measuring

the catalytic activity for a series of reactants of varying size. Product shape-selectivity can be observed and the most studied example is the synthesis of near pure p-xylene from toluene over ZSM-5-based catalysts. With product shape-selectivity, several products are formed within the zeolite pore space and are able to convert into each other. At least one of the products has a smaller kinetic diameter than the others and therefore it diffuses through the zeolite pores at a higher rate than the other products. As the fast diffusing species moves out of the zeolite crystals, the other compounds convert to this species (thus allowing the catalysis to continue; if interconversion were not possible then the larger molecules would clog the zeolite pore space). A good test for the existence of product shape-selectivity is to monitor the product distribution as a function of increasing the zeolite crystal size; the larger the crystal the greater the selectivity to the faster diffusing species.

To date, proven examples of transition-state shape-selectivity are rare. The example illustrated in Figure 2.6.1 shows that the cyclization of dienes can take place in the zeolite mordenite while no reaction occurs in ZSM-5 even though there are active sites available to perform the reaction. This is due to a lack of sufficient pore space to form the transition-state since cyclopentadiene will adsorb into the pores of ZSM-5. Often times the lack of a particular product, e.g., one of the trimethylbenzenes in the disproportionation of m-xylene, is construed as evidence for transition-state

shape-selectivity. However, selectivities of this type can result from product shape-selectivity as well. Thus, one test to distinguish between transition-state and product shape-selectivity is to observe the product distribution as the crystal size is varied; there should be no variation in the product composition if transition-state shape-selectivity is the controlling process while such is not the case with product-shape selectivity. In conclusion, significant progress has been made in rationally developing zeolite catalysts that function via reactant shape-selectivity and to some extent with product shape-selectivity. However, very little work has concentrated on the purposeful use of transition-state selectivity.

In addition to acid-mediated catalysis with zeolites, base catalysis and oxidation chemistries are now performed with zeolites.[97] A particularly germane example for this review is the oxidation catalysis by the use of the titanosilicate TS-1 (has the structure of ZSM-5).[103,104] TS-1 is the pure-silica version of the zeolite ZSM-5 in which ~ 1-2 atomic percent of the silicon atoms are substituted by tetravalent titanium atoms. This material is capable of catalyzing a very broad spectrum of oxidation reactions (see Figure 2.6.2) using aqueous H_2O_2 as the oxidant at temperatures below 373K. TS-1 has revolutionized zeolite catalysis and one reason for doing so is that it demonstrated that low temperature liquid-phase reactions are commercially feasible with a zeolite-based catalyst (phenol to hydroquinone and catechol and cyclohexanone to the oxime are now both practiced on commercial

scale and the epoxidation of olefins is near commercialization). TS-1 is able to accomplish these chemistries using aqueous H_2O_2 as the oxidant. It is well known that titanium compounds are not able to catalyze oxidation reactions if water is present, *e.g.*, the Sharpless asymmetric, homogeneous epoxidation of allyl alcohols and Shell's heterogeneous titanium on amorphous silica catalyst for propylene epoxidation. How is it that TS-1 is able to remain active in the presence of water? Khouw *et al.* addressed this issue.[105] TS-1 is hydrophobic. Organic reactants are adsorbed into the hydrophobic pore space, oxidized and displaced by other reactant molecules. That is to say, the more hydrophobic reactants partition from the bulk solution phase into the hydrophobic pore space and in doing so readily displace products (more hydrophilic since they are oxidized forms of the reactant) and water (from the H_2O_2) back into the bulk solvent phase. This behavior is similar to that observed in certain enzymes, *i.e.*, partitioning of substrates from the aqueous solution to the hydrophobic active site that excludes water and then releases the product back to the aqueous phase, *e.g.*, methane to methanol with methane monooxygenase. Thus, in addition to shape-selectivity, it is possible to control the partitioning of reactants/products from the solvent to the intrazeolitic reaction site by tuning the hydrophilic/hydrophobic nature of the zeolite.[106]

Zeolites can be synthesized using organic molecules as "templates." As pointed out by Davis and Lobo, the specificity between the organic guest

and the zeolite host is as yet not sufficient to invoke true templating in the sense that this term is used in biological contexts.[96] Here, we will call the organic species structure-directing agents (SDAs) since they have been shown to dictate the final outcome of a zeolite synthesis.   Figure 2.6.3 illustrates a schematic of a reasonable proposal for the synthesis of a zeolite (ZSM-5) that employs a SDA (tetrapropylammonium cation, TPA).[107] Initially, the hydrophobic hydration sphere of TPA is partially or completely replaced by silicate species. Favorable van der Waals contacts between the alkyl groups of the TPA and the hydrophobic silicate species likely provide the enthalpic driving force while release of ordered water to the bulk aqueous phase provides an additional entropic driving force for the assembly process.[108] It is via these organic-inorganic interactions that the geometric correspondence between the organic SDA and the zeolite pore architecture arises.[96,107-109] These composite species have recently been identified by NMR techniques[107] and trapped by silylation methods.[107b] The organic-inorganic species then combine to form entities of size around 5-7 nm (identified by *in situ* SAXS[110] and cryo-TEM[111] studies).   These nanostructured entities are proposed to be the nucleation sites for crystal growth.[112] A complete discussion of the mechanistic details and references for the experimental evidence supporting the proposal shown here can be found elsewhere.[112] What is important about this type of zeolite synthesis (in the context of this review) is that the inorganic species are organized by the

organic molecules via numerous non-covalent, *i.e.*, weak, interactions that ultimately determine the kinetic pathway of the crystallization process (all zeolites are metastable phases that are produced by kinetically controlled synthetic processes). Thus, like the self assembly processes for amorphous "imprinted" materials (see previous sections), zeolite synthesis employs relatively weak, non-covalent intermolecular interactions to direct the synthesis.

It is obvious that not just any organic molecule can serve as a SDA for zeolite synthesis. The properties necessary for structure-direction to occur in the synthesis of high-silica zeolites have been discussed previously.[96,108,113] What is clear from the organics that have been shown to function as SDAs is that they have intermediate hydrophobicity.[107] Presumably this allows the organics to remain as isolated molecules in aqueous solutions with hydrophobic hydration spheres.[107] If the organic molecules interact too strongly with water, then silica can never be organized by the organic species.[107c]

Although a complete mechanistic picture is not available, the known general features of the assembly process lead to strategies for zeolite synthesis by design.[112] Demonstrated examples of designing SDAs to product desired zeolite pore architectures exist.[114,115] An interesting example of the design of zeolite pore architecture is due to Zones and coworkers.[114] Using the linear diquaternary ammonium cation shown in

Figure 2.6.4, Zones prepared a zeolite that contains linear nonintersecting pores (in the as-prepared material the diquat is the guest species in the pores). In order to force the synthesis to produce a zeolite with intersecting pores, Zones added another ring to the diquat to "break the symmetry" of the molecule about the long axis of the diquat. In doing so, linear nonintersecting pores are not able to form and a new zeolite with intersecting pores was formed by *a priori* design of the SDA. Additionally, a single attempt to not only control the pore space geometry but also the placement of atoms into specific crystallographic sites has been reported.[116]

Returning to the objective of prepared zeolite catalysts by design, to date there is no clear example of a zeolite catalyst that was prepared by *a priori* design. However, this goal is being pursued by numerous groups throughout the world. Although zeolites can be prepared via the use of SDAs, no use of a TSA-SDA has appeared. One obvious limitation to the use of a TSA-SDA with zeolites compared to amorphous materials is that the amorphous materials have more conformations available for maximizing guest-host interactions since they are not constrained by symmetry as in the case of a crystalline solid like a zeolite. Regardless, future work on *a priori* design of zeolite catalysts needs to concentrate further on exploiting transition-state selectivity and this will require not only the successful construction of the pore architecture but also the placement of the catalytically active element. Initial efforts in one important subarea of the

overall concept have appeared. Arhancet and Davis have prepared the first zeolite to show chiral properties. Zeolite beta is an intergrowth of two crystal types, one of which can form an enantiomorphic pair. Arhancet and Davis used a chiral SDA to produce a zeolite beta that had a very slight enrichment in one of the enantiomorphs and this material revealed asymmetric catalysis with low enantiomeric excess.[96] These results show that in principle, a chiral zeolite catalyst can be prepared. Lobo and Davis also demonstrated that zeolite materials with chirality should be able to exist and not form intergrowths; i.e., a zeolite analogous to d, ℓ – quartz. Again, it is expected that a chiral SDA would be necessary to prepare a single enantiomorph. Thus, we believe the potential is high for the synthesis of new zeolite-based catalysts by rational design and believe that if such is done it will exploit transition-state shape-selectivity rather than the more traditional reactant and product shape-selectivities.

2.7   Comparisons

From the aforementioned discussions on catalytic antibodies, imprinted polymers, imprinted amorphous metal oxides and zeolites, it is clear that each catalytic system contains advantages and disadvantages when considering their use as commercially viable catalysts. Here, we compare and contrast these materials.

Tables 2.7.1 and 2.7.2 list comparisons between the various imprinted catalytic systems described in this review. The antibody catalyst can show high activity and selectivity that can be attributed to the imprinting process via a TSA imprint. Although the activity is not as high as with enzymes, it can be more than sufficient for practical application in numerous circumstances. The difficulties with antibody catalysts are their preparation methods, their "robustness" (lack of stability in harsh chemical and/or physical environments) and their low productivity. Here, we denote productivity as the product formed per unit volume of reactor. Although antibody catalysts show high turnover frequencies, the concentrations of the reactants are normally very low and the possible regeneration of the catalyst is currently unknown. Thus, catalytic antibodies will likely find use in small scale syntheses where high selectivities are required.

Imprinted polymer catalysts can yield higher productivities and catalyst "robustness" than catalytic antibodies. However, the polymer catalysts thus far have shown low reaction rates. The imprinted polymers typically reveal low number densities of active sites and site heterogeneity. If the imprinted sites had a significantly higher turnover frequency relative to the non-imprinted sites, then site heterogeneity need not be such a significant issue. The problem is that to obtain high catalytic activity, a high binding affinity is likely necessary in these materials. A high binding affinity without flexibility around the catalytic site would likely lead to low activity (refer to

enzyme model of induced fit) since it would be very difficult to design an appropriate TSA to give high binding without product inhibition (see previous discussions on endothermic *vs.* exothermic reactions). Thus, a better strategy is most likely to prepare imprinted polymers of greater homogeneity with a controlled transition-state stabilization that minimizes product inhibition.

Imprinted amorphous metal oxides show nearly the same features and suffer from the same problems as the imprinted polymers except that the metal oxides do not have the range of functional groups available with polymers to create active sites without grafting of other moieties onto the surface of the metal oxides; only hydroxyl groups and Lewis acid centers (for example, tri-coordinated Al^{3+}) are available as catalytic sites.

Zeolites reveal numerous properties that allow them to be commercially viable catalysts, *e.g.*, high active site density, "robustness" and shape selectivity. However, the design of a zeolite catalyst via a TSA has not occurred. Although there are limited examples of transition-state shape-selective catalysis with zeolites, none of these were designed *a priori.* The limitations imposed by the crystalline nature of zeolites will likely impede the use of the TSA imprinting methodology. Additionally, zeolites suffer from the same lack of functional groups as described for amorphous metal oxides. In spite of these shortcomings, zeolites are and will continue to be one of the most important materials used commercially as catalysts.

However, there will be numerous reactions where the zeolite does not contain the appropriate functional group for catalytic action and/or the selectivity, *e.g.*, enantioselectivity, necessary for application. It is for these reasons that the aforementioned imprinted systems should be explored as catalysts.

Throughout this review we have discussed the positive and negative features of using TSA imprints to synthesize catalytic materials. It is clear from this presentation that the TSA paradigm in imprinting materials for catalysis is alive and well. However, as with other newly developing fields, the number of control experiments and direct comparisons between different catalytic materials still needs improvement. We expect these shortcomings to disappear as the field matures. As we look to the future, the target of mimicking enzyme catalysis appears closer due to continued improvements on the synthesis of nanostructured materials.

2.8　　　References

[1]　Wulff, G. *ACS Symp. Ser.* **1986**, *308*, 186.

[2]　Shea, K. J. *Trends Polymer Sci.* **1994**, *2*, 166.

[3]　a. Mosbach, K. *Trends Biochem. Sci.* **1994**, *19*, 9.
　　 b. Mosbach, K; Ramström, O. *Bio/Technology* **1996**, *14*, 163.

[4]　Kempe, M.; Mosbach, K. *J. Chromatography* **1995**, *694*, 3.

[5]　Vidyasankar, S.; Arnold, F. H. *Curr. Op. Biotech.* **1995**, *6*, 218.

[6]　*Chem. Eng. News* **1949**, *27(13)*, 913.

[7]　Pauling, L. *J. Am. Chem. Soc.* **1940**, *62*, 2643.

[8]　Dickey, F. H. *Proc. Natl. Acad. Sci. USA* **1949**, *35*, 227.

[9]　Dickey, F. H. *J. Phys. Chem.* **1955**, *59*, 695.

[10]　Haldeman, R. G.; Emmett, P. H. *J. Phys. Chem.* **1955**, *59*, 1039.

[11]　Curti, R.; Colombo, U. *J. Am. Chem. Soc.* **1952**, *74*, 3961.

[12]　Wulff, G.; Sarhan, A. *Angew. Chem. Int. Ed. Engl.* **1972**, *11*, 341.

[13]　Fischer, E. *Ber. Dtsch. Chem. Ges.* **1890**, *23*, 2611.

[14]　Koshland, D. E. Jr. *Proc. Natl. Acad. Sci. USA* **1958**, *44*, 98.

[15]　Koshland, D. E. Jr. *Angew Chem. Int. Ed. Engl.* **1994**, *33*, 2375.

[16]　(a) Fersht, A., Enzyme Structure and Mechanism, 2nd ed.; W. H. Freeman: New York, 1985. (b) Creighton, T. E., Proteins: Structure and Molecular Properties, 2nd ed.; W. H. Freeman: New York, 1993.

[17]　Gerstein, M.; Lesk, A. M.; Chothia, C. *Biochem.* **1994**, *33*, 6739.

[18]　Affleck, R.; Xu, Z. F.; Suzawa, V.; Focht, K.; Clark, D. S.; Dordick, J. S. *Proc. Natl. Acad. Sci. USA* **1992**, *89*, 1100.

[19]　Pauling, L. *Chem. Eng. News* **1946**, *24*, 1375.

[20]   Radzicka, A.; Wolfenden, R. *Science* **1995**, *267*, 90.

[21]   (a) Boudart, M. *Chem. Rev.* **1995**, *95*, 661. (b) Weisz, P. *CHEMTECH* **1982**, *22*, 424.

[22]   Pauling, L. *Am. Sci.* **1948**, *36*, 51.

[23]   Tramontano, A.; Janda, K. O.; Lerner, R. A. *Science* **1986**, *234*, 1566.

[24]   Pollack, S. J.; Jacobs, J. W.; Schultz, P. G. *Science* **1986**, *234*, 1570.

[25]   Schultz, P. G.; Lerner, R. A. *Acc. Chem. Res.* **1993**, *26*, 391.

[26]   Schultz, P. *Acc. Chem. Res.* **1989**, *22*, 287.

[27]   Schultz, P.; Lerner, R. A.; Benkovic, S. J. *Chem. Eng. News* **1990**, *68*(22), 26.

[28]   Stewart, J. D.; Liotta, L. J.; Benkovic, S. J. *Acc. Chem. Res.* **1993**, *26*, 396.

[29]   Schultz, P. G.; Lerner, R. A. *Science*, **1995**, *269*, 1835.

[30]   Haynes, M. R.; Stura, E. A.; Hilvert, D.; Wilson, I. A. *Science* **1994**, *263*, 646.

[31]   Hilvert, D.; Carpenter, S. H.; Nared, K. D.; Auditor, M. T. M. *Proc. Natl. Acad. Sci. USA* **1989**, *85*, 4953.

[32]   Hilvert, D.; Nared, K. D. *J. Am. Chem. Soc.* **1988**, *110*, 5593.

[33]   Jackson, D. Y.; Liang, M. N.; Bartlett, P. A.; Schultz, P. G. *Angew. Chem. Int. Ed. Engl.* **1992**, *31*, 182.

[34]   Chook, Y. M.; Ke, H.; Lipscomb, W. N. *Proc. Natl. Acad. Sci. USA* **1993**, *90*, 8600.

[35]   Thorn, S. N.; Daniels, R. G.; Auditor, M. T. M.; Hilvert, D. *Nature* **1995**, *373*, 228.

[36]   Kemp, D. S.; Cox, D. D.; Paul, K. G. *J. Am. Chem. Soc.* **1975**, *97*, 7312.

[37] Stewart, J. D.; Benkovic, S. J. *Nature* **1995**, *375*, 388.

[38] Shevlin, G. S.; Hilton, S.; Janda, K. D. *Bioorg. Med. Chem. Lett.* **1994**, *4*, 297.

[39] Wulff, G. *Angew. Chem. Int. Ed. Engl.* **1995**, *34*, 1812.

[40] Whitcombe, M. J.; Rodriguez, M. E.; Villar, P.; Vulfson, E. *J. Am. Chem. Soc.* **1995**, *117*, 7105.

[41] (a) Kempe, M.; Mosbach, K. *J. Chromatography* **1995**, *691*, 317. (b) Kempe, M.; Mosbach, K. *Int. J. Peptide Protein Res.* **1994**, *44*, 603. (c) Ramström, O.; Nicholls, I. A.; Mosbach, K. *Tetrahedr. A* **1994**, *4*, 649. (d) Sellergren, B. Ph.D. Thesis, University of Lund, Sweden, 1988. (e) Andersson, L. I. Ph.D. Thesis, University of Lund, Sweden, 1990. (f) Norrlöw, O. Ph.D. Thesis, University of Lund, Sweden, 1986. (g) Kempe, M. Ph.D. Thesis, University of Lund, Sweden, 1994. (h) Fischer, L.; Müller, R.; Ekberg, B.; Mosbach K. *J. Am. Chem. Soc.* **1991**, *113*, 9358.

[42] (a) Hunter, L. *Prog. Stereochem.* **1954**, *1*, 222. (b) Pimentel, G. C.; McClellan, A. I. *The Hydrogen Bond*; W.H. Freeman: New York, 1960.

[43] Sellergren, B.; Shea, K. J. *J. Chromatography* **1993**, *635*, 31.

[44] (a) Tao, Y.; Ho, T. *J. Chem. Soc. Chem. Commun.* **1988**, 417. (b) Norrlöw, O.; Månsson, M. O..; Mosbach, K. *J. Chromatography* **1987**, *396*, 374.

[45] Wulff, G.; Heide, B.; Helfmeier, G. *J. Am. Chem. Soc.* **1986**, *108*, 1089.

[46] Wulff, G.; Heide, B.; Helfmeier, G. *React. Polym.* **1987**, *6*, 299.

[47] Adamson, A. W., *Physical Chemistry of Surfaces*; John Wiley & Sons: Toronto, 1976.

[48] Sellergren, B. *Makromol. Chem.* **1989**, *190*, 2703.

[49] Sellergren, B.; Shea, K. J. *J. Chromatography* **1995**, *690*, 29.

[50] Andersson, L.I.; Müller, R.; Vlatakis, G.; Mosbach, K. *Proc. Natl. Acad. Sci. USA* **1995**,*92*, 4788.

[51] Shea, K. J.; Sasaki, D. Y. *J. Am. Chem. Soc.* **1991**, *113*, 4109.

[52] Sellergren, B. *Chirality* **1989**, *1*, 63.

[53] Mosbach, K. *Protein Engr.* **1995**, *8 (supplement)* 54.

[54] Andersson, L. I.; Nicholls, I. A.; Mosbach, K. *ACS Symp. Ser.* **1995**,*586*, 89.

[55] Vlatakis, G.; Andersson, L. I.; Müller, R.; Mosbach, K. *Nature* **1993**, *361*, 645.

[56] Levine, I. N. *Physical Chemistry*, 3rd ed.; McGraw Hill: New York, 1988.

[57] Jencks, W. P. *Catalysis in Chemistry and Enzymology*, Dover: New York, 1969.

[58] (a) Hammond, G.S. *J. Am. Chem. Soc.* **1955**, *77*, 334. (b) Lewis, E. *Techniques of Chemistry Volume VI*, 3rd ed; John Wiley & Sons: New York, 1973.

[59] (a) Conformations of molecules were minimized in energy using Dreiding 2.21 Force Field. *Ab initio* calculations were performed on minimized structures with MOPAC6 using AM1 Hamiltonian and Geometry Optimization with Cerius^2 version 1.6 molecular mechanics software. The calculated enthalpies represent the standard enthalpies of reaction. Note that in reaction **H**, $NaBH_3CN$ was used instead of $LiAlH_4$ in the enthalpy of reaction calculation, due to the fact that MOPAC6 and AM1 are not able to accommodate Li-containing molecules. We note that although the absolute magnitudes of the enthalpies calculated with this method may not be correct, especially for reactions conducted in aqueous media, it is important to emphasize that only the relative trends in the enthalpies with respect to exothermicity are significant for the purpose of evaluating the merit of the Hammond postulate in predicting the plausability of conducting a particular reaction on an imprinted material. (b) Mayo, S. L.; Olafson, B. D.; Goddard III, W. A. *J. Phys. Chem.* **1990**, *94*, 8897.

[60] Hilvert, D. *Curr. Op. Struct. Biol.* **1994**, *4*, 612.

[61] Hsieh, L. C.; Yonkovich, S.; Kochersperger, L.; Schultz, P. G. *Science* **1993**, *260*, 337.

[62] Leonhardt, A.; Mosbach, K. *React. Polym.* **1987**, *6*, 286.

[63] Robinson, D.; Mosbach, K. *J. Chem. Soc. Chem. Commun.* **1989**, 969.

[64] Ohkubo, K.;Urata, Y.; Hirota, S.; Honda, Y.; Fujishita, Y.; Sagawa, T. *J. Mol. Catal.* **1994**, *93*, 189.

[65] Ohkubo, K.; Urata, Y.; Hirota, S.; Honda, Y.; Sagawa, T. *J. Mol. Catal.* **1994**, *87*, L21.

[66] Andersson, L. I.; Mosbach, K. *Makromol. Chem. Rapid Commun.* **1989**, *10*, 491.

[67] Motomura, T.; Inoue, K.; Kobayashi, K.; Aoyama, Y. *Tetrahedron Lett.* **1991**, 32, 4757.

[68] (a) Ohkubo, K.; Urata, Y.; Hirota, S.; Funakoshi, Y.; Sagawa, T.; Usui, S.; Yoshinaga, K. *J. Mol. Catal. A* **1995**, *101*, L111. (b) Reference 68a reports the difference in the activation free energies between the most catalytically active polymer (TP1') and the uncatalyzed reaction (None) to be 6.4 kcal/mol. This corresponds to a relative rate increase of more than 41,300 for TP1' over None at 303 K, which is significantly larger than the reported experimentally measured value of 3.7.

[69] Müller, R.; Andersson, L. I.; Mosbach, K. *Makromol. Chem. Rapid Commun.* **1993**, *14*, 637.

[70] Beach, J. V.; Shea, K. J. *J. Am. Chem. Soc.* **1994**, *116*, 379.

[71] Shokat, K. M.; Leumann, C. J.; Sugasawara, R.; Schultz, P. G. *Nature* **1989**, *338*, 269.

[72] Damen, J.; Neckers, D. C. *J. Am. Chem. Soc.* **1980**, *102*, 3265.

[73] Wulff, G.; Vietmeier, J. *Makromol. Chem.* **1989**, *190*, 1727.

[74] Byström, S.; Börje, A.; Akermark, B. *J. Am. Chem. Soc.* **1993**, *115*, 2081.

[75] Sellergren, B.; Shea, K. J. *Tetrahedron A* **1994**, *8*, 1403.

[76] Martin, M. T.; Angeles, T. S.; Sugasawara, R.; Aman, N.; Napper, A. D.; Darsley, M. J.; Sanchez, R. I.; Booth, P.; Titmas, R. C. *J. Am. Chem. Soc.* **1994**, *116*, 6508.

[77] (a) Shea, K. J.; Thompson, E. A. *J. Org. Chem.* **1978**, *43*, 4253. (b) Shea, K. J.; Thompson, E. A.; Pandey, S. D.; Beauchamp, P. S. *J. Am. Chem. Soc.* **1980**, *102*, 3149.

[78] Mathew, J.; Buchart, O. *Bioconjugate Chem.* **1995**, *6*, 524.

[79] Schwanghart, A.-D.; Backmann, W.; Blasche, G. *Chem. Ber.* **1977**, *110*, 778.

[80] Andersson, L. I.; Sellergren, B.; Mosbach, K. *Tetrahedron Lett.* **1984**, *25*, 5211.

[81] Morihara, K.; Kurihara, S.; Suzuki, J. *Bull. Chem. Soc. Jpn.* **1988**, *61*, 3991.

[82] (a) Morihara, K.; Nishihata, E.; Kojima, M.; Miyake, S. *Bull. Chem. Soc. Jpn.* ***1988***, *61*, 3999. (b) Morihara, K.; Tanako, E.; Takeuguchi, Y.; Miyazaki, K.; Yamamoto, N.; Sagawa Y.; Kawamoto, E.; Shimada, T. *Bull. Chem. Soc. Jpn.* **1989**, *62*, 499.

[83] Shimada, T.; Kiyoko, N.; Morihara, K. *Bull. Chem. Soc. Jpn.* **1992**, *65*, 954.

[84] (a) Morihara, K.; Doi, S.; Takiguchi, M.; Shimada, T. *Bull. Chem. Soc. Jpn.* **1993**, *66*, 2977. (b) Morihara, K.; Iijima, T.; Usui, H.; Shimada, T. *Bull. Chem. Soc. Jpn.* **1993**, *66*, 3047. (c) Morihara, K.; Nishihata, E.; Kojima, M.; Miyake, S. *Bull. Chem. Soc. Jpn.* **1993**, *66*, 906.

[85] Shimada, T.; Kurazono, R.; Morihara, K. *Bull. Chem. Soc. Jpn.* **1993**, *66*, 836.

[86] (a) Matsuishi, T.; Shimada, T.; Morihara, K. *Bull. Chem. Soc. Jpn.* **1994**, *67*, 748. (b) Morihara, K.; Takiguchi, M.; Shimada, T. *Bull. Chem. Soc. Jpn.* **1994**, *67*, 1078. (c) Shimada, T.; Horose, R.; Morihara, K. *Bull. Chem. Soc. Jpn.* **1994**, *67*, 227.

[87] Morihara, K.; Kurokawa, M.; Kamata, Y.; Shimada, T. *J. Chem. Soc. Chem. Commun.* **1992**, 358.

[88] Bernhard, S.; Gutfreund, H. *Proceedings of the International Symposium on Enzyme Chemistry* **1957**, Tokyo and Kyoto.

[89] Hamilton, C. L.; Niemann, C.; Hammond, G. S. *Proc. Natl. Acad. Sci. USA* **1966**, *55*, 664.

[90] Heilmann, J.; Maier, W. F. *Angew. Chem. Int. Ed. Engl.* **1994**, *33*, 471.

[91] Ahmad, W. R.; Davis, M. E., *Catal. Lett.* **1996**, *40*, 109.

[92] Napper, A. D.; Benkovic, S. J.; Tramontano, A.; Lerner, R. A. *Science* **1987**, *23*, 1041.

[93] Heilmann, J.; Maier, W. F. *Z. Naturforsch. B* **1995**, *50*, 460.

[94] Davis, M. E. *Ind. Eng. Chem. Res.* **1991**, *30*, 1675.

[95] Venuto, P. B. *Microporous Mater.* **1994**, *2*, 297.

[96] Davis, M. E.; Lobo, R. F. *Chem. Mater.* **1992**, *4*, 756.

[97] Davis, M. E. *Acc. Chem. Res.* ***1993, 26, 111.***

[98] Csicsery, S. M. *Zeolites* **1984**, *4*, 202.

[99] Weisz, P. B.; Frilette, V. J.; Maatman, R. W.; Mower, E. B. *J. Catal.* **1962**, *1*, 307.

[100] Anderson, M. W.; Klinowski, J. *Nature* **1989**, *339*, 220.

[101] Kucherov, A. V.; Slinkin, A. A.; Gitis, K. M.; Isagulants, G. V. *Catal. Lett.* **1988** *1*, 311.

[102] Khouw, C. B.; Davis, M. E. *ACS Symp. Ser.* **1993**, *517*, 206.

[103] Perego, G.; Bellussi, C.; Corno, C.; Taramasso, M.; Buonomo, F. *Stud. Sur. Sci. Catal.* **1986**, *28*, 129.

[104] Notari, B. *Stud. Sur. Sci. Catal.* **1988**, *37*, 413.

[105] Khouw, C. B.; Dartt, C. B.; Labinger, J. A.; Davis, M. E. *J. Catal.* ***1994***, *149*, 195.

[106] Li, H. X.; Annen, M. J.; Chen, C. Y.; Arhancet, J. P.; Davis, M. E. *J. Mater. Chem.* **1991**, *1*, 79.

[107] (a) Burkett, S. L.; Davis, M. E. *J. Phys. Chem.* **1994**, *98*, 4647. (b) Burkett, S. L.; Davis, M. E. *Chem. Mater.* **1995**, *7*, 920. (c) Burkett, S. L.; Davis, M. E. *Chem. Mater.* **1995**, *7*, 1453.

[108] Helmkamp, M. M.; Davis, M. E. *Ann. Rev. Mater. Sci.* **1995**, *25*, 161.

[109] Gies, H.; Marler, B. *Zeolites* **1992**, *12*, 42.

[110] (a) Iton, L. E.; Trouw, F.; Brun, T. O.; Epperson, J. E.; White, J. W.; Henderson, S. J. *Langmuir* **1992**, *8*, 1045. (b) Dokter, W. H.; van Garderen, H. F.; Beelen, T. P. M.; van Santen, R. A.; Bras, W. *Angew. Chem. Int. Ed. Engl.* **1995**, *34*, 73.

[111] Regev, O.; Cohen, Y.; Kahet, E.; Talmon, Y. *Zeolites* **1994**, *14*, 314.

[112] Davis, M. E. *Stud. Sur. Sci. Catal.* **1995**, *97*, 35.

[113] Lobo, R. F.; Zones, S. I.; Davis, M. E. *J. Incl. Phenom.* **1995**, *47*, 21.

[114] (a) Zones, S. I.; Olmstead, M. N.; Santilli, D. S. *J. Am. Chem. Soc.* **1992**, *164*, 4195. (b) Lobo, R. F.; Pan, M.; Chan, I.; Medrud, R. C.; Zones, S. I.; Crozier, P. A.; Davis, M.E. *J. Phys. Chem.* **1994**, *98*, 12040.

[115] Schmitt, K. O.; Kennedy, G. J. *Zeolites* **1994**, *14*, 635.

[116] Li, H. X.; Camblor, M. A.; Davis, M. E. *Microporous Mater.* **1994**, *3*, 117.

	Relative Adsorption Power[a] for:			
Silica Gel Imprinted With	Methyl Orange	Ethyl Orange	Propyl Orange	Butyl Orange
methyl orange $\left(R = CH_3 \right)^b$	3.5	1.6	1.1	1.1
ethyl orange $\left(R = CH_2CH_3 \right)$	2.5	9	2.1	2.2
propyl orange $\left(R = CH_2CH_2CH_3 \right)$	2.3	5	20	6
butyl orange $\left(R = CH_2CH_2CH_2CH_3 \right)$	1.5	2.8	5	15

a Relative adsorption power is defined as the ratio of the adsorption power of an imprinted gel to that of an non-imprinted gel. The adsorption power of a gel is the concentration of the adsorbate in the gel divided by the concentration of the adsorbate in the supernatant solution.[8]

b
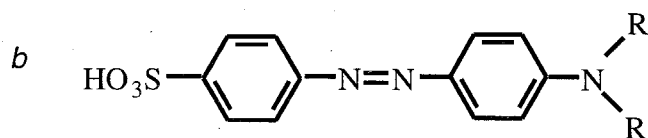
Table 2.1.1. Specific adsorption results from Dickey.[8]

No.	Reaction	Ref.
1	α-proton exchange of phenylalaninanalide	66
2	photodimerization of *trans*-cinnamic acid	72
3	stereoselective synthesis of threonine and allothreonine	73
4	stereoselective synthesis of *trans*-1,2-cyclopropanedicarboxylic acid	77
5	hydrolysis of adenosine triphosphate	78

Table 2.4.1.   Reactions on imprinted polymers.

Table 2.4.2. Standard heats of reaction for selected antibody, imprinted polymer and imprinted silica catalyzed reactions.

Table is four pages long including this page.
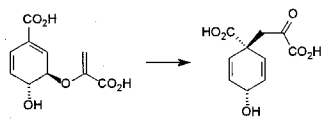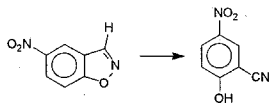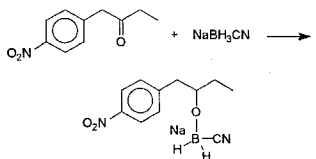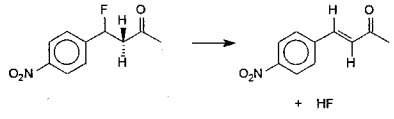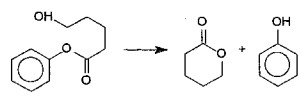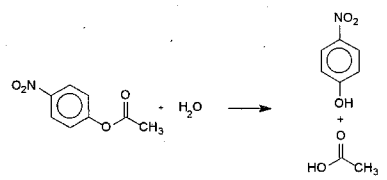
No	Reaction	Type [b]	ΔH kcal/mol	Kinetic Information [a]	Ref.
A		AB	-12.9	$k_{cat}/k_{uncat} > 2.0\times10^6$	31-33
B		AB	-51.99	$k_{cat}/k_{uncat} = 2.1\times10^4$	35
C		AB	-34.57	$k_{cat}/k_{uncat} = 1.7\times10^6$	61
D		AB and POL	-3.67	$k_{cat}/k_{uncat} = 1.5\times10^3$ (AB) $k_{cat}/k_{uncat} = 7.5$ (P) TOF= 14/day (P)	69-71
E		AB [c] and S	-1.78	$k_{cat}/k_{uncat} = 167$ (AB) not reported for silica	92, 93
F		POL	-5.83	$k_{cat}/k_{uncat} = 6.7$	62-65

Table 2.4.2. (Continued)
Standard heats of reaction for selected antibody, imprinted polymer and imprinted silica catalyzed reactions.

G

POL	-15.69	$k_{cat}/k_{uncat} = 3.7$	68

H

POL	-29.52 (Path A)	not reported	74
	-27.09 (Path B)		

I

POL	-84.39	$k_{cat}/k_{hom}^{d)} = 10$	75

J

S	-4.84	not reported	81

Table 2.4.2. (Continued)
Standard heats of reaction for selected antibody, imprinted polymer and imprinted silica catalyzed reactions.

K (structures)

S	+10.84	$k_{cat}/k_{uncat} = 33.4$	83, 85

L (structures)

S	+9.23	$k_{cat}/k_{uncat} = 1.52$	87

M (structures)

S	-3.98	not reported	90

[a] k_{cat} = rate constant for the catalyzed reaction system, k_{uncat} = rate constant for the non-imprinted material (polymer or silica) or solution background reaction rate (antibody).

[b] AB = antibody, POL = polymer, S = silica; TOF is the turnover frequency.

[c] The antibody catalyzed reaction was analogous to that shown with a substituent group at the δ-carbon.

[d] A homogeneous reaction was carried out with phenol-imidazole for comparison. The reported k_{cat}/k_{hom} represents the rate constant of the imprinted polymer divided by that afforded by the homogeneous system.

Table 2.4.2. (Continued)

Standard heats of reaction for selected antibody, imprinted polymer and imprinted silica catalyzed reactions.

82

Solvent	Dipole Moment* (Debyes)	Relative Rate[†] (k_{cat}/k_{uncat})
acetonitrile	3.92	2.2
ethanol	1.69	1.5
benzene	0	7.5

* Data from *CRC Handbook of Chemistry and Physics*, 63rd ed.; Weast, R.C. Ed.; CRC Press: Boca Raton, FL, 1982, pp E59 - E61.

[†] Relative rate represents rate constant of imprinted polymer catalyst (k_{cat}) divided by the rate constant of non-imprinted polymer catalyst (k_{uncat}).

Table 2.4.3. Dependence of the Beach and Shea imprinted polymer catalyzed reaction rate on solvent polarity (adapted from ref. 70).

Catalytic System	Solvent	Relative Rate* (k_{cat} / k_{uncat})	Binding Constant (mM)
Catalytic Antibody	aqueous	1485	0.182
Imprinted Polymer	benzene	3.5 (unoptimized) 7.5 (optimized)	27 (unoptimized)

* Catalytic rate constant, k_{cat}, denotes rate constant with imprinted polymer or antibody. Control rate constant, k_{uncat}, denotes background rate constant of non-imprinted polymer or solution without antibody. Beach and Shea (ref. 70) report two different relative rate constants based on optimized and unoptimized reaction conditions.

Table 2.4.4. Comparison of catalytic antibody (adapted from ref. 71) and Beach and Shea imprinted polymer (adapted from ref. 70) for the dehydrofluorination reaction.

Polymer Template	%* α-truxillic	% β-truxinic	% δ-truxinic
α-truxillic acid	100	0	0
β-truxinic acid	47	53	0
δ-truxinic acid	47.3	0	52.7

* Stereochemical composition (mol %) of acid in reaction products.

Table 2.4.5. Results on the stereochemical control of the photochemical reaction of trans-cinnamate ester using polymers imprinted with α-truxillic, β-truxinic and δ-truxinic acids (adapted from ref. 72).

Silica Imprinted With	Distance r [nm]	Apparent Binding Constants With		Selectivity (ratio of binding constants)
		12	**13**	
10	0.72	4.91	2.58	1.74
11	1.05	9.07	13.77	1.67

Table 2.5.1.   Selectivity of modified silicas (adapted from ref. 45).

Catalyst imprinted With	$10^{-2} \times k_{cat}$ [a) [M^{-1}s^{-1}]	$10^4 \times K_m$ [b) [M]	$10^{-5} \times k_{cat}/K_m$ [M^{-2}s^{-1}]	Charge on Benzoyl Oxygen [c)
13	1.89	2.70	7.00	-0.481
14	4.04	3.36	12.02	-0.478
15	33.36	4.06	82.23	-0.478 & -0.534
control (no imprint)	6.79	18.0	3.77	-

a) k_{cat} = rate constant for the catalyzed reaction.

b) K_m = Michaelis constant.

c)   Equilibrium charge on imprint oxygen determined here using the Dreiding force field[59b] algorithm in the Cerius² software package.

Table 2.5.2.   Kinetic parameters for the 2,4-dinitrophenolysis of benzoic anhydride (adapted from refs. 83, 85) and imprint oxygen Lewis basicities.

Catalyst Type	Ease of Preparation	Robustness	Regeneration	Asymmetric Conversions	Reaction Rates	Productivity
Antibody	difficult	low	unknown	proven	can be high	low
Polymer	moderate	moderate	proven	proven	low	low
Amorphous Metal Oxide	moderate	moderate	unknown	questionable	low	low
Zeolite	moderate	high	excellent	questionable	can be high	good

Table 2.7.1. Comparisons of imprinted catlysts: overall behavior.

Catalyst Type	TSA Concept of Selectivity	Range of Functionalities for Active Site	Active Site Density of Catalyst	Active Site Homogeneity	Active Site Density in Reactor
Antibody	proven	broad	high	excellent	low
Polymer	likely	broad	low	poor	moderate
Amorphous Metal Oxide	questionable	narrow	low	poor	moderate
Zeolite	no	narrow	high	good	high

Table 2.7.2. Comparison of imprinted catalysts: catalyst properties.
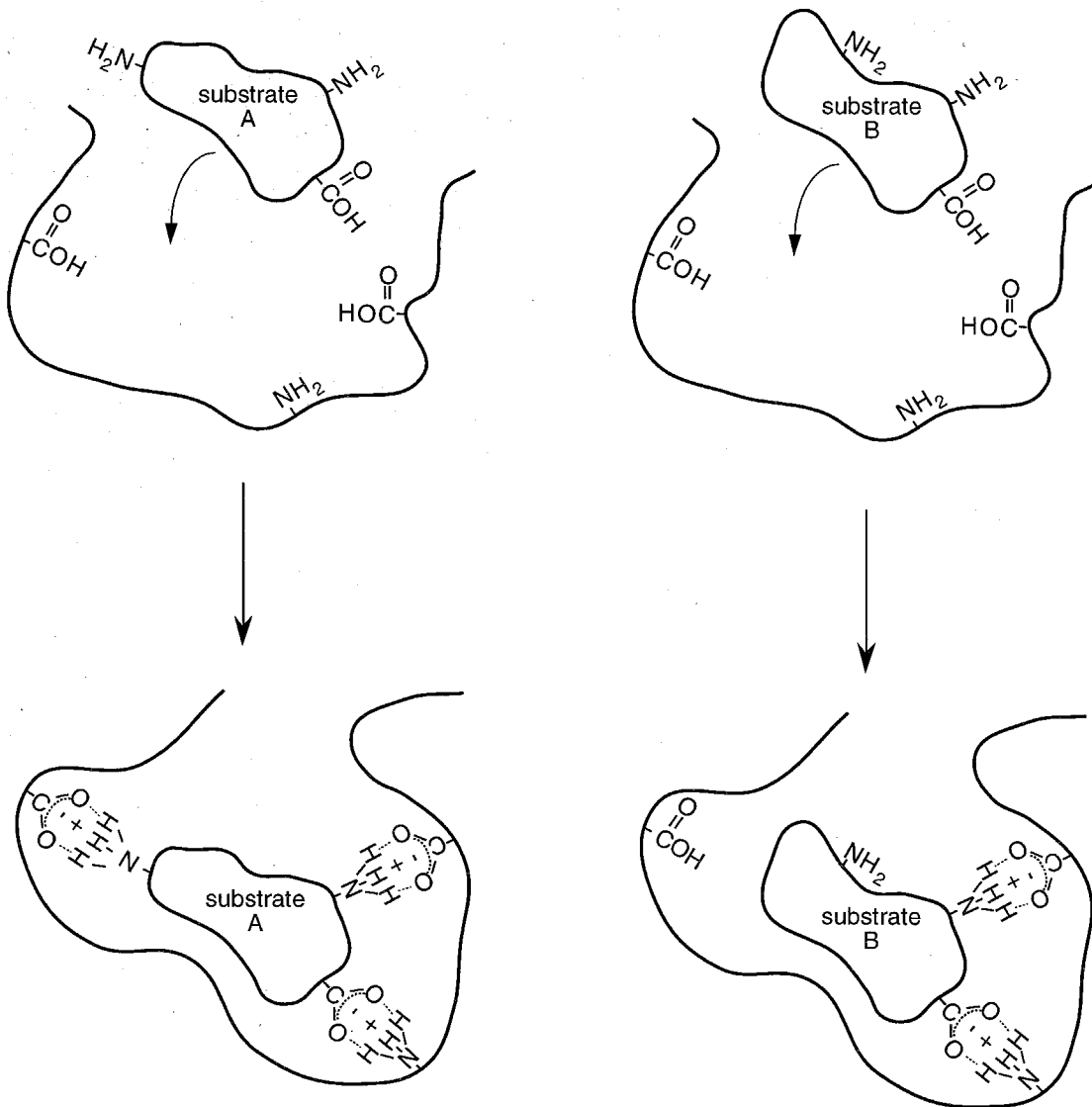
Figure 2.2.1.   Schematic of the induced fit mechanism for enzyme mediated catalysis. On the left, substrate A binding induces a change in the enzyme to bring the functional groups into alignment and thus allows catalysis to occur. On the right, the binding of substrate B causes a misalignment of one functional group and catalysis does not proceed (adapted from ref. 15).
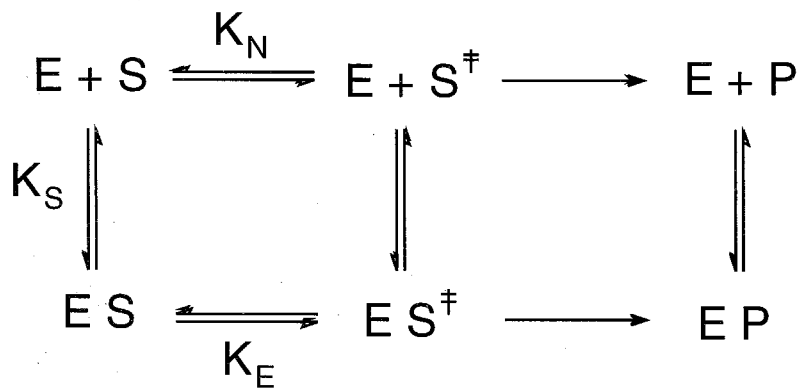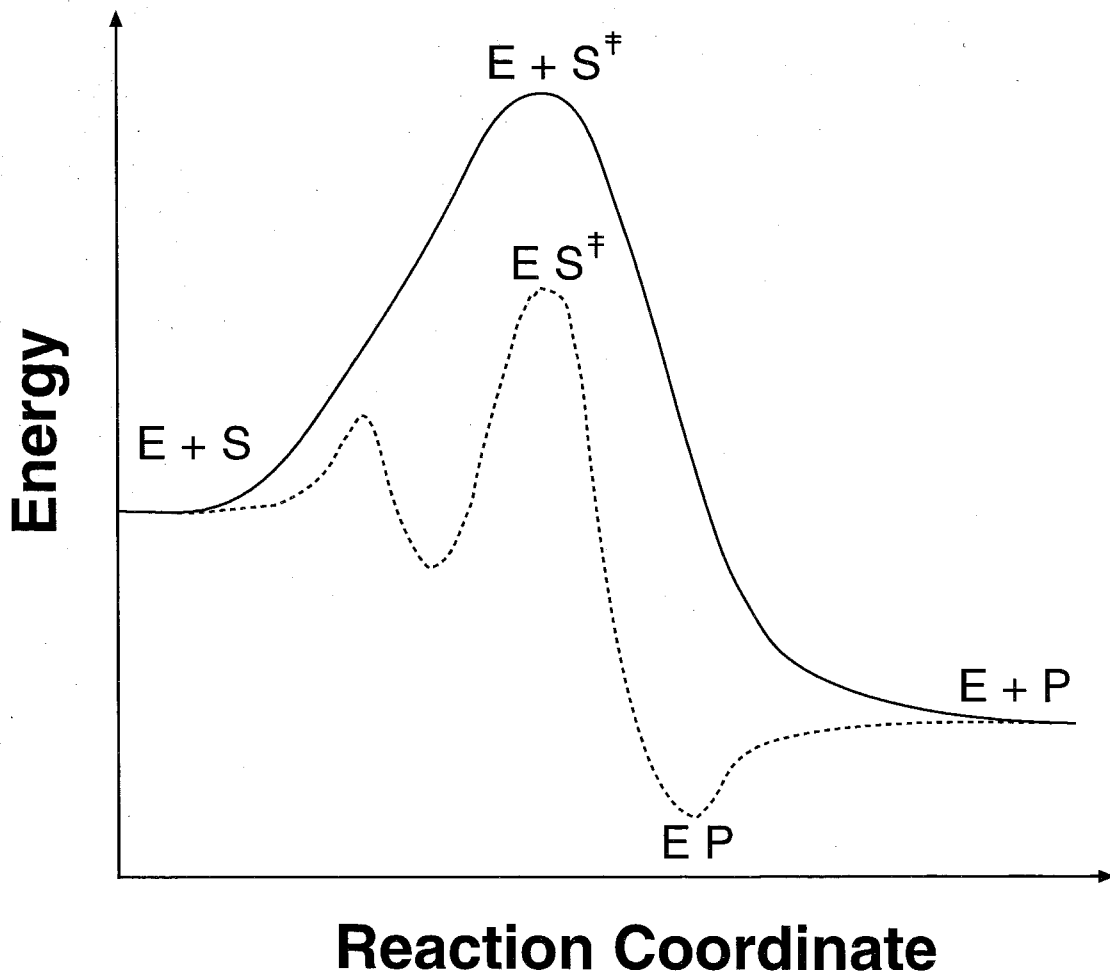
Figure 2.2.2. Energy-reaction pathways for hypothetical single substrate enzymatic and corresponding nonenzymatic reaction.
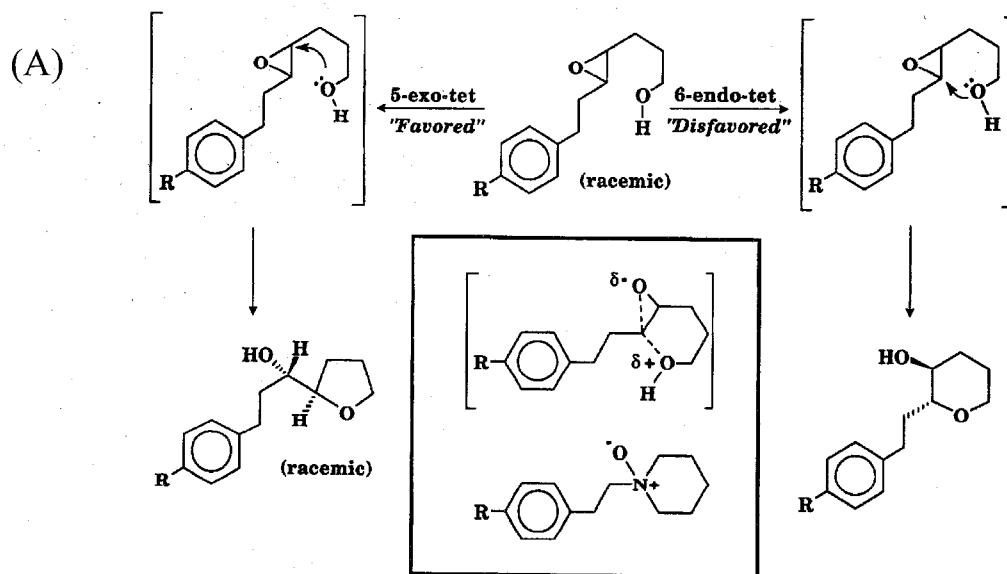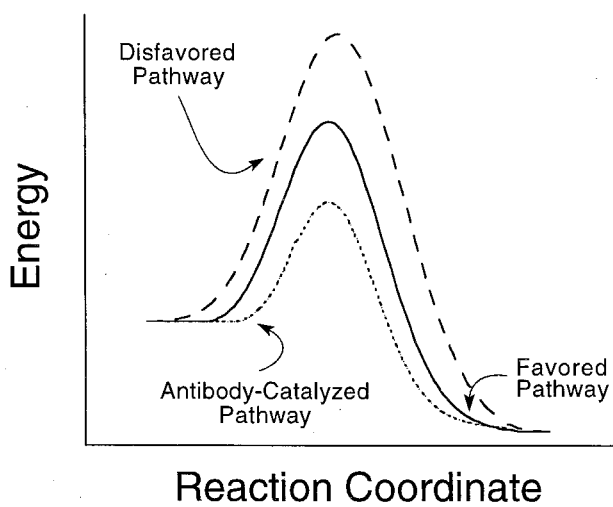
Figure 2.3.1. (A) Schematic of a disfavored reaction achieved using a catalytic antibody (pathway ending in the six-membered ring product). Inset: the N-oxide TSA (imprint) used to generate the catalytic antibody (bottom) and the proposed intermediate (top). (B) Schematic of energy-reaction pathways for reactions shown in A (from ref. 25).
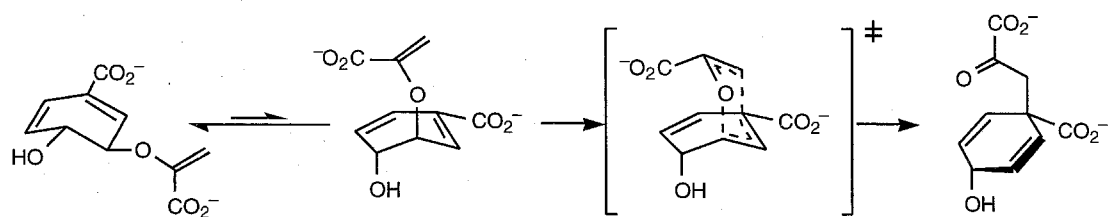
Figure 2.3.2. The Claisen rearrangement of (-)-chorismate to form prephenate. Reprinted with permission from ref. 30. Copyright 1994 American Association for the Advancement of Science.
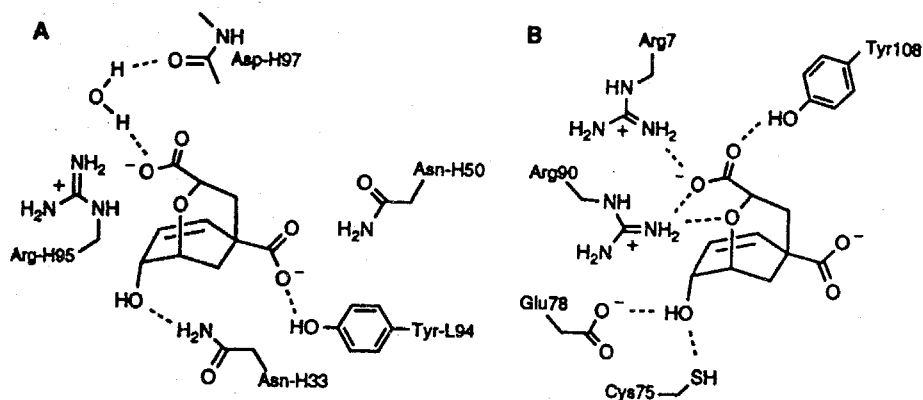
Figure 2.3.3. Schematic diagram comparing the hydrogen bonding and electrostatic interactions of the transition-state analogue with relevant side chains in an antibody (**A**) and enzyme (**B**). Dashed lines indicate hydrogen bonds. Bonds are not indicated for residues at distances greater than 3.3 Å from the TSA. Reprinted with permission from ref. 30. Copyright 1994 American Association for the Advancement of Science.
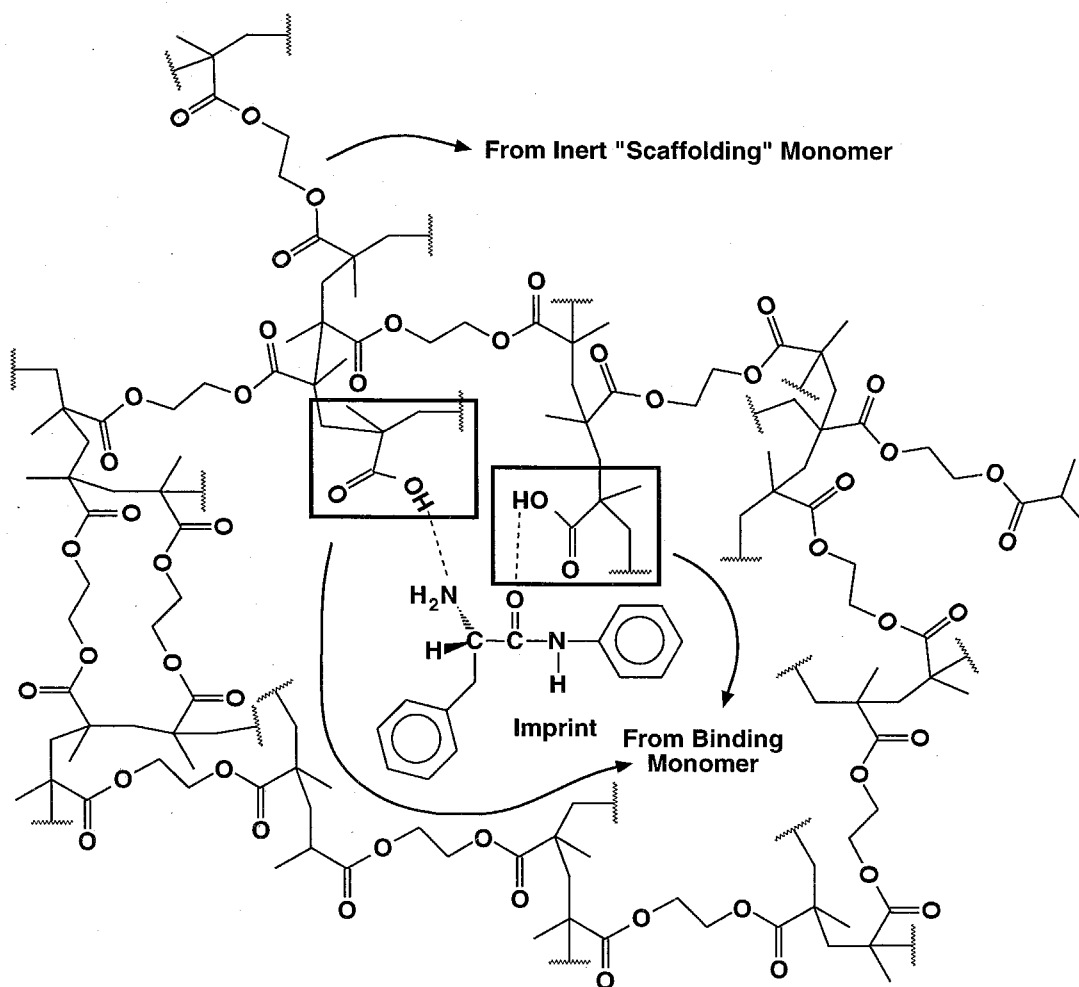
Figure 2.4.1. Schematic diagram showing the configuration of inert "scaffolding" monomer, binding monomer, and imprint in a typical imprinted polymer (adapted from ref. 43). Polymerization has been significantly truncated for purposes of clarity.
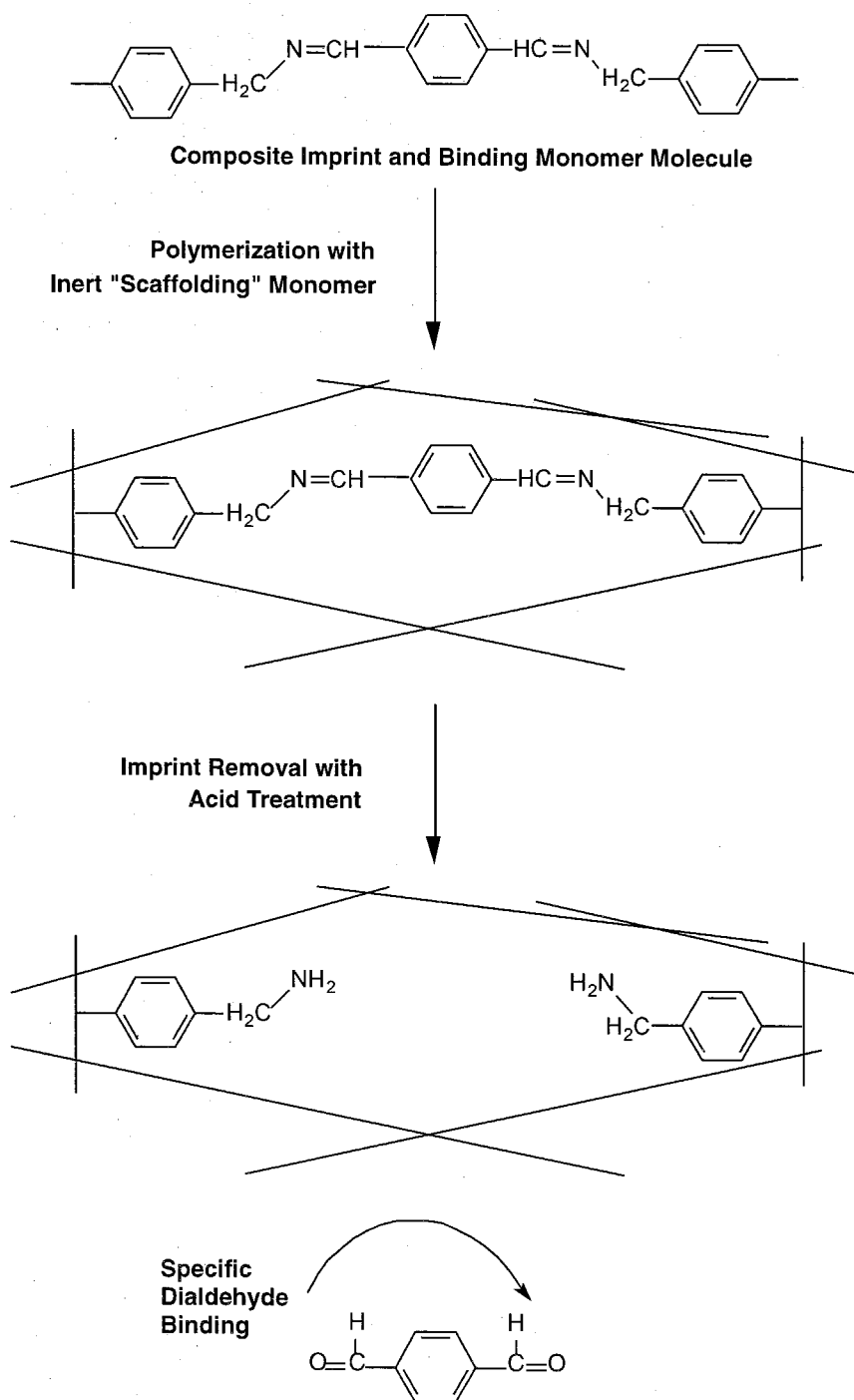
Figure 2.4.2. Example of an imprinted polymer preparation for the binding of a dialdehyde using the controlled distance method (adapted from ref. 46).
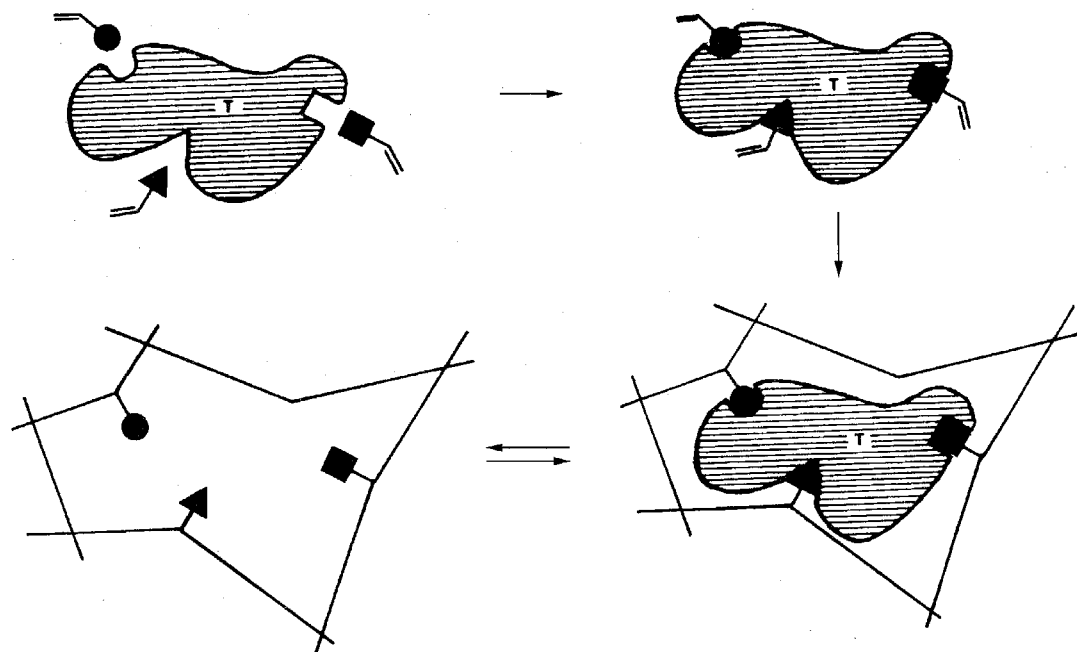
Figure 2.4.3.   Schematic representation of the self assembly method in polymer imprinting. Reprinted with permission from ref. 1. Copyright 1986 The American Chemical Society.
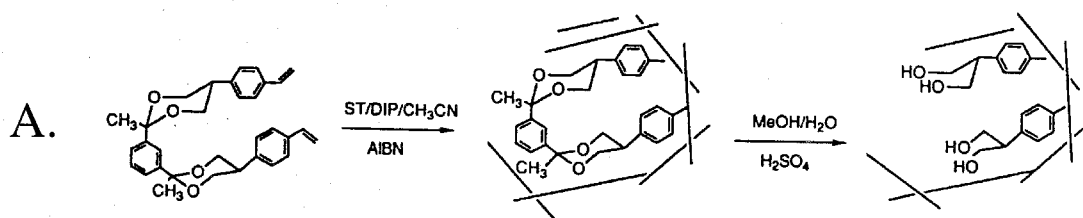
A. Polymer Synthesis
B. Imprint Rebinding

TWO POINT REBINDING   ONE POINT REBINDING
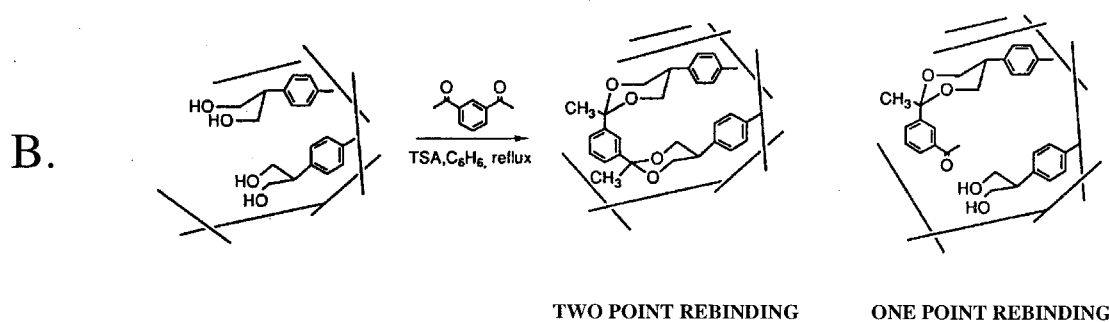
Figure 2.4.4.   (a) Preparation of imprinted polymer by Shea and Sasaski for covalent binding of diketone and (b) Binding of a diketone in imprinted nanopore yielding both one point and two point rebinding (adapted from ref. 51).
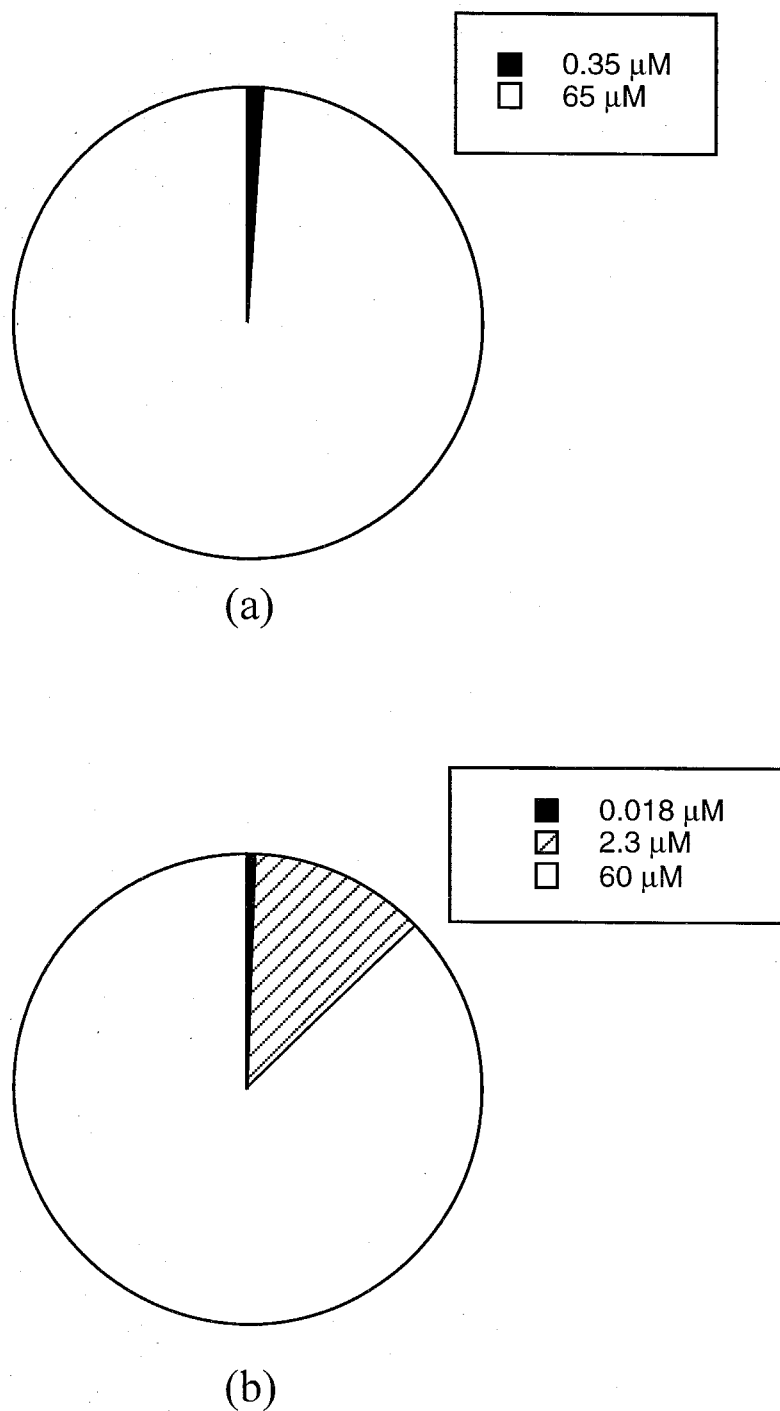
Figure 2.4.5. Fraction of binding sites found in (a) theophylline imprinted polymer and (b) diazepam imprinted polymer. Data taken from ref. 55.
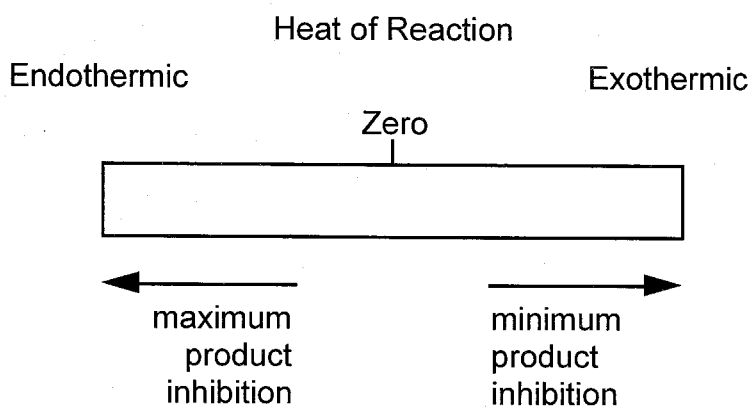
Figure 2.4.6. Schematic representation of the relationship between enthalpy of reaction and the degree of product inhibition expected for a rigid catalyst such as an imprinted polymer (or imprinted silica).
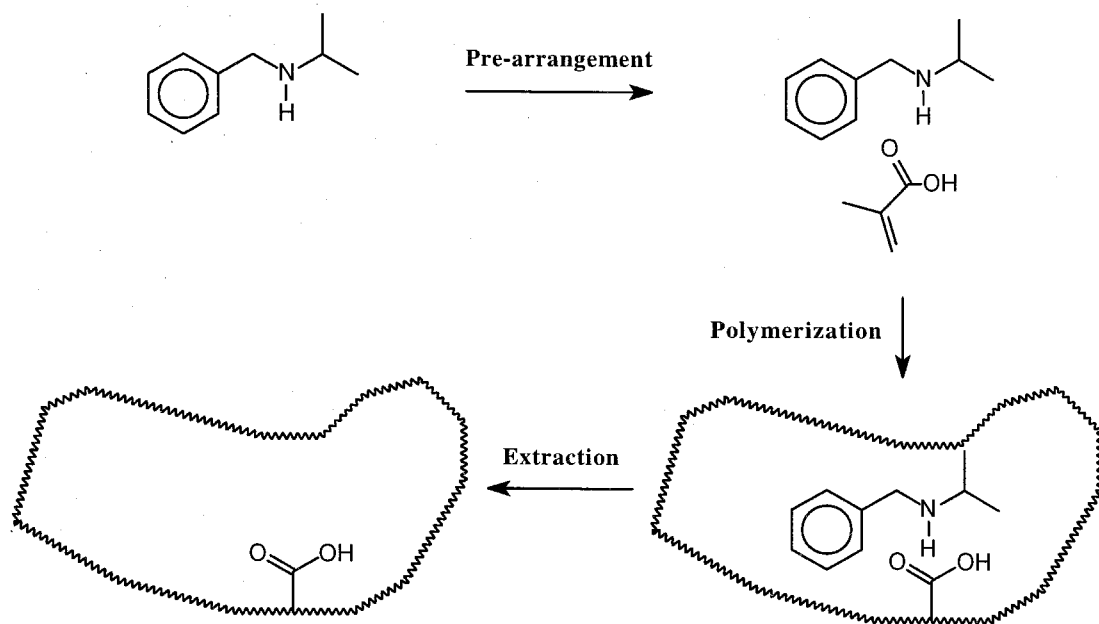
Figure 2.4.7. Polymer imprinting scheme used by Müller *et al.* for the deydrofluorination reaction (adapted from ref. 69).
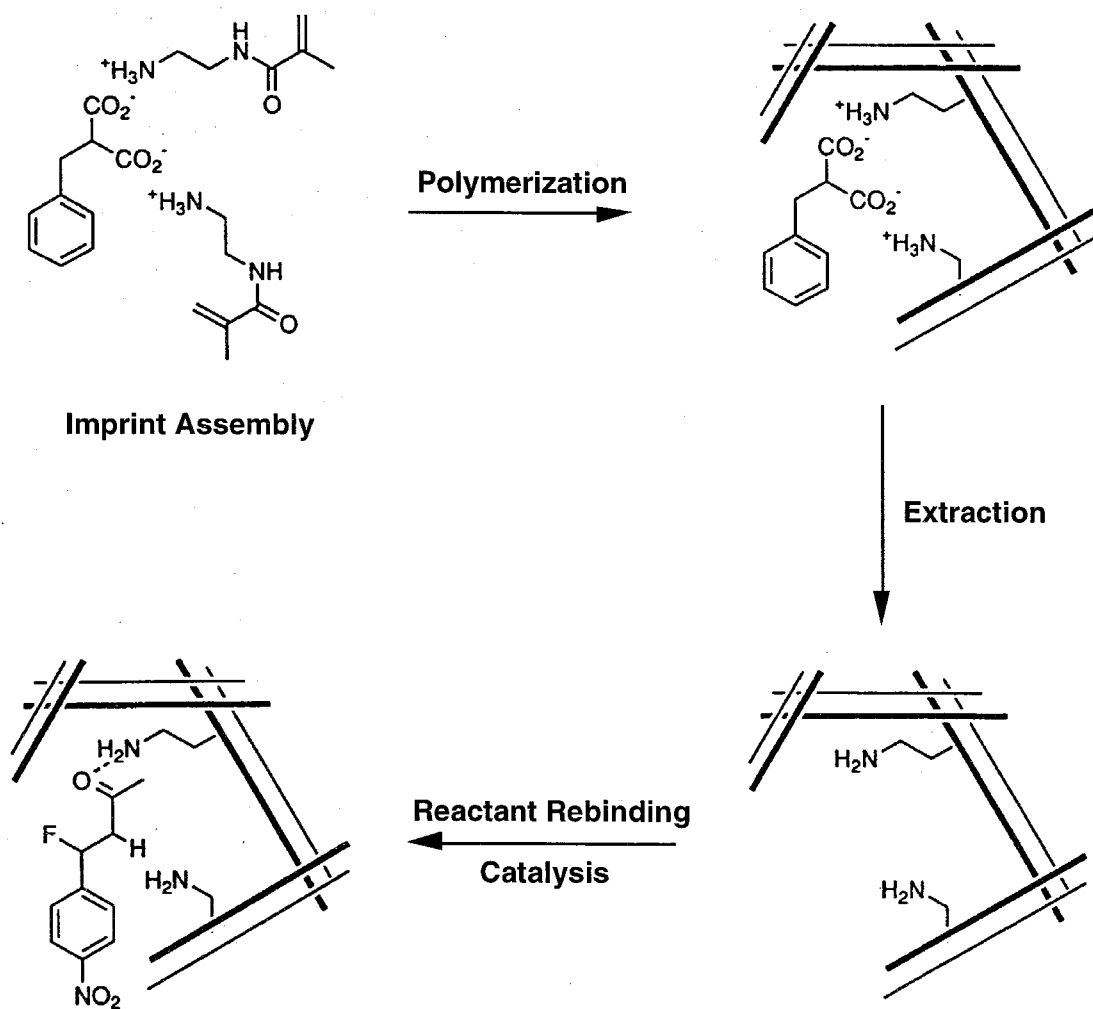
Figure 2.4.8. Polymer imprinting scheme used by Beach and Shea for the dehydrofluorination reaction (adapted from ref. 70).
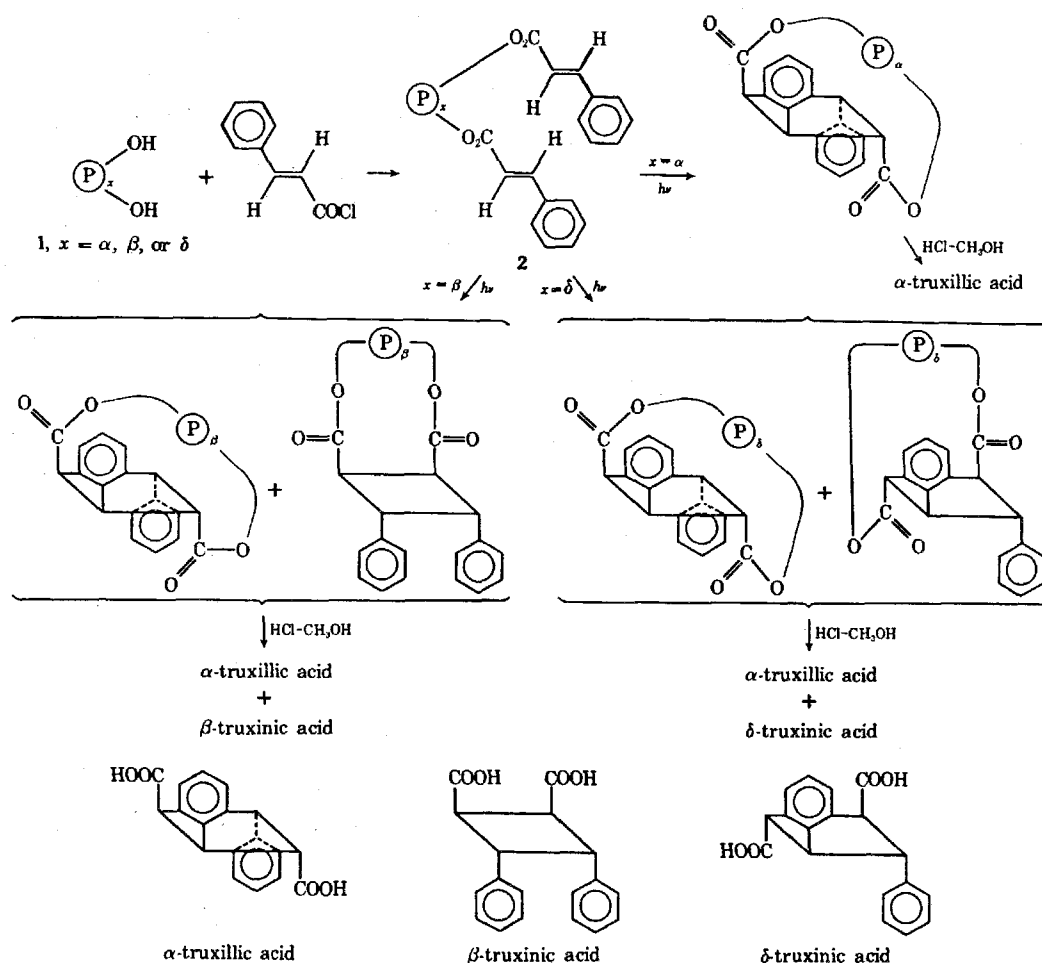
Figure 2.4.9. Polymer imprinting and catalysis scheme used by Damen and Neckers for the stereochemical control of the photochemical dimerization of trans-cinnamate esters. "P" represents a general imprinted nanopore in the polymer framework. Reprinted with permission from ref. 72. Copyright 1980 The American Chemical Society.
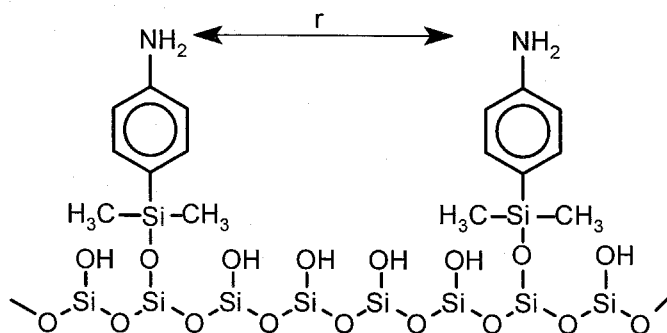
Figure 2.5.1. Representation of two amino groups located at a fixed distance, r, on the surface of silica formed by cleaving compounds **10** or **11** (adapted from ref. 45).
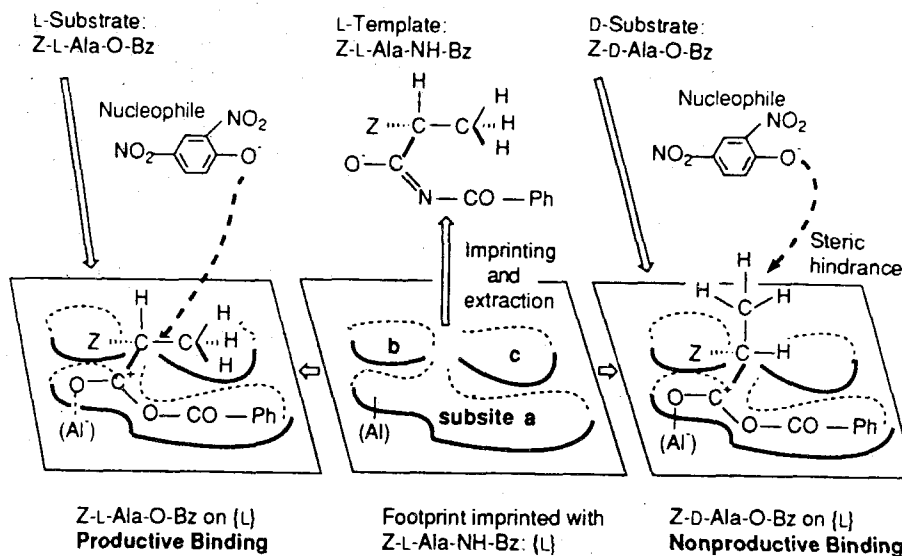
Figure 2.5.2. The proposed mechanism of enantioselectivity for the 2,4 dinitrophenolysis of **17**: chiral L- molecular footprints are produced by **16** and consist of three sites denoted a, b and c corresponding to substructures -CO-NH-Bz, Z-NH- and methyl (not a-hydrogen) of the alanine residue. **Productive Binding**: The L-substrate binds to the footprint through a 3-point interaction maintaining the same a-methyl configuration as the imprint; this places the carbonyl group of the reaction center for activation on the Lewis acid site (Al), thus allowing transformation by nucleophilic attack with 2,4-dinitrophenoxide. **Non-productive Binding**: The D-substrate binds to the footprint through another 3-point adsorption as in b) except that the hydrophobic α-hydrogen replaces the methyl group. Consequently the methyl groups shield the carbonyl compound from nucleophilic attack. The abbreviations refer to the following moieties:
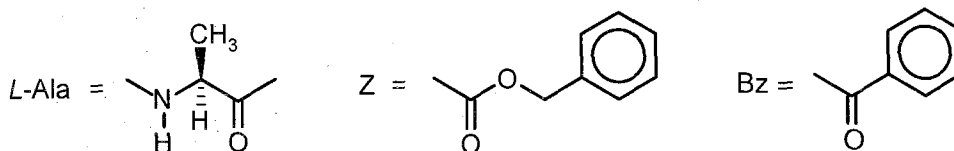
Reactant Shape Selectivity (discrimination between size of reactant molecules).

Product Shape-Selectivity (discrimination between products formed in the intrazeolitic pore space).

Transition-state Shape-Selectivity (transition state is too large to form in the intrazeolitic space).
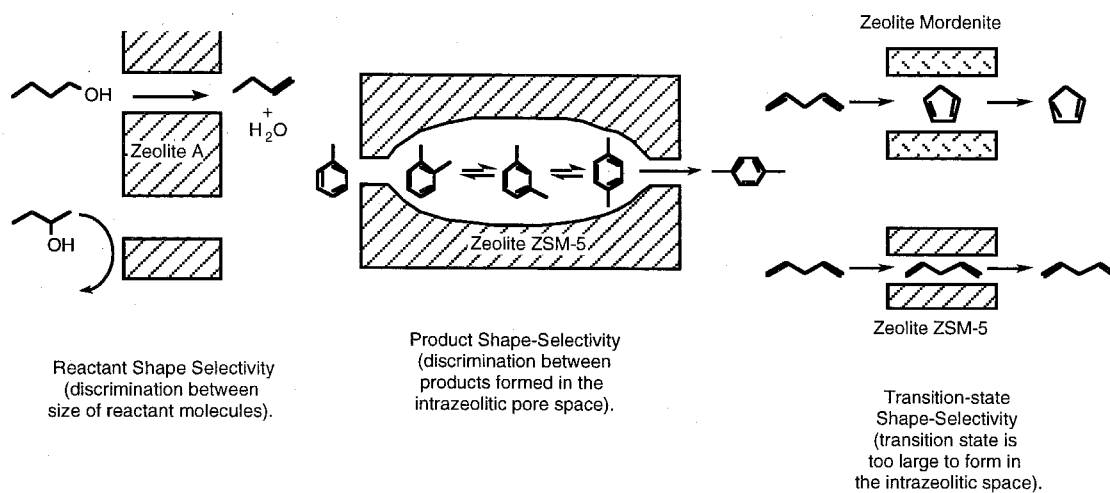
Figure 2.6.1. Schematic representations of the types of primary shape-selectivity.
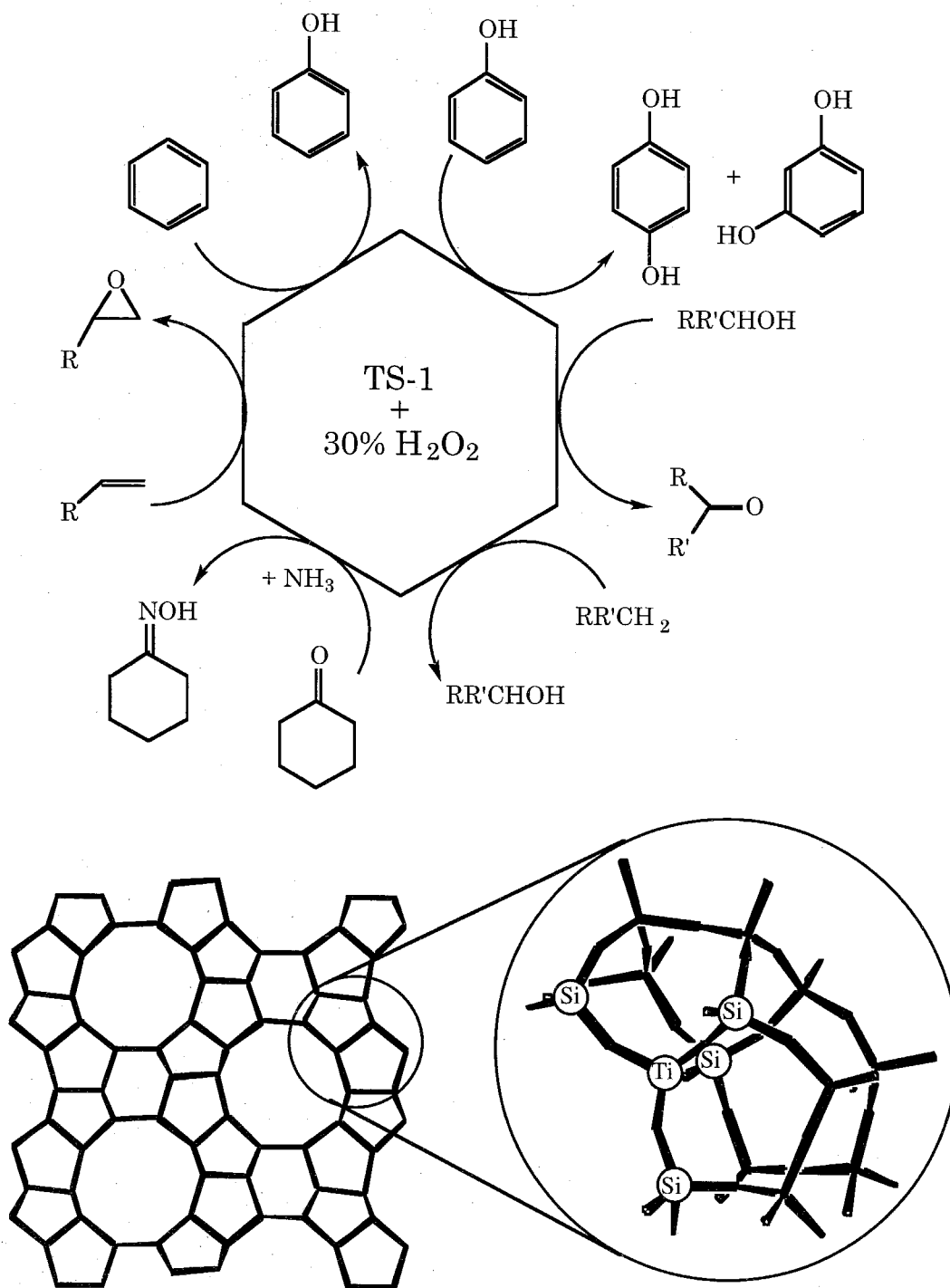
Figure 2.6.2.   Types of reactions catalyzed by TS-1 (schematic of titanium site in TS-1 is provided also).
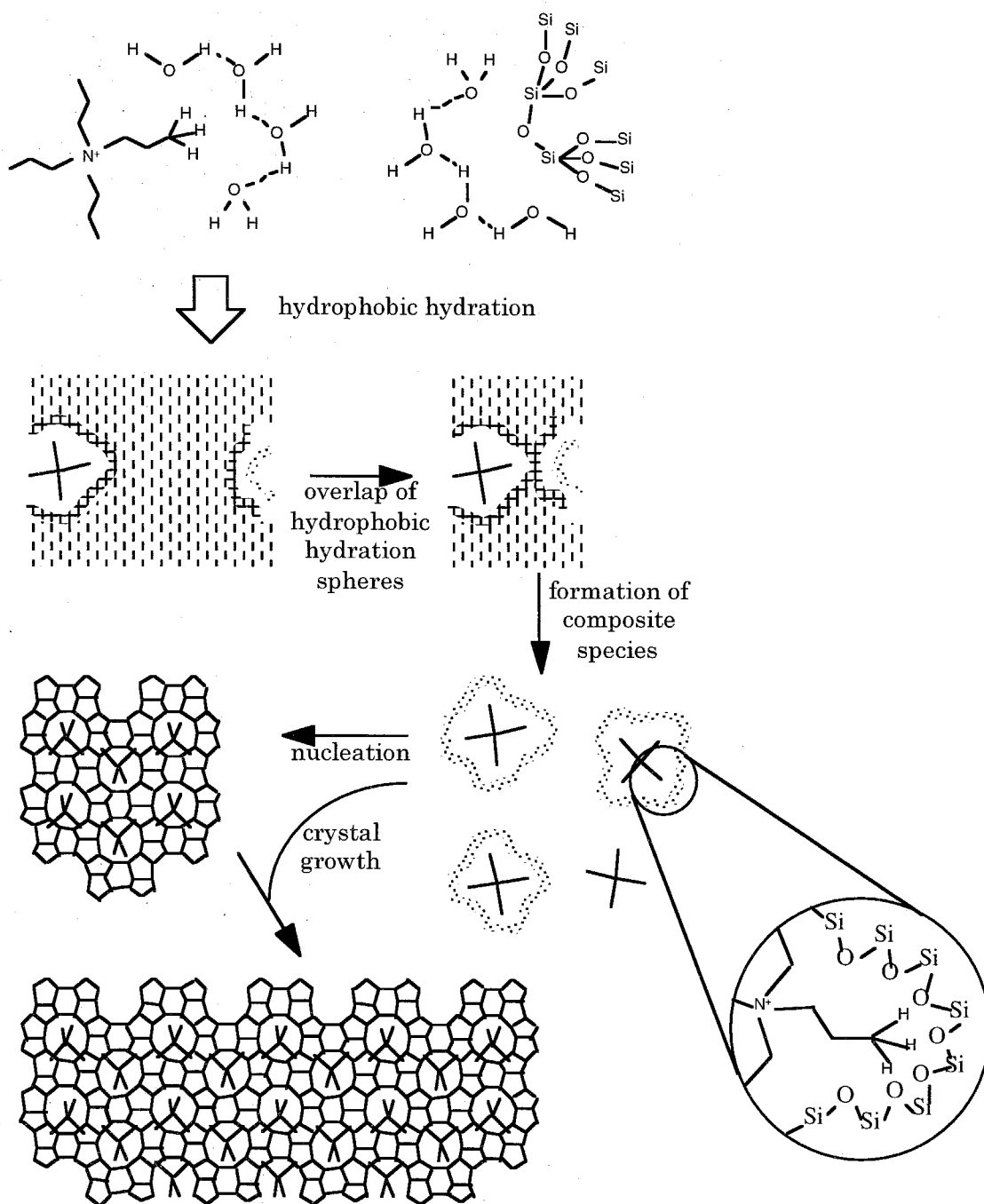
Figure 2.6.3. Schematic of proposed mechanism for the synthesis of ZSM-5 (adapted from ref. 107).

ZSM-12

10-ring

12-ring

SSZ-26
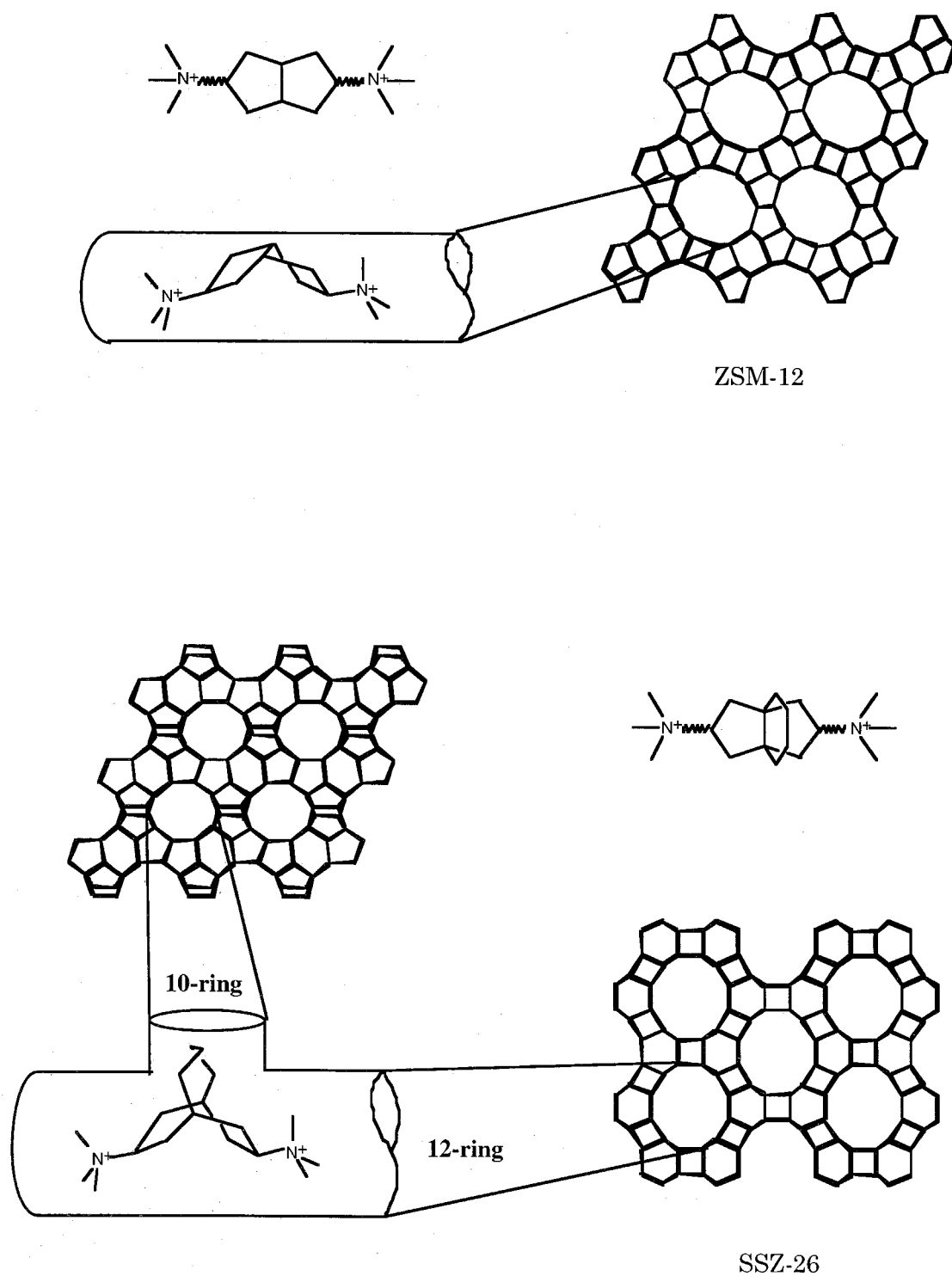
Figure 2.6.4   Schematic representations of organic SDA's and zeolites formed (adapted from ref. 114).

CHAPTER THREE

INVESTIGATIONS INTO THE MECHANISMS OF MOLECULAR RECOGNITION WITH IMPRINTED POLYMERS

Investigations into the Mechanisms of Molecular Recognition with Imprinted Polymers

Alexander Katz and Mark E. Davis

Chemical Engineering, California Institute of Technology, Pasadena, CA

Abstract.

The nature of molecular recognition in an imprinted polymer that is formed by the self-assembly of a binding monomer and an imprint through non-covalent interactions is investigated. The system studied uses ethylene glycol dimethacrylate, methacrylic acid and L-phenylalanine anilide as the crosslinking monomer, binding monomer and imprint, respectively, to assemble the imprinted polymer. A proposal for the self-assembly mechanism between the binding monomer and imprint that occurs during polymer synthesis is derived from a single crystal X-ray structure of a crystal containing binding monomer and imprint and from ^{1}H NMR and FTIR spectroscopy of solutions of these components. These studies show the presence of a salt-bridge interaction that leads to a 1:1 molecular complex between methacrylic acid and L-phenylalanine anilide and provide no evidence for the formation of higher order molecular complexes. Macroscopic phase separation is observed between the imprint and binding monomer and the crosslinking monomer in this system prior and subsequent to polymerization. These findings suggest a mechanism for enantioselective molecular recognition in the imprinted polymer involving remaining, occluded imprint molecules, which can provide for binding via imprint-imprint intermolecular interactions. Support for this mechanism is

provided from polymers prepared using a combination of imprint and mimic, L-phenylalanine 4-vinylanilide; the latter remains covalently bonded into the polymer and is shown to increase the rebinding of imprint while not significantly affecting the binding of the opposite enantiomer. Elucidation of this mechanism provides insight into the nature of site heterogeneity in imprinted polymer systems.

3.1 Introduction

A frequently-used method for the molecular imprinting of materials is that of non-covalent self-assembly.[1] The major advantage of this approach is its ease of implementation due to the fact that the imprinted site self-assembles during the synthesis process to generate binding interactions that are reversible and in many ways similar to interactions used by natural systems such as enzymes and antibodies (Scheme 3.1.1).[2] However, despite the growing acceptance of the method of non-covalent, molecular imprinting by self-assembly as a strategy for preparing templated materials, a significant problem that remains inherent to these materials is a strong binding site heterogeneity.[3] The objective of our work is to study the origins of binding site heterogeneity in these imprinted polymers by understanding the molecular level phenomena governing the imprinting effect and the subsequent capability of the imprinted polymer to perform molecular recognition. To this end, we investigated one of the most studied non-covalent, molecular imprinting systems that was originally introduced by

Mosbach and colleagues.[4] The system is comprised of a hydrophobic crosslinking monomer, ethylene glycol dimethacrylate **1** that serves as the mechanical support for the imprinted site and a binding monomer, methacrylic acid **2** that is proposed to form favorable hydrogen bonding and electrostatic interactions with the imprint L-phenylalanine anilide **3** (L-PheNHPh). Imprinted polymers that utilize the imprint L-PheNHPh have reported enantioselectivities of up to thirteen (defined as the ratio of the capacity factors of the L- and D- enantiomers (chromatographic)),[5] and other polymers using **1** and **2**, but other imprints have been reported to function as catalysts[6] that have shown enantioselectivity.[7]
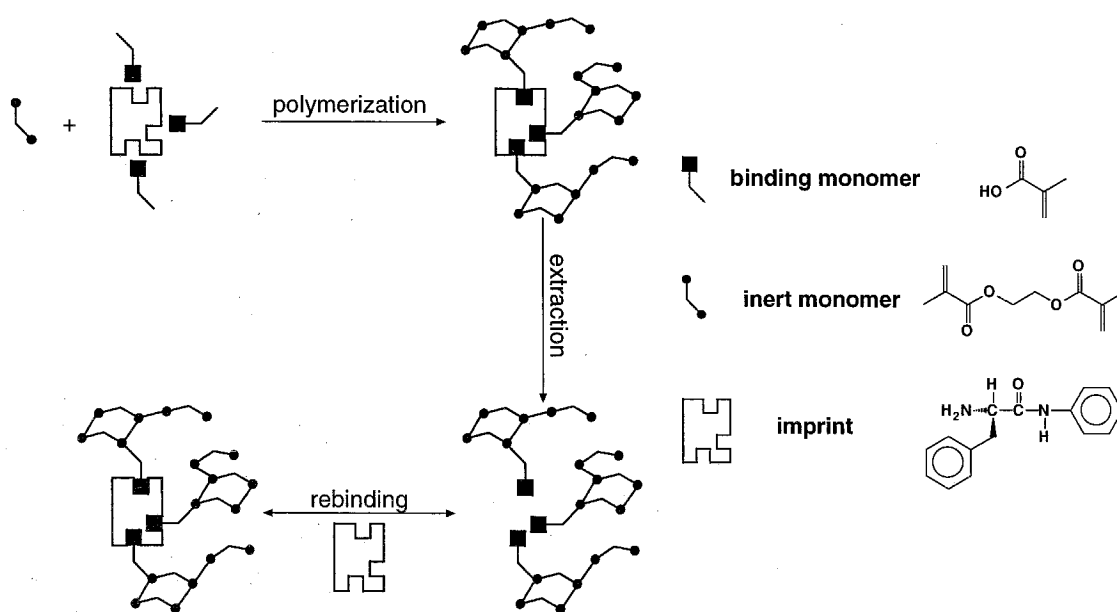
Scheme 3.1.1. Illustration of molecular imprinting by non-covalent self-assembly assuming that the imprint molecules are well-isolated from each other.

The primary goal of our work is to determine whether non-covalent, molecular imprinting by self-assembly in the L-PheNHPh system can fundamentally give rise to isolated molecular binding sites (Scheme 3.1.1) or to a phase separated composite involving a lattice of binding sites associated with one another via imprint-imprint intermolecular interactions (Scheme 3.1.2), or a combination of both situations. This ultimately reduces to a question of whether the imprint is homogeneously distributed throughout the polymer or whether it is clustered on some length scale that is accessible to a re-adsorbing species.

1

2

3

4
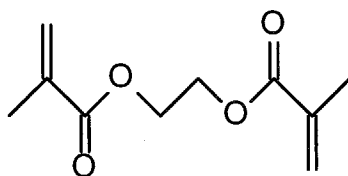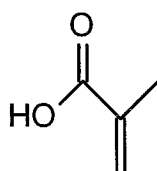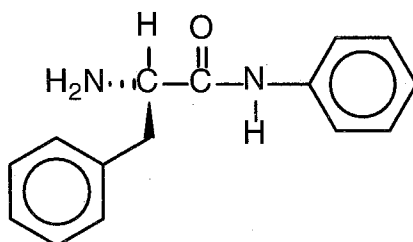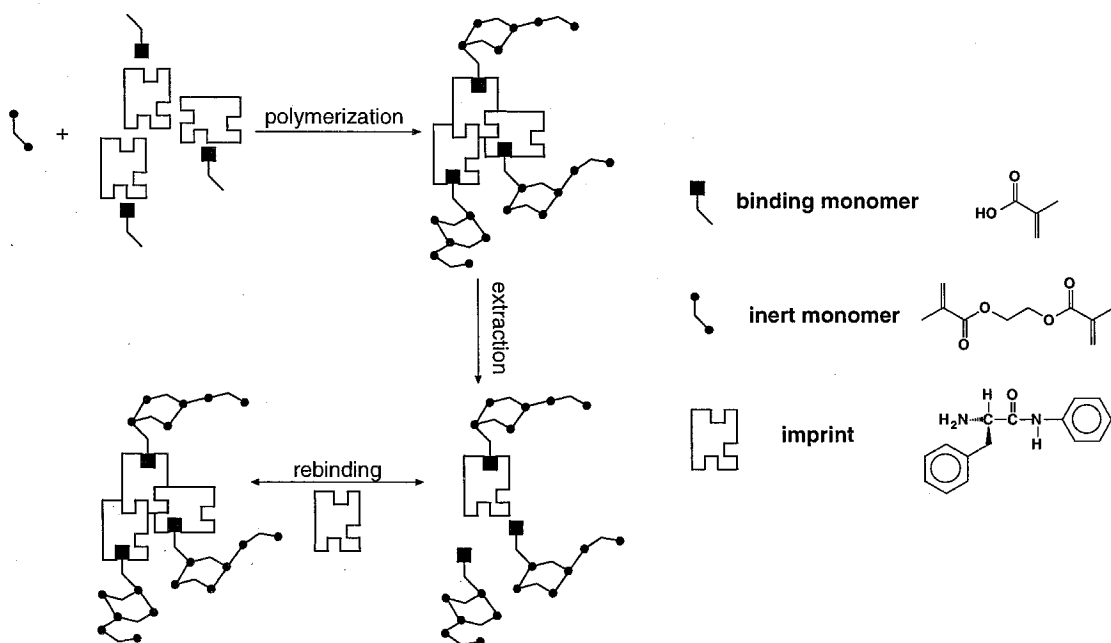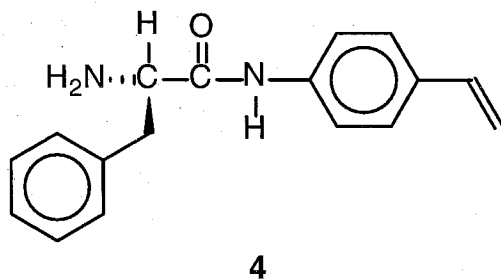
Scheme 3.1.2. Illustration of molecular imprinting by self-assembly assuming that the imprint molecules are not well isolated from each other. In this scenario, in addition to having binding monomer-imprint interactions, imprint-imprint interactions are also significant. The mechanism of molecular recognition here involves a combination of recrystallization-type interactions between adjacent imprint molecules and single point binding interactions between imprint and binding monomer.

To address this issue experimentally, we prepared a vinyl-containing mimic of the imprint **3**, the 4-vinylanilide derivative of phenylalanine, **4**. This mimic was chosen because of the analogy to **3** in terms of possible functional group interactions with **2**, its size complementarity to **3** and because it can be covalently incorporated into the imprinted material upon polymerization. Thus, the addition of **4** to the polymerization process allows some control over the amount of isolated imprint remaining in the polymer following imprint extraction. For the mechanism represented by Scheme 3.1.1, the addition of a small fraction of **4** to **3** as imprint into a molecularly imprinted polymer should slightly decrease the observed enantioselectivity and imprint adsorption capacity as compared with a material prepared only with **3** since there are fewer open binding sites available due to the presence of the covalently bound and unextractable imprint **4**. For the mechanism represented by Scheme 3.1.2, the addition of **4** should cause a significant increase in the observed enantioselectivity and imprint adsorption capacity, since there are more nucleation sites available for the recrystallization-type interactions.[8]

3.2   Results and Discussion

3.2.1   Characterization of the Self-Assembly Process

The interaction between L-PheNHPh and **2** has been investigated previously.[4] It was suggested that the binding monomer **2** and the imprint **3** self-assemble to form 3:1 complexes in the solution phase (in equilibrium with 2:1 and 1:1 complexes) prior to polymerization. These interactions were argued to be conserved during the polymerization process to subsequently

provide the basis for molecular recognition in the final imprinted material according to the mechanism depicted in Scheme 3.1.1.[9] Here, we collected ^{1}H NMR spectra from titrating as much as five equivalents of **2** with **3** at four different temperatures in both deuterated acetonitrile and chloroform (at the concentration of **3** corresponding to an imprinted polymer synthesis prior to polymerization). The most significant change in the ^{1}H NMR chemical shift occurs from the exchangeable proton of the ion pair between **2** and **3** as observed previously[4] (shown in Figure 3.2.1 as a function of the number of acid equivalents added). The ^{1}H NMR titration curves serve as a sensitive calibration for determining the number of acid equivalents in a solution of **2** and **3** (*vide infra*). FTIR can be used to analyze for the possibility of other hydrogen bonding interactions besides the ion pair interaction discussed above.[10] The carbonyl vibration of **3** was monitored by FTIR spectroscopy when titrating up to five molar equivalents of **2** at room temperature in chloroform solution. It is well established that hydrogen bonding has the general effect of broadening and lowering the frequency of the carbonyl stretch.[11] The results are presented in Figures 3.2.2 - 3.2.4 and indicate that there is little effect of acid addition on the carbonyl band of **3**. Indeed the frequency and width of the **3** carbonyl band remain virtually identical over the full concentration range of **2** investigated.[12] The spectroscopic evidence above provides no evidence for hydrogen-bonding interactions between **2** and **3** other than the single-point salt-bridge interaction. We note that it is not possible to rigorously dismiss the presence of other hydrogen bonding interactions separate from the salt-bridge interaction based solely on the spectroscopic evidence above, as the lack of spectroscopic signature upon

acid titration may be a result of a transition in the mode of hydrogen bonding in this system from intra-molecular to inter-molecular.

Upon addition of all monomers and free-radical initiator, phase separation can be observed optically in this system. As can be seen in Figure 3.2.5 (a small amount of chlorophenol red dye was used to help visualize the distribution of imprint **3** in the imprinted polymer mixture prior to polymerization), the mixture prior to polymerization is separated into two phases: one rich in imprint **3** that is stained dark by the dye (bottom) and one containing little imprint **3** that is clear (top). Figure 3.2.6 shows the visual appearance of an as-made L-PheNHPh imprinted polymer. In our hands, the degree of visually observable phase separation in a L-PheNHPh imprinted polymer varied from none (clear) to almost complete phase separation as shown in Figure 3.2.6, and we have found that small variations in the experimental procedure (such as the extent of dryness of solvents and monomers used in the imprinted polymer syntheses) can cause variability in the results (precise details therefore provided in the Experimental Section). It is important to note in this regard, that the materials used to collect adsorption data in all of the work presented here were from optically clear polymers, and optical photographs of these polymers are shown in Figures 3.2.7 and 3.2.8.

It is possible to isolate the needles precipitated from within the polymers shown in Figure 3.2.6 (some needles float to the top of the polymer during polymerization and can be subsequently scraped off with a spatula). Liquid phase ^{1}H NMR spectra of the needles dissolved in deuterated chloroform suggest that the needles are comprised of **2** and **3** in a molar ratio of 1:1.[13]

The ^{1}H and ^{13}C NMR spectra from the solution obtained by dissolving the needles in deuterated chloroform provide no evidence for the incorporation of **1** into the collected material and suggest that **2** and **3** can phase separate from **1** in the imprinted polymer as observed in the liquid phase prior to polymerization. To further characterize the complex formed between **2** and **3**, single-crystals were grown in a more controlled manner from a chloroform solution containing four molar equivalents of **2** relative to the concentration of **3**.[14]   Figure 3.2.9 shows an ORTEP plot and a stereoscopic representation for the structure solution of the crystal of **2** and **3** (crystallographic data are included in Tables 3.2.1 - 3.2.7).   The 1:1 stoichiometric composition of the crystal is consistent with the solution ^{1}H NMR and FTIR spectroscopic results discussed above.   The three molar equivalents of methacrylic acid remaining in the solution phase were confirmed by ^{1}H NMR experiments on the mother liquor after crystallization, indicating that acid in amounts greater than one equivalent is excluded from the **2-3** crystal under the conditions investigated.   It is important to emphasize for comparison that there are examples of self-assembled crystal systems that are comprised of acid-base building units and where more than one equivalent of acid is found to incorporate into the crystal via additional interactions.[15] To summarize information from the X-ray crystal structure solution, in the **2-3** crystal, there is a single point binding between **2** and **3** via the salt-bridge made by the acid proton and the amine, and there are no other independent interactions between **2** and **3** evident.   In terms of transferring chiral information between molecules in the crystal, the bond distances in Figure 3.2.9 show that there are two intermolecular interactions

that could potentially be responsible for this: a hydrogen bonding interaction between O1 and the H of N2 (labeled H22N) on an adjacent imprint molecule (fixes the position of the carbonyl oxygen) and an additional interaction between O1 and H of C15 (labeled H15) on an adjacent imprint molecule (fixes the position of the benzyl group).[16] These three intermolecular interactions (one between binding monomer and imprint and two between imprint and imprint) could be used for chiral molecular recognition in a manner consistent with Scheme 3.1.2.

3.2.2   *Polymer Prepared with Imprint Mimic*

In order to obtain insight into the mechanism of molecular recognition exhibited by the L-PheNHPh imprinted polymer, the significance of remaining imprint in the polymer subsequent to extraction was investigated. By synthesizing imprinted polymers without (**P1**) and with (**P2**) the synthetic mimic of **3** that is covalently retained in the imprinted material following extraction, **4**, the influence of remaining imprint can be ascertained. Wulff et al. used **4** as a mimic since it is close in terms of size and chemical functionality to the imprint **3**.[17] The approach here differs from Wulff et al. in that the mimic **4** is used in combination with **3**. Below, the complementary roles of the imprint and mimic are discussed for the mechanism depicted in Scheme 3.1.2. The mimic **4** can dissolve within a cluster of **2** and **3** at the self-assembly stage of imprinting.[18] This is facilitated in the present study by using a relatively small amount of **4** as imprint (100 ppm) in conjunction with **3**, since at these small fractions of **4**, the phase separation of **4** from **3** that might occur at higher amounts is minimized. Upon polymerization, both **2**

and **4** are covalently incorporated into the imprinted material (the symbols **2'** and **4'** will be used to refer to the covalently incorporated molecules of **2** and **4** respectively). It is expected that **4'** participates in similar intermolecular bonding to **2'** and adjacent molecules of **3**, as does **3**.[18] Upon extraction, the imprint molecules of **3** surrounding **4'** are removed. This results in regions of isolated **4'**. These <u>isolated</u> molecules of **4'** that are covalently bound to the polymer framework and interact with **2'** function as centers for rebinding in the mechanism of Scheme 3.1.2. If on the other hand the molecular recognition mechanism resembles that of Scheme 3.1.1, some of the imprinted binding pockets will be lost due to the covalent binding of **4'**. However, the addition of 100 ppm of **4** should have a small effect on the observed adsorption capacity and enantioselectivity.

Three imprinted polymers were synthesized and they are described in Table 3.2.8: **P1** is a reference polymer imprinted with **3**, **P2** is an imprinted polymer comprised of 100 ppm **4** and the remainder **3** as imprint and **P3** is a reference polymer imprinted solely with **4**. All polymers have the same morphology as ascertained by scanning electron microscopy and are macroporous as judged by nitrogen adsorption measurements (**P1**, **P2** and **P3** have BET surface areas within experimental error of each other and were on the order of 4 m^2/g). It is noteworthy that the percentage of **4** extracted from **P3** is of the same order of magnitude as the percentage of unreacted double bonds after complete monomer conversion in similar crosslinked systems.[19] This result suggests that **4** is covalently incorporated into the framework of the imprinted polymer. The relative amounts of **3** extracted in chloroform for **P1** and **P2** are consistent with those reported

elsewhere[3e] for L-PheNHPh imprinted polymer extraction in acetonitrile and acetonitrile/acetic acid.[20] It is often argued that the unextractable imprint is located in solvent "inaccessible" regions and can therefore be ignored from the point-of-view of participating in the imprinted polymer mechanism of molecular recognition.[21] This argument is reasonable if molecular recognition in the imprinted polymer follows Scheme 3.1.1. In this configuration, imprint that is unextractable occupies a templated site that could otherwise be used for molecular recognition and renders it inactive because of a lack of void space for adsorption. However, if Scheme 3.1.2 controls the molecular recognition in the imprinted material, then a small amount of residual imprint remaining in the polymer can still be significant from the perspective of serving as a nucleation center for adsorption (*vide infra*). Therefore, Scheme 3.1.2 cannot be disqualified on the basis of the amount of imprint extracted from the polymer, unless this number is 100%.

Table 3.2.9 presents adsorption data for separately adsorbing **3** and its enantiomer onto **P1** and **P2** in chloroform solvent at room temperature.[22] The magnitude of the amount of imprint adsorbed in **P1** and **P2** relative to the maximum number of theoretical sites based on the amount of imprint extracted from the polymer varies from a minimum of approximately 1.06% (D-enantiomer in **P2**) to a maximum of approximately 1.88% (L-enantiomer in **P2**). These values are consistent with those reported for other L-PheNHPh imprinted polymer systems.[3f] The effect of the 100 ppm addition of **4** is evident. The final solution concentration of **3** is 18.6±12% more for **P1** than for **P2** with the same initial conditions for adsorption (same adsorption conditions). That is to say, **P2** adsorbed 11.5±7% more **3** than

did **P1** under identical conditions. Thus, one molecule of **4'** acts as an adsorption center for 19 ± 11 molecules of **3** at the conditions used in the adsorption experiment.[23] The data in Table 3.2.9 have been reproduced on at least two different synthesis batches of materials and the adsorption experiments repeated approximately a dozen times on each of the materials.

3.3. Summary

The nature of the molecular recognition phenomena in the L-PheNHPh imprinted polymer system has been investigated. Our results show that: (i) macroscopic phase separation of **2-3** from the remainder of the crosslinked network can occur, (ii) solution spectroscopic and single crystal X-ray data provide no evidence for multiple-point interactions between **2** and **3** and (iii) the addition of **4'** into the polymer causes the adsorption of several molecules of **3** per **4'** (should be zero according to Scheme 3.1.1). These observations suggest that the mechanism schematically illustrated in Scheme 3.1.2 does contribute to the enantioselective molecular recognition exhibited by this imprinted polymer system under equilibrium binding conditions. The origin of enantioselective adsorption in Scheme 3.1.2 arises from weak interactions between an occluded molecule of **3** (or **4'**) and the molecules of **3** adsorbing from the fluid phases in a manner suggested above for the interactions occurring in the crystals of **2-3**.

The minimum active fraction of imprint that remains unextractable and participates in this type of adsorption mechanism can be estimated if the ratio of nineteen molecules of **3** per **4'** is assumed for molecules of **3** adsorbing per occluded **3**. With polymer **P1**, the calculation yields that only

0.087% of the initial amount of imprint that remains unextractable will be sufficient to account for the adsorption of **3** by **P1**. In other words, the extraction of imprint needs to be greater than 99.9% complete before the mechanism shown in Scheme 3.1.2 can be ruled out on the basis of mass balances.

Although one cannot disqualify the possibility that multiple mechanisms can occur in any real material, we suggest that Scheme 3.1.2 is the dominant one in the adsorption behavior of the L-PheNHPh imprinted polymer system under <u>equilibrium binding conditions</u>. In general, we cannot rule out the possibility that a very small number of sites like those represented in Scheme 3.1.1 exist (they could be below the detection limit of all of the methods used herein). These sites could provide for selective binding of very low concentrations of adsorbate[3d-g] and for separations by column chromatographic methods.[24] However, if such is the case, it is clear that one origin for site heterogeneity is that depicted in Scheme 3.1.2.[25]

3.4. Experimental Section

3.4.1 General Methods

All solvents and chemicals were purchased at the highest grade commercially available. These materials were not purified further except when used for the synthesis of the imprinted polymers. Solvents for the imprinted polymer syntheses were prepared as follows. Chloroform (EM Science Omnisolve Grade) was washed with distilled water three times followed by washings with saturated sodium bicarbonate and brine solutions. The chloroform was dried with calcium chloride for a period of 12

hours and subsequently dried with phosphorous pentoxide for a period of 24 hours. The chloroform was then distilled under positive argon pressure from the phosphorous pentoxide. Ethylene glycol dimethacrylate (Aldrich) was washed three times with 15% aqueous NaOH followed by washings with saturated sodium bicarbonate and brine solutions. The ethylene glycol dimethacrylate was dried with calcium chloride for a period of 12 hours and subsequently dried with calcium hydride for a period of 24 hours. It was then degassed by sonication and distilled under a vacuum of 300 mTorr from calcium hydride. Methacrylic acid (Aldrich) was dried for 24 hours with calcium chloride and distilled from the calcium chloride under a vacuum of 1 Torr prior to use for the imprinted polymer syntheses. All ^{1}H and ^{13}C NMR spectra were recorded using a General Electric QE 300 Plus spectrometer operating at 300.3 and 75.5 MHz respectively. Reported chemical shifts are relative to the central peak of the CHD_2CN heptet at 1.930 ppm (relative to TMS) for deuterated acetonitrile solvent or the $CHCl_3$ singlet at 7.240 ppm (relative to TMS) for deuterated chloroform. Liquid phase ^{19}F NMR spectra were recorded at 282.203 MHz in ^{19}F-labeled CCl_3F solvent using a Varian 300 MHz spectrometer. Weight measurements were performed using a Mettler AE 260 Deltarange balance (one tenth of a milligram resolution). Room temperature was controlled to be 24 ^oC (±1 ^oC) unless otherwise specified.

3.4.2   Synthesis of L-Phenylalanine Anilide

To a mixture of 105 mmol of N-t-BOC-phenylalanine (28 g) and 103 mmol of hydroxybenzotriazole (15.7 g) in 320 mL CH_2Cl_2 was added 116 mmol of dicyclohexylcarbodiimide (24 g) over ice cooling. Subsequently 116 mmol of aniline (10.6 mL) were added to the reaction mixture over ice cooling The reaction mixture was stirred at room temperature and monitored by TLC using 9:1 chloroform/methanol as eluent and Silica Gel 60 F_{254} plates (EM Science). The insoluble dicyclohexyl urea was filtered and the crude solution was redissolved in $CHCl_3$, washed with 0.1 M HCl/saturated sodium bicarbonate/brine solutions and dried over magnesium sulfate. The resulting solution was evaporated to a viscous oil and eluted through a silica gel column packed with Silica Gel 60 (EM Science) using 2.5:1 hexane:ethyl acetate as eluent. The crude product comprising N-t-BOC-phenylalanine anilide was recrystallized in chloroform/hexane at room temperature to give 88 mmol of transparent platelet crystals of N-t-BOC-phenylalanine anilide (30 g; yield 84%). Deprotection was initiated by adding neat trifluoroacetic acid under ice cooling to the crystals. The deprotection reaction was conducted at room temperature and monitored by a bubbler. When gas evolution had completely stopped the trifluoroacetic acid was evaporated to a viscous transparent oil. The oil was made basic and was extracted repeatedly with chloroform, washed with distilled water/saturated sodium bicarbonate/brine solutions and dried over potassium carbonate. Transparent platelets of the target compound were recrystallized from chloroform/hexane to give 62 mmol of product (14 g; yield 59%); mp 72 °C (uncorrected) [lit.[26] 71-72 °C]; $[\alpha]^{22}_D$ -136.7° (c 0.3, $CHCl_3$) [lit.[27] $[\alpha]^{20}_D$

+137 (c 0.3, CHCl$_3$) for D-Phenylalanine Anilide]. ^{1}H NMR (CDCl$_3$): 1.55 (2H, s, NH_2); 2.77 (1H, dd, J = 9.6 Hz, 13.8 Hz, CHH); 3.38 (1H, dd, J = 3.9 Hz, 13.8 Hz, CHH); 3.73 (1H, dd, J = 3.9 Hz, 9.6 Hz, CH); 7.08 - 7.62 (10H, m, Ph-H); 9.45 (1H, brs, CONH). ^{13}C{^{1}H} NMR (CDCl$_3$): 40.8 (Ph-CH$_2$); 56.9 (CHCO); 119.5 (CH); 124.2 (CH); 127.0 (CH); 128.9 (CH); 129.0 (CH); 129.4 (CH); 137.8 (C$_q$); 172.5 (C=O). *Anal.* Calcd for C$_{15}$H$_{16}$N$_2$O: C, 74.97; H, 6.71; N, 11.66. Found: C, 74.84; H, 6.85; N, 11.65.

3.4.3   Synthesis of L-Phenylalanine 4-Vinylanilide

To a mixture of 77 mmol of N-FMOC-L-Phenylalanine (30 g) and 83 mmol of 4-vinyl aniline (9.75 mL) in 250 mL THF under ice cooling and an argon atmosphere was added 80 mmol of diisopropylcarbodiimide (12.5 mL). The reaction mixture was stirred for approximately 3 hours at room temperature. Upon filtering the insoluble urea and evaporating the solvent, a crude product was crystallized from 500 mL of methanol. The crystals were filtered and washed with methanol. 68 mmol of N-FMOC-L-phenylalanine vinylanilide was isolated (33.2 g; yield 88%). Deprotection was performed by treating the crystals with a 5 vol% piperidine solution in THF overnight at room temperature. The THF was evaporated and the resulting crude flocculent precipitate was dissolved in ethyl acetate, evaporated to an oily residue and purified through a silica gel column packed with Silica Gel 60 using a gradient solvent mixture starting with 3-5% ethyl acetate in CH$_2$Cl$_2$ and ramping to 70% ethyl acetate in CH$_2$Cl$_2$ once the FMOC-piperidine complex was removed from the column as monitored by TLC using 8:2 CH$_2$Cl$_2$/ethyl acetate as eluent and Silica Gel 60 F$_{254}$ plates. Transparent

platelets of the desired L-phenylalanine vinyl anilide product were recrystallized from chloroform/hexane to give 43 mmol of product (11 g; yield 56%); mp 75 °C (uncorrected) [lit.[17] 79 °C]; $[\alpha]^{22}_{577}$ -101.7 ° (c 0.87, acetone). Enantiomeric purity was evaluated by derivitizing the final product with the NMR resolving agent S-(-)-α-methoxy-α-(trifluoromethyl)-phenylacetic acid; a single peak in the liquid phase ^{19}F NMR spectrum of the derivitized product was obtained.[28] ^1H NMR (CDCl$_3$): 1.53 (2H, s, N$\underline{H}_2$); 2.79 (1H, dd, J = 9.6 Hz, 13.8 Hz, C$\underline{H}$H); 3.39 (1H, dd, J = 3.8 Hz, 13.8 Hz, CH$\underline{H}$); 3.73 (1H, dd, J = 3.9 Hz, 9.6 Hz, CH); 5.22 (1H, d, J = 10.9 Hz, vinyl C$\underline{H}$H); 5.72 (1H, d, J = 17.6 Hz, vinyl CH$\underline{H}$); 6.70 (1H, dd, J = 10.9 Hz, 17.6 Hz); 7.25 - 7.61 (9H, m, Ar-$\underline{H}$); 9.52 (1H, s, CON$\underline{H}$). $^{13}C\{^1H\}$ NMR (CDCl$_3$): 40.8 (Ph-CH$_2$); 56.9 (CHCO); 113.0 (vinyl CHH); 119.5 (CH); 126.9 (CH); 127.0 (CH); 128.9 (CH); 129.4 (CH); 133.6 (C$_q$); 136.3 (CH); 137.4 (C$_q$); 137.8 (C$_q$); 172.5 (C=O). *Anal.* Calcd for C$_{17}$H$_{18}$N$_2$O: C, 76.67 H, 6.81; N, 10.52. Found: C, 76.43; H, 6.69; N, 10.49.

3.4.4   *Titration Experiments via ^1H NMR and FTIR Spectroscopies*

The samples for the titration studies were individually prepared in scintillation vials by weighing out portions of L-phenylalanine anilide and methacrylic acid to correspond to the desired number of equivalents for the particular sample being prepared. Chloroform or acetonitrile (deuterated for NMR) was then added so as to maintain an overall concentration of L-phenylalanine anilide of 0.1 M in the final solutions. The samples were then degassed for 15 minutes in a sonicator prior to analysis. For the titration experiments measured by ^1H NMR, all spectra were recorded at the

temperature stated in Figure 3.2.1 within a deviation of 0.2 ºC. For the case of the FTIR titration, all spectra were recorded at room temperature on a Nicolet System 800 FTIR spectrometer with a 0.1 mm path length, CaF_2 solution phase cell (Spectra Tech FT04-757) by averaging 256 scans.

3.4.5 X-ray Structure Determination Crystal Growth

10 mL of a 0.2 M solution of L-phenylalanine anilide in $CHCl_3$ were placed in a 20 mL scintillation vial and four molar equivalents of methacrylic acid (0.678 mL) were added. The open vial was then placed in a covered cylindrical TLC tank (10×20 cm) that was filled partially with hexane and carefully held there at room temperature. After a period of 3 days long needles were observed optically in the solution. A portion of these needles were extracted with tweezers under a polarizing microscope and used as specimens for the X-ray structure solution.

3.4.6 X-ray Structure Determination

Data were collected at room temperature on a Syntex (Crystal Logic) diffractometer with Cu Kα X-rays. The structure was solved by direct methods and refined to a final agreement factor of R = 5.8% and R_w = 6.0% for 803 reflections with F > 2σ(F). Calculated hydrogen positions were included in the structural analysis.

3.4.7 P1 Imprinted Polymer Reaction Mixture

A previously reported recipe was followed for all imprinted polymer syntheses.[3g] In a 38 mL pressure tube (Ace Glass 8648-29), 0.7209 g of L-phenylalanine anilide imprint and 5.1 mL $CHCl_3$ were combined. Upon complete dissolution of the imprint, 1.017 mL of methacrylic acid and 11.32 mL of ethylene glycol dimethacrylate were added. To this mixture 5.25 mL $CHCl_3$ containing 0.1232 g of azo-bis-isobutyronitrile were added. Finally 6 mL of $CHCl_3$ was added. The mixture was sealed with a septum for further processing.

3.4.8 P2 Imprinted Polymer Reaction Mixture

In a 38 mL pressure tube (Ace Glass 8648-29), 0.4806 g of L-phenylalanine anilide imprint and 4.4 mL $CHCl_3$ were combined. Upon complete dissolution of the imprint, 0.678 mL of methacrylic acid and 7.54 mL of ethylene glycol dimethacrylate were added. To this mixture, 3.5 mL $CHCl_3$ containing 0.0821 g of azo-bis-isobutyronitrile were added. 2 mL of $CHCl_3$ was added. Finally 1 mL of a 0.2 mM solution (2×10^{-7} mol total) of L-phenylalanine 4-vinylanilide in $CHCl_3$ was added to the reaction mixture, and the mixture was sealed with a septum for further processing.

3.4.9 P3 Imprinted Polymer Reaction Mixture

In a 38 mL pressure tube (Ace Glass 8648-29), 0.5327 g of L-phenylalanine 4-vinylanilide imprint and 5.0 mL $CHCl_3$ were combined. Upon complete dissolution of the imprint, 0.678 mL of methacrylic acid and 7.54 mL of ethylene glycol dimethacrylate were added in the order listed. To this

mixture, 3.5 mL $CHCl_3$ containing 0.0821 g of azo-bis-isobutyronitrile were added. Finally 2.4 mL of $CHCl_3$ was added. The mixture was sealed with a septum for further processing.

3.4.10   Imprinted Polymer Synthesis and Extraction

The sealed pressure tubes were freeze thaw degassed by submerging the tubes in liquid nitrogen and holding the frozen tubes under a vacuum of 100 mTorr for a period of at least 15 minutes for each cycle. Each sample was freeze thaw degassed in this manner for three cycles. The tubes were then thawed and charged with a positive pressure of argon. The tubes were placed in ice-filled liquid nitrogen dewars and temperature equilibrated. These dewars were then placed under a water cooled medium-pressure mercury vapor lamp (Conrad Hanovia 550 W) for a period of 24 hours. During this time the tubes were turned and the ice in the dewars changed three times to maintain a constant temperature of 0 °C during the entire polymerization.[29] Upon completion of the polymerization, the tubes were taken out of the dewars and crushed. The polymers were ground in a ball mill (Spex 8000) and dry sieved (Spex 3536) to a size between 100 mesh (149 µm) and 200 mesh (74 µm). The sieved polymer particles were dried at room temperature for a period of 24 hours in a 10 mL airless flask connected to a vacuum manifold to remove residual solvent (40 mTorr). The weighed polymers were placed in a cellulose extraction thimble (Whatman 2800199) and Soxhlet extracted in $CHCl_3$ for a period of 24 hours.[30] The extracted polymers were dried at room temperature for a period of 24 hours in a 10 mL airless flask on a vacuum manifold (40 mTorr). The extract was filtered

directly into a clean scintillation vial using a 0.7 μm pore size GF/F Filter Media syringe filters (Whatman 6825-1307). The extract was diluted, and its UV absorbance value was recorded at a fixed wavelength of 260.0 nm and a 1 second integration time using a Beckman DU-640 spectrophotometer and blackened standard size UV cells (Starna 29BQ10). The amount extracted was calculated directly from this absorbance value using a theoretical maximum amount extracted of 0.2179 mmol imprint per gram of solvent-free as-synthesized polymer and ε (260 nm) = 8523 M^{-1} (for **P3** the theoretical maximum amount is 0.2166 mmol imprint per gram of solvent-free as-synthesized polymer and ε (260 nm) = 15083 M^{-1}).

3.4.11 Liquid Phase Dye Visualization Procedures

In a disposable culture tube, 0.0961 g of L-phenylalanine anilide imprint, 0.4 mg chlorophenol red dye (Sigma) and 0.5 mL $CHCl_3$ were combined. Upon complete dissolution of the imprint, 136 μL of methacrylic acid and 1.5 mL of ethylene glycol dimethacrylate were added. To this mixture 0.7 mL $CHCl_3$ containing 16 mg of azo-bis-isobutyronitrile were added. Finally 0.98 mL $CHCl_3$ was added.

3.4.12 Batch Adsorption Experiments with Imprinted Polymers

In a short form 1 dram (4 mL) vial covered with a Teflon cap (Qorpak 5200), 40 mg of imprinted polymer and 4.0 mL of D- or L-phenylalanine anilide at a concentration of 6.18×10^{-5} M in $CHCl_3$ (target absorbance value of 0.5265 in $CHCl_3$ since ε (260 nm) = 8523 M^{-1}) were added into the vial. The vial was covered, and the mixture in the vial was stirred using a flea micro stirring bar

(Bel-Art) at room temperature. The solutions in the vials were equilibrated for a period of 24 hours at these conditions. Afterwords, the contents of the vial were filtered directly into a UV cuvette using a 0.7 µm pore size GF/F Filter Media syringe filters (Whatman 6825-1307). All UV measurements were performed at a fixed wavelength of 260.0 nm and a 1 second integration time using a Beckman DU-640 spectrophotometer and blackened standard size UV cells (Starna 29BQ10).

3.5. References

[1]   (a) Wulff, G. In *Polymeric Reagents and Catalysts*; Ford, W. T., Ed.; ACS Symposium Series 308; American Chemical Society: Washington, DC, 1986. (b) Ekberg, B.; Mosbach, K. *Trends Biotech.* **1989**, *7*, 92.

[2]   (a) Mosbach, K. *Trends, Biochem. Sci.* **1994**, *19*, 9. (b) Mosbach, K. U.S. Patent 5 110 833, 1992. (c) Andersson, L. I.; Nicholls, I. A.; Mosbach, K. In *Immunoanalysis of Agrichemicals*, Nelson, J. O.; Karu, A. E.; Wong, R. B., Eds.; ACS Symposium Series 586; American Chemical Society: Washington, DC, 1995. (d) Ansell, R. J.; Ramström, O.; Mosbach, K. *Clin. Chem.* **1996**, *42*, 1506.

[3]   (a) Matsui, J.; Miyoshi, Y.; Doblhoff-Dier, O.; Takeuchi, T. *Anal. Chem.* **1995**, *67*, 4404. (b) Matsui, J.; Kaneko, A.; Miyoshi, Y.; Yokoyama, K.; Tamiya, E.; Takeuchi, T. *Anal. Lett.* **1996**, *29*, 2071. (c) Tomioka, Y.; Kudo, Y.; Hayashi, T.; Nakamura, N.; Niizeki, M.; Hishinuma, T.; Mizugaki, M. *Biol. Pharm. Bull.* **1997**, *20*, 397. (d) Sellergren, B.; Shea, K. J. *J. Chromatogr.* **1995**, *690*, 29. (e) Sellergren, B. *Chirality* **1989**, *1*, 63. (f) Sellergren, B. *Makromol. Chem.* **1989**, *190*, 2703. (g) Sellergren, B.; Shea, K. J. *J. Chromatogr.* **1993**, *635*, 31.

[4]   Sellergren, B.; Lepistö, M.; Mosbach, K. *J. Am. Chem. Soc.* **1988**, *110*, 5853.

[5]   Sellergren, B.; Shea, K. J. *J. Chromatogr.* **1993**, *654*, 17.

[6]   Davis, M. E.; Katz, A.; Ahmad, W. R. *Chem. Mater.* **1996**, *8*, 1820.

[7]   Sellergren, B.; Shea, K. J. *Tetrahedron A* **1994**, *5*, 1403.

[8]   (a) The relation implied between the number of nucleation sites and the enantioselectivity relies on the concept of continuous overloading of binding sites in this system as discussed in ref. 3(d)-(g) For other discussion of nucleation sites formed from residual imprint in an imprinted polymer system, see: (b) Dickey, F. H. *Proc. Natl. Acad. Sci. USA* **1949**, *35*, 227. (c) Dickey, F. H. *J. Phys. Chem.* **1955**, *59*, 695. (d) Morrison, J. L.; Worsley, M.; Shaw, D. R.; Hodgson, G. W. *Can. J. Chem.* **1959**, *37*, 1986.

[9]   A minimum of three independent binding interactions are required for enantioselective molecular recognition (see Ogsten, A. G. *Nature* **1948**, *162*, 963). For discussion related to a more modern application, see for example: Arena, G.; Bonomo, R.; Casella, L.; Gullotti, M.; Impellizzeri, G.; Maccarrone, G.; Rizzarelli, E. *J. Chem. Soc. Dalton Trans.* **1991**, 3203 and discussion therein.

[10]   There are several literature examples that show spectroscopic evidence for multi-point hydrogen bonding interactions. Significant IR shifts are observed for the N-H stretching vibrations corresponding to each of the three functional groups involved in the hydrogen bonding between the adenine and uracil derivatives 2,6-diamino-9-ethylpurine and 1-cyclohexyl-5-bromouracil (Kyogoku, Y., Lord, R. C., and Rich, A. *Proc. Natl. Acad. Sci. USA* **1967**, *57*, 250).

[11]   (a) Sherry, D. A. In *The hydrogen bond - recent developments in theory and experiments*; Schuster, P., Zundel, G., and Sandorfy, C., Eds.; North-Holland Publishing Company: Amsterdam, Holland,

1976. (b) Bellamy, L. J. *The Infrared Spectra of Complex Molecules Volume 2*, 2nd ed.; Chapman and Hall: New York, New York 1980.

[12] Liquid phase ^{13}C NMR in deuterated chloroform was used to corroborate the FTIR results. To avoid accidental overlap of the carbonyl carbon resonances between **3** and the acid **2**, a titration experiment was performed with the structurally similar propionic acid and **3** using the same experimental conditions described in the manuscript for the FTIR titration. It has been previously established that a hydrogen bond involving the C=O functional group shifts the carbonyl carbon resonance downfield (Kalinowski, H., Berger, S., and Braun, S. *Carbon-13 NMR Spectroscopy*, John Wiley & Sons, 1988). No downfield shift in the carbonyl carbon resonance of **3** was observed during the course of titrating up to four molar equivalents of propionic acid.

[13] ^{1}H NMR of the isolated crystals was performed under the same conditions as those used in Figure 3.2.1 (the crystal was dissolved at the same concentration of **3** in deuterated chloroform). Integration of the exchangeable proton yielded three protons indicative of a 1:1 molar ratio of **2** and **3** in the crystal. By measuring the chemical shift of the exchangeable proton at 23 °C to be 5.24 ppm (5.27 ppm predicted from Figure 3.2.1), it was further determined that the crystal comprised a 1:1 molar ratio of **2** and **3**.

[14] In an attempt to resolve any potential differences between material grown in the polymer during material synthesis and crystals grown for

the single crystal study as described in the manuscript, X-ray powder diffraction on the single crystals and the collected material from the polymer synthesis was performed. The overlap in the X-ray powder diffraction patterns indicates that the material formed under polymerization conditions is indeed structurally the same with that synthesized under more careful conditions to yield large single crystals.

[15]   Félix, O., Hosseini, M. W., DeCian, A., and Fischer, J. *Angew. Chem. Int. Ed. Engl.* **1997**, *36*, 102.

[16]   For an example of the interaction between an amide carbonyl oxygen and an aryl hydrogen, see: Johnson, S. W.; Eckert J.; Barthes, M.; McMullan, R.K.; Muller, M. *J. Phys. Chem.* **1995**, *99*, 16253.   Other examples of amide carbonyl oxygen and aryl interactions can be found in : (a) Bone, R.; Lu, Tianbao, Illig, C. R.; Soll, R. M.; Spurlino, J. C. *J. Med. Chem.* **1998**, *41*, 2068.   (b) Hibbert, F.; Mills, J. F.; Nyburg, S. C.; Parkins, A. W. *J. Chem. Soc., Perkin Trans. 2* **1998**, 629. (c) Brandstetter, H.; Kühne, A.; Bode, W.; Hubert, R.; von der Saal, W.; Wirthensohn; K.; Engh, R. A. *J. Biol. Chem.* **1996**, *271*, 29988.

[17]   Wulff, G.; Best, W.; Akelah, A. *React. Polym.* **1984**, *2*, 167.

[18]   A crystal **C1** was synthesized from a chloroform solution containing initially 70 mol% **3** and 30 mol% **4** as the amino-acid derivative content and four molar equivalents of methacrylic acid by using the same procedures for crystal growth as described in the Experimental Section.   Most major reflections in the X-ray powder pattern of this

crystal overlap with the crystal synthesized from **3** alone, indicating that the species comprising both crystals are similar in their orientation and positioning. Based on the integration of the vinyl proton resonances of the ^{1}H NMR of dissolved crystal **C1** in deuterated chloroform, it was estimated that the content of **4** in the crystal **C1** was approximately 21 mol%, indicating 70 mol% incorporation of **4** from the mother liquor into the crystal. A single amine proton resonance was observed in the ^{1}H NMR of dissolved crystal **C1** in deuterated chloroform, which is consistent with the similarity of **4** and **3** in interacting with **2** in the solution phase.

[19] Hjertberg, T.; Hargitai, T.; Reinholdsson, P. *Macromolecules* **1990**, *23*, 3080.

[20] Further Soxhlet extraction of **P1** in a mixture of 7:3 MeOH:Acetic Acid (v:v) for 24 hours and chloroform for 36 hours resulted in a polymer posessing an adsorption capacity for the imprint in the amount of less than 1% relative to **P1**. Furthermore no increase in the enantioselectivity was observed by comparison to **P1**. Confocal fluoresence microscopy (Biorad 600 Confocal Fluoresence Microscope using excitation wavelength of 568 nm and emission wavelength of longpass filter 50% level at 587 nm) was used to observe occluded imprint following extraction. An imprinted polymer was synthesized and processed for this purpose according to the same experimental procedure as for **P1** only using L-phenylalanine β-naphthylamide (Sigma) as the imprint. The faint fluorescence

observed in the extracted polymer signifies that some imprint still remains in the polymer subsequent to extraction.

[21] Sellergren, B.; Ekberg, B.; Mosbach, K. *J. Chromatogr.* **1985**, *347*, 1.

[22] As determined by Wulff et al. (ref. 16), the reference polymer **P3** did not possess enantioselectivity for **3** at the adsorption conditions used in this investigation. This result does not preclude the validity of either Scheme 3.1.1 or 3.1.2, since no imprint has been extracted for the creation of void spaces.

[23] Assuming an average of 93% imprint extraction from the imprinted polymers, one obtains that there are 8.5196×10^{-3} mmol theoretical binding sites per 40 mg of extracted imprinted polymer (based on the amount of imprint originally in the polymer prior to extraction). **P1** adsorbed the equivalent 1.68% of the theoretical maximum of sites with **3** while **P2** adsorbed the equivalent of 1.88% of the theoretical maximum of sites with **3**. Upon calculating the difference between these two polymers and dividing it by the fraction of **4** in **P2** (0.01%) gives 19 ± 11 molecules of **3** adsorbed per fragment of **4**. This is an underestimate of the value because a small fraction of **4** is extracted after synthesis and prior to adsorption.

[24] Kempe, M. and Mosbach, K. *J. Chromatogr.* **1995**, *694*, 3.

[25] Sellergren, B. and Lepistö, M. *J. Org. Chem.* **1989**, *54*, 6010.

[26] Ikota, N.; Hanaki, A. *Heterocycles* **1984**, *22*, 2227.

[27] Yamaguchi, S. In *Asymmetric Synthesis*; Morrison, J. D., Ed.; Academic Press: New York, 1983; Vol. 1.

[28]   O'Shannessy, D. J.; Ekberg, B.; Mosbach, K. *Anal. Biochem.* **1989**, *177*, 144.

[29]   Prior to extracting any of the polymers, the rates of mass transfer under the adsorption conditions used (at room temperature) were investigated.   The average time to achieve mass-transfer limited equilibration in a L-PheNHPh imprinted polymer (prepared identically to the procedure given for **P1**) is on the order of 10 minutes for the L- and D- enantiomers of **3** with the particle sizes used in this work.

Formula	C19 H21 N2 O3
Fw	325.39
Cryst Syst	monoclinic
Space Group	P21
Cryst Color	colorless
Cryst Habit	plate
a, Å	12.76(1)
b, Å	6.100(5)
c, Å	11.646(9)
β, deg	98.64(3)
Z	2
V, Å^3	896(1)
ρ (calcd), g cm^{-3}	1.206
radiation, λ	Cu k$_\alpha$ 1.5418
abs coeff (μ), mm^{-1}	0.630
F(000), e	346
temp, K	298
diffractometer	Syntex (Crystal Logic)
scan mode, speed (deg/min)	θ-2θ, 3.0
2θ range, deg	7.0 - 115.0
total data collcd, unique data saved	1435, 803 (I> 2σ(I))
no. of parms refined	216
final shift/error, max and avg	0.002, 0.001
max resid density, e/Å^3	0.38
$R = \sum \lvert\, \lvert F_o\rvert - \lvert F_c\rvert\,\rvert / \sum \lvert F_o\rvert$	0.058
$R_w = \left(\sum w(\lvert F_o\rvert - \lvert F_c\rvert)^2 / \sum w(\lvert F_o\rvert)^2 \right)^{1/2}$	0.060
$GOF = \left(\sum w(\lvert F_o\rvert - \lvert F_c\rvert)^2 /(No - Nv) \right)^{1/2}$	1.689

Table 3.2.1. Details of data collection and structure refinement for **2-3** crystal.

Atom	x	y	z	$U_{eq} \times 10^3$
N1	0.7663(6)	0.2778	0.7649(6)	57(5)
N2	1.0211(5)	0.4262(18)	0.9238(5)	49(5)
O1	0.9077(5)	0.0610(16)	0.8347(6)	64(5)
O2	1.1862(5)	0.1444(19)	0.9546(6)	82(6)
O3	1.1219(5)	-0.1879(17)	0.9282(5)	66(5)
C1	0.6840(7)	-0.0778(23)	0.7959(8)	61(8)
C2	0.6000(8)	-0.2231(24)	0.7636(9)	69(8)
C3	0.5220(9)	-0.1728(27)	0.6727(10)	82(10)
C4	0.5234(9)	0.0207(27)	0.6156(9)	82(10)
C5	0.6058(7)	0.1720(21)	0.6455(8)	62(8)
C6	0.6843(7)	0.1175(22)	0.7366(8)	51(7)
C7	0.8702(7)	0.2421(24)	0.8103(8)	49(7)
C8	0.9394(6)	0.4453(18)	0.8200(8)	48(7)
C9	0.9934(7)	0.4761(20)	0.7120(8)	61(7)
C10	0.9143(7)	0.5224(23)	0.6034(8)	61(8)
C11	0.8923(8)	0.3676(24)	0.5135(10)	82(10)
C12	0.8190(10)	0.4107(31)	0.4176(11)	102(12)
C13	0.7699(10)	0.6089(36)	0.4045(11)	101(12)
C14	0.7870(9)	0.7556(26)	0.4926(12)	94(11)
C15	0.8599(8)	0.7194(22)	0.5893(8)	69(9)
C16	1.1972(8)	-0.0577(26)	0.9321(8)	58(8)
C17	1.3072(7)	-0.1278(23)	0.9133(8)	56(7)
C18	1.3198(8)	-0.3580(26)	0.8902(10)	87(10)
C19	1.3891(7)	0.0241(25)	0.9217(9)	90(10)

$$U_{eq} = [1/(6\pi^2)] \times \Sigma_i \Sigma_j \beta_{ij} a_i \cdot a_j$$

Table 3.2.2.   Fractional atomic coordinates and equivalent isotropic thermal paramters ($Å^2$) with e.s.d.'s of the refined parameters in parenthesis for **2-3** crystal.

Atom	x	y	z
H1	0.7418	-0.1105	0.8615
H2	0.5997	-0.3681	0.8036
H3	0.4612	-0.2758	0.6521
H4	0.4641	0.0531	0.5516
H5	0.6077	0.3119	0.6012
H8	0.8968	0.5812	0.8250
H9	1.0320	0.3372	0.7005
H9	1.0450	0.6004	0.7233
H11	0.9341	0.2286	0.5187
H12	0.7977	0.2916	0.3599
H13	0.7253	0.6484	0.3294
H14	0.7420	0.8899	0.4901
H15	0.8769	0.8372	0.6488
H1N	0.7448	0.4342	0.7506
H21N	1.0906	0.3361	0.9410
H22N	1.0038	0.3944	1.0089
H18A	1.2816	-0.4493	0.9420
H18B	1.3960	-0.4022	0.9001
H18C	1.2874	-0.3830	0.8076
H19A	1.3812	0.1605	0.9670
H19B	1.4530	0.0003	0.8830

Table 3.2.3.   Final fractional atomic coordinates for H-Atoms for **2-3** crystal.

From	To	Distance
N1	C7	1.37(1)
N1	C6	1.43(1)
N2	C8	1.477(9)
O1	C7	1.22(1)
O2	C16	1.27(1)
O2	O3	2.19(1)
O3	C16	1.24(1)
C1	C6	1.38(1)
C1	C2	1.40(1)
C2	C3	1.37(1)
C3	C4	1.36(1)
C4	C5	1.40(1)
C5	C6	1.39(1)
C7	C8	1.52(1)
C8	C9	1.53(1)
C9	C10	1.52(1)
C10	C15	1.39(1)
C10	C11	1.41(1)
C11	C12	1.37(1)
C12	C13	1.36(2)
C13	C14	1.35(2)
C14	C15	1.37(1)
C16	C17	1.51(1)
C17	C19	1.39(1)
C17	C18	1.44(1)

Table 3.2.4. Interatomic distances (Å) involving non-H atoms with e.s.d's in parentheses for **2-3** crystal.

From	Thru	To	Angle
C7	N1	C6	127.7(9)
C6	N1	O1	101.3(6)
C6	C1	C2	118.2(9)
C3	C2	C1	120(1)
C4	C3	C2	121(1)
C3	C4	C5	121(1)
C6	C5	C4	117(1)
C1	C6	C5	122(1)
C1	C6	N1	122.1(9)
C5	C6	N1	116(1)
O1	C7	N1	123.8(9)
O1	C7	C8	121.3(8)
N1	C7	C8	114.7(9)
N2	C8	C7	109.1(8)
N2	C8	C9	109.4(7)
C7	C8	C9	111.5(8)
C10	C9	C8	112.4(7)
C15	C10	C11	117.0(9)
C15	C10	C9	121(1)
C11	C10	C9	122(1)
C12	C11	C10	121(1)
C13	C12	C11	121(1)
C14	C13	C12	119(1)
C13	C14	C15	122(1)
C14	C15	C10	120(1)
O3	C16	O2	121(1)
O3	C16	C17	123(1)
O2	C16	C17	116(1)
C19	C17	C18	124(1)
C19	C17	C16	120(1)
C18	C17	C16	116(1)

Table 3.2.5. Bond angles (degrees) involving non-H atoms with e.s.d's in parentheses for **2-3** crystal.

Atom	$U_{11} \times 10^3$	$U_{22} \times 10^3$	$U_{33} \times 10^3$	$U_{12} \times 10^3$	$U_{13} \times 10^3$	$U_{23} \times 10^3$
N1	52(5)	40(5)	77(5)	3(5)	-2(4)	2(5)
N2	33(4)	63(6)	48(4)	3(4)	-7(3)	5(4)
O1	54(4)	47(5)	85(5)	4(4)	-9(4)	-2(4)
O2	48(4)	61(5)	138(7)	-5(4)	18(4)	-20(5)
O3	61(4)	46(5)	94(5)	-11(4)	19(4)	4(4)
C1	60(7)	61(8)	65(7)	10(7)	16(5)	0(7)
C2	63(7)	59(7)	91(8)	-4(7)	28(6)	-5(7)
C3	62(8)	100(11)	84(9)	-30(8)	11(7)	-22(9)
C4	75(8)	97(10)	68(8)	-18(8)	-6(6)	5(8)
C5	55(6)	69(8)	55(7)	-12(6)	-17(5)	0(6)
C6	50(6)	46(6)	57(7)	-3(5)	5(5)	-8(6)
C7	49(6)	61(8)	38(5)	8(6)	8(5)	7(6)
C8	45(6)	39(6)	62(6)	2(5)	14(5)	-1(5)
C9	57(6)	67(8)	62(6)	-6(6)	21(6)	-3(6)
C10	55(6)	71(9)	60(8)	8(6)	19(6)	8(7)
C11	88(9)	79(9)	80(8)	0(7)	18(7)	-36(8)
C12	119(12)	114(13)	64(9)	-10(11)	-12(8)	-46(10)
C13	106(10)	131(13)	64(9)	-4(10)	3(7)	-8(11)
C14	100(9)	93(10)	89(9)	16(9)	14(8)	3(10)
C15	78(7)	68(9)	58(7)	6(7)	-1(6)	-19(6)
C16	62(7)	65(9)	45(6)	15(7)	4(5)	-11(7)
C17	46(6)	63(8)	62(6)	10(6)	19(5)	-4(6)
C18	70(8)	85(10)	110(9)	16(8)	26(7)	20(9)
C19	55(6)	89(10)	133(10)	-12(7)	33(7)	-40(8)

The complete temperature factor is

$$\exp[-2\pi^2(a^{*2}U_{11}h^2 + b^{*2}U_{22}k^2 + c^{*2}U_{33}l^2$$

$$+ 2a^*b^*U_{12}hk + 2a^*c^*U_{13}hl + 2b^*c^*U_{23}kl)] .$$

Table 3.2.6.   Anisotropic temperature factors for **2-3** crystal.

Table 3.2.7.   Observed and calculated structure factor listing for **2-3** crystal.

Table is five pages long including this page.
Table contains 803 reflections.
Scale factor is 9.245
Actual F is the printed F divided by the scale factor.

K	L	FO	FC
****	H = 0	****	
0	2	53	50
0	3	88	89
0	4	144	137
0	5	40	38
0	6	223	212
0	7	214	203
0	8	83	82
0	9	129	124
0	10	60	60
0	12	49	56
1	1	267	260
1	2	44	43
1	3	290	308
1	4	112	116
1	5	29	28
1	6	121	122
1	7	76	71
1	9	61	64
1	10	38	50
1	11	43	36
2	0	93	93
2	1	127	127
2	2	75	78
2	3	81	80
2	4	203	193
2	5	121	121
2	7	125	126
2	8	78	90
2	9	76	79
3	1	140	134
3	2	47	42
3	3	42	42
3	4	147	145
3	6	43	43
3	8	49	55
4	1	72	67
4	2	79	82
4	3	37	40
4	5	62	65
4	10	35	28
5	1	48	61
5	2	85	93
5	3	53	37
5	4	52	60
5	8	43	36
6	0	42	52
6	1	35	42
6	2	53	52
6	3	53	65
6	4	38	50
****	H = 1	****	
0	-10	40	56

K	L	FO	FC
0	-9	63	61
0	-8	108	105
0	-7	53	50
0	-6	42	41
0	-5	141	137
0	-4	426	412
0	-3	926	999
0	-2	32	32
0	1	157	175
0	2	427	460
0	3	456	465
0	4	495	495
0	5	184	179
0	6	54	49
0	7	30	22
0	8	122	122
0	9	170	175
1	-11	43	55
1	-10	78	71
1	-8	46	39
1	-7	121	123
1	-6	167	170
1	-5	66	69
1	-4	153	153
1	-3	123	118
1	-2	650	656
1	-1	355	351
1	0	336	331
1	1	535	537
1	2	181	176
1	3	263	267
1	4	74	85
1	5	74	79
1	6	116	116
1	7	77	74
1	8	84	75
1	9	64	63
1	11	52	55
2	-11	70	65
2	-10	49	42
2	-7	74	80
2	-6	31	30
2	-5	148	141
2	-4	65	63
2	-3	80	77
2	-2	198	197
2	-1	101	103
2	0	221	214
2	1	113	104
2	2	244	241
2	3	66	65
2	4	68	68
2	5	96	98
2	6	88	103
2	7	71	74

K	L	FO	FC
2	8	45	26
2	9	45	46
3	-5	91	86
3	-4	61	62
3	-3	146	148
3	-2	169	166
3	-1	136	134
3	0	96	90
3	2	197	188
3	3	114	107
3	5	106	103
3	6	52	49
3	7	62	64
3	8	53	55
3	9	62	64
4	-10	41	39
4	-8	47	27
4	-6	44	44
4	-5	56	57
4	-4	53	48
4	-3	57	59
4	-2	41	39
4	-1	59	56
4	0	44	40
4	1	92	90
4	2	90	89
4	3	63	65
5	-6	36	28
5	-5	54	57
5	-4	45	41
5	-2	68	74
5	-1	42	13
5	1	111	112
5	2	95	95
5	6	39	37
5	7	38	29
6	-2	48	43
6	-1	55	59
6	1	44	33
6	2	44	47
6	3	61	66
****	H = 2	****	
0	-11	73	73
0	-9	73	72
0	-7	78	80
0	-6	55	56
0	-5	262	248
0	-4	468	464
0	-3	255	256
0	-2	34	31
0	-1	72	76
0	0	117	135
0	1	87	100
0	2	315	352

K	L	FO	FC
0	3	91	87
0	4	139	132
0	5	142	139
0	6	221	217
0	8	82	76
1	-10	74	75
1	-9	78	69
1	-8	57	56
1	-7	70	68
1	-6	99	107
1	-5	121	127
1	-4	166	168
1	-3	436	434
1	-2	321	324
1	-1	476	469
1	0	380	385
1	1	53	53
1	2	116	114
1	3	150	157
1	4	148	151
1	5	246	234
1	6	33	43
1	7	46	48
1	8	81	81
1	9	93	107
2	-9	38	40
2	-7	36	39
2	-4	131	126
2	-2	137	137
2	-1	99	94
2	0	298	290
2	1	182	187
2	2	191	192
2	3	228	230
2	4	73	73
2	5	63	57
2	9	91	98
3	-6	43	52
3	-5	87	84
3	-4	42	35
3	-3	121	122
3	-2	105	104
3	-1	294	282
3	0	217	214
3	1	87	84
3	2	205	194
3	3	106	106
3	4	42	44
3	5	66	69
3	6	76	76
3	8	53	58
3	9	42	56
3	10	38	38
4	-8	44	35
4	-7	51	50

Table 3.2.7 (Continued).
Observed and calculated structure factor listing for **2-3** crystal.

K	L	FO	FC	K	L	FO	FC	K	L	FO	FC	K	L	FO	FC
4	-4	79	77	2	-6	82	83	0	-2	51	53	3	10	34	37
4	-3	52	58	2	-5	152	139	0	0	131	131	4	-9	45	51
4	-2	31	33	2	-4	37	31	0	1	237	252	4	-8	43	33
4	-1	91	88	2	-3	94	97	0	2	114	121	4	-5	89	92
4	0	81	84	2	-1	133	125	0	3	128	117	4	-4	70	68
4	1	51	54	2	0	243	240	0	4	245	231	4	-3	73	81
4	3	38	23	2	1	250	236	0	5	158	141	4	-2	61	65
4	6	70	67	2	2	110	108	0	6	90	86	4	-1	149	137
5	-7	48	50	2	3	78	80	0	7	52	51	4	0	56	54
5	-5	40	38	2	4	129	117	0	8	63	69	4	1	65	63
5	-4	45	51	2	5	39	39	0	10	41	28	4	3	49	47
5	-3	60	57	2	6	62	65	1	-12	40	54	4	5	72	75
5	-2	73	79	2	8	101	104	1	-9	43	21	4	6	57	57
5	-1	71	68	2	10	46	43	1	-8	55	56	4	8	44	56
5	0	103	102	3	-7	41	39	1	-7	135	130	5	-7	48	45
5	1	120	119	3	-6	46	47	1	-6	118	107	5	-6	57	59
5	6	59	51	3	-5	63	65	1	-5	276	277	5	-3	45	48
6	-1	62	60	3	-4	35	37	1	-4	186	188	5	-2	51	52
6	1	39	43	3	-3	136	130	1	-3	137	149	5	-1	60	70
				3	-2	142	144	1	-2	264	270	5	0	77	74
****	H =	3	****	3	-1	96	92	1	-1	338	333	5	2	80	85
0	-11	90	81	3	0	119	108	1	0	336	345	5	3	35	50
0	-10	35	26	3	1	31	29	1	1	166	164	5	5	43	56
0	-8	95	95	3	2	172	166	1	2	199	201	5	6	37	48
0	-7	88	83	3	3	109	107	1	4	88	83	6	0	46	35
0	-5	372	361	3	4	74	75	1	5	104	101	6	2	34	29
0	-4	226	216	3	5	127	126	1	6	55	50				
0	-3	119	120	3	7	53	63	1	7	91	90	****	H =	5	****
0	-2	561	590	3	9	47	27	2	-11	33	38	0	-10	38	44
0	-1	658	697	4	-6	58	60	2	-9	58	61	0	-9	41	25
0	2	96	97	4	-4	45	44	2	-8	44	43	0	-6	77	80
0	3	224	224	4	-1	32	33	2	-5	82	88	0	-5	59	56
0	4	315	314	4	0	105	103	2	-4	217	210	0	-4	225	226
0	6	106	105	4	2	72	71	2	-3	53	51	0	-3	257	267
0	7	59	53	4	3	66	63	2	-2	148	152	0	-2	234	245
0	8	34	35	4	4	77	77	2	-1	254	245	0	-1	138	127
1	-11	65	63	4	5	51	49	2	0	193	179	0	0	39	46
1	-10	49	59	5	-6	63	68	2	1	241	226	0	1	59	60
1	-8	75	74	5	-4	84	85	2	2	57	54	0	2	25	27
1	-6	194	192	5	-3	141	131	2	3	77	84	0	3	167	169
1	-5	42	43	5	-2	88	88	2	4	59	62	0	4	50	48
1	-4	192	191	5	1	46	53	2	5	42	46	0	5	42	49
1	-3	358	374	5	2	58	68	2	6	94	90	0	6	95	96
1	-2	455	472	5	4	32	34	2	8	50	52	1	-10	41	41
1	-1	230	237	5	5	42	45	3	-6	52	52	1	-9	51	48
1	0	106	100	5	6	53	52	3	-5	83	78	1	-8	66	70
1	1	138	152	6	-2	56	49	3	-3	60	65	1	-7	43	52
1	2	40	44	6	-1	53	54	3	-1	108	101	1	-6	93	99
1	3	145	152					3	0	77	68	1	-5	139	133
1	4	176	170	****	H =	4	****	3	1	47	45	1	-4	134	136
1	6	116	108	0	-8	147	136	3	2	96	103	1	-3	245	243
1	8	52	48	0	-7	154	145	3	6	91	100	1	-2	224	222
1	9	68	71	0	-6	52	50	3	7	67	79	1	-1	199	199
2	-8	69	60	0	-4	83	81	3	8	39	42	1	0	85	85
2	-7	40	46	0	-3	211	216	3	9	46	46	1	1	88	84

Table 3.2.7 (Continued).

Observed and calculated structure factor listing for **2-3** crystal.

K	L	FO	FC	K	L	FO	FC	K	L	FO	FC	K	L	FO	FC
1	2	68	71	5	3	47	49	3	-5	77	78	2	-6	49	53
1	3	266	254	5	6	36	29	3	-4	103	104	2	-5	117	115
1	4	206	196	6	-1	36	24	3	-3	61	56	2	-4	53	58
1	5	78	79	6	0	46	40	3	-3	61	56	2	-3	49	52
1	6	37	27					3	0	89	82	2	-2	111	103
1	7	42	36	****	H =	6	****	3	1	41	43	2	-1	96	88
2	-11	46	44	0	-10	43	38	3	2	116	117	2	0	93	91
2	-10	38	21	0	-9	38	44	3	3	58	69	2	1	98	89
2	-9	47	47	0	-8	113	104	3	4	78	85	2	3	81	86
2	-8	57	56	0	-6	124	123	3	5	74	80	2	4	114	115
2	-7	73	74	0	-5	160	155	3	6	54	53	2	5	114	108
2	-6	72	60	0	-4	37	30	3	7	48	50	2	6	59	61
2	-5	198	207	0	-3	64	62	3	8	43	33	2	7	64	59
2	-4	144	143	0	-2	132	135	4	-6	91	94	2	8	53	46
2	-3	144	140	0	0	32	25	4	-5	63	73	3	-7	50	63
2	-2	180	190	0	1	182	183	4	-4	49	40	3	-6	42	46
2	-1	177	166	0	2	31	23	4	-3	88	85	3	-5	115	119
2	0	50	54	0	3	247	244	4	-2	48	53	3	-4	99	94
2	1	127	117	0	4	34	26	4	-1	59	62	3	-2	91	93
2	2	160	151	0	5	52	45	4	0	117	127	3	-1	31	34
2	3	54	57	1	-8	41	33	4	1	70	74	3	0	39	33
2	4	81	90	1	-7	66	68	4	2	44	48	3	1	49	31
2	6	84	95	1	-6	90	93	4	5	75	81	3	3	72	66
2	7	71	74	1	-5	128	126	4	6	52	45	3	4	79	76
2	8	103	112	1	-4	136	138	5	-2	58	58	3	5	48	59
2	10	37	33	1	-3	142	142					3	6	52	48
3	-9	51	56	1	-2	211	210	****	H =	7	****	4	-8	39	44
3	-8	44	49	1	-1	97	96	0	-11	45	44	4	-7	39	49
3	-6	73	69	1	0	231	218	0	-7	43	22	4	-4	113	124
3	-4	34	44	1	1	235	227	0	-6	92	89	4	-3	127	128
3	-3	75	72	1	2	60	61	0	-5	106	101	4	-2	40	27
3	-2	107	106	1	4	42	36	0	-4	39	42	4	1	44	40
3	-1	51	49	1	5	103	105	0	-3	71	62	4	3	95	101
3	0	45	45	1	6	57	54	0	-2	129	117	4	4	95	88
3	1	70	65	1	7	51	49	0	-1	41	35	4	5	48	37
3	4	64	53	1	8	34	30	0	0	51	38	5	2	61	58
3	5	53	44	1	9	46	40	0	1	171	175	5	3	63	55
3	6	100	100	2	-8	46	60	0	2	63	70				
3	8	57	61	2	-7	58	57	0	3	124	123	****	H =	8	****
3	9	39	38	2	-6	89	95	0	5	45	34	0	-2	85	75
4	-5	89	94	2	-5	135	133	0	8	41	52	0	-1	151	146
4	-4	98	98	2	-4	72	75	1	-8	56	62	0	3	62	62
4	-3	74	76	2	-3	44	43	1	-7	36	42	1	-6	79	81
4	-2	90	89	2	-2	143	141	1	-6	99	97	1	-5	85	90
4	0	124	122	2	-1	92	84	1	-5	53	50	1	-4	53	65
4	1	80	81	2	0	42	50	1	-4	86	86	1	-3	54	55
4	2	46	47	2	1	64	63	1	-3	74	67	1	-2	74	81
4	3	49	60	2	2	62	73	1	0	126	120	1	-1	91	94
4	4	50	55	2	3	108	106	1	1	108	112	1	1	50	50
4	5	86	82	2	4	163	160	1	3	74	69	1	2	38	42
4	8	47	44	2	7	93	88	1	4	40	42	1	3	45	50
5	-7	33	28	2	8	70	75	1	5	53	51	1	4	77	72
5	-6	42	34	3	-8	44	51	1	6	80	79	1	5	94	97
5	-1	50	43	3	-7	87	91	1	7	87	90	1	6	54	69
5	2	64	70	3	-6	56	60	2	-9	51	39	1	7	33	29
								2	-7	54	59				

Table 3.2.7 (Continued).

Observed and calculated structure factor listing for **2-3** crystal.

K	L	FO	FC	K	L	FO	FC	K	L	FO	FC	K	L	FO	FC
1	8	37	34	0	3	86	91	0	0	166	174	1	-5	72	74
2	-8	47	60	0	5	47	46	0	1	55	57	1	-4	52	60
2	-7	60	65	1	-7	57	64	0	3	104	115	1	-3	54	54
2	-6	52	40	1	-6	60	72	0	5	95	85	1	-2	73	81
2	-5	104	101	1	-4	137	135	0	7	47	38	1	1	47	39
2	-4	50	53	1	-3	102	112	1	-9	35	14	1	2	44	50
2	-2	74	74	1	-2	58	65	1	-7	55	51	1	3	50	49
2	-1	79	80	1	0	43	55	1	-6	62	71	1	4	32	41
2	0	100	99	1	1	59	58	1	-2	63	65	2	-6	47	46
2	1	60	69	1	2	122	128	1	-1	85	78	2	-4	44	24
2	2	47	50	1	3	82	88	1	0	80	78	2	-2	49	64
2	3	126	127	1	4	100	95	1	1	113	111	2	-1	78	77
2	4	79	77	1	5	70	71	1	2	93	92	2	0	83	80
2	5	92	94	2	-7	75	66	1	3	38	36	2	3	45	45
2	8	50	31	2	-5	43	48	1	4	39	37	3	-2	35	40
3	-9	52	51	2	-4	68	66	2	-8	36	38	3	-1	54	57
3	-8	50	44	2	-3	41	37	2	-6	70	69	3	2	52	40
3	-7	55	59	2	-2	44	44	2	-5	70	68	3	3	38	32
3	-6	50	46	2	-1	85	91	2	-4	75	76	4	-3	37	32
3	-3	73	69	2	1	42	36	2	0	55	50				
3	-2	36	44	2	2	74	68	2	1	47	52	**** H = 12 ****			
3	-1	43	38	2	3	52	53	2	2	61	62	0	-6	54	66
3	0	34	35	2	4	65	56	2	4	88	83	0	-1	108	104
3	2	46	48	2	7	35	45	3	-7	63	63	0	1	58	57
3	3	109	108	3	-9	41	39	3	-5	37	51	1	-1	70	65
3	4	61	63	3	-7	38	43	3	-3	71	70	1	3	62	52
3	5	58	61	3	-6	72	75	3	-2	44	37	2	-5	41	33
3	6	34	34	3	-5	48	60	3	-1	51	51	2	-4	45	34
4	-6	52	60	3	-2	42	42	3	0	64	54	2	-2	48	46
4	-3	42	35	3	0	91	92	3	2	45	51	2	-1	39	40
4	-1	56	54	3	1	78	82	4	-3	36	45	2	1	39	36
4	0	90	98	3	3	65	69	4	0	32	32				
4	1	98	102	4	-3	57	47					**** H = 13 ****			
4	2	46	36	4	3	39	46	**** H = 11 ****				0	-3	45	36
5	-3	42	34	5	-3	32	32	0	-5	67	70	0	-2	92	94
5	-2	45	54	5	-2	43	45	0	-4	70	66	0	0	52	50
				5	-1	41	38	0	-3	45	42	0	1	49	45
**** H = 9 ****								0	-2	49	42	1	-2	35	34
0	-10	39	41	**** H = 10 ****				0	0	55	52	1	-1	41	45
0	-9	46	40	0	-4	39	39	0	2	142	148	1	0	51	49
0	-5	58	40	0	-3	92	84	0	3	76	84	1	1	34	36
0	-4	104	100	0	-2	35	31	0	6	35	29	2	-4	46	38
0	0	70	73	0	-1	48	51	1	-6	43	22				

Table 3.2.7 (Continued).
Observed and calculated structure factor listing for 2-3 crystal.

Polymer	Composition of Imprint (mole)	% Imprint Extracted
P 1	reference polymer, 100% **3**	93.2
P 2	99.99% **3** and 0.01% **4**	92.7
P 3	reference polymer, 100% **4**	4.3

Table 3.2.8.   Summary of synthesized imprinted polymers.

Solution	L-PhNHPh Solution (µM)	D-PhNHPh Solution (µM)	L-PhNHPh Adsorbed (µmol/g)	D-PhNHPh Adsorbed (µmol/g)
Blank	61.9	61.7	0.0	0.0
P 1	26.1±1.2	38.5±1.2	3.58±0.12	2.32±0.12
P 2	22.0±1.2	39.1±1.2	4.00±0.12	2.27±0.12

a) *Absorbance measurements performed at 260 nm in distilled chloroform.*

Table 3.2.9. Adsorption of enantiomers of PheNHPh with imprinted polymers.[a] The reported values are the solution and adsorbed concentrations for the various polymers.
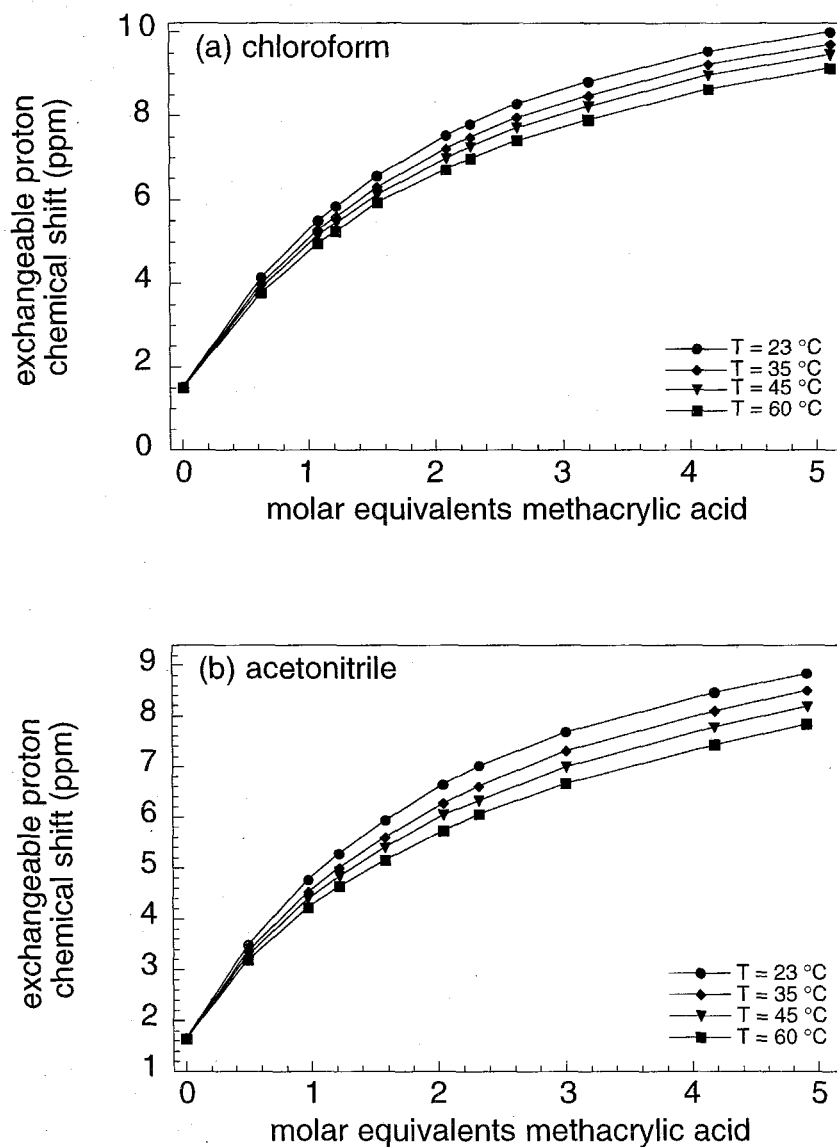
Figure 3.2.1. Shift of the exchangeable proton of **3** versus molar equivalents of **2** added in chloroform solvent (a). Shift of the exchangeable proton of **3** versus molar equivalents of **2** added in acetonitrile solvent (b). Investigation performed at the concentration of **3** used in imprinted polymer synthesis.
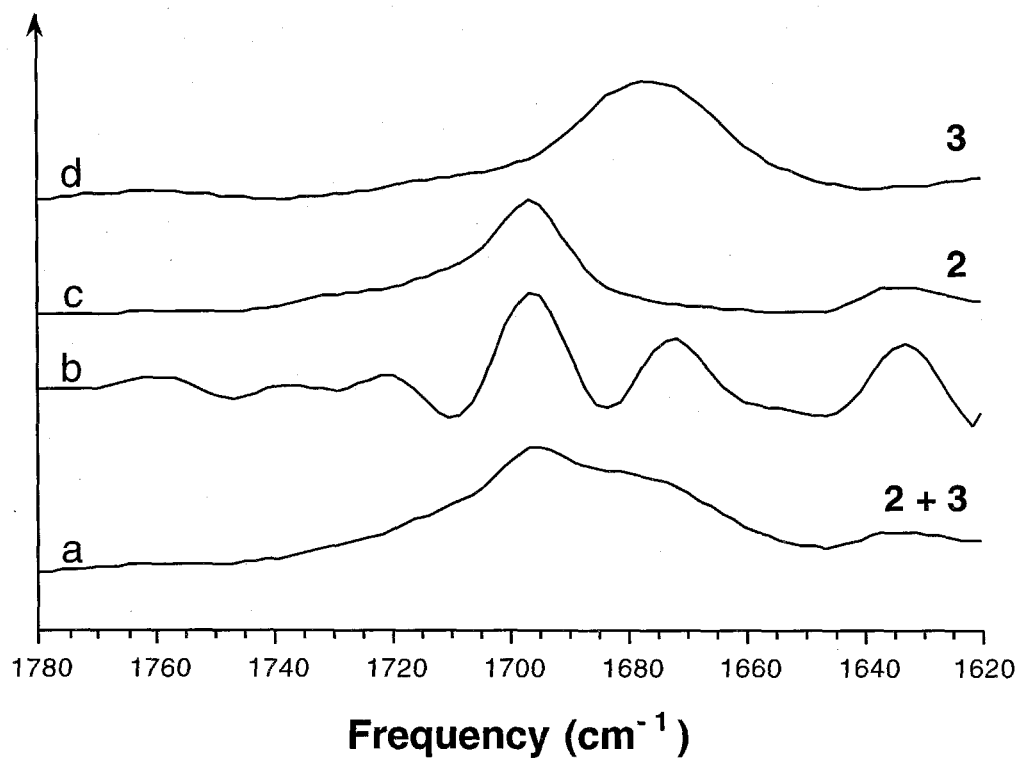
Figure 3.2.2. Infrared spectra of (a) one equivalent of **2** in a chloroform solution of (0.1 M) **3**, (b) Fourier self-deconvolution of spectrum in (a), (c) (0.2 M) **2** in a chloroform solution and (d) (0.1 M) **3** in a chloroform solution. Investigation performed at the concentration of **3** used in imprinted polymer synthesis for (a), (b) and (d).

Frequency (cm⁻¹)
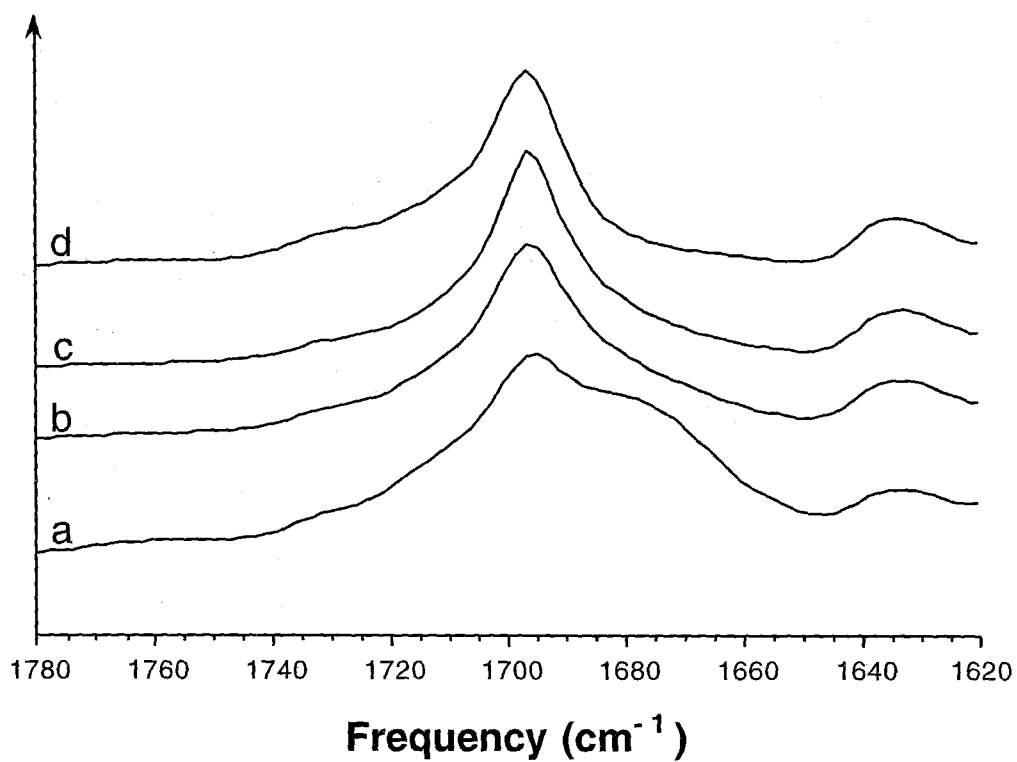
Figure 3.2.3. Infrared spectra of (a) one equivalent of **2**, (b) three equivalents of **2**, (c) five equivalents of **2** and (d) **2** (0.2 M) in a chloroform solution. Investigation performed at the concentration of **3** used in imprinted polymer synthesis in (a), (b) and (c).
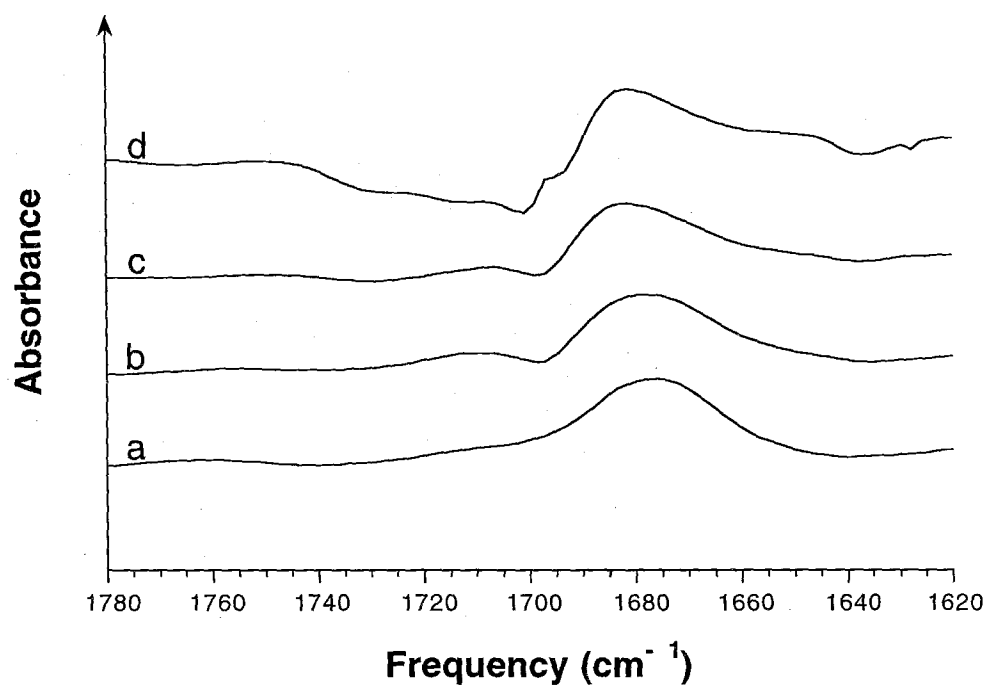
Figure 3.2.4. (a) Infrared spectrum of **3** in chloroform solution at the concentration used in imprinted polymer synthesis. (b) - (d) Infrared spectra obtained by the subtraction of the spectrum in Figure 3(d) from: (b) Figure 3(a) (one equivalent of **2**), (c) Figure 3(b) (three equivalents of **2**) and (d) Figure 3(c) (five equivalents of **2**).
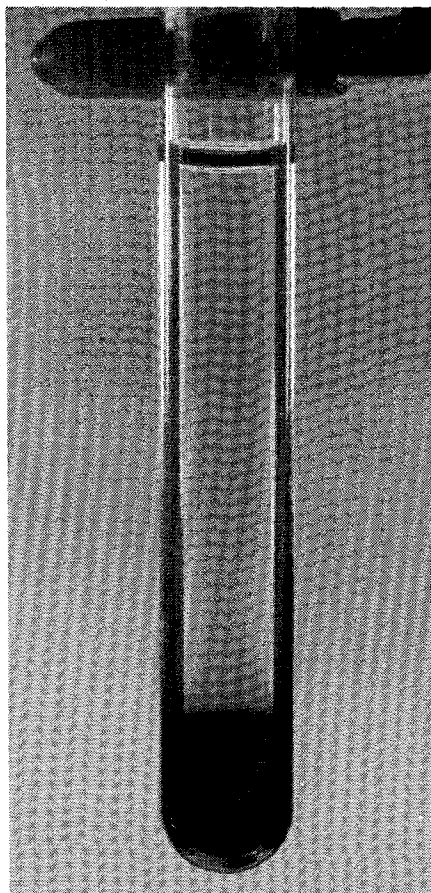
Figure 3.2.5. Optical photograph of L-PheNHPh imprinted polymer synthesis mixture prior to polymerization. A small quantity of chlorophenol red dye was added to facilitate the visualization of the **2-3** rich phase (lower layer) separate from the **1** rich phase (upper layer).
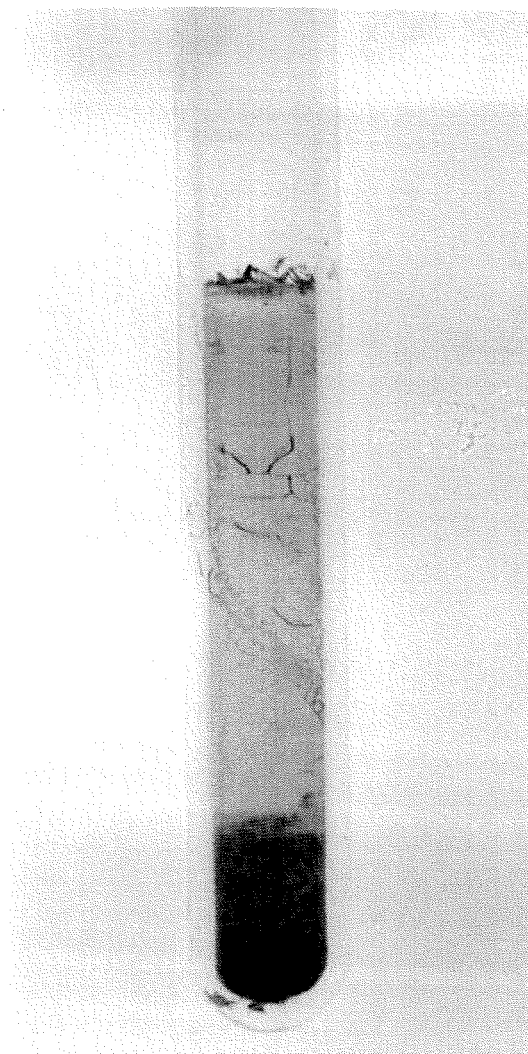
Figure 3.2.6. Optical photograph of an as-made L-PheNHPh imprinted polymer. The phase separation in this case is localized to upper and lower layers as in the case preceding polymerization represented in Figure 3.2.5.
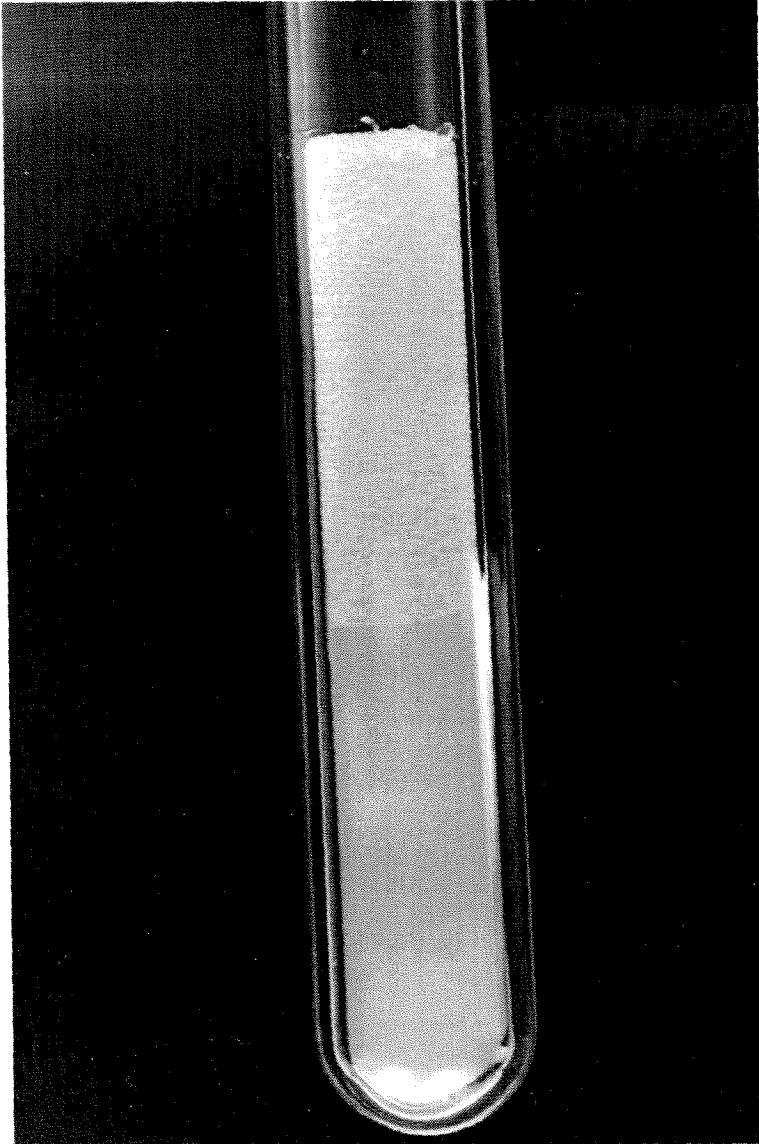
Figure 3.2.7. Optical photograph of as-made **P1**.

Figure 3.2.8.   Optical photograph of as-made **P2**.
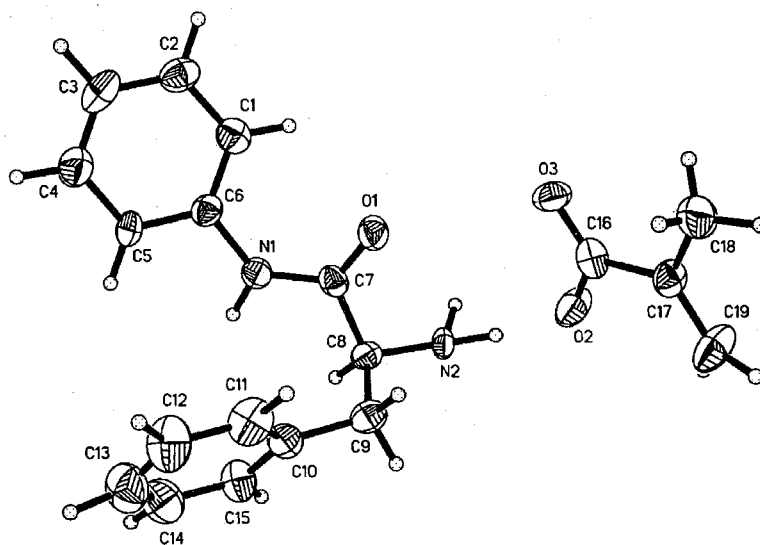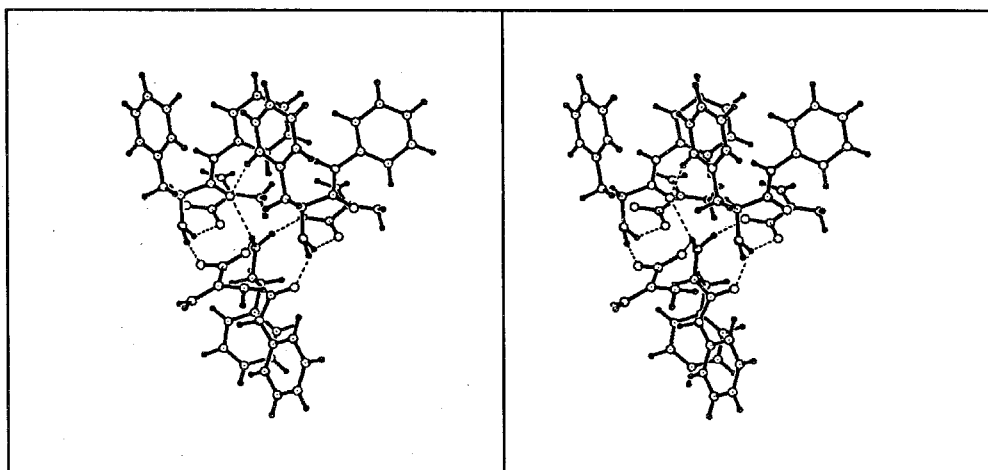
Figure 3.2.9. (a) ORTEP plot of the structure and atom labeling scheme for **2-3** crystal. Thermal ellipsoids are drawn at the 30% probability level, and labels for hydrogen atoms are omitted for clarity. (b) Stereoscopic representation of the intermolecular bonding involved in the **2-3** crystal. Interatomic distances were used to identify hydrogen bonds, and these are labeled with dashed lines.

CHAPTER FOUR

A NEW METHOD FOR THE MOLECULAR IMPRINTING OF SILICA WITH AMINE FUNCTIONALITY

Abstract

A new method for molecularly imprinting the three-dimensional pore space of silica with amine functionality has been developed. Imprinted silicas containing up to three amines per templated site are synthesized and characterized by FTIR and ^{29}Si and ^{13}C NMR spectroscopies. The silicas are microporous and reveal microporosity beyond that of the inherent pore volume of acid catalyzed sol-gel generated silicas upon removal of the imprint. The increase in porosity is consistent with the extent of imprint removed. The amines that reside in the microporous void space are able to bind molecules such as benzoic acid and acetylacetone and also perform shape-selective catalysis. Fluorescence measurements with a pyrenebutyric acid probe molecule were performed on the imprinted silica containing three amines per imprinted site and compared to the silica containing one amine per imprinted site. The results demonstrate that the imprinting process employed here gives control over local functional group ordering and provides a foundation from which further investigations towards elucidating quantitative distance information can be developed.

4.1   Introduction

An area of much current attention is the synthesis of supramolecular structures that possess convergently positioned chemical functional groups

within a molecular cleft.[1]   In these instances, functional groups are positioned relative to one another for concerted catalysis in a manner reminiscent of enzymatic systems, with the molecular structure surrounding the cleft serving as a mechanically rigid framework to prevent collapse of the catalytic groups.[2]   Several *molecular* systems exhibiting such order have been synthesized for the particular case of nitrogen-containing functionality positioned in a convergent manner, and in these instances metal chelation[3] and anion recognition[4] have been demonstrated along with small molecule binding and catalysis.[5]   In addition to *molecular* systems, there is also extreme interest in preparing *solid* materials that contain convergently positioned chemical functionality, where the functionality is immobilized on a solid support that serves the dual role of providing a rigid molecular framework and porosity.   The advantages inherent in positioning functionality off of a *solid* as opposed to a *molecular* scaffold are shown in Scheme 4.1.1. The approach involving the solid (framework for mechanical support is outside of the functional groups) creates a natural environment for convergent positioning of chemical functionality, whereas the approach involving the molecular scaffold (framework for mechanical support is typically inside of the functional groups) creates a natural environment for divergent positioning. This is not to rule out that a certain type of positioning cannot be created, but rather to say that each approach has an intrinsic geometric preference for creating a certain type of functional group order.

solid scaffold approach

imprint synthesis

+ CF ⟶

CF CF
CF
CF

+

monomer

imprinted material synthesis

convergent positioning

CF CF
CF
CF

⟵ **imprint deprotection**

CF CF
CF
CF

molecular scaffold approach

supramolecular synthesis

+ CF ⟶ CF CF CF CF **divergent positioning**
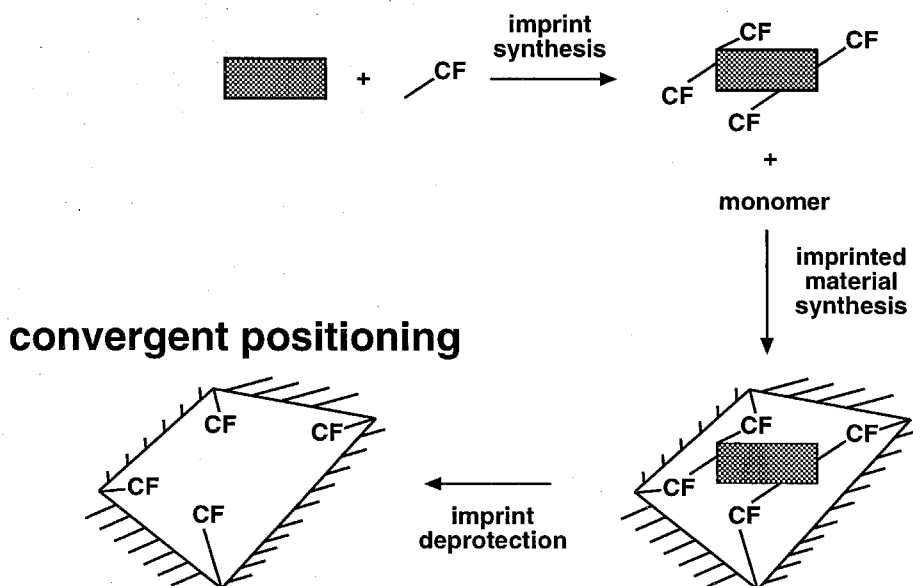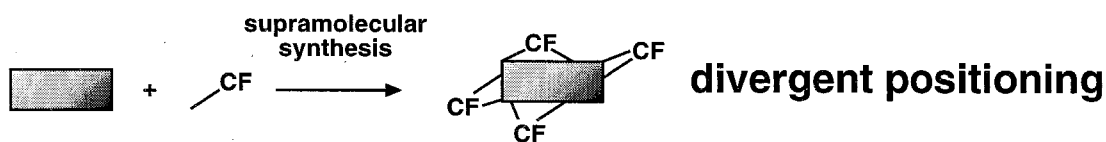
Scheme 4.1.1. Illustration comparing the use of molecular and solid, material-based scaffolds for the organization of chemical functionality (CF) within a cleft. The lines in the figure connecting CF represent covalent bonds.

Thus, in order to achieve convergent positioning, which is the preferred embodiment for catalysis, solid-based scaffolds may provide a useful alternative to molecular ones, especially in instances where such

positioning is difficult to achieve in the latter. Another important comparative issue between the solid and molecular scaffold approaches is the potential to afford shape-selectivity for catalysis via the three-dimensional porosity encompassing the convergently positioned chemical functionality in the solid. This aspect of the solid-based approach is discussed further in Sections 4.4.9 and 4.4.10.

The synthetic methodology for creating order in a solid material on the length-scale of a small molecule, catalytic site is provided for by the method of molecular imprinting.[6] In the past, this method has been used to organize one, two and three nitrogen-containing functionalities (in the form of an imine) on the surface of a silica particle with the use of aromatic rings as a template.[7] The template was removed in these instances with the use of an acid-catalyzed deprotection process to yield convergently positioned amines on a surface.

4.2. New Imprinting Method

The aforementioned approach has been limited to the postsynthetic positioning of amines on the surface of silica particles. My objective is to develop an imprinting method that allows the convergent positioning of amines within a three-dimensional void space of controlled dimensions in silica. By using a single aromatic ring as an organizing moiety for proof of concept experiments, silicas containing one (one point), two (two point) and

three (three point) amines positioned symmetrically within micropores of approximately 1-2 nm in size were synthesized. These amines are represented schematically in Figure 4.2.1 as they would appear in the three point material. Here, I developed a covalent imprinting strategy[8] to position amines with desired geometry. Advantages of this approach include the ability to create a homogeneous distribution of imprinted sites (based on Langmuirian adsorption profiles of imprinted sites),[8a] which is in contrast to molecular imprinting methods that are based on non-covalent interactions (see Chapter 3).[9] My approach involves the synthesis of a benzyl carbamate imprint in which the amines are positioned relative to the aromatic ring and are rendered non-nucleophilic in their protected carbamate state during the process of material synthesis via acid-catalyzed sol-gel hydrolysis and condensation. The resulting organosilane carbamate is used as the imprint and is copolymerized via acid-catalyzed sol-gel methods with a suitable silica monomer such as tetraethylorthosilicate (TEOS) to create a clear and brittle glass. A solid-phase deprotection is then performed to hydrolyze the carbamate C-N bond directly on the silica and generate the amine functionality from the carbamate within the imprinted material *in-situ*. The result is a molecularly imprinted configuration of convergent amines (for the two and three point materials). This complete process is outlined for the three point material in Scheme 4.2.1 below.
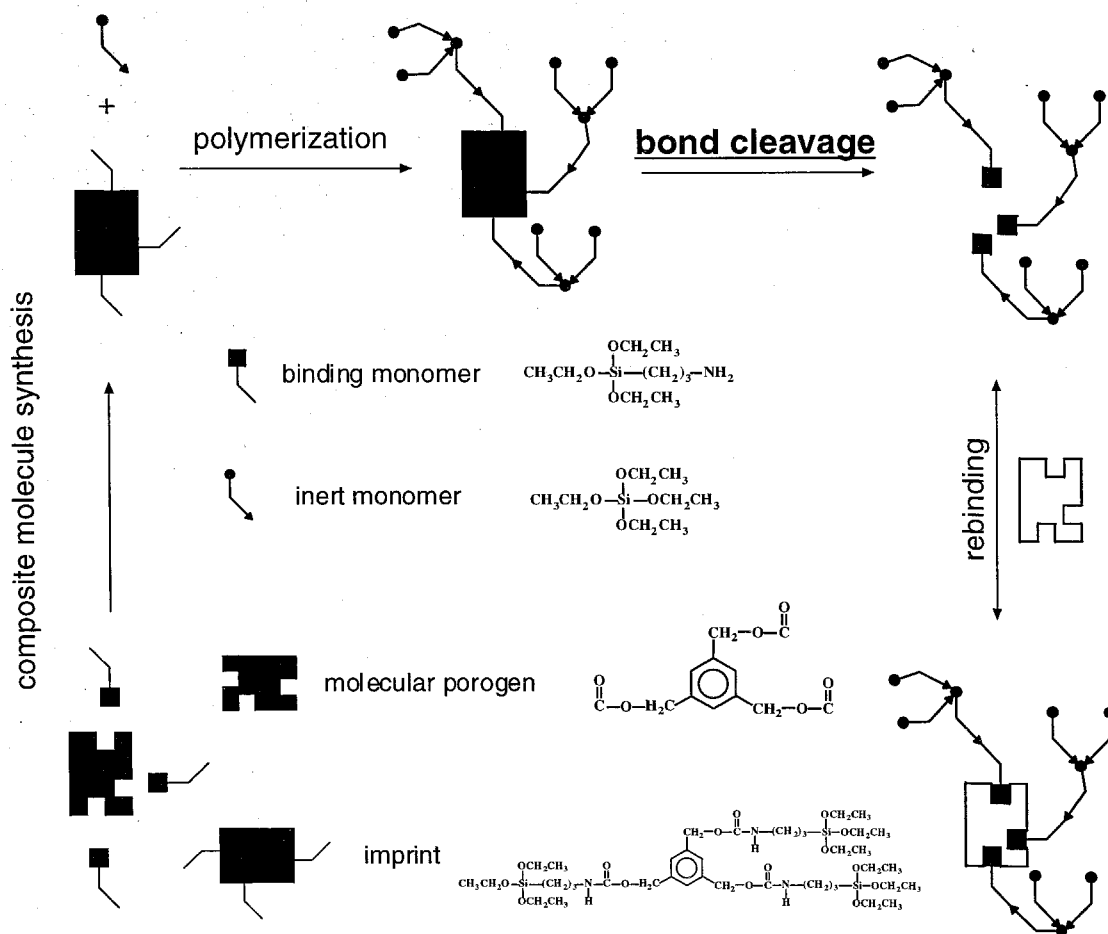
Scheme 4.2.1. Diagram illustrating the various steps involved in creating a molecularly imprinted silica by the controlled distance approach. In the center of the scheme are examples of typical monomers and imprints used and include 3-aminopropyltriethoxysilane as binding monomer, tetraethylorthosilicate as inert crosslinking monomer, and [3-(triethoxysilyl)propyl]-1,3,5-benzenetriyltris(methylene)carbamate as imprint.

4.3. Imprint and Material Synthesis

4.3.1   Synthesis of 1
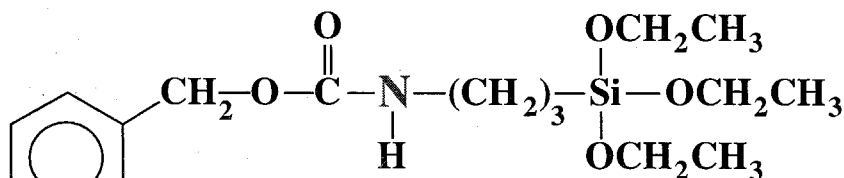
3-(triethoxysilyl)propyl-benzylcarbamate

1

To 42 mmol (10 mL) of 3-aminopropyltriethoxysilane in 50 mL of anhydrous ether, 40 mmol (5.6 mL) of triethylamine were added. Under ice cooling, 40 mmol (5.7 mL) of benzyl chloroformate were added dropwise to this mixture via dry syringe. The reaction mixture was stirred for a period of 1 hour at room temperature, evaporated to an oil, dissolved in chloroform, and extracted with pH 2.0 aqueous HCl, saturated sodium bicarbonate, and saturated brine. The organic phase was dried over magnesium sulfate and purified by flash chromatography. The final product was recovered as a transparent oil (yield 80%). ^{1}H NMR (CDCl$_3$): 0.620 (2H, t, C$\underline{H}_2$); 1.21 (3H, t, OCH$_2$C$\underline{H}_3$); 1.56 - 1.66 (2H, m, C$\underline{H}_2$); 3.13 - 3.2 (2H, m, C$\underline{H}_2$); 3.8 (2H, q, OC$\underline{H}_2$CH$_3$); 5.07 (2H, brs, C$\underline{H}_2$O); 5.30 (1H, t, N$\underline{H}$); 7.25 - 7.33 (5H, m, Ar-H). ^{13}C{^{1}H} NMR (CDCl$_3$): 8.13 ($\underline{C}$H$_2$); 18.8 (OCH$_2\underline{C}$H$_3$); 23.8 ($\underline{C}$H$_2$); 44.0 ($\underline{C}$H$_2$); 58.9 (O$\underline{C}$H$_2$CH$_3$); 66.9 ($\underline{C}$H$_2$O); 128.5 ($\underline{C}$H); 128.6 ($\underline{C}$H); 130.0 ($\underline{C}$H); 137.3 ($\underline{C}_q$); 157 ($\underline{C}$=O). ^{29}Si NMR (CDCl$_3$): -45.61 ($\underline{Si}$(OCH$_2$CH$_3$)$_3$CH$_2$). *Anal.* Calcd for C$_{17}$H$_{29}$O$_5$NSi: C, 57.43; H, 8.22; N, 3.94; Si, 7.90. Found: C, 57.54; H, 8.56; N, 4.05; Si, 7.96.

4.3.2　Synthesis of 2

$$CH_3CH_2O-\overset{\overset{\displaystyle OCH_2CH_3}{|}}{\underset{\underset{\displaystyle OCH_2CH_3}{|}}{Si}}-(CH_2)_3-\overset{\overset{\displaystyle O}{||}}{\underset{\underset{\displaystyle H}{|}}{N}-C}-O-H_2C$$

$$CH_2-O-\overset{\overset{\displaystyle O}{||}}{C}-\overset{\overset{\displaystyle}{|}}{\underset{\underset{\displaystyle H}{|}}{N}}-(CH_2)_3-\overset{\overset{\displaystyle OCH_2CH_3}{|}}{\underset{\underset{\displaystyle OCH_2CH_3}{|}}{Si}}-OCH_2CH_3$$
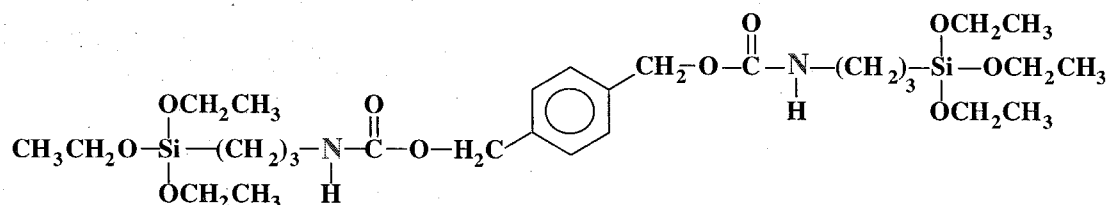
[3-(triethoxysilyl)propyl]-1,4-phenylenebis(methylene)carbamate

2

To 24 mmol (3. 89 g) of 1,1'-carbonyldiimidazole in 20 mL of dry THF, a catalytic amount of sodium ethoxide (ca 5 mg) was added. Subsequently 12 mmol (1.66 g) of 1,4-benzenedimethanol were dissolved in 20 mL of dry THF and were added dropwise under ice cooling to the reaction mixture. The flocculent precipitate formed was redissolved by heating the reaction mixture to ca 50 °C and stirring for an additional hour at room temperature. Subsequently 26 mmol (6.2 mL) of 3-aminopropyltriethoxysilane were added dropwise under ice cooling. The reaction mixture was allowed to stir for an additional 3 hours at room temperature and monitored by TLC. The THF was evaporated, and the crude product was redissolved in ether. Excess imidazole was removed by vacuum filtration, and the crude product was purified by silica chromatography (Silica Gel 60 and 1.4/1.0 v/v hexane:ethyl acetate). The solid recovered from the silica gel column was recrystallized in chloroform/hexane to give white platelets (yield 41%). ^{1}H NMR (CDCl$_3$): 0.624 (4H, t, C$\underline{H}_2$); 1.21 (6H, t, OCH$_2$C$\underline{H}_3$); 1.57 - 1.67 (4H, m, C$\underline{H}$); 3.15 - 3.22 (4H, m, C$\underline{H}_2$); 3.81 (4H, q, OC$\underline{H}_2$CH$_3$); 5.07 (4H, brs, C$\underline{H}_2$O); 5.17 (2H, t, N$\underline{H}$); 7.32 (4H, s, Ar-H). ^{13}C{^{1}H} NMR (CDCl$_3$): 7.63 ($\underline{C}$H$_2$); 18.3

(O$\underline{C}$H$_2$CH$_3$); 23.3 ($\underline{C}$H$_2$); 43.5 ($\underline{C}$H$_2$); 58.5 (O$\underline{C}$H$_2$CH$_3$); 66.2 ($\underline{C}$H$_2$O); 128.2

($\underline{C}$H); 136.6 ($\underline{C}_q$); 156.4 ($\underline{C}$=O). ^{29}Si NMR (CDCl$_3$): -45.7 ($\underline{Si}$(OCH$_2$CH$_3$)$_3$CH$_2$).

Anal. Calcd for C$_{28}$H$_{52}$O$_{10}$N$_2$Si$_2$: C, 53.14; H, 8.28; N, 4.43; Si, 8.87. Found: C, 53.22; H, 8.48; N, 4.37; Si, 8.74.
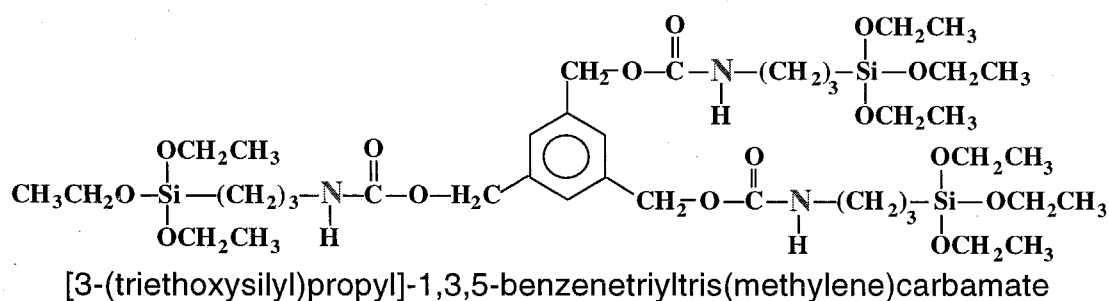
4.3.3   Synthesis of *3*

[3-(triethoxysilyl)propyl]-1,3,5-benzenetriyltris(methylene)carbamate

3

To 36 mmol (5.84 g) of 1,1'-carbonyldiimidazole in 20 mL of dry THF, a catalytic amount of sodium ethoxide (ca 5 mg) was added. Subsequently 12 mmol (2.02 g) of 1,3,5-benzenetrimethanol were dissolved in 20 mL of dry THF and were added dropwise under ice cooling to the reaction mixture. The reaction mixture was stirred for 1.75 hours at room temperature. Subsequently 40 mmol (9.3 mL) of 3-aminopropyltriethoxysilane were added dropwise under ice cooling. The reaction mixture was allowed to stir for an additional 2 hours at room temperature as monitored by TLC. The THF was evaporated and the crude product was redissolved in ether. Excess imidazole was removed by vacuum filtration, and the crude product was purified by silica chromatography with Silica Gel 60 using 1.4/1.0

hexane:ethyl acetate as eluent. A white wax-like solid was recovered from the silica gel column (yield 55%). ^{1}H NMR (CDCl$_3$): 0.632 (6H, t, C$\underline{H}_2$); 1.22 (9H, t, OCH$_2$C$\underline{H}_3$); 1.58 - 1.68 (6H, m, C$\underline{H}_2$); 3.15 - 3.22 (6H, m, C$\underline{H}_2$); 3.81 (6H, q, OC$\underline{H}_2$CH$_3$); 5.05 (6H, brs, C$\underline{H}_2$O); 5.30 (3H, t, N$\underline{H}$); 7.25 (6H, s, Ar-H). ^{13}C{^{1}H} NMR (CDCl$_3$): 7.61 ($\underline{C}$H$_2$); 18.3 (OCH$_2$$\underline{C}H_3$); 23.3 ($\underline{C}H_2$); 43.5 ($\underline{C}H_2$); 58.4 (O$\underline{C}H_2CH_3$); 66.0 ($\underline{C}H_2$O); 127.1 ($\underline{C}$H); 137.4 ($\underline{C}_q$); 156.3 ($\underline{C}$=O). ^{29}Si NMR (CDCl$_3$): -45.7 ($\underline{Si}$(OCH$_2CH_3$)$_3CH_2$). *Anal.* Calcd for C$_{39}H_{75}O_{15}N_3Si_3$: C, 51.46; H, 8.30; N, 4.62; Si, 9.26. Found: C, 51.48; H, 8.50; N, 4.53; Si, 9.12.

4.3.4 Synthesis of 1,3,5-benzenetrimethanol

Synthesis was accomplished using methodology described elsewhere,[10] by reduction of the commercially available benzene trimethyl ester. To a suspension containing 300 mmol of lithium aluminum hydride dissolved in 333 mL of 1:1 THF:ether, 40 mmol (100 g) of trimethylbenzene-1,3,5-tricarboxylate was added dropwise and stirred for 5 hours under reflux. It was then cooled to room temperature and 300 mL of water was slowly added to quench reaction. The resulting slurry was stirred overnight. The solution was filtered, dried with sodium sulfate, and evaporated to dryness with ethanol. A brown oil was obtained upon evaporation. This was extracted three times with ethyl acetate (3 x 200 mL) and recrystallized with hot ethyl acetate to give platelets (50% yield). ^{1}H NMR (CD$_3$OD): 4.59 (6H, s, C$\underline{H}_2$); 4.87 (3H, s, O$\underline{H}$); 7.24 (3H, s, C$\underline{H}$). ^{13}C{^{1}H} NMR (CD$_3$OD): 63.45 ($\underline{C}$H$_2$); 123.8 ($\underline{C}$H); 141.3 ($\underline{C}_q$).

*4.3.5   Synthesis of **4***

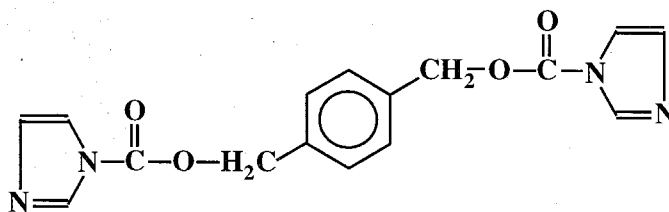[N-imidazole]-1,4-phenylenebis(methylene)carboxylate

4

To 24 mmol (3.892 g) of 1,1'-carbonyldiimidazole in 20 mL of dry THF, a catalytic amount of sodium ethoxide (ca 5 mg) was added. Subsequently 12 mmol (1.66 g) of 1,4-benzenedimethanol were dissolved in 20 mL of dry THF and were added dropwise under ice cooling to the reaction mixture. After 30 minutes (followed by TLC), the reaction vessel was cooled in an ice bath and a flocculent precipitate was formed. This precipitate was collected via vacuum filtration and recrystallized in chloroform:hexane to yield 7.6 mmol of brilliant white powder (2.5 g; yield 63%). ^{1}H NMR (CDCl$_3$): 5.41 (1H, s, C$\underline{H}_2$); 7.04 (1H, s, C$\underline{H}$); 7.41 (1H, s, C$\underline{H}$); 7.47 (2H, s, C$\underline{H}$); 8.12 (1H, s, C$\underline{H}$). ^{13}C{^{1}H} NMR (CDCl$_3$): 69.8 ($\underline{C}$H$_2$); 117.7 ($\underline{C}$H); 129.7 ($\underline{C}$H); 131.4 ($\underline{C}$H); 135.6 ($\underline{C}_q$); 137.7 ($\underline{C}$H); 194.1 ($\underline{C}$=O).

4.3.6   Silica Synthesis

Imprinted silicas were synthesized via acid-catalyzed, sol-gel hydrolysis and condensation. These conditions were chosen so as to ensure comparable hydrolysis rates between the organosilane imprint and the silica

source tetraethylorthosilicate (TEOS) and to obtain a clear gel with a polymer-like micro-state (as opposed to base-catalyzed sol-gels that are known to be colloidal and cloudy).[11]   A high ethanol/water content was used to create a gel with significant microporosity (*vide infra*). The amount of imprint used in the sol-gel synthesis corresponds to 2 mole percent of imprint silicon relative to TEOS silicon. A typical procedure was to dissolve 0.7338 g of **1** for 1 point material synthesis (no imprint for 0 point, 0.6532 g of **2** for 2 point and 0.6263 g of **3** for 3 point) into 193.5 mL of dry ethanol in a 16 ounce jar (Qorpak 7534). 23.0 mL of TEOS were added to this mixture. Finally 64.5 mL of pH 2.0 aqueous HCl were added to the gel mixture. The mixture was covered loosely with a jar cap and stirred for 24 hours at 8 ^{o}C. It was then covered with weighing paper and stirred for 12 hours at 15 ^{o}C and for 8 days at room temperature. With approximately 3/4 of an inch of liquid head remaining in the jar after this period, the mixture was transferred to a 40 ^{o}C oven and covered loosely with a jar cap. The mixture was aged in the oven for 10 days after which time gelation had occurred and the cap removed. The resulting glass monoliths were further aged in an oven for a period of 8 days at a temperature of 40 ^{o}C. The final gels had an approximate imprint content of 0.283 mmol imprint nitrogen/g of as-made material as determined from the mass balance. A thermogravimetric analysis (TGA) on the as-made materials showed that the gels can be

heated to over 200 °C in air without any detectable decomposition of imprint if such further processing was desired. The as-made imprinted silica monoliths were ground into a powder of particles less than 10 μm in diameter via a ball mill and repetitive wet-sieving in dry ethanol. The resulting powder was dried under ambient conditions and Soxhlet extracted with acetonitrile refluxing in calcium hydride for a period of 24 hours to remove water and ethanol from the silica. The silica was then separately washed with 25 mL/g of silica with chloroform and pentane and allowed to dry. At this stage, the imprinted material is referred to as extracted. The extracted material was further processed prior to deprotection by capping surface hydroxyl groups at room temperature by treating the extracted silica with an equimolar mixture of chlorotrimethylsilane and 1,1,1,3,3,3-hexamethyldisilazane for a period of 24 hours (6.3 mL of 1,1,1,3,3,3-hexamethyldisilazane and 3.7 mL chlorotrimethylsilane per gram of extracted silica). Typical weight increases after the capping procedure were approximately 5 wt %. Subsequent to capping, the silica was washed with 50 mL/g of silica with anhydrous THF, anhydrous acetonitrile, chloroform, and pentane, and allowed to dry in a dessicator under ambient conditions. The resulting silica is referred to as capped.

4.3.7   Silica Deprotection: Imprint Cleavage

The silica deprotection strategy was chosen by the process discussed in Section 4.4.2 below. Silica deprotection was performed by adding 15 mL of a 0.25M TMSI in dry acetonitrile per gram of capped silica and stirring the resulting slurry in the dark for 12 hours under argon. Increasingly higher temperatures were used to affect deprotection in the multiple point materials; thus, 40 ^{o}C for the one point material, 70 ^{o}C for the two point material and 80 ^{o}C for the three point material were used. The deprotected silica was collected via vacuum filtration and washed with 30 mL/g of silica with dry acetonitrile, methanol, saturated aqueous sodium bicarbonate, methanol, and acetonitrile. The deprotected silica was then Soxhlet extracted for 24 hours each with acetonitrile refluxing in calcium hydride and chloroform. Finally, the silica was collected via vacuum filtration, washed with 25 mL per gram separately with chloroform and pentane, and dried in a dessicator under ambient conditions. The resulting silica is referred to as deprotected.

4.4. Results and Discussion

4.4.1   Imprinted Silica Characterization Before Deprotection

An optical photograph of the as-made zero point, one point, two point and three point imprinted silicas is shown in Figure 4.4.1. All gels are optically

transparent as expected for materials prepared via acid-catalyzed, sol-gel hydrolysis and condensation.[11]

Figure 4.4.2 shows the infrared spectra of the capped materials illustrated in Figure 4.4.1. Notice the absence of significant hydroxyl stretching bands in the region above 3000 cm^{-1}, the presence of the carbamate carbonyl at 1700 cm^{-1} and a weaker amide II band at 1550 cm^{-1} in the imprint-containing materials. The latter two bands are more evident in the FTIR subtraction spectra between the capped and deprotected materials (vide infra). Figure 4.4.3 shows typical ^{13}C CP/MAS NMR spectra for extracted one point (4.4.3a), capped two point (4.4.3c) and extracted three point (4.4.3e) materials. The spectra prove that the imprint is intact following sol-gel synthesis and silica capping procedures. The following are the resonance assignments for the one, two and three point materials: CP-MAS ^{13}C NMR of extracted one point material: 9.5 ($\underline{C}H_2$); 23.2 ($\underline{C}H_2$); 43.5 ($\underline{C}H_2$); 67.4 ($\underline{C}H_2O$); 128.7 ($\underline{C}H$); 136.8 ($\underline{C}_q$); 158.7 ($\underline{C}=O$), CP-MAS ^{13}C NMR of capped two point material: 9.6 ($\underline{C}H_2$); 23.8 ($\underline{C}H_2$); 43.9 ($\underline{C}H_2$); 67.4 ($\underline{C}H_2O$); 128.2 ($\underline{C}H$); 137.4 ($\underline{C}_q$); 158.2 ($\underline{C}=O$), CP-MAS ^{13}C NMR of extracted three point material: 9.2 ($\underline{C}H_2$); 22.6 ($\underline{C}H_2$); 43.5 ($\underline{C}H_2$); 66.9 ($\underline{C}H_2O$); 126.5 ($\underline{C}H$); 137.8 ($\underline{C}_q$); 158.7 ($\underline{C}=O$). Note that in the spectra shown in Figure 4.4.3 a weak resonance at approximately 17.3 ppm that is attributable to a residual ethoxy methyl group and a resonance at approximately 55.0 ppm that is attributable to a residual ethoxy methylene group can be observed in some

of the samples. The intensities of these resonances (even compared with imprint which is present in a 2 mol % concentration relative to silicon in the imprinted silicas) indicate the high degree of hydrolysis achieved in the silicas during their synthesis. The small peak located at approximately 118.3 ppm is due to residual acetonitrile solvent.

The bulk silicon environment in the imprinted silicas was investigated by ^{29}Si block decay NMR. A typical spectrum is shown in Figure 4.4.4 for a zero point material. In this particular case it was found by integrating the areas of the respective peaks that 60% of the quaternary silicon is Q^4 ($Si(OSi)_4$) and 40% of the quaternary silicon is Q^3 ($Si(OSi)_3O$). There was no detectable amount of Q^2 silicon with this method (see ^{29}Si CP/MAS NMR discussion below where this fraction is amplified via cross-polarization and is observable). Typical amounts of TMS in the capped materials are less than 7% of the silicon (TMS in spectrum shown cannot be accurately quantified due to the presence of unwashed capping reagents as exemplified by the features immediately upfield and downfield from the main TMS peak). Figure 4.4.5 shows typical ^{29}Si CP/MAS NMR spectra of the capped one, two and three point silicas, where the integrity of the silicon-carbon bond is evident in the predominant T^3 ($Si(OSi)_3$-C) resonance at -66±1 ppm for the one, two and three point imprinted silicas (-68 ppm reported for T^3 and -58 ppm reported for T^2 resonance of surface functionalized aminopropyl silica).[12] A smaller fraction of the imprint is bound to the framework with two

oxide linkages per silicon (note shoulder on T^3 peak at -58±1 ppm), and there is no detectable imprint bound to the framework with less than two anchors per imprint silicon (no detectable T^1 silicon). The spectra in Figure 4.4.5 demonstrate that approximately equal degrees of condensation of the imprint in the one, two and three point silicas exist and thus indicate that increased steric demands for the multiple point imprints did not result in lower degrees of imprint condensation to the silica framework.

4.4.2 Deprotection Process

The objective of the deprotection process is to cleave the carbamate bond and generate porosity around which the imprinted amines are convergently positioned. The reaction needs to be performed in a manner that does not destroy the integrity of the silica framework. This requires a deprotection strategy that will selectively hydrolyze the carbamate functionality without hydrolyzing silica. To assess the effectiveness of a particular deprotection method, a high-silica faujasite (FAU) (Tosoh HUA-390 with Si/Al ca 300) was used as a substitute for the amorphous sol-gel-derived silica. The crystallinity of the zeolite permits the use of diffraction-based methods to study the degree of integrity of the silica material framework. Figure 4.4.6 illustrates the results of using this model system on two different deprotection strategies: sodium peroxide treatment[13] and trimethylsilyliodide. Although sodium peroxide is a proven reagent for the cleavage of amide bonds and

their corresponding transformation to the free amines and acids,[14] it is

unsuitable for use in the current imprinting method due to its non-specific

hydrolysis of the silica framework (base-catalyzed). In comparison, the

Lewis acid trimethylsilyliodide (TMSI) cleaves benzyl carbamates to amines

and benzyl iodides via a silyl carbamate intermediate in the reaction

sequence shown in Scheme 4.4.1.[15] TMSI is specific to the carbamate

functionality and does not destroy the integrity of the bulk silica framework,

as evidenced by the same X-ray powder diffraction intensities (within

experimental error) before and after deprotection for FAU shown in Figure

4.4.6.[16]
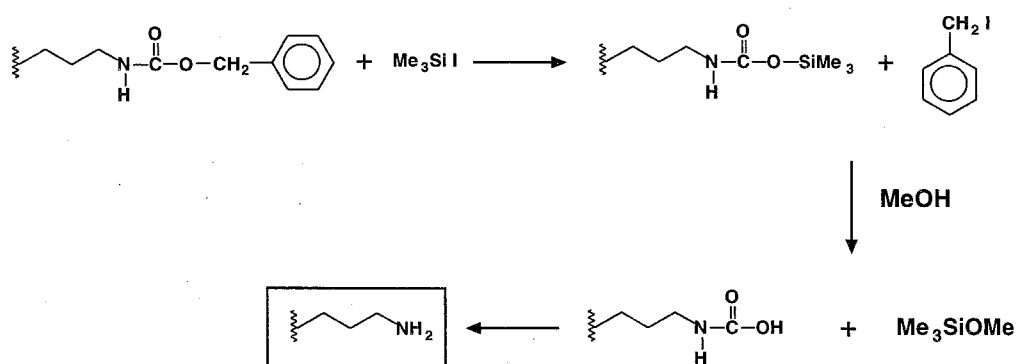
Scheme 4.4.1. Illustration of carbamate deprotection with TMSI. The first step is a transesterification reaction to convert the benzylcarbamate to the trimethylsilylcarbamate. Treatment with a suitable OH source yields the free carbamic acid, which spontaneously loses CO_2 to provide the free amine.

The X-ray-based crystallinity investigation of zeolite FAU above confirms that TMSI does not alter the *bulk* crystallinity of the silica. However, it could still be possible that although long-range order in the amorphous material is maintained, *local* order indicative of silica immediately adjacent to where carbamate cleavage is occurring may be compromised. This will be so provided a significant amount of HI is not generated during the deprotection procedure (can occur if there are a large number of OH groups remaining since the TMSI will react with these groups to TMS-cap them and make HI as a by-product of the capping reaction). The HI can subsequently serve as an acid catalyst for the hydrolysis and degradation of the silica framework. Note that for the zeolite model used this is not a particularly significant problem due to the extremely low silanol defect density in the *crystalline* silica. However, in the amorphous silica, there are silanol sites as evidenced by the fraction of Q^3 silicon (as discussed in Section 4.4.1). To decrease the generation of HI during imprinted silica deprotection, the silica is TMS-capped under neutral conditions before deprotection is initiated, with a neat, equimolar mixture of chlorotrimethylsilane and 1,1,1,3,3,3-hexamethyldisilazane.

To investigate the significance of this possibility as it relates directly to the TMSI-based deprotection method, ^{29}Si CP/MAS NMR spectroscopy was used to study the degree of condensation of T-silicon (silicon connected directly to the carbon tether in imprint) in the imprinted silicas before and

after deprotection. The results of this investigation are presented in Figure 4.4.5. As can be seen from the spectra, there are no observable changes that indicate a decrease in the degree of condensation of T-silicon in the one, two and three point imprinted silicas before and after deprotection. This conclusion strongly suggests that there is no *local* hydrolysis of silica occurring in the vicinity of imprint deprotection. To summarize, the TMSI-based deprotection protocol provides reactivity for only the organic portion of the imprinted silicas and does not appear to alter the silica framework, either in the long-range order or in the local vicinity of where deprotection is occurring.

4.4.3   *Imprinted Silica Characterization After Deprotection*

Figure 4.4.7 shows scanning electron micrographs (SEMS) of a deprotected two point material. The particles have no macroscopic porosity on the length-scale of the SEM, and the particle sizes are consistent with the method of preparation described above. No evidence of flocculent particles indicative of partially hydrolyzed silica is observed.

The deprotection process illustrated in Figure 4.2.1 can be followed using ^{13}C CP/MAS NMR. This spectroscopic method can be employed as a sensitive analytical method to investigate the extent of deprotection by measuring the decrease in the resonances corresponding to the functional groups being cleaved from the silica (carbonyl, aromatic, and benzyl

methylene). Figure 4.4.3 shows ^{13}C CP/MAS NMR of deprotected one, two and three point materials (corresponding protected spectra discussed in Section 4.4.1). The peak assignments are consistent with those reported in the literature for aminopropylated silica particles;[12] CP-MAS ^{13}C NMR of deprotected 1-point material: 9.7 ($\underline{C}H_2$); 22.9 ($\underline{C}H_2$); 42.8 ($\underline{C}H_2$); 129 ($\underline{C}H$) (weak), CP-MAS ^{13}C NMR of deprotected two point material: 10.5 ($\underline{C}H_2$); 23.1 ($\underline{C}H_2$); 43.2 ($\underline{C}H_2$) (the two point material also shows some residual ethoxy moieties resulting from incomplete condensation and hydrolysis at 54.1 ($CH_3\underline{C}H_2O$) and 17.5 ($\underline{C}H_3CH_2O$) ppm), CP-MAS ^{13}C NMR of deprotected three point material: 10.1 ($\underline{C}H_2$); 21.7 ($\underline{C}H_2$); 43.0 ($\underline{C}H_2$); 128.1 ($\underline{C}H$) (weak); 139.2 ($\underline{C}H$) (weak); 158.9 ($\underline{C}=O$) (weak). The degree of deprotection achieved in the one and two point materials as judged from the decrease in areas of the carbamate resonances from these spectra is $85\pm10\%$. This results in a number density of approximately 0.27 mmol amines/g of deprotected silica. The three point material, despite a higher deprotection temperature of 80 °C, maintained a higher amount of imprint. The NMR spectrum in Figure 4.4.3f shows some aromatic resonance remaining in the three point material. This amount is disproportionate with the carbonyl intensity of the imprint, as judged from the spectrum of the capped three point material, in Figure 4.4.3e. Further investigation and optimization of deprotection conditions is necessary for the three point material. However, an estimate of the deprotection achieved is $70\pm15\%$

based on the integration of the aromatic resonances between the protected and deprotected silicas.

The deprotection process can also be followed by the disappearance of the carbonyl stretching band of the carbamate in the imprint via infrared spectroscopy. The subtraction spectrum between the capped and the deprotected materials yields the infrared spectrum of the imprint immobilized in the silica. These spectra are shown in Figure 4.4.8 for the one, two, and three point imprinted silicas. Note the strong carbonyl band at 1700 cm^{-1} and the amide II band at approximately 1550 cm^{-1}. The frequency of the carbonyl band is significantly shifted toward lower frequency from its value in a non-interacting CCl_4 environment which was measured to be 1729 cm^{-1} for the one, two and three point imprints. This is consistent with a significant interaction between the silica framework and the imprint and suggests the formation of a shape selective pocket surrounding the imprint in the silica preceding deprotection.

### 4.4.4 Creation of Microporosity via Imprinting Process

Todate in the molecular imprinting field, there has not been a single account of increased porosity generated by the imprinting process. Here, we investigated the argon adsorption isotherms at liquid nitrogen temperatures of a two point material before deprotection (whose NMR spectrum is shown in Figure 4.4.3c), and a two point material after

deprotection (whose NMR spectrum is shown in Figure 4.4.3d). The argon adsorption isotherms are shown in Figure 4.4.9. Most notable is the significant increase in argon uptake in going from the protected (washed in acetonitrile and chloroform similar to deprotected material to remove residual capping reagents prior to adsorption) to the deprotected two point imprinted silica. This creation of microporosity is expressed in the subtraction isotherm represented in Figure 4.4.10 (the two point deprotected isotherm subtracted from the two point protected one). Here, the difference in volume adsorbed between the two materials reaches a limiting value of approximately 27 cm^3 STP/g. Using Cerius^2 molecular mechanics software,[17] a molecular volume of the fragment of imprint removed from the two point material during deprotection was calculated to be 450 $Å^3$, and this corresponds to a bulk density of organic fragment within the silica of 0.7 g/cm^3. Hence, the argon adsorption value of the difference in volume between the two point protected and deprotected materials represents a value of approximately 0.25 mmol amines/g or 80% deprotection. These values are consistent with those obtained from the solid state NMR data presented in Figure 4.2.2, which represents data from the same batch of materials (see Section 4.2.2). Because most of the difference in adsorption capacity is observed below a relative pressure of 0.1, the porosity generated by the imprinting process in the two point material is in the microporous regime (as it should be based on the size of the imprint fragment removed).

Alternatively, this increase in microporosity afforded by imprinted silica deprotection can be represented in the form of a pore size distribution by the method of Horvath-Kawazoe.[18] Figure 4.4.11 shows pore size distributions for the two point imprinted silica before and after deprotection. The increase in porosity accompanying two point deprotection corresponds to the length-scale of imprint fragment removal.

4.4.5   Presence of Imprinted Primary Amine Functionality

The presence of amine functionality in the deprotected materials was investigated by treating the deprotected material with five molar equivalents of acetylacetone in a pH 7.4 phosphate-saline (PBS) buffer at room temperature.   Acetylacetone reacts with primary amines to form a carbinolamine that subsequently collapses to a Schiff base. A stable covalent interaction with the primary amine of the deprotected silica is then formed when the Schiff base undergoes tautomerization to an enamine that has a strong ultraviolet absorption at approximately 316 nm.[19] This process is summarized in Scheme 4.4.2 below.
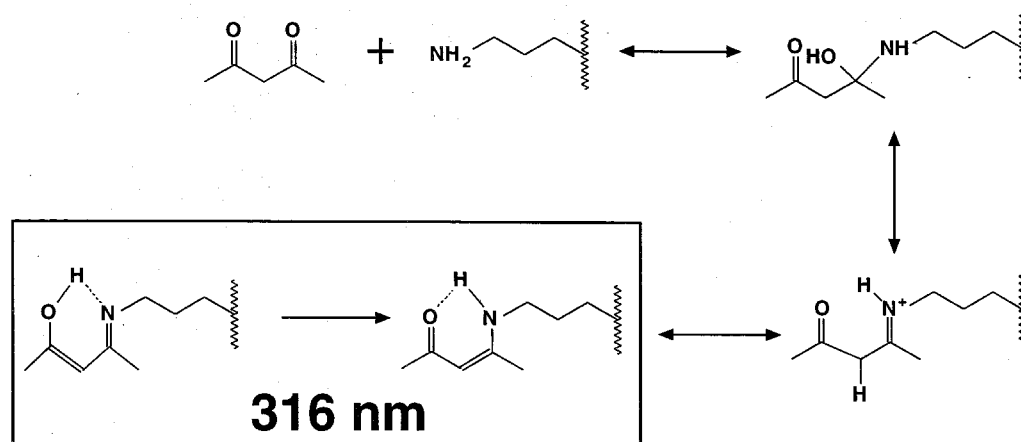
Scheme 4.4.2. Illustration of various intermediates formed during reaction of acetylacetone with primary amine of imprinted silica.

Figure 4.4.12 shows the diffuse-reflectance, ultraviolet spectrum of the acetylacetone-treated one point material. The prominent peak at 316 nm is indicative of the enamine formation and indicates the presence of a primary amine moiety in the deprotected material.

4.4.6 Quantifying Number of Amines with Benzoic Acid Adsorption

The number density of amines created during the imprinting process was estimated by non-covalent association of adsorbed benzoic acid from chloroform to the amine sites (the adsorption experiment was monitored by UV spectrophotometry). The results are presented in Table 4.4.1 for the same batches of one, two, and three-point silicas as were used for generating the data shown in Figure 4.4.3. All of the imprinted silicas investigated have amines resulting from the imprinting process. The number

density of amines accessible to benzoic acid is consistent with the values determined by NMR for the one and two point materials and is somewhat smaller than that determined from solid-state NMR for the three point material. This may be due to steric considerations (difficulty with getting several acids into a limited void space).

4.4.7 Functional Group Positioning via Fluorescence Investigation

Pyrenebutyric acid (PBA) was used as a fluorescence probe molecule to ascertain the molecular-level positioning of amines in the one and three point silicas. The basic fluorescence characteristics of PBA are summarized in Scheme 4.4.3. PBA was adsorbed into the zero, one and three point silicas. The silicas were then Soxhlet extracted in chloroform for 24 hours to remove physisorbed PBA (the silicas were extracted simultaneously in separate thimbles). Subsequently, the fluorescence of these materials at 340 nm (near maximum in UV spectrum) was analyzed. The fluorescence emission spectra are shown in Figure 4.4.13. The three point material shows significant excimer emission relative to the one point and reference materials. This is consistent with the concept of three amines being tightly positioned approximately 7 Å apart. The three point material has a monomer to excimer ratio that is approximately 24 times smaller than that of the one point material and 1.8 times smaller than that of the zero point material, where the PBA is non-specifically physisorbed in microporous voids.

monomer   excimer

emission ca 400 nm   emission ca 470 nm

Scheme 4.4.3. Diagram illustrating the fluorescence properties of PBA. When two PBA molecules can come to within approximately 3 Å of each other in a stacked configuration, excimer emission can occur, which can be accurately quantified by fluorescence measurements. These photophysics form the basis for the use of PBA as a distance probe for the imprinted silicas.

The results of this comparison are presented in Table 4.4.2. The PBA fluorescence study above suggests at least some degree of control over functional group positioning in the imprinted materials, as the one point silica gave a fluorescence signature consistent with well-isolated amines and the three point material gave a fluorescence signature consistent with local ordering of the amines, in comparison with a control zero point silica containing no amines. However, the fluorescence study does not provide quantitative information about how the amines are positioned relative to one another in the imprinted silicas or a sampling of all

imprinted sites (approximately one percent of sites sampled with this method as determined by UV assay on hydrolyzed silicas in 1N NaOH).[20]

4.4.8   Diacid Binding into One and Two Point Materials

In an attempt to provide further proof of amine positioning in the imprinted silicas, a study of diacid binding to the imprinted materials was performed. A diacid in principle has the capability to interact with both amines in the two point imprinted silica, if the spacer between the carboxyl groups of the acid is sufficiently long to permit interaction. Thus, experiments with diacids of different lengths were used in order to investigate whether a difference in binding could be observed in going from a configuration where only one salt-bridge interaction should be possible to a configuration where two salt-bridge interactions can occur between the diacid and the amines of the imprinted silica. Adipic (6 carbon), malonic (3 carbon) and oxalic (2 carbon) acids were used for the binding study (adipic and malonic diacids are anticipated to be long enough to interact with the two amines in the two point material assuming a hydrogen bonding distance of ca 3 Å between the carboxyl carbon and the amine nitrogen). The diacids were adsorbed into the one and two point materials at a coverage corresponding to full, fifty percent, and ten percent of the amines available in the silicas assuming monodentate binding of diacid, as determined by the benzoic acid titration method (*vide supra*), from a mixed cyclohexane:methyl t-butyl ether solvent

system (9:1 (v:v) for oxalic and malonic acids and 7:3 (v:v) for adipic acid). The adsorptions were followed by liquid-phase infrared spectroscopy, and from this it was determined that the binding of the diacids was quantitative for all of the experimental conditions investigated. The position of the infrared band corresponding to the carbonyl stretch of the adsorbed diacid, as determined by subtraction spectra of the bound and unbound silicas, is represented in Table 4.4.3 for the three acids under the experimental conditions investigated. No difference in carbonyl shift is observed between the one and two point silicas. Furthermore, there is no change in the infrared spectrum of the adsorbed diacids in going from ten percent to full loading in the two point material. These results are inconsistent with the concept of bidentate binding of diacid. In going from full loading in the two point material, where only monodentate binding of diacid should be possible, as in the one point material, to ten percent loading in the two point material, where bidentate binding should be favored, a change in the diacid binding should occur that is indicative of a monodentate to bidentate transition.

To decrease the significance of entropy, infrared spectroscopy was performed at liquid nitrogen temperatures to further favor a multi-dentate binding configuration of the diacid in the two point material. No change in the main carboxylate band is observed in going to liquid nitrogen temperatures for the adipic and malonic acids (data in Table 4.4.3). For

malonic and adipic acids, however, a new band higher in frequency to the original carboxylate band appeared at liquid nitrogen temperatures in the ten percent-loaded silicas. The source of this band may be due to physisorbed acid interacting with a small concentration of silanols on the surface of the silica (*vide infra*).

In stark contrast to the amine-containing silicas, the zero point silica physisorbed malonic and oxalic acid and shows two bands in the carbonyl region at room temperature. For oxalic acid the lower-frequency band of these two bands is in the same range as the carboxylate anion band in the imprinted materials. For malonic acid the lower band is not quite as depressed in frequency as the band observed in the imprinted materials. For both oxalic and malonic acids, the high-frequency band observed in the carbonyl region of the zero-point material is not in the frequency range of carboxylate anion and likely corresponds to weakly physisorbed diacid (data in Table 4.4.3).

Based on the infrared spectroscopy results, it is likely that internal silanol groups (recall that there is Q^3 silicon in the materials) of silica, probably due to their greater number density than the corresponding imprinted amines, are not inert towards the diacids. These silanols may have prevented a true bidentate binding configuration from occurring to the imprinted amines in the two point material. It is possible that one attachment may have been with the amine, for example, as evidenced by the carboxylate anion bands reported

in Table 4.4.3, but the other carboxyl of the diacid may bind to surface

hydroxyls rather than to the imprinted amines. This suggested scenario is

illustrated in Scheme 4.4.4. At this time, however, it remains unknown as to

why true bidentate binding is not observed.

4.4.9 Imprinted Material Binding Characteristics

Several other reagents were adsorbed into the imprinted silicas,

including the dicarboxylate **4**. The results of these experiments are

presented in Table 4.4.4.

favorable **more favorable**
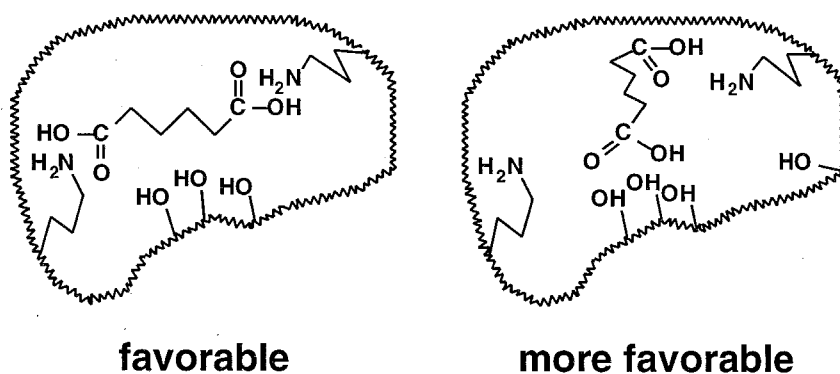
Scheme 4.4.4. Illustration of diacid binding in two point material to generate a single interaction with imprinted amine and a single interaction with silanol groups (preferred) in imprinted silica.

It is interesting that despite the similarity of the transition state for the

covalent attachment of **4** and acetylacetone discussed in Section 4.4.5, **4**

did not bind covalently to the imprinted one and two point silicas. The

dicarboxylate **4** is able to physisorb into the silica pore system to the same

extent with the one and two point silicas (upon exposing the one and two point silicas to **4** approximately 60% adsorbed into the silica, but it is extracted out and not observed in the infrared spectrum of the treated silicas following a brief wash with chloroform). The vital question is, given the similarity in the possible covalent binding mechanism between **4** and acetylacetone, why did **4** not bind while acetylacetone did? A likely explanation is shape-selectivity of the imprinted cavity, which allows the tetrahedral carbon transition state but does not permit it with a bulky group such as imidazole off of the carbonyl carbon during nucleophilic attack by the imprinted amine. Other examples of reagents that bind to surface functionalized amines but not to the imprinted amines are copper(II) acetate and 2,4,6-trinitrobenzene sulfonic acid (TNBS) (although in these instances the problem of partitioning and covalent attachment has not been separated).

4.4.10   Catalysis

As an example of the shape-selectivity discussed in a previous section, a Knoevenagel C-C bond forming reaction was performed with a bifunctional reactant. The reaction investigated is shown in Scheme 4.4.5 below. It is observed that the monofunctional product was produced while the difunctional product is not during the course of reaction over both the one point and two point imprinted materials. This is a further testament to the
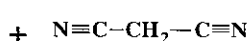
shape selectivity phenomena alluded to in Section 4.4.9. The results showing the selectivity of the imprinted materials in comparison with a surface-functionalized, aminopropylated silica, which does not exhibit shape-selectivity for this reaction, are shown in Figure 4.4.14. As can be observed from this phase-plot, the surface functionalized silica generates a certain amount of monofunctional product before the exclusive production of the bifunctional product begins. That is to say, at a limiting value of the monofunctional product concentration (as predicted from elementary reaction kinetics theory), the synthesis of the bifunctional product becomes significant. However, in contrast, the imprinted materials do not follow such a trend and continue to produce monofunctional product at a concentration that is greater than two times the value at which monofunctional product is converted into difunctional product in the surface-functionalized material. The data in Figure 4.4.14 can be alternatively represented as time-dependent product concentrations for the imprinted and surface functionalized catalysts, and these data are shown in Figures 4.4.15 and 4.4.16 for the monofunctional and bifunctional products, respectively. The reaction rates as computed from the initial curve in the conversion of dialdehyde starting material per unit time are shown in Figure 4.4.17. As can be seen, the initial rates of the imprinted materials are somewhat lower than that of the surface functionalized silica (by a factor of approximately 4.5). The reduction in rate is expected because of the fact that the imprinted

silicas are microporous while the surface functionalized silica is not. However, the main point is that the imprinted materials have the capability to discriminate based on shape, as the examples in this section and the previous one demonstrate.
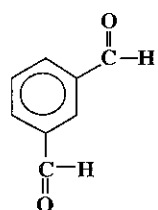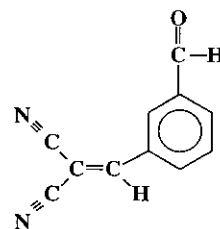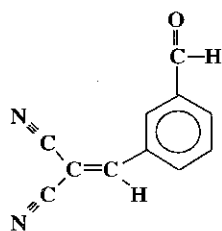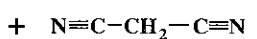

isophthalaldehyde malononitrile → monofunctional product
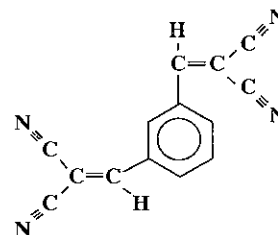
monofunctional product malononitrile → bifunctional product

Scheme 4.4.5. Illustration of Knoevenagel reaction of isophthalaldehyde and malononitrile to make monofunctional and bifunctional product via base catalysis.

4.5 Conclusions

A new method of molecular imprinting silica with amine functionality has been developed. The method has been characterized at different stages of the imprinting process by solid-state NMR and FTIR spectroscopies. The imprinted silicas synthesized with this approach are unique in that they show

porosity being created by the imprinting process at the length scale of the imprint. The final imprinted silicas display the presence of primary amine functionality and possess shape-selectivity for catalysis and covalent binding of molecules.

A most vital issue is whether the positioning of the amines in the two and three point materials has been accomplished. Pyrene-probe-based fluorescence measurements seem to suggest that it has, since they show a significant amount of excimer in the three point material and a significant amount of monomer in the one point material. These two extremes would otherwise be difficult to achieve in practice, as exemplified by the mixed fluorescence behavior of the zero point control in comparison. However, due to the low sampling percentage (approximately one percent of the total number of imprinted sites) inherent to the fluorescence technique, it is difficult to generalize the results of the fluorescence study to make a conclusion pertaining to the degree of homogeneity in the imprinted sites. Steady-state fluorescence measurements do not provide the necessary quantitative information to assess how far apart the amines may be. As a result, the problem of quantitatively characterizing the imprinting process at its most fundamental level, as to the control of functional group positioning on the sub-nanometer length scale, has yet to be accomplished.

4.6   Recommendations

In addressing the issue of quantitative determination of functional group positioning, several key pieces of information can be learned from the studies mentioned above.   In designing the ideal probe molecule for characterizing the imprinting process, it is best to use a dual functional molecule. On one end it should bind <u>covalently</u> to the imprinted site in a monodentate fashion so that problems dealing with monodentate binding of potentially bidentate adsorbates can be avoided and so that the binding can be quantitative and not influenced by factors such as silanol groups or solvent environments.[8b]   On the other end of the probe molecule, there should be a distance-sensitive moiety (based on either charge transfer, EPR-activity or other spectroscopic signature). Thus far there has been no characterization of an imprinted material with such a designed probe molecule, which could make the characterization relatively unambiguous and straightforward.

In addition to the issue of the design of such a universal probe molecule for a particular imprinting system, other methods of analytical characterization, such as those based on fluorescence-lifetime measurements and advanced solid-state NMR techniques, may yield valuable microscopic information as well about the imprinted environment.

4.7   Experimental Section

4.7.1   General

FTIR spectra were obtained using a Nicolet System 800 Spectrophotometer with KBr pellets. A homemade infrared dewar was used (CaF_2 windows) for the liquid nitrogen temperature, infrared acquisitions. A CaF_2 solution cell with 0.1 mm path length (Spectra Tech FT04-757) was used for quantitative solution phase FTIR work. A Scintag XDS-2000 diffractometer equipped with a germanium solid state detector was used to obtain X-ray (Cu-Kα radiation) powder diffraction patterns. Solid-state NMR spectroscopy was performed on a Bruker AM 300 spectrometer equipped with solids accessories. Samples were packed into 7 mm ZrO_2 rotors and spun in air at approximately 4 kHz. Typical recycle delays were 60 seconds. Scanning electron micrographs were recorded on a Etec Autoscan instrument. Gas chromatography was performed on a Hewlett-Packard HP 5890 Series II instrument.

4.7.2   Fluorescence Measurements

Pyrenebutyric acid (PBA) was purchased from Aldrich Chemical Co. at 99.3% (by gas-chromatography) purity. The purchased acid was recrystallized in benzene a total of two times prior to use in fluorescence experiments. A typical procedure was to add 200 mg of imprinted silica to 32 mg of PBA in 160 mL of chloroform. Adsorptions were performed with

cooling stirrers at a temperature of 5 °C and for the duration of 1 week. The silica was collected by centrifugation. The zero, one and three point silicas were subsequently Soxhlet extracted in chloroform for 24 hours in one batch (separate thimbles). The samples were stored in argon-sealed vials prior to fluorescence measurement. Steady-state fluorescence measurements were performed at room temperature on a Hitachi FS-4500 fluorimeter equipped with a front surface attachment using the following parameters: 700 V excitation voltage for one point material (950 V for two and three point materials), 15 nm/min scan speed, 2.5 nm excitation slit width, 2.5 nm emission slit width and 340 nm excitation wavelength. Spectra were collected as uncorrected. The silica samples were later dissolved in 1 N NaOH at 80 °C, and their pyrene content was quantified using UV spectrophotometry at 342.2 nm and an extinction coefficient of 36844 M^{-1}.

4.7.3 Acetylacetone Binding

500 µl of methanol were added to 300 mg of one point silica. Subsequently 30 mL of pH 7.4 phosphate-saline (PBS) buffer were added, and 31 µl of acetylacetone were added to this mixture. The resulting slurry was stirred for 6 hours at room temperature, after which time it was filtered and washed with 45 mL of pentane. The sample was dried under ambient conditions prior to analysis. Ultraviolet spectra were acquired on a Cary-3 spectrophotometer equipped with a Labsphere specular reflectance

accessory. Subsequent Soxhlet extraction of acetylacetone-bound one point silica in acetonitrile for 24 hours did not alter the diffuse-reflectance UV spectrum, thus indicating covalent attachment of the enamine. Infrared spectrocopy on the extracted, acetylacetone-bound one point silica revealed a band at 1637 cm^{-1} corresponding to the enamine carbonyl stretch.

4.7.4   *Benzoic Acid Titration Experiments*

5.0 mg of imprinted silica were equilibrated in a 4 mL vial with a 9.3 x 10^{-4} chloroform solution of benzoic acid. The slurries were stirred for an equilibration period of four days. After this time, the vials were emptied into a syringe equipped with a 0.7 µm glass fiber filter (Whatman). The benzoic acid concentration was analyzed by UV spectrophotometry at 275 nm using an extinction coefficient of 1076 M^{-1}.

4.7.5   *Dicarboxylate 4 Experiments*

60 mg of one and two point imprinted silica (same batch as discussed in Section 4.4.6) were equilibrated with 4 mL of a 1.48 mM solution of **4** in chloroform at 50 °C for 24 hours. The equilibration conditions were chosen so as to have an equimolar concentration of amines and carboxylic acid functionalities. UV spectrophotometry on the solutions after equilibration was performed at 270 nm using an extinction coefficient of 256. The results indicate that 61.5 percent of **4** in solution originally adsorbed into the one

point material and 60.8 percent of **4** in solution originally adsorbed into the two point material. The materials were washed with 60 mL of chloroform and dried in a dessicator prior to infrared spectroscopy.

4.7.6   *Knoevenagel Catalysis*

1.5 mmol isophthalaldehyde and 3.0 mmol malononitrile were combined in 5 ml acetonitrile solvent with 8 mg hexamethylbenzene (internal standard) at 80 °C. Subsequently 30 mg imprinted silica or 6 mg surface functionalized, silica catalyst were added (equal number of amines). The reaction vial was magnetically stirred with a micro stir bar (Bel-Art) continuously. The imprinted catalysts both contained approximately 0.2 mmol amine sites/g catalyst, and the surface functionalized contained 1 mmol amines/g catalyst.

4.8. References

[1]   Rebek, Jr., J. *J. Heterocycl. Chem.* **1990**, *27*, 111.

[2]   (a) Wolfe, J.; Muehldorf, A.; Rebek, Jr., J. *J. Am. Chem. Soc.* **1991**, *113*, 1454. (b) Pieters, R. J.; Huc, I.; Rebek, Jr., J. *Tetrahedron* **1995**, *51*, 485. (c) Rojas, C. M. and Rebek, Jr., J. *Bioorg. Med. Chem. Lett.* **1996**, *6*, 3013.

[3]   Vögtle, F.; Ibach, S.; Nieger, M.; Chartroux, C.; Krüger, T.; Stephan, H.; Gloe, K. *Chem. Commun.* **1997**, 1809.

[4]   Davis, A. P.; Perry, J. J.; Williams, R. P. *J. Am. Chem. Soc.* **1997**, *119*, 1793.

[5]   (a) Lindsey, J. S.; Kearney, P. C.; Duff, R. J.; Tjivikua, P. T.; Rebek, Jr., J. *J. Am. Chem. Soc.* **1988**, *110*, 6575. (b) Hage, R.; Iburg, J. E.; Kerschner, J.; Koek, J. H.; Lempers, E. L. M.; Martens, R. J.; Racheria, U. S.; Russell, S. W.; Swarthoff, T.; van Vliet, M. R. P.; Warnaar, J. B.; van der Wolf, L.; Krijnen, B. *Nature* **1994**, *369*, 637. (c) Jubian, V.; Dixon, R. P.; Hamilton, A. D. *J. Am. Chem. Soc.* **1992**, *114*, 1120.

[6]   Wulff, G. In *Polymeric Reagents and Catalysts*; Ford, W. T., Ed.; ACS Symposium Series 308; American Chemical Society: Washington, DC, 1986.

[7]   (a) Wulff, G.; Heide, B.; Helfmeier, G. *J. Am. Chem. Soc.* **1986**, *108*, 1089. (b) Wulff, G.; Heide, B.; Helfmeier, G. *Reactive Polymers* **1987**, *6*, 299. (c) Tao, Y.; Ho, Y. *J. Chem. Soc., Chem. Commun.*

1988, *6*, 417. (d) Hwang, K; Yakura, Y.; Ohuchi, F. S.; Sasaki, T. *Mater. Sci. and Eng. C* **1995**, *3*, 137. (e)

Tahmassebi, D. C. and Sasaki, T. *J. Org. Chem.* **1994**, *59*, 679.

[8] (a) Whitcombe, M. J.; Rodriguez, M. E.; Villar, P.; Vulfson, E. *J. Am. Chem. Soc.* **1995**, *117*, 7105. (b) Shea, K. J. and Sasaki, D. Y. *J. Am. Chem. Soc.* **1991**, *113*, 4109. (c) Wulff, G.; Kirstein, G. *Angew. Chem. Int. Ed. Engl.* **1990**, *29*, 684.

[9] (a) Matsui, J.; Miyoshi, Y.; Doblhoff-Dier, O.; Takeuchi, T. *Anal. Chem.* **1995**, *67*, 4404. (b) Matsui, J.; Kaneko, A.; Miyoshi, Y.; Yokoyama, K.; Tamiya, E.; Takeuchi, T. *Anal. Lett.* **1996**, *29*, 2071. (c) Tomioka, Y.; Kudo, Y.; Hayashi, T.; Nakamura, N.; Niizeki, M.; Hishinuma, T.; Mizugaki, M. *Biol. Pharm. Bull.* **1997**, *20*, 397. (d) Sellergren, B.; Shea, K. J. *J. Chromatogr.* **1995**, *690*, 29.

[10] (a) Cochrane, W. P.; Pauson, P. L.; Stevens, T. S. *J. Chem. Soc. (C)* **1968**, 630. (b) Houk, J. and Whitesides, G. M. *J. Am. Chem. Soc.* **1987**, *109*, 6825.

[11] Brinker, C. J.; Keefer, K. D.; Schaefer, D. W.; Ashley, C. S. *J. Non-Cryst.* **1982**, *48*, 47.

[12] Sudhölter, E. J. R.; Huis, R.; Hays, G. R.; Alma, N. C. M. *J. Colloid and Interface Sci.* **1985**, *103*, 554.

[13] 60 mg of silica to be deprotected were suspended in 10 mL distilled water. 1.3 g of sodium peroxide were added, and the mixture was

stirred for 9 hours at 70 °C. Subsequently 10 mL of ethanol were added to the mixture, and the silica was filtered, washed with ethanol and dried under ambient conditions prior to X-ray measurement.

[14] Vaughn, H. L. and Robbins, M. D. *J. Org. Chem.* **1975**, *40*, 1187.

[15] Olah, G. A. and Narang, S. C. *Tetrahedron* **1982**, *38*, 2225.

[16] 54.6 mg of zeolite were weighed out for X-ray measurement in acquiring the powder patterns of the zeolite before and after deprotection (for quantitative comparison). Deprotection was performed at 40 °C for a period of 4 hours. Subsequently the zeolite was washed with acetonitrile, chloroform and methanol and dried under vacuum prior to X-ray analysis.

[17] The free volume function was used with a Van Der Waals scale factor of 1.00, medium grid spacing and a probe radius of 1.6 Å (corresponding to solvent radius) on the fragment of the two point imprint that is removed during deprotection. The geometry of the fragment was optimized using the Dreiding force field prior to the free volume calculation.

[18] Horvath, G.; Kawazoe, K. J. *J. Chem. Eng. Jpn.* **1983**, *16*, 470.

[19] Barbas III, C. F.; Heine, A.; Zhong, G.; Hoffmann, T.; Gramatikova, S.; Björnestedt, R.; List, B.; Anderson, J.; Stura, E. A.; Wilson, I. A.; Lerner, R. A. *Science* **1997**, *278*, 2085.

[20] This concentration of pyrene probe in silica is consistent with other pyrene-based, fluorescence investigations of silica. For example see: (a) Avnir, D.; Busse, R.; Ottolenghi, M.; Wellner, E.; Zachariasse, K. A. *J. Phys. Chem.* **1985**, *89*, 3521. (b) Ramamurthy, V.; Sanderson, D. R.; Eaton, D. F. *Photochem. and Photobiol.* **1992**, *56*, 297.

Material	BA Adsorbed (mmol/g silica) [a]	Percentage Deprotected [b]
Zero Point	0.02	N / A
One Point	0.23	73
Two Point	0.23	73
Three Point	0.07	22

a) BA represents benzoic acid. See Experimental Section for details.
b) Computed based on theoretical maximum of 0.31 mmol amine/g silica from material balance.

Table 4.4.1. Adsorption capacity of zero, one, two and three point silicas for benzoic acid.

Material	Monomer / Excimer [a]
Zero Point	1.3
One Point	17
Three Point	0.7

a) Represents monomer intensity (377 nm) divided by excimer intensity (467.6 nm).

Table 4.4.2. Monomer to excimer ratio measured from fluorescence emission of pyrenebutyric acid adsorbed in zero, one and three point imprinted silicas.

Material	Diacid	Loading Level[a]	Temp.	Carbonyl Band Frequency [b]
Zero Point	oxalic acid	50%	296 °K	1744 ± 10 and 1649 ± 10 cm^{-1}
One Point	oxalic acid	50%	296 °K	1654 ± 10 cm^{-1}
One Point	oxalic acid	100%	296 °K	1650 ± 5 cm^{-1}
Two Point	oxalic acid	50%	296 °K	1652 ± 10 cm^{-1}
Two Point	oxalic acid	100%	296 °K	1653 ± 5 cm^{-1}
Zero Point	malonic acid	50%	296 °K	1734 ± 10 and 1618 ± 10 cm^{-1}
One Point	malonic acid	50%	296 °K	1576 ± 10 cm^{-1}
One Point	malonic acid	100%	296 °K	1585 ± 5 cm^{-1}
Two Point	malonic acid	10%	296 °K	1588 ± 10 cm^{-1}
Two Point	malonic acid	10%	77 °K	1710 ± 10 and 1586 ± 10 cm^{-1}
Two Point	malonic acid	50%	296 °K	1582 ± 10 cm^{-1}
Two Point	malonic acid	100%	296 °K	1586 ± 5 cm^{-1}
Two Point	malonic acid	100%	77 °K	1588 ± 5 cm^{-1}
One Point	adipic acid	50%	296 °K	1569 ± 10 cm^{-1}
Two Point	adipic acid	50%	296 °K	1562 ± 10 cm^{-1}
Two Point	adipic acid	10%	296 °K	1558 ± 10 cm^{-1}
Two Point	adipic acid	10%	77 °K	1558 ± 10 and 1653 ± 15 cm^{-1}

a) Loading level represents fraction of amines bound in imprinted silica assuming monodentate binding of diacid. Adsorptions were performed at room temperature over a period of 24 hours in 4 mL of solvent at diacid concentrations corresponding to 2.735 mM (50% loading and 100% loading) and 0.547 mM (10% loading). 50 mg of the zero point material was used for all adsorption experiments.

b) Solution bands for: 1) oxalic acid bands at 1744.5 cm-1 and 1774.7 cm^{-1}, 2) malonic acid bands at 1741.4 cm^{-1}, 1755.9 cm^{-1} and 1779.3 cm^{-1} and 3) adipic acid a band at 1741.6 cm^{-1}.

Table 4.4.3.   Infrared bands of adsorbed diacids in imprinted silicas.

Material [a]	Reagent [b]	Physisorbed Attachment [c]	Covalent Attachment [d]
Surface-amine	benzoic acid	yes	N/A
Imprinted	benzoic acid	yes	N/A
Surface-amine	trinitrobenzene sulfonate	yes	yes
Imprinted	trinitrobenzene sulfonate	no	no
Surface-amine	copper(II) acetate	yes	yes
Imprinted	copper(II) acetate	no	no
Surface-amine	acetylacetone	yes	yes
Imprinted	acetylacetone	yes	yes
Surface-amine	dicarboxylate **4**	yes	yes
Imprinted	dicarboxylate **4**	yes	no

a) Surface-amine represents silica particle with aminopropyl groups on interior surface. Imprinted represents one, two and three point imprinted silicas.

b) 2,4,6-trinitrobenzene sulfonate was equilibrated in DMF with silica. Absorbance was monitored by UV spectrophotometry using extinction coefficient of 2732 M^{-1} at 300 nm at room temperature and 80 °C. Copper(II) acetate was equilibrated with materials in acetonitrile. Absorbance was monitored by UV spectroscopy. See Experimental Section for details on acetylacetone and dicarboxylate **4** procedures.

c) Physisorption that is reversible upon silica washing.

d) Covalent attachment refers to binding that is not reversible upon silica washing.

Table 4.4.4. Reagents treated with imprinted silicas and silica particles with aminopropyl groups dispersed on surface.
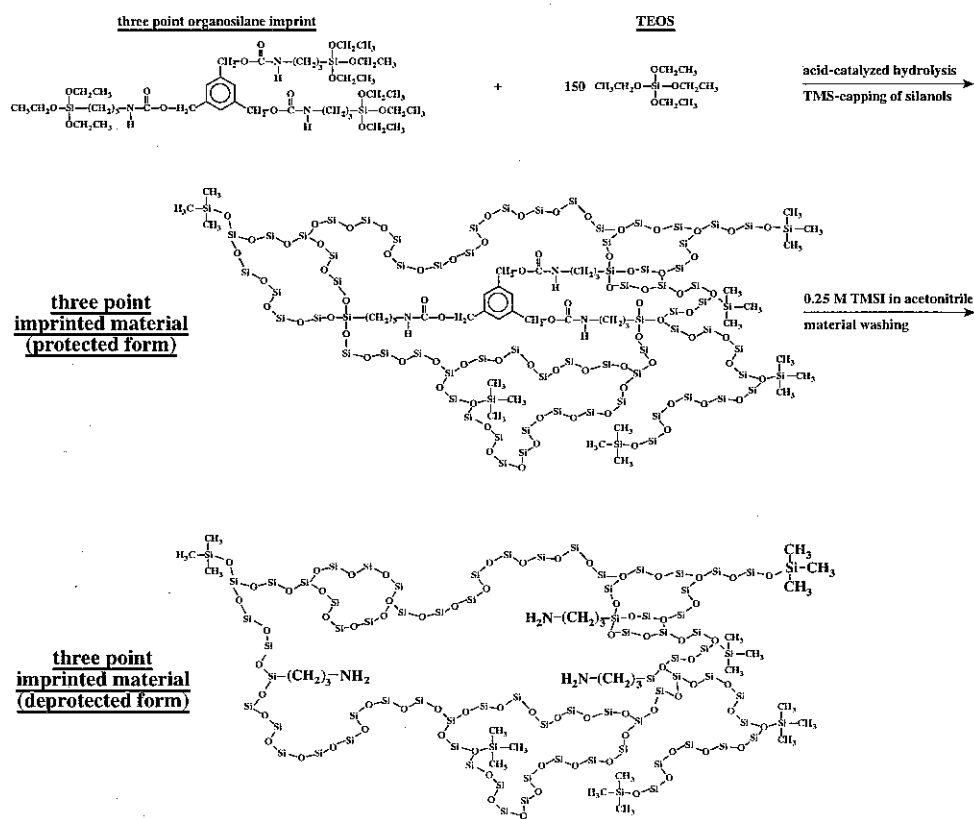
Figure 4.2.1. Illustration showing synthesis of three point imprinted silica encompassing all of the steps shown in Scheme 4.2.1.
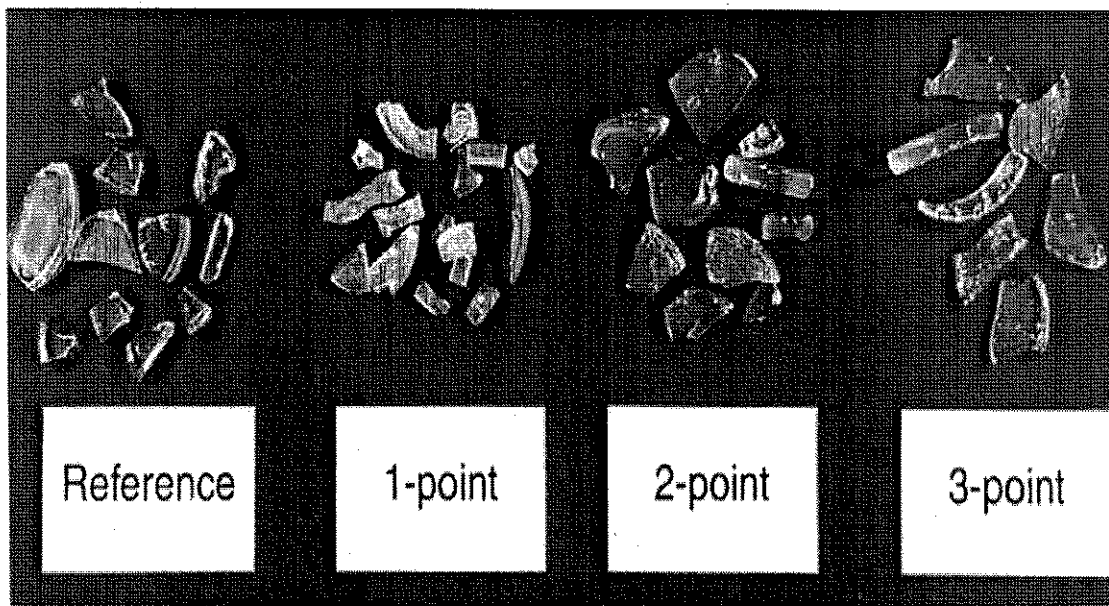
Figure 4.4.1. Optical photograph of zero (reference), one, two and three point imprinted silicas.
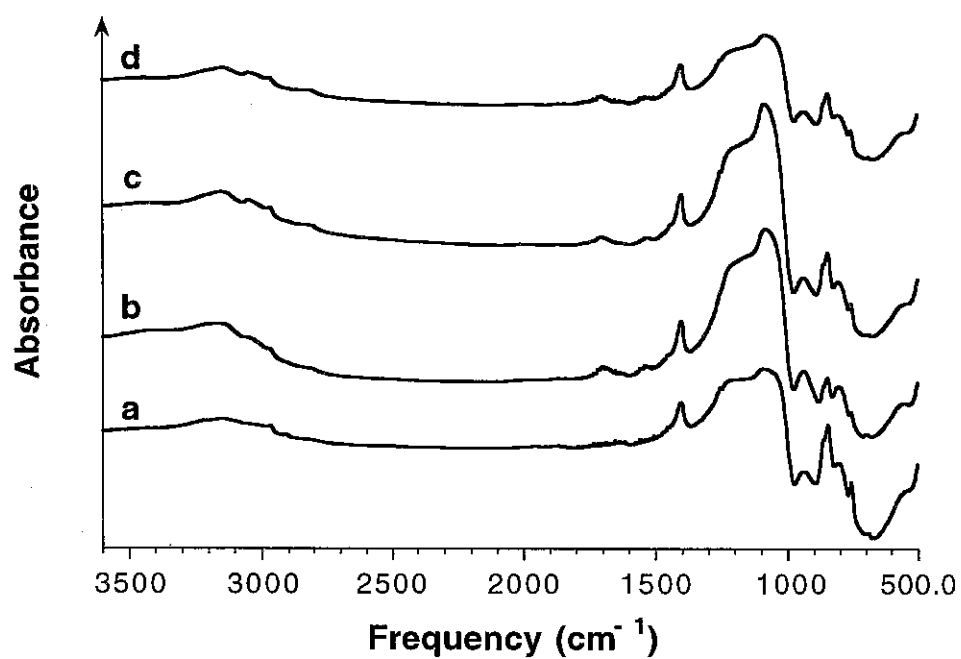
Figure 4.4.2.   Infrared spectra of the (a) capped zero point, (b) capped one point, (c) capped two point and (c) capped three point imprinted silicas.
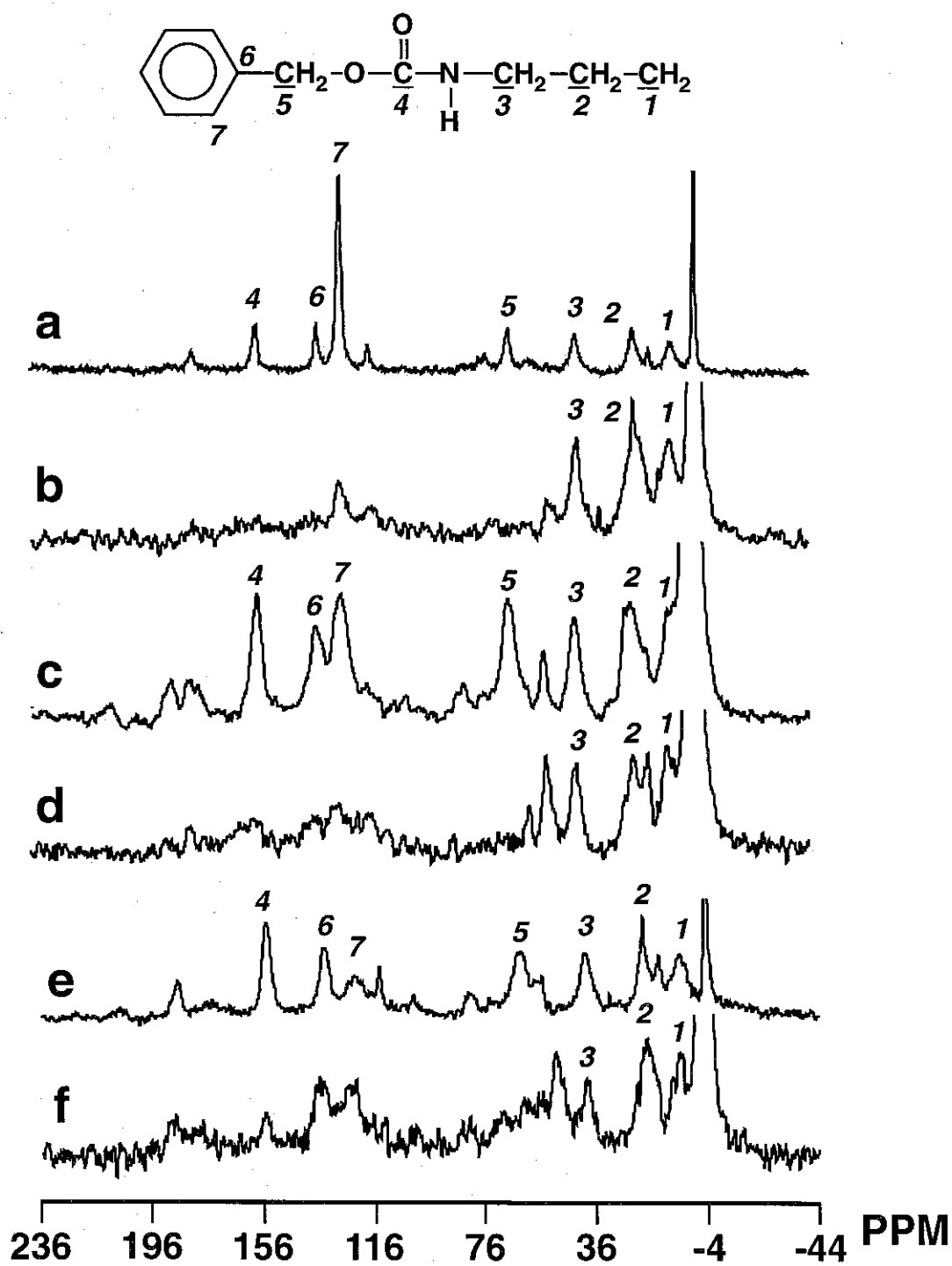
214

Figure 4.4.3. ^{13}C CP/MAS NMR spectra for (a) extracted one point, (b) deprotected one point, (c) capped two point, (d) deprotected two point, (e) extracted three point, (f) deprotected three point imprinted silicas.
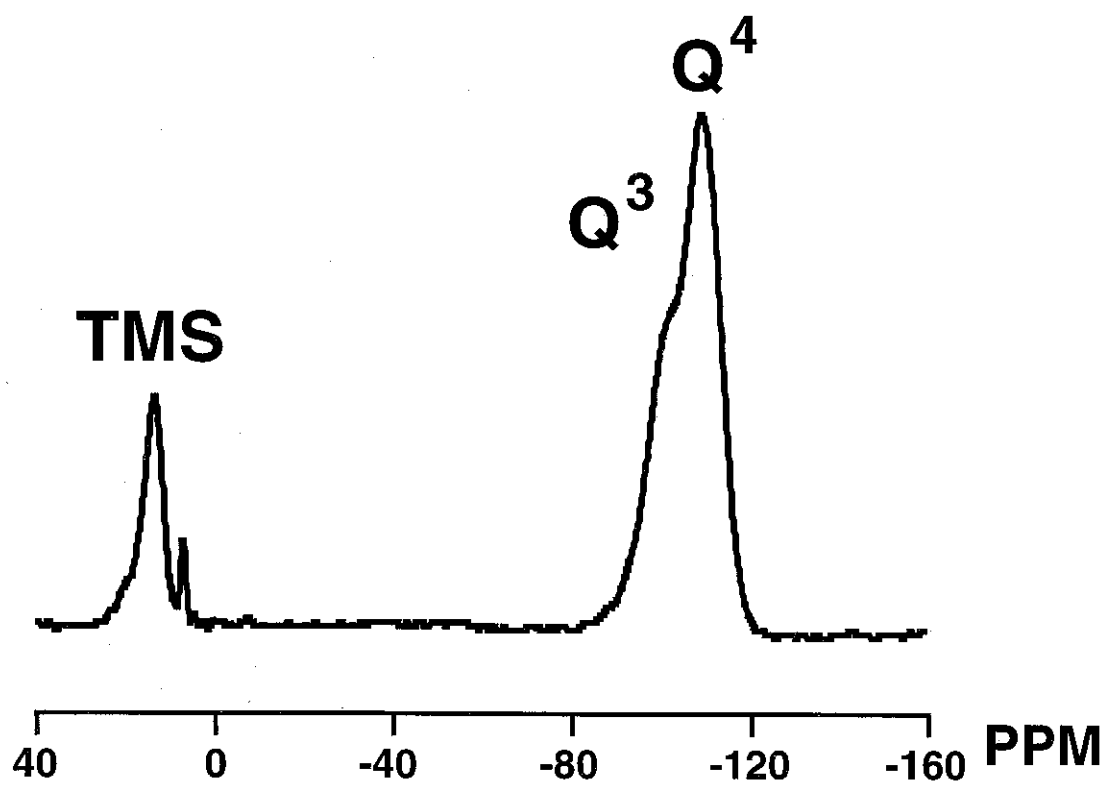
Figure 4.4.4. ^{29}Si block decay NMR spectrum for capped zero point material.
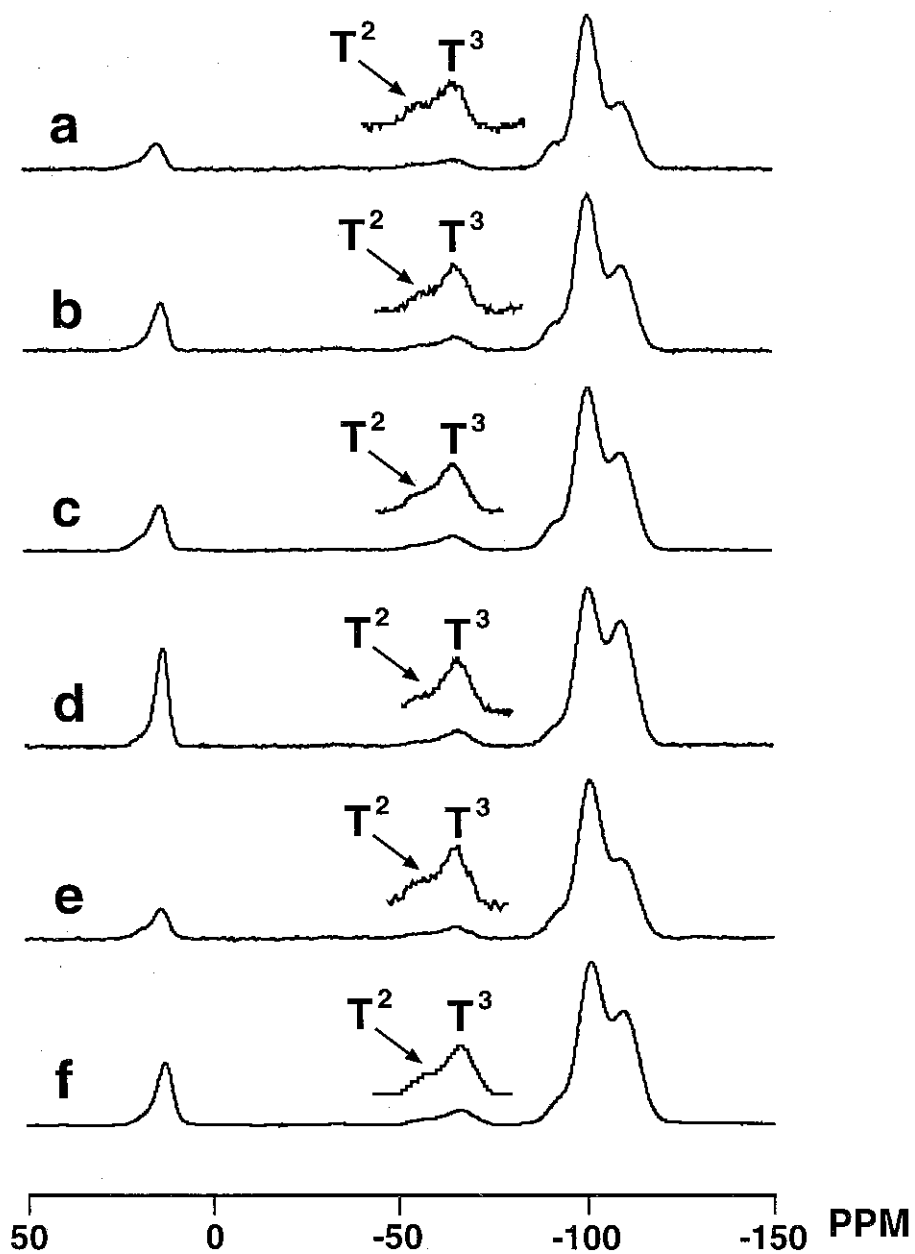
Figure 4.4.5. ^{29}Si CP/MAS NMR spectra of the (a) capped one point, (b) deprotected one point, (c) capped two point, (d) deprotected two point, (e) capped three point, (f) deprotected three point imprinted silicas.
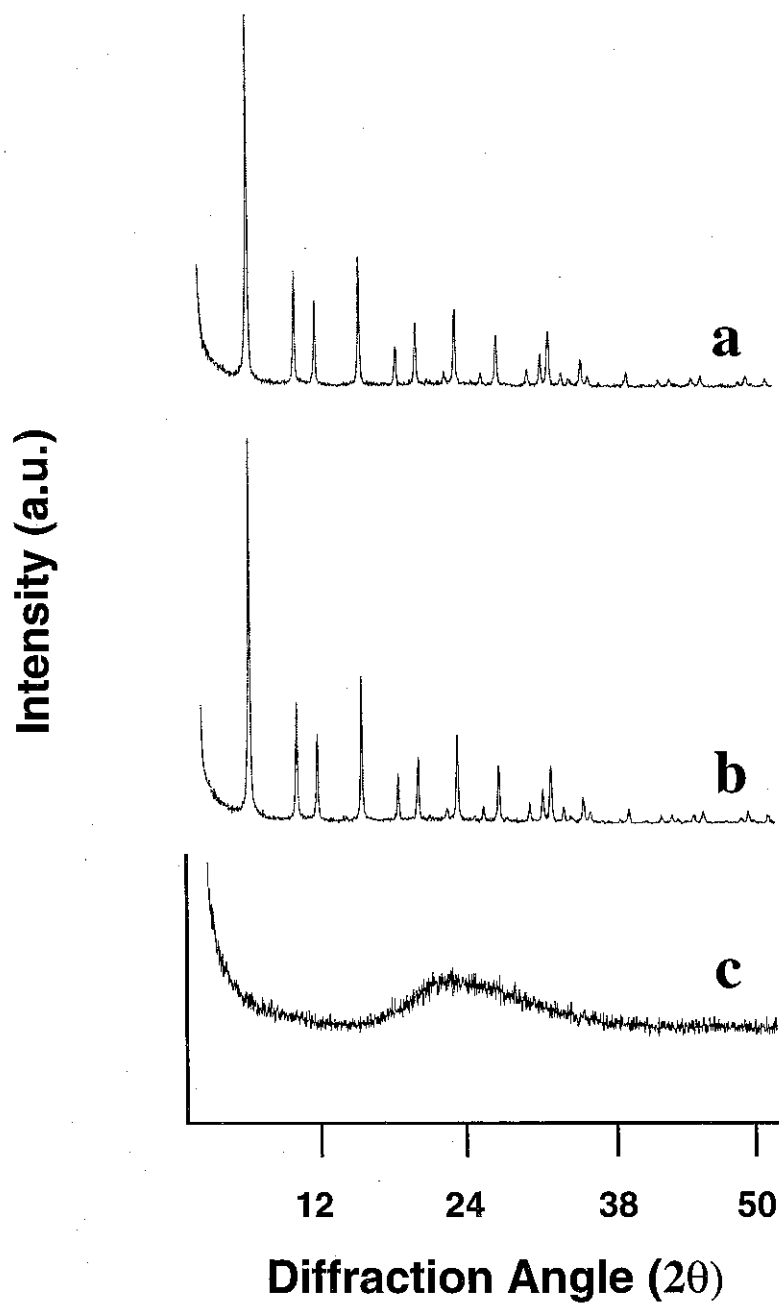
Figure 4.4.6.   X-ray powder diffraction patterns for (a) high silica faujasite, (b) TMSI deprotected high silica faujasite, (c) sodium peroxide deprotected high silica fajasite.
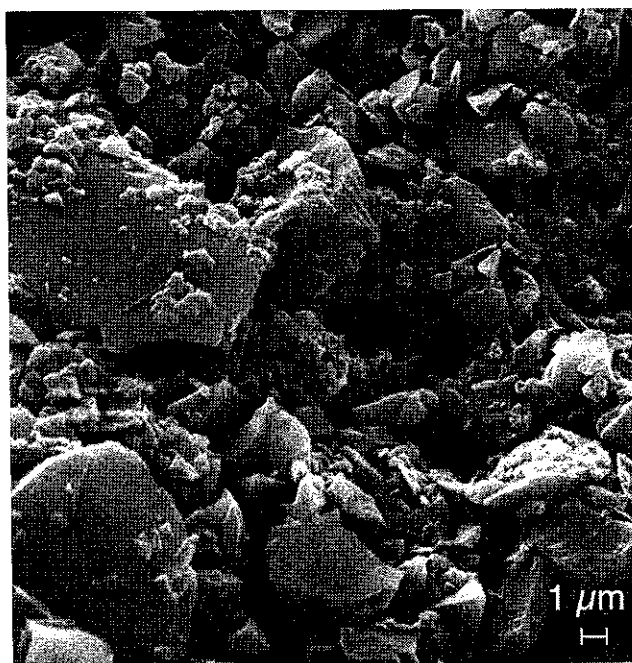
Figure 4.4.7. Scanning electron micrographs of two point deprotected material.
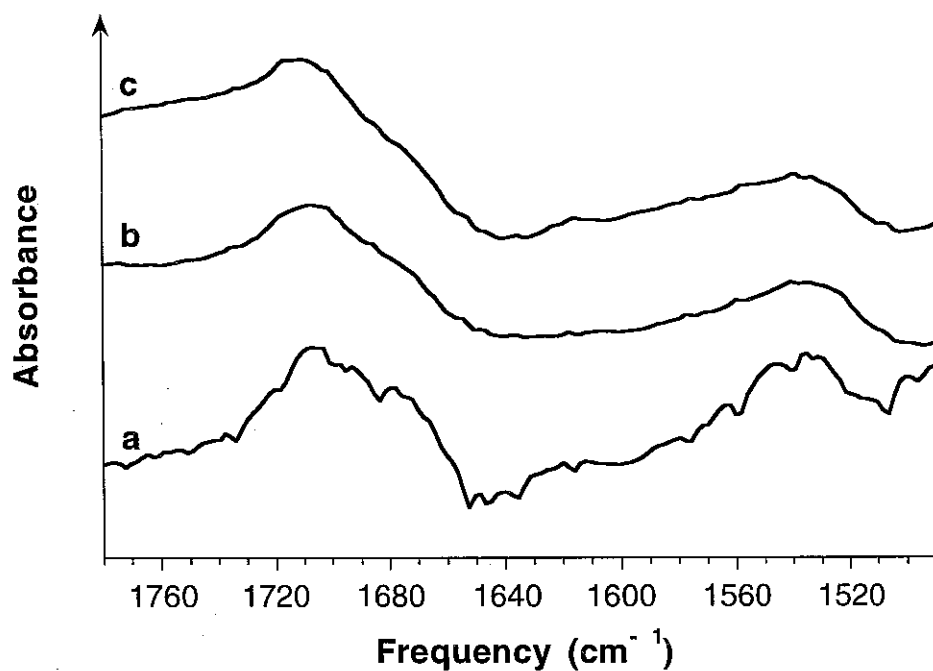
Figure 4.4.8. Subtraction spectra between capped and deprotected silicas for (a) one point, (b) two point, and (c) three point imprinted silicas.
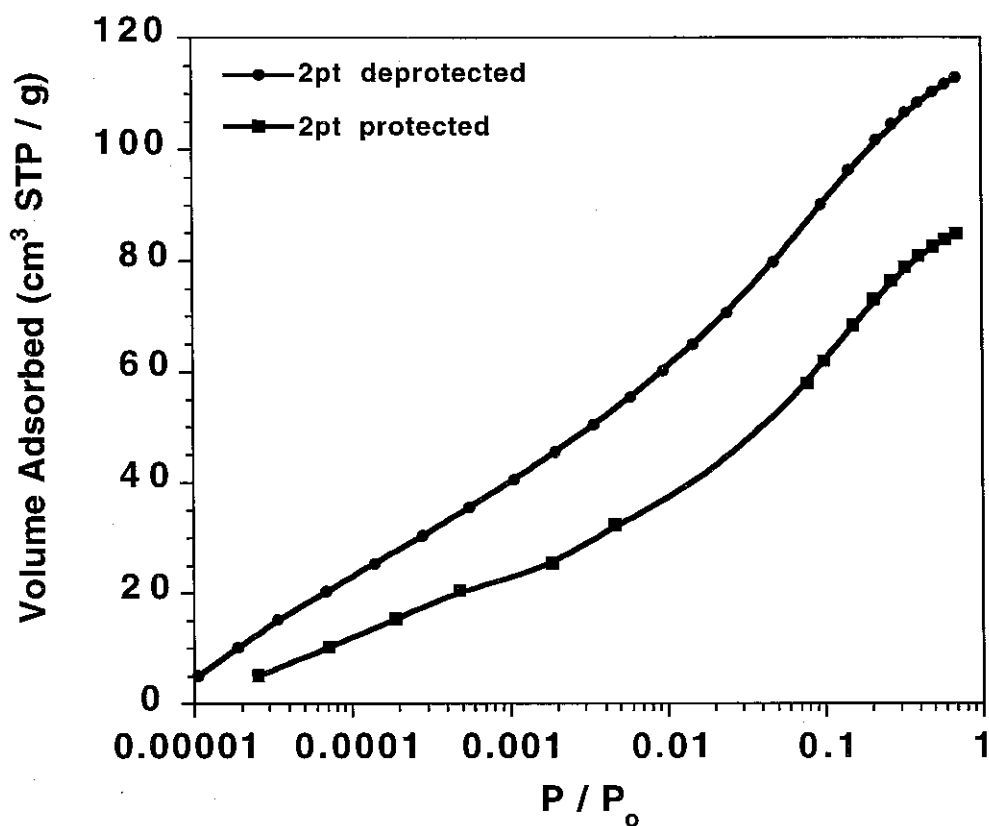
Figure 4.4.9.   Argon adsorption isotherms for two point deprotected (top), zero point deprotected (middle), and two point capped (protected) (bottom) imprinted silicas.
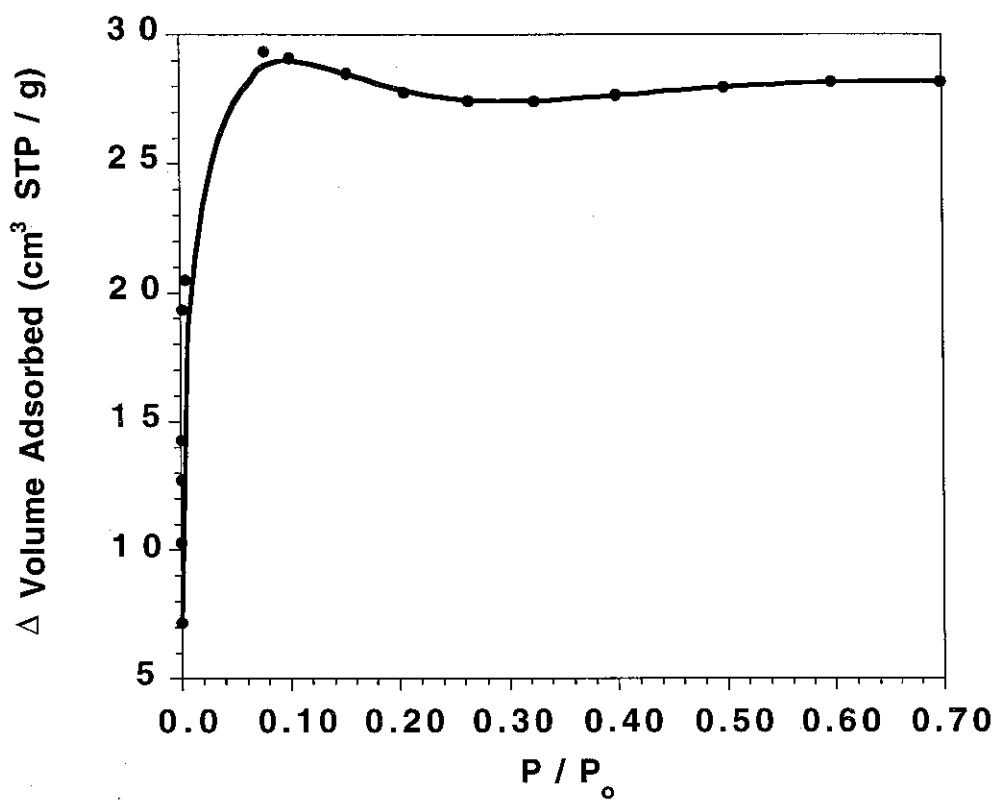
Figure 4.4.10. Difference isotherm between two point deprotected and two point capped (protected) imprinted silicas.
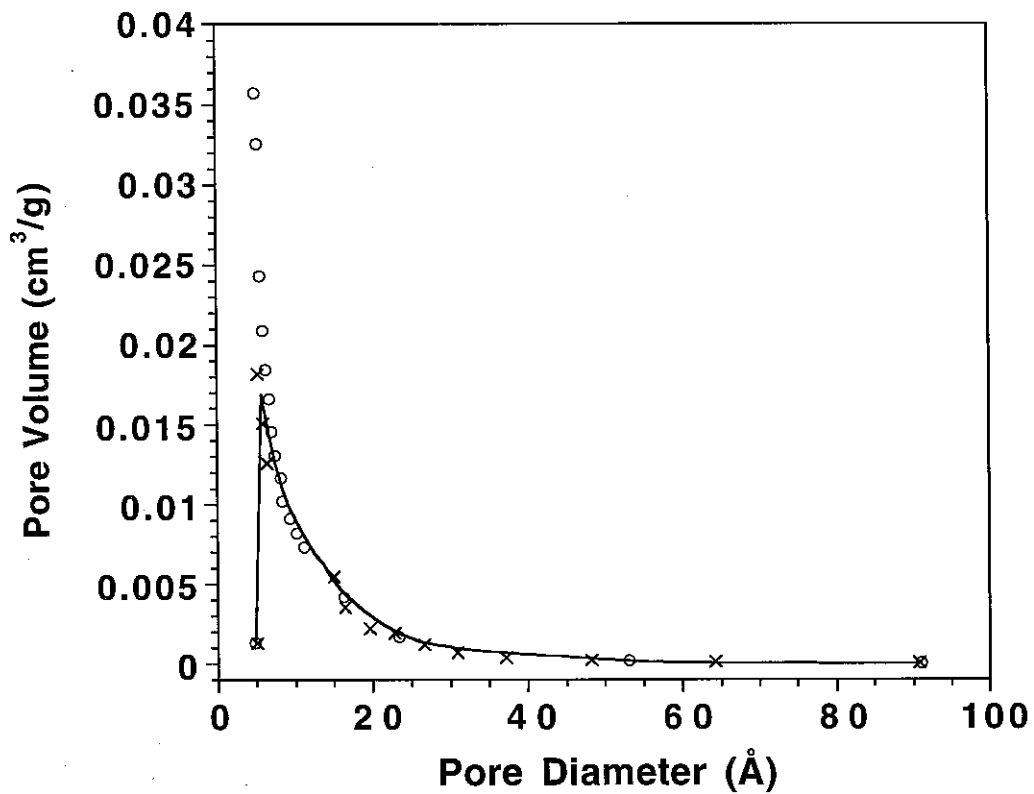
Figure 4.4.11. Pore size distribution plot obtained by the using method of Horvath-Kawazoe (ref. 18) for two point deprotected (o) and capped (protected) (X).
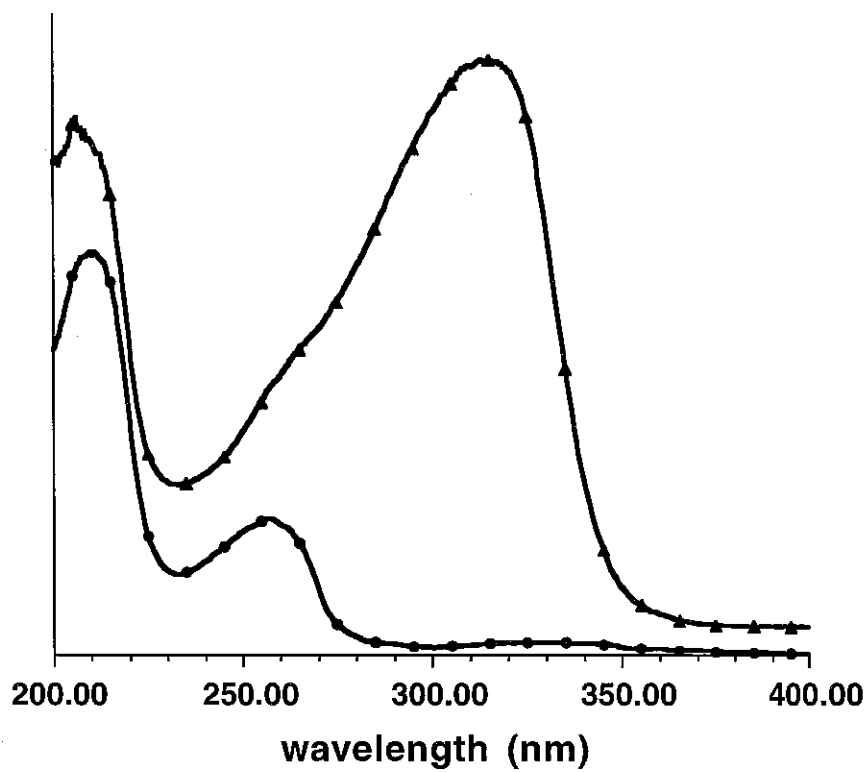
Figure 4.4.12. Diffuse-reflectance, ultraviolet spectra of one point material (lower with filled circles) and one point silica treated with acetylacetone (upper with filled triangles). The broad band in the upper spectrum is at 316 nm.
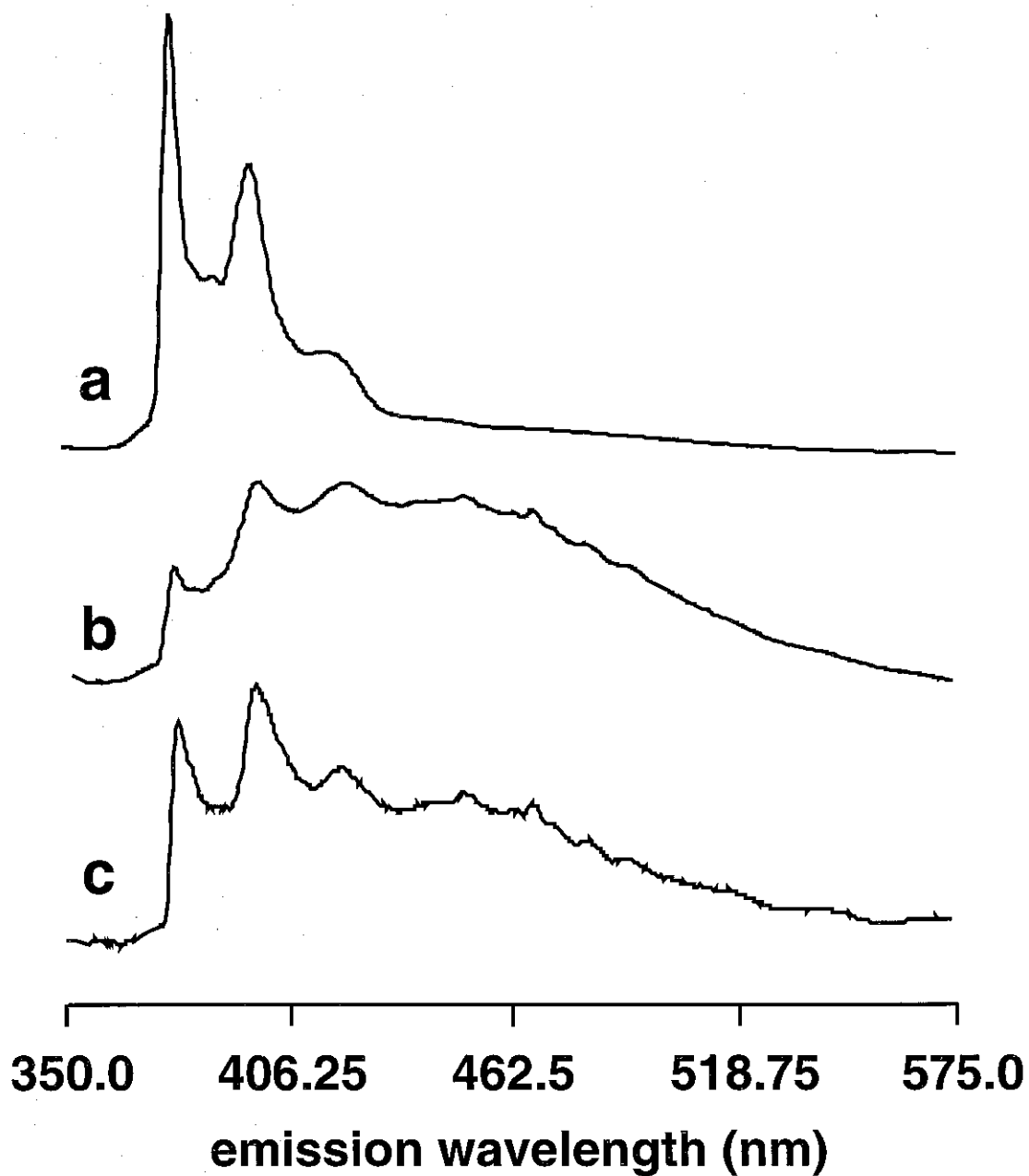
Figure 4.4.13. Emission spectra measured at an excitation frequency of 340 nm for pyrenebutyric acid bound into the (a) one point, (b) three point and (c) zero point imprinted silicas.
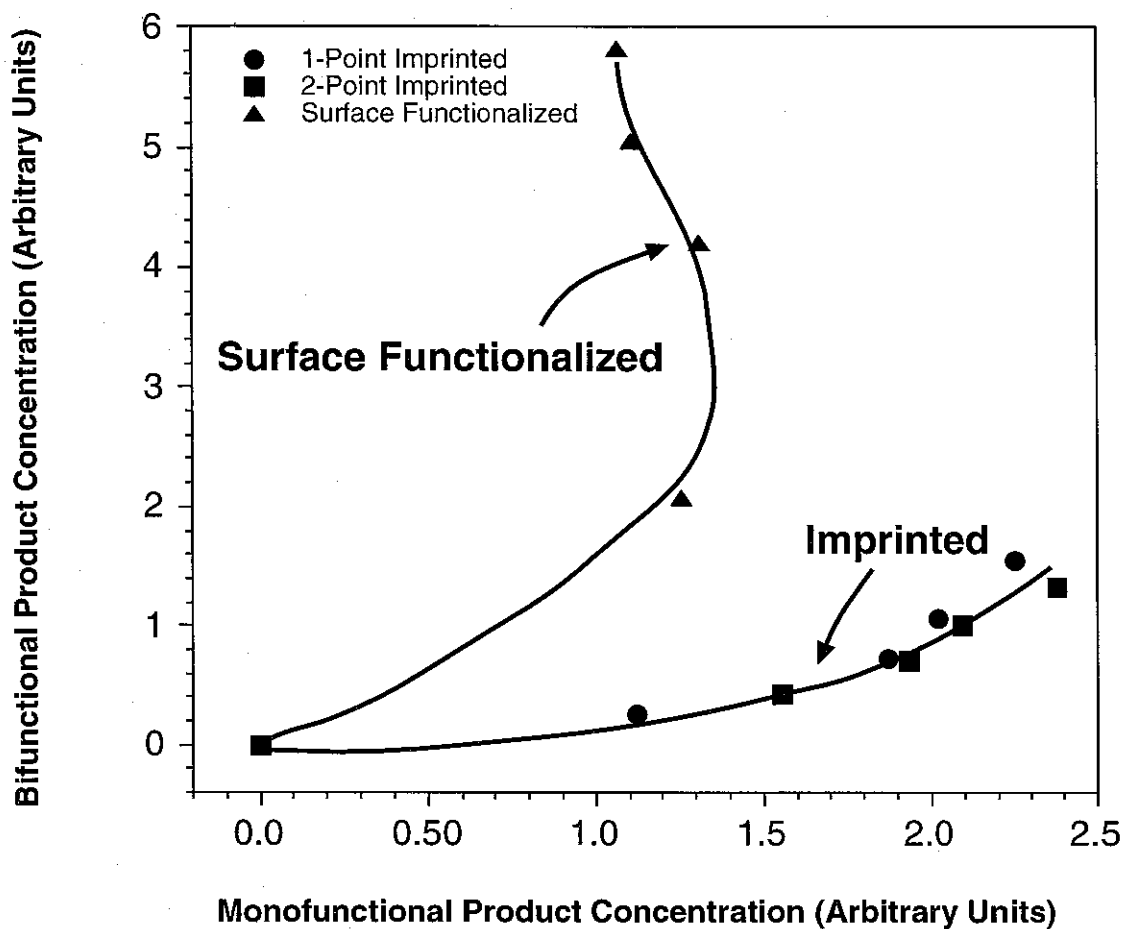
Figure 4.4.14. Phase plot representation of monofunctional product solution concentration versus bifunctional product solution concentration for the Knoevenagel condensation of isophthalaldehyde and malononitrile. Filled triangles represent aminopropyl, surface functionalized silica, filled circles represent the one-point imprinted silica, and filled squares represent the two-point imprinted silica.
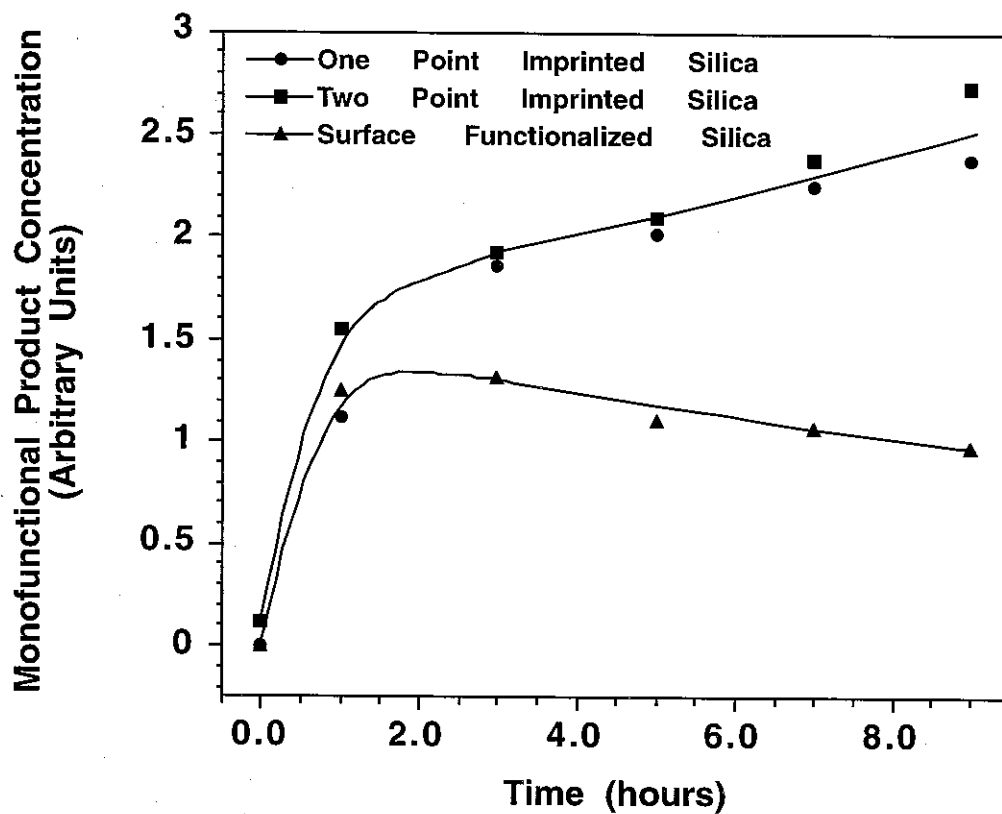
Figure 4.4.15. Monofunctional product solution concentration versus time for the Knoevenagel condensation of isophthalaldehyde and malononitrile. Filled triangles represent aminopropyl, surface functionalized silica, filled circles represent the one-point imprinted silica, and filled squares represent the two-point imprinted silica.

Figure 4.4.16. Bifunctional product solution concentration versus time for the Knoevenagel condensation of isophthalaldehyde and malononitrile. Filled triangles represent aminopropyl, surface functionalized silica, filled circles represent the one-point imprinted silica, and filled squares represent the two-point imprinted silica.
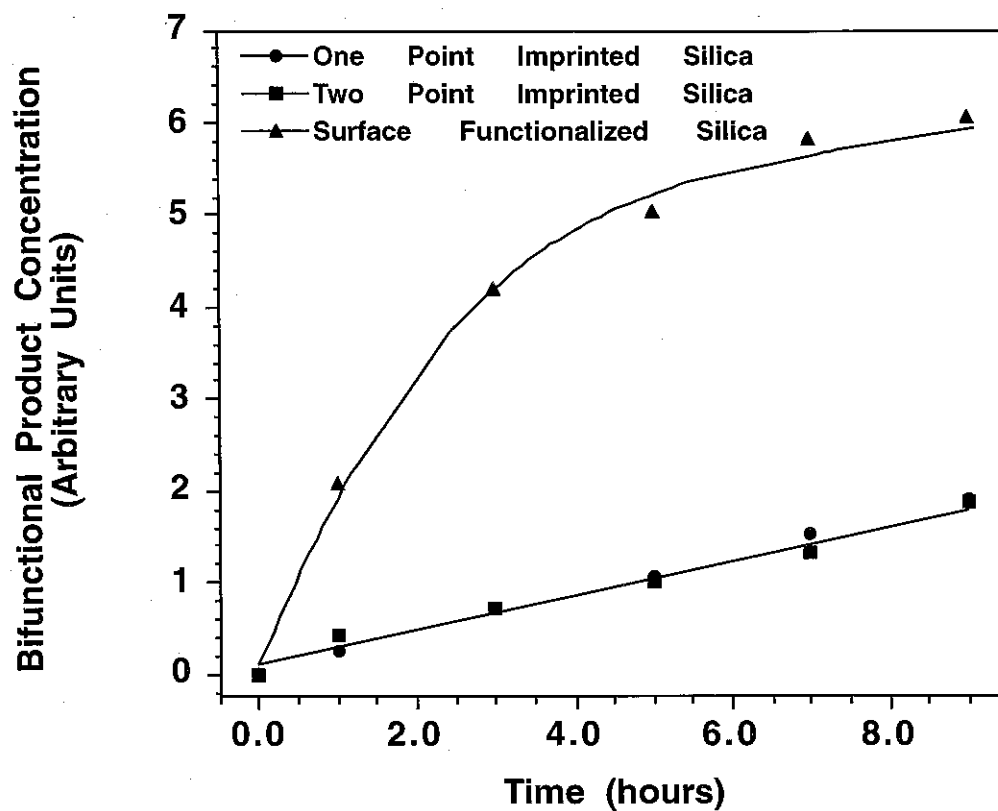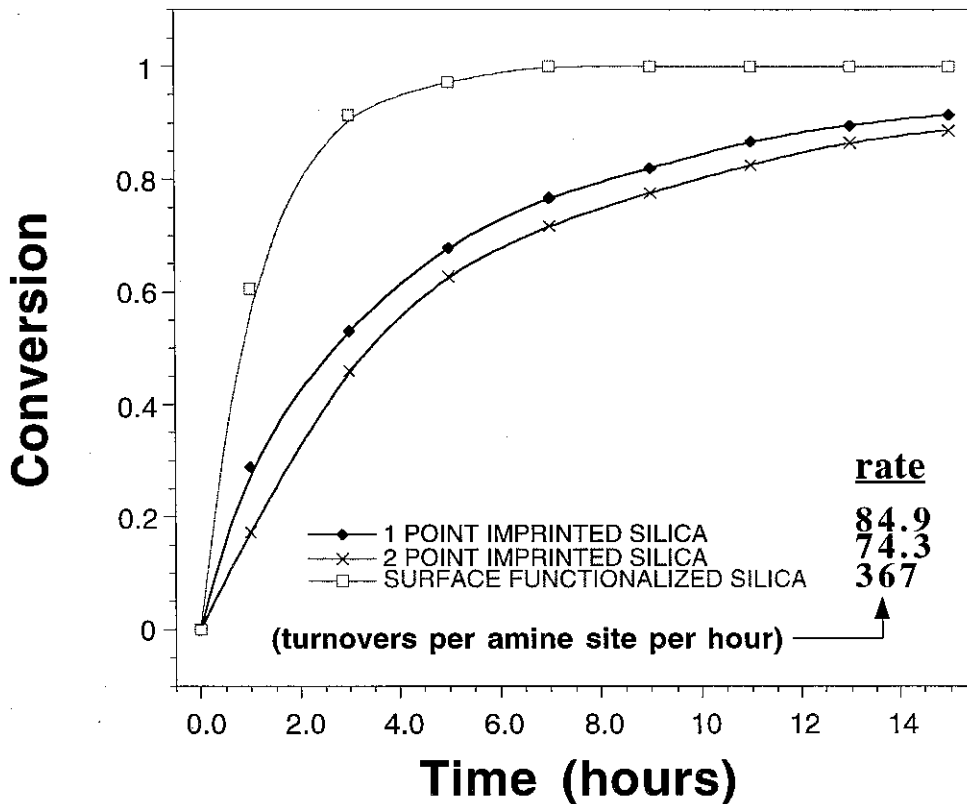
Figure 4.4.17. Conversion of isophthalaldehyde versus time for the Knoevenagel condensation of isophthalaldehyde and malononitrile. Filled circles represent aminopropyl, surface functionalized silica, filled diamonds represent the one-point imprinted silica, and filled squares represent the two-point imprinted silica. The rates given in the right-hand-corner of the graph represent initial rates in turnovers per amine site per hour.

CHAPTER FIVE

SUMMARY

Summary

The molecular imprinting of materials for catalysis presents many challenges. On one hand, it is non-covalent interactions which, in the end, control the success or failure of an imprinted catalyst. However, as my studies in Chapters 3 and 4 conclude, using these same types of interactions as a driving force for the imprinting process (by imprinting with the self-assembly method) or its characterization (by non-covalent binding of bifunctional reagents) can lead to binding site heterogeneity and a lack of general control in binding, respectively. This led me to develop an imprinting strategy based on a controlled distance approach that uses covalent interactions to achieve functional group positioning within the rigid framework provided for by silica. This approach, although conceptually simple, has provided significant insight into the basics of the molecular imprinting process. For the first time in the synthesis of imprinted materials, this approach gives a material with a measurable porosity increase at the microporous length scale of the imprint over a non-imprinted material. In turn, this microporosity, in which the imprinted functional groups are themselves imbedded within, provides for shape-selective catalysis and adsorption. However, none of these properties explicitly exploits the local positioning of the amines in the two and three point materials. Pyrene fluorescence measurements on a material prepared with three amines per imprinted site gives a spectroscopic signature characteristic of the "ordered

functionality" while the material with one amine per imprinted site gives a signature corresponding to isolated functionality (which is itself a unique material from the perspective of *isolated* organic imbedded in a siliceous network). Despite these advances much interesting work remains to be done in making the characterization of the imprinting process more quantitative for the *rapid* evaluation of imprinting approaches. I have given some suggestions for the next steps to take in this regard based on my own triumphs and failures in characterizing the new imprinted silica system described in Chapter 4.

The ultimate test of an imprinted system, however, is its performance in the catalytic application that it was designed for. As more complexity is built into newly developed imprinting approaches, the proof of concept may be in the catalysis that was sought out for by the imprinting in the first place. Indeed this is one of the areas of molecular imprinting that has a large potential to grow by building on the knowledge of biological systems; some of which are discussed in Chapter 2. Currently the degree of progress in other fields emulating biological catalysis exceeds imprinted materials (fields such as protein oligomer enzyme mimics, catalytic antibodies, immobilized "natural" systems and synthetic peptide mimics). In a way, these more advanced disciplines provide a feeding ground to the field of molecular imprinting towards mimicking aspects of enzyme catalysis. Thus, progress can forseeably be made in imprinting by applying the lessons

learned from these communities onto well-defined, imprinting based systems, and some of these are summarized in Chapter 2.

At the other end of the spectrum, more progress on the materials challenges confronting the imprinting field must be made in the more immediate future. These include: 1) the synthesis of amorphous, microporous materials with a higher degree of crosslinking and larger pore dimensionality (> 15 Å); 2) the homogeneous incorporation of organic functionality within a microporous material framework and 3) expansion on the diversity of synthetic imprinting strategies for different types of functional groups with varying mechanical rigidity and chemical properties. Although progress in these areas does not necessarily require an imprinting approach, there is little doubt that further knowledge in these areas will open up more opportunities to build on the complexity of the other fields mentioned above and in the design of new catalysts via molecular imprinting.